OSCILLOTHERAPEUTICS - TOWARD REAL-TIME CONTROL OF PATHOLOGICAL OSCILLATIONS IN THE BRAIN, 2nd Edition

EDITED BY: Yuichi Takeuchi, Takeshi Kawano, Qun Li, Tatsuya Mima and Jun Nagai

PUBLISHED IN: Frontiers in Behavioral Neuroscience,
Frontiers in Human Neuroscience,
Frontiers in Systems Neuroscience and
Frontiers in Computational Neuroscience

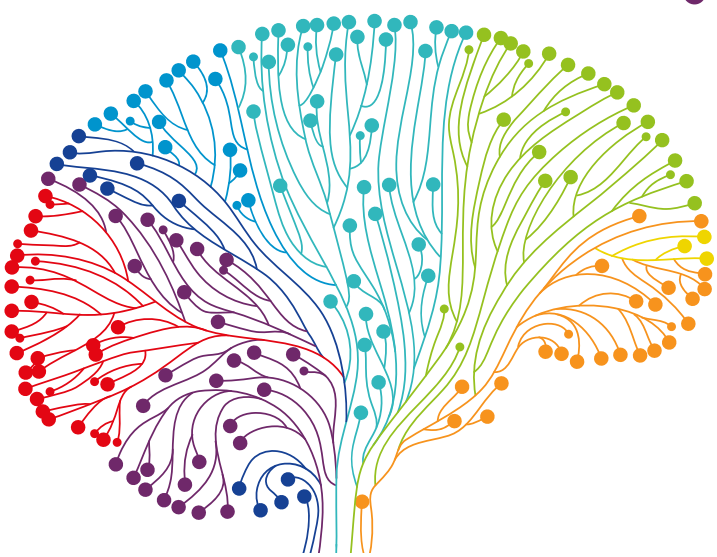

frontiers Research Topics

frontiers

ISSN 1664-8714
ISBN 978-2-83251-255-5
DOI 10.3389/978-2-83251-255-5

About Frontiers

Frontiers is more than just an open-access publisher of scholarly articles: it is a pioneering approach to the world of academia, radically improving the way scholarly research is managed. The grand vision of Frontiers is a world where all people have an equal opportunity to seek, share and generate knowledge. Frontiers provides immediate and permanent online open access to all its publications, but this alone is not enough to realize our grand goals.

Frontiers Journal Series

The Frontiers Journal Series is a multi-tier and interdisciplinary set of open-access, online journals, promising a paradigm shift from the current review, selection and dissemination processes in academic publishing. All Frontiers journals are driven by researchers for researchers; therefore, they constitute a service to the scholarly community. At the same time, the Frontiers Journal Series operates on a revolutionary invention, the tiered publishing system, initially addressing specific communities of scholars, and gradually climbing up to broader public understanding, thus serving the interests of the lay society, too.

Dedication to Quality

Each Frontiers article is a landmark of the highest quality, thanks to genuinely collaborative interactions between authors and review editors, who include some of the world's best academicians. Research must be certified by peers before entering a stream of knowledge that may eventually reach the public - and shape society; therefore, Frontiers only applies the most rigorous and unbiased reviews.
Frontiers revolutionizes research publishing by freely delivering the most outstanding research, evaluated with no bias from both the academic and social point of view. By applying the most advanced information technologies, Frontiers is catapulting scholarly publishing into a new generation.

What are Frontiers Research Topics?

Frontiers Research Topics are very popular trademarks of the Frontiers Journals Series: they are collections of at least ten articles, all centered on a particular subject. With their unique mix of varied contributions from Original Research to Review Articles, Frontiers Research Topics unify the most influential researchers, the latest key findings and historical advances in a hot research area! Find out more on how to host your own Frontiers Research Topic or contribute to one as an author by contacting the Frontiers Editorial Office: frontiersin.org/about/contact

OSCILLOTHERAPEUTICS - TOWARD REAL-TIME CONTROL OF PATHOLOGICAL OSCILLATIONS IN THE BRAIN,
2nd Edition

Topic Editors:
Yuichi Takeuchi, Hokkaido University, Japan
Takeshi Kawano, Toyohashi University of Technology, Japan
Qun Li, University of Szeged, Hungary
Tatsuya Mima, Ritsumeikan University, Japan
Jun Nagai, RIKEN Center for Brain Science (CBS), Japan

Publisher's note: In this 2nd edition, the following article has been added: Takeuchi Y, Li Q, Kawano T, Nagai J and Mima T (2022) Editorial: Oscillotherapeutics - toward real-time control of pathological oscillations in the brain. *Front. Behav. Neurosci.* 16:1021616. doi: 10.3389/fnbeh.2022.1021616

Citation: Takeuchi, Y., Kawano, T., Li, Q., Mima, T., Nagai, J., eds. (2023). Oscillotherapeutics - Toward Real-Time Control of Pathological Oscillations in the Brain, 2nd Edition. Lausanne: Frontiers Media SA.
doi: 10.3389/978-2-83251-255-5

Table of Contents

frontiers | Frontiers in Behavioral Neuroscience

TYPE Editorial
PUBLISHED 08 September 2022
DOI 10.3389/fnbeh.2022.1021616

OPEN ACCESS

EDITED AND REVIEWED BY
Rainer Spanagel,
University of Heidelberg, Germany

*CORRESPONDENCE
Yuichi Takeuchi
ytake@pharm.hokudai.ac.jp

SPECIALTY SECTION
This article was submitted to Pathological Conditions, a section of the journal Frontiers in Behavioral Neuroscience

RECEIVED 17 August 2022
ACCEPTED 23 August 2022
PUBLISHED 08 September 2022

CITATION
Takeuchi Y, Li Q, Kawano T, Nagai J and Mima T (2022) Editorial: Oscillotherapeutics - toward real-time control of pathological oscillations in the brain. *Front. Behav. Neurosci.* 16:1021616. doi: 10.3389/fnbeh.2022.1021616

Editorial: Oscillotherapeutics - toward real-time control of pathological oscillations in the brain

Yuichi Takeuchi[1,2]*, Qun Li[2], Takeshi Kawano[3], Jun Nagai[4] and Tatsuya Mima[5]

[1]Department of Biopharmaceutical Sciences and Pharmacy, Faculty of Pharmaceutical Sciences, Hokkaido University, Sapporo, Japan, [2]MTA-SZTE "Momentum" Oscillatory Neuronal Networks Research Group, Department of Physiology, University of Szeged, Szeged, Hungary, [3]Department of Electrical and Electronic Information Engineering, Toyohashi University of Technology, Aichi, Japan, [4]Laboratory for Glia-Neuron Circuit Dynamics, RIKEN Center for Brain Science, Saitama, Japan, [5]The Graduate School of Core Ethics and Frontier Sciences, Ritsumeikan University, Kyoto, Japan

KEYWORDS

oscillation, oscillopathy, neurological disorders, psychiatric disorders, closed-loop control, brain stimulation

Editorial on the Research Topic
Oscillotherapeutics - toward real-time control of pathological oscillations in the brain

The aim of this Research Topic: Oscillatory brain activities reflect and affect network activities in the brain. They support many physiological functions from motor control to cognition and emotion (Buzsáki, 2006; Nambu et al., 2020). Abnormal oscillatory brain activities are commonly observed in neurological and psychiatric disorders including epilepsy, Parkinson's disease, Alzheimer's disease, schizophrenia, anxiety/trauma-related disorders, major depressive disorders, and addiction (Leuchter et al., 2015; Takeuchi et al., 2021b). Therefore, these disorders can be considered as common oscillation defects "oscillopathies," despite having distinct behavioral manifestations (Takeuchi and Berényi, 2020; Földi et al., 2021).

Recent advances in brain activity measurements and analyses have allowed us to study the pathological oscillations of each disorder as a possible biomarker of symptoms (Hultman et al., 2018). Furthermore, emerging brain stimulation technologies enable time- and space-targeted interventions of the pathological oscillations of neurological and psychiatric disorders. These interventions are possible therapeutic targets for regulating disorder symptoms (Tyler et al., 2018; Vöröslakos et al., 2018; Takeuchi et al., 2021a).

This Research Topic was organized to provide a comprehensive overview of pathological oscillations in neurological and psychiatric disorders. It was also aimed at examining correlations or causal relationships between pathological oscillations and the symptoms of disorders. These relationships were analyzed for the possible use of oscillations as biomarkers or therapeutic targets.

This Research Topic covers animal, human, and computational studies in the oscillotherapeutics field. Good animal models that accurately reflect the neurological and psychiatric symptoms of patients are necessary for providing the oscillotherapeutics proof-of-concept for future translational research. Clinical studies may test the proof-of-concept provided from animal research *via* solving clinical issues. Computational studies can prospectively or retrospectively provide a theory that explains pathological oscillations or their interventions.

Statistics on this Research Topic: The Research Topic was open from November 20, 2020 to December 31, 2021. It had been viewed over 37 thousand times at the time this editorial was prepared in June 2022. Ten articles were accepted after rigorous and constructive reviewing processes.

Section 1: Reviews

Mokhothu and Tanaka gave a concise overview of physiological and non-physiological high frequency oscillations in hippocampus-related temporal lobe epilepsy in animals and humans.

Okonogi and Sasaki reviewed how neuronal oscillations in the limbic brain structure were engaged in emotional behaviors and altered by psychiatric changes such as anxiety and depression.

Section 2: Animal studies

Acerbo et al. introduced a novel non-thermal electroporation technique to ablate neurons in a seizure focus with reduced vascular damage and accelerated tissue recovery.

Tomar et al. investigated the impacts of acute and chronic stress on spatial coding and gamma oscillations in the hippocampal CA1 region of mice.

Adlan et al. investigated sleep architecture and brain oscillatory patterns in a multiple-hit model for schizophrenic rats with impaired cognitive functions.

Wada et al. reported diminished "rubber tail task"-related expression of the immediate early gene (c-Fos) in the posterior parietal cortex of a transgenic mouse line that exhibits autistic-like phenotypes.

Section 3: Clinical and computational studies

Nakajima et al. reported the case of a patient with Parkinson's disease whose local field potential fluctuations were less evident inside the hospital than outside after receiving chronic-adaptive deep brain stimulation of the subthalamic nuclei.

Ogawa et al. reported topographical distributions of desynchronization of electroencephalography recordings during volitional swallow in two amyotrophic lateral sclerosis patients.

Cimenser et al. reported that rhythmic gamma sensory stimulation improved the sleep and daily living activity of mild to moderate Alzheimer's disease patients.

Nobukawa et al. showed that applying chaotic resonance induced by a reduced region of orbit feedback signals may provide a promising treatment option for attention-deficit hyperactivity disorder.

Summary

This is the first collection of articles in oscillotherapeutics research.

Author contributions

All authors listed have made a substantial, direct, and intellectual contribution to the work and approved it for publication.

Acknowledgments

We are grateful to all authors of this Research Topic and also the reviewers for their constructive feedback.

Conflict of interest

The authors declare that the research was conducted in the absence of any commercial or financial relationships that could be construed as a potential conflict of interest.

Publisher's note

References

Buzsáki, G. (2006). *Rhythms of the Brain*. Oxford University Press.

Földi, T., Lorincz, M. L., and Berényi, A. (2021). Temporally targeted interactions with pathologic oscillations as therapeutical targets in epilepsy and beyond. *Front. Neural Circuits* 15, 784085. doi: 10.3389/fncir.2021.784085

Hultman, R., Ulrich, K., Sachs, B. D., Blount, C., Carlson, D. E., Ndubuizu, N., et al. (2018). Brain-wide electrical spatiotemporal dynamics encode depression vulnerability. *Cell* 173, 166–180.e14. doi: 10.1016/j.cell.2018.02.012

Leuchter, A. F., Hunter, A. M., Krantz, D. E., and Cook, I. A. (2015). Rhythms and blues: modulation of oscillatory synchrony and the mechanism of action of antidepressant treatments. *Ann. N. Y. Acad. Sci.* 1344, 78–91. doi: 10.1111/nyas.12742

Nambu, A., Tsuda, I., and Mima, T. (2020). Oscillology: nonlinear neural oscillations. *Neurosci. Res.* 156, 1–4. doi: 10.1016/j.neures.2020.05.007

Takeuchi, Y., and Berényi, A. (2020). Oscillotherapeutics time-targeted interventions in epilepsy and beyond. *Neurosci. Res.* 152, 87–107. doi: 10.1016/j.neures.2020.01.002

Takeuchi, Y., Harangozó, M., Pedraza, L., Földi, T., Kozák, G., Li, Q., et al. (2021a). Closed-loop stimulation of the medial septum terminates epileptic seizures. *Brain* 144, 885–908. doi: 10.1093/brain/awaa450

Takeuchi, Y., Nagy, A. J., Barcsai, L., Li, Q., Ohsawa, M., Mizuseki, K., et al. (2021b). The medial septum as a potential target for treating brain disorders associated with oscillopathies. *Front. Neural Circuits* 15, 701080. doi: 10.3389/fncir.2021.701080

Tyler, W. J., Lani, S. W., and Hwang, G. M. (2018). Ultrasonic modulation of neural circuit activity. *Curr. Opin. Neurobiol.* 50, 222–231. doi: 10.1016/j.conb.2018.04.011

Vöröslakos, M., Takeuchi, Y., Brinyiczki, K., Zombori, T., Oliva, A., Fernández-Ruiz, A., et al. (2018). Direct effects of transcranial electric stimulation on brain circuits in rats and humans. *Nat. Commun.* 9, 483. doi: 10.1038/s41467-018-02928-3

frontiers in Behavioral Neuroscience

REVIEW
published: 09 June 2021
doi: 10.3389/fnbeh.2021.698753

Theta-Range Oscillations in Stress-Induced Mental Disorders as an Oscillotherapeutic Target

*Toya Okonogi and Takuya Sasaki**

Laboratory of Chemical Pharmacology, Graduate School of Pharmaceutical Sciences, The University of Tokyo, Tokyo, Japan

Emotional behavior and psychological disorders are expressed through coordinated interactions across multiple brain regions. Brain electrophysiological signals are composed of diverse neuronal oscillations, representing cell-level to region-level neuronal activity patterns, and serve as a biomarker of mental disorders. Here, we review recent observations from rodents demonstrating how neuronal oscillations in the hippocampus, amygdala, and prefrontal cortex are engaged in emotional behavior and altered by psychiatric changes such as anxiety and depression. In particular, we focus mainly on theta-range (4–12 Hz) oscillations, including several distinct oscillations in this frequency range. We then discuss therapeutic possibilities related to controlling such mental disease-related neuronal oscillations to ameliorate psychiatric symptoms and disorders in rodents and humans.

Keywords: oscillations, emotion, depression, anxiety, hippocampus, amygdala, prefrontal cortex

OPEN ACCESS

Edited by:
Yuichi Takeuchi,
Osaka City University, Japan

Reviewed by:
Brendon O. Watson,
University of Michigan, United States
Thomas John McHugh,
RIKEN Brain Science Institute (RIKEN BSI), Japan

***Correspondence:**
Takuya Sasaki
tsasaki@mol.f.u-tokyo.ac.jp

Specialty section:
This article was submitted to Pathological Conditions, a section of the journal Frontiers in Behavioral Neuroscience

Received: *22 April 2021*
Accepted: *14 May 2021*
Published: *09 June 2021*

Citation:
Okonogi T and Sasaki T (2021) Theta-Range Oscillations in Stress-Induced Mental Disorders as an Oscillotherapeutic Target. Front. Behav. Neurosci. 15:698753. doi: 10.3389/fnbeh.2021.698753

INTRODUCTION

The accumulation of mental stress loads is a primary risk factor for psychiatric disorders such as major depressive disorder (MDD), anxiety disorders, and posttraumatic stress disorder (PTSD) (Yehuda and LeDoux, 2007; Arnsten, 2015). A number of studies have revealed that brain regions such as the medial prefrontal cortex (mPFC), cingulate cortex, amygdala (AMY), hippocampus (HPC), and hypothalamus play crucial roles in the regulation of affective and visceral functions and undergo marked changes in their activity caused by stress-induced mental disease (Greicius et al., 2007; Sheline et al., 2010; Nugent et al., 2015; Tovote et al., 2015; Drysdale et al., 2017). In particular, the HPC-PFC-AMY circuit is a core network formed by long-range projections (Caliskan and Stork, 2019) in which the ventral HPC (vHPC) and the mPFC transfer sensory and contextual information to the basolateral amygdala (BLA) (Orsini et al., 2011; Ciocchi et al., 2015) and the BLA, in turn, transfers information of negative valence back to the mPFC and vHPC (Ishikawa and Nakamura, 2003; Senn et al., 2014; Kim et al., 2016; Burgos-Robles et al., 2017).

To date, a key technique to understand the basic neuronal mechanisms and devise therapeutic strategies based on pathophysiology is the recording of electrophysiological signals that represent brain activity patterns and provide great temporal resolution at the millisecond scale. The mammalian forebrain generates extracellular field potentials containing a mixture of diverse neural oscillations at frequency bands ranging from 0.1 to 250 Hz (in health) and up to 500 Hz (in disease) that show dynamic changes associated with arousal levels, emotional valence, and memory

Abbreviations: AMY, amygdala; BLA, basolateral amygdala; LFP, local field potential; mPFC, medial prefrontal cortex; PTSD, posttraumatic stress disorder; vHPC, ventral hippocampus.

performance (Buzsaki and Draguhn, 2004; Buzsaki et al., 2012; Buzsaki and Watson, 2012). In addition to representing the activity patterns of individual brain areas, electrical signals from multiple brain regions are sensitive to changes in their functional connectivity defined as their correlational power changes and coherence. A number of clinical studies have reported altered patterns of electroencephalogram (EEG) oscillatory signals in depressed patients, such as altered power and functional coupling in the alpha (8–13 Hz) and gamma (30–100 Hz) bands in the frontal cortex (Jesulola et al., 2015; Fitzgerald and Watson, 2018; Grunewald et al., 2018). Similarly, in PTSD patients, resting electrical signals in the PFC show decreased alpha power-mediated inhibition and increased gamma power, suggesting hypofunction in the PFC (Huang et al., 2014; Clancy et al., 2017). Accumulated evidence from these studies suggests that brain field potential signals serve as a physiological sign of mood disorders (Iosifescu, 2011; Baskaran et al., 2012; Buzsaki and Watson, 2012; Fitzgerald and Watson, 2018).

On the other hand, at microscopic levels, a number of studies from animal models to human patients have demonstrated stress-related molecular and cellular mechanisms that could lead to psychiatric disorders (Krishnan and Nestler, 2008; Arnsten, 2015; McEwen et al., 2015). However, it remains largely unknown how these mechanisms are integrated in the expression of psychiatric symptoms and behavioral phenotypes. The necessity to bridge the gap between these insights also highlights the importance of electrical field signals as a measure to estimate neuronal network-level dynamics. In particular, animal experiments allow us to directly measure local field potential (LFP) signals from target brain regions with high signal-to-noise ratios and compare how their oscillatory patterns dynamically change with emotional behavior in both health and disease. Such basic non-clinical experiments are crucial for devising novel therapeutic strategies, including drug discovery and timed interventions on brain activity, which have been termed oscillotherapeutics (Takeuchi and Berenyi, 2020).

This paper introduces recent techniques to measure brain LFP signals from freely moving rodents, summarizes recent reports showing anxiety- and fear-related changes in LFP patterns, especially focusing on the HPC-PFC-AMY circuit, observed in non-pathological animals, and then describes how LFP signals from these brain regions are affected by stress accumulation. Finally, we discuss potential therapeutic strategies to ameliorate stress-induced psychiatric disorders based on oscillatory LFP patterns.

METHODS FOR OSCILLOTHERAPEUTIC STUDIES USING RODENTS

Multisite Recordings of Local Field Potentials (LFPs) in Freely Moving Rodents

A key experimental technique related to oscillotherapeutics in rodent research is chronic electrophysiological recordings of extracellular signals representing collective oscillatory field potentials from neuronal populations and spike patterns from individual neurons in freely moving animals (**Figure 1A**). A number of studies have utilized various types of recording electrodes, such as tetrode arrays and silicon probes (**Figure 1B**), that enable multisite (tens or hundreds of sites) recordings from target brain regions. These electrodes are chronically implantable for several months and are flexibly movable to adjust the depth of electrodes with micrometer precision in the brain tissue after implantation using microdrives. Recent advancements in 3D printer technology make it easy to customize plastic parts to accommodate these electrodes into a microdrive (**Figure 1C**). For example, we recently created a recording device to cover wide ranges of cortical regions from anterior to posterior and from medial and lateral parts in rodents (**Figure 1B**, left) (Konno et al., 2019; Nakayama et al., 2019). Conveniently, most of the CAD files designed by developers for multichannel recordings are now available from cloud-based repositories, such as Mendeley data, and laboratory websites, which enables researchers to freely create these devices. Furthermore, wireless recording systems are recently available (Zuo et al., 2012; Martinez et al., 2018; Iturra-Mena et al., 2019), which are especially useful for stress research because they reduce the physical stress of animals.

In addition to brain electrophysiological recordings, we conceived a recording approach in which a multichannel recording device extends to the collection of bioelectrical signals from peripheral organs, such as electrocardiogram (ECG) signals, electromyogram (EMG) signals (Okada et al., 2016; Okonogi et al., 2018; Shikano et al., 2018), olfactory bulb respiratory (Resp) signals (Kuga et al., 2019), and vagus nerve (VN) signals (Shikano et al., 2019) (**Figure 1D**), all of which can be captured by a single recording device. This recording method is useful for precisely monitoring signals representing changes in peripheral organ activity related to emotion, stress, and mental disorders, in addition to simple behavioral phenotypes.

Realtime Manipulation of Local Field Potentials

Electrophysiological recordings, compared with imaging techniques, provide higher temporal resolution at millisecond timescales, allowing real-time detection of electrical signals and precisely timed interventions involving neuronal activity immediately upon the emergence of target features in the signals (e.g., signal amplitude, phase, and spikes), a so-called closed-loop neurostimulation system (**Figures 2B,C**). On-demand stimulation protocols based on this system enable a high-quality physiological experimental design for both basic and pathological studies. As an example of targeting transient brain signals, time-specific stimulation during seizure events can inhibit subsequent seizure-like behavior in epilepsy animal models (Berenyi et al., 2012; Takeuchi et al., 2021). At frequencies lower than 10 Hz, phase-targeting stimulation (e.g., peaks and troughs of a given oscillation) is an effective technique to test their contributions to brain functions. For instance, theta (4–12 Hz) phase-specific manipulations of neuronal activity in the hippocampus and the subthalamic nucleus have been shown to induce memory enhancement and parkinsonian symptoms,

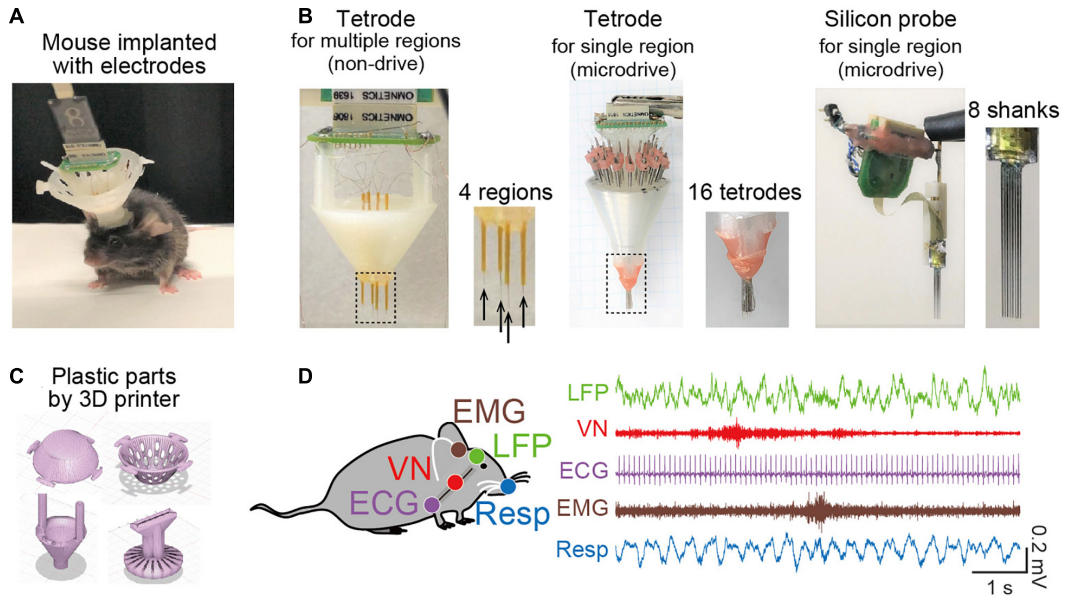

FIGURE 1 | Recent recording methods to study brain oscillations in rodents. **(A)** A picture of a mouse implanted with an electrode assembly. **(B)** Typical electrode assemblies with multiple recording sites. (Left) Tetrode arrays to target several separated brain regions. The dotted region is magnified in the right panel, showing the electrode tips (indicated by arrows). (Middle) A microdrive with multiple tetrode arrays to record spike patterns of neurons in a target region. (Right) A microdrive with 8-shanks silicon probes to record spike patterns of neurons in a target region. **(C)** Typical CAD illustrations of plastic parts created by a 3D printer. **(D)** Simultaneous electrophysiological recordings of a brain LFP signal, a vagus nerve (VN) signal, an ECG signal, an EMG signal, and a Respiration (Resp) signal.

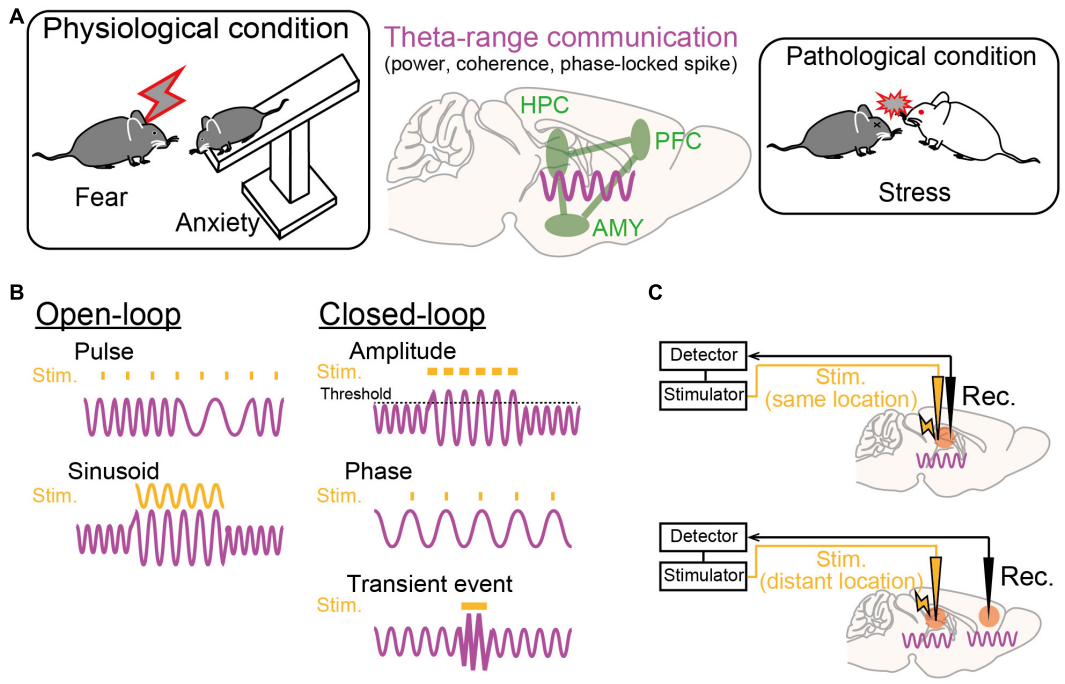

FIGURE 2 | Theta-range oscillations as a target of oscillotherapeutics. **(A)** Recent studies suggest that theta-range (4–12 Hz) oscillations in the HPC-PFC-AMY circuit are crucial for emotional behavior and susceptibility to stress. **(B)** Examples of stimulation patterns (orange) upon brain oscillatory signals (magenta) in the open-loop and closed-loop systems. **(C)** (Top) Closed-loop stimulation is applied to the brain region where a target brain signal is recorded. (Bottom) Closed-loop stimulation is applied to a brain region that is different from the brain region where a target signal is recorded.

respectively (Siegle and Wilson, 2014; Cordon et al., 2018). Additional details of applications to studies of emotion and psychiatric disease are described later.

THETA-RANGE OSCILLATIONS IN THE HPC-PFC-AMY CIRCUIT RELATED TO EMOTIONAL BEHAVIOR

Dysregulation of emotions and increased anxiety are crucial hallmarks of stress-induced mental disorders in both animal models and human patients. Regarding rodent studies, behavioral paradigms have been established to subjectively estimate the levels of emotional valence and anxiety. From these behavioral experiments, a number of studies with genetic and pharmacological approaches have suggested that the HPC-PFC-AMY regions is a hub network related to fear and anxiety-like behavior (as reviewed by Tovote et al., 2015). In particular, electrophysiological studies have indicated the importance of theta-range (4–12 Hz, including multiple distinct oscillations) LFP signals in the HPC-PFC-AMY circuit related to emotional behavior as potential substrates for temporal circuit coordination and long-term plasticity in neuronal networks (**Figure 2A**; as reviewed by Caliskan and Stork, 2019). Experimentally, such low-frequency signals are a good model for a closed-loop system (e.g., phase-targeting stimulation) to test their causal roles in behavior and to associate neuronal activity patterns with single spike levels. Here, we focus on several major findings of theta-range LFP oscillations in the HPC-PFC-AMY regions observed in non-pathological animals, which are subsequently discussed in later chapters from the perspective of pathology. Details regarding the involvement of the other oscillations and the other brain regions are beyond the scope of this paper.

Fear

Fear is an adaptive component of transient responses to internal and external aversive events such as potentially threatening stimuli. Fear conditioning tests are often used to assess rodents' learned fear, in which a conditioned stimulus (e.g., auditory stimulus) is paired with an aversive unconditioned stimulus. During an acquisition phase of fear conditioning, the mPFC-BLA circuit has been shown to increase 4-Hz LFP power (Karalis et al., 2016; Davis et al., 2017). During REM sleep periods after fear conditioning, the vHPC-mPFC-BLA circuit exhibits long-lasting enhancement of theta (4–12 Hz) power and interregional theta synchrony for hours (Popa et al., 2010; Ognjanovski et al., 2014; Totty et al., 2017), possibly serving as a substrate to consolidate fear memories (Boyce et al., 2016). During retrieval phases where the same conditioned stimulus is applied, similar tendencies of the two types of LFP oscillations are detected; increased mPFC-BLA 4-Hz (Dejean et al., 2016; Karalis et al., 2016; Ozawa et al., 2020) and HPC-mPFC-BLA theta (4–12 Hz) oscillations (Seidenbecher et al., 2003; Likhtik et al., 2014; Stujenske et al., 2014), each of which entrain oscillatory spike patterns of cell ensembles in this frequency band. Note that Karalis et al. (2016) suggested that the mPFC-BLA 4-Hz oscillation is distinct from the theta oscillations with higher frequency ranges as they are generated through different mechanisms. First, medial septum inactivation selectively eliminated the theta oscillations, possibly via the HPC, while the mPFC 4-Hz oscillation remained intact, which suggests that medial septum is an upstream brain region providing theta-locked inputs to the hippocampus (Buzsaki, 2002) but not 4 Hz-locked inputs to the mPFC. Second, HPC theta oscillations appear to represent atropine-sensitive type 2 theta oscillations as they are specific to periods of immobility (Seidenbecher et al., 2003) and responses to danger (e.g., predator odor) (Mikulovic et al., 2018). This insight suggests that HPC-mPFC-BLA theta oscillations depend on cholinergic inputs, possibly through the medial septum. Third, dmPFC interneurons exhibit spike patterns phase-locked to 4-Hz oscillations (Karalis et al., 2016) and selective activation of dmPFC parvalbumin (PV)-expressing interneurons replicates dmPFC 4-Hz oscillation (Dejean et al., 2016). These results suggest that dmPFC 4-Hz oscillation is intrinsically induced from the inhibitory neuronal circuit in the dmPFC.

Manipulation of the mPFC 4-Hz oscillations is useful to test their causal roles in fear expression and retrieval. Karalis et al. (2016) has demonstrated that optogenetic induction of dmPFC 4-Hz oscillations drives conditioned freezing and Dejean et al. (2016) has demonstrated that inhibition of dmPFC principal neurons in the descending phase of the oscillation increased conditioned freezing. These results suggest the sufficiency of dmPFC 4-Hz oscillations in the induction of learned freezing behavior.

Conditioned fear memories are extinguished by repeated presentations of the conditioned stimulus alone without presentation of an unconditioned stimulus, which is termed extinction learning. Consistent with increased theta oscillations during freezing throughout the phases of fear conditioning, theta coupling across the HPC-mPFC-BLA regions declined as animals underwent extinction learning, whereas it recurred during extinction recall (Lesting et al., 2011). Davis et al. (2017) demonstrated that increased power of a 3–6-Hz BLA oscillation, possibly classified as a 4-Hz oscillation, induced postextinction fear memory retrieval. In contrast, outcompeting this BLA oscillation by chemogenetic inhibition of BLA parvalbumin-positive interneurons (Davis et al., 2017) or 8-Hz sinusoidal stimulation (Ozawa et al., 2020) could inhibit the recurrence of fear behavior following extinction learning, which suggests the necessity of a 4-Hz oscillation in fear extinction recall and/or the induction of conditioned freezing.

Anxiety

Anxiety is an emotional state characterized by an unpleasant state with heightened awareness even without actual exposure to danger. Anxiety-like behavior in rodents is generally assessed in an elevated plus maze (EPM) test or an open field (OF) test. Through these behavioral tests, a number of studies have suggested that the expression of both fear and anxiety is mediated by the HPC-PFC-AMY circuit, possibly through overlapping neuronal mechanisms (Tovote et al., 2015). As a typical example, mice lacking serotonin 1A receptors showing higher anxiety-like behavior in an EPM test exhibited larger increases in HPC theta (4–12 Hz) power (Gordon et al., 2005). In contrast, treatment

with anxiolytics, such as serotonin 1A receptor agonists and benzodiazepines, has been shown to exhibit decreases in HPC theta oscillations (Zhu and McNaughton, 1995). Adhikari et al. (2010) recorded LFP signals simultaneously from the mPFC and vHPC in mice engaging in an EPM test. They showed that theta-frequency communication between the mPFC and vHPC was specifically augmented under anxiogenic environments in an EPM and an OF and correlated with behavioral performance (Adhikari et al., 2010). At a single-neuron level, mPFC neuronal firing patterns were precisely entrained by vHPC theta oscillations (Adhikari et al., 2011), which were related to anxiogenic behavior in an EPM. Together with the fact that the vHPC neurons preferentially send anxiety-related information to the mPFC (Ciocchi et al., 2015), it is conceivable that vHPC theta oscillations lead to mPFC theta-locked spiking activity, and such theta-locked mPFC neuronal activity is crucial for the expression of anxiety. This idea was further supported by the observation that artificial oscillatory activation of mPFC-projecting vHPC neurons at a theta (8-Hz) frequency increased anxiety-like behavior in an EPM test (Padilla-Coreano et al., 2019). In addition, Likhtik et al. (2014) demonstrated that mPFC theta oscillations precede BLA spiking activity and that coherence and power changes at the theta band in the mPFC-BLA circuit predicted stay time in anxiogenic environments. These results all suggest that interregional coordination of neuronal population activity in theta bands in the vHPC-mPFC-BLA circuit is crucial for the expression of anxiogenic behavior. Together with the observations of fear-related theta-range oscillations, anxiogenic behavior and fear behavior may be expressed partly through a common mechanism: theta-range power increases as a means for enhanced synchronization and entrainment of the HPC-PFC-AMY circuit.

OSCILLATIONS IN THE HPC-PFC-AMY CIRCUIT RELATED TO STRESS-INDUCED PSYCHIATRIC DISORDERS

The findings of theta-range oscillations in the HPC-PFC-AMY circuit from non-pathological animals related to fear and anxiety-like behavior suggest that stress susceptibility and stress-induced dysregulation of emotion may be due to altered interplay based on these oscillatory communications. In rodents, behavioral and physiological changes reminiscent of depressive symptoms are induced by repeated exposures to chronic social defeat stress in which a mouse is defeated by a larger animal; this procedure has been utilized as an excellent murine model with etiological, predictive, discriminative and face validity (Berton et al., 2006; Golden et al., 2011; Abe et al., 2019). Socially defeated mice with impaired extinction learning, possibly replicating a PTSD symptom, showed increased theta (4–8 Hz) synchronization between the PFC and AMY (Narayanan et al., 2011). In addition, defeated mice with depressive-like behavior showed increased power of a PFC 2–7-Hz oscillation during interactions with an aggressor mouse (Kumar et al., 2014), which entrained beta (14–23 Hz) coherence between the AMY and ventral tegmental area (VTA) (Hultman et al., 2016). These stress-sensitive changes in oscillatory patterns possibly represented an increase in the 4-Hz or theta oscillations based on their frequency bands and common properties. Consistently, increased theta (4–12 Hz) power in the vHPC-mPFC-BLA circuit has also been reported in a chronic unpredictable stress model (Jacinto et al., 2013; Oliveira et al., 2013). Taken together, these findings suggest that stressed animals appear to exacerbate aversive emotion-related oscillations in the HPC-PFC-AMY circuit that originally operated in non-pathological conditions.

Notably, the power of this 2–7-Hz PFC oscillation differs across individual animals even before stress exposure, and these differences can predict the manifestation of subsequent stress-induced depression-like behavior (Kumar et al., 2014). This finding suggested that LFP signals can serve as a predictive factor of vulnerability to mental stress in individual animals. Recently, this idea of predictive stress vulnerability has been expanded to multiple brain regions, including the nucleus accumbens (NAc) and VTA, in addition to the HPC-PFC-AMY circuit. An elegant study with a machine learning algorithm by Hultman et al. (2018) identified several patterns of prestress LFP power and coherence in frequency bands ranging from 1 to 50 Hz across these brain regions and termed these patterns electome factors. These factors differentiate early life-associated stress vulnerability and stress susceptibility that can be reversed by antidepressants. Our group applied a similar strategy to LFP signals recorded from multiple cortical areas and demonstrated that rats with lower theta power and higher delta power correlations across the cortical regions before stress exposure were more likely to exhibit irregular heartbeat signals after stress load (Nakayama et al., 2019). In the future, these new types of studies with multivariate statistics and machine learning algorithms on large-scale physiological datasets are expected to reveal how the core region, i.e., the HPC-PFC-AMY circuit, and neuromodulatory regions, such as the NAc and VTA, functionally interact with each other. These new approaches are expected to provide a more comprehensive entire picture of functional organizations of brain networks that have not been defined by existing statistics with limited dimensions.

TIME-TARGETED INTERVENTIONS TOWARD OSCILLOTHERAPEUTICS FOR PSYCHIATRIC DISORDERS

While LFP oscillatory signals in the HPC-PFC-AMY circuit related to stress-induced symptoms are beginning to be revealed (**Figure 2A**), they remain correlative and leave open questions as to whether they are causal factors for the pathogenesis of mental disorders. Addressing these issues will help identify true therapeutic targets of endogenous oscillatory signals in the development of oscillotherapeutics. Ideal research strategies are to selectively manipulate target ongoing oscillatory signals using open-loop or closed-loop systems and test their phenotypic effects. In open-loop interventions, external stimulation with

sinusoidal waveforms, mimicking oscillatory signals, or pulse trains is applied without feedback from biological oscillatory signals (**Figure 2B**, left). In closed-loop interventions, stimulation is applied with the appearance of target brain signals, enabling on-demand stimulation with reference to brain states while avoiding out-of-target overstimulation (**Figure 2B**, right). Target signal variables to be detected are transient neuronal events with certain amplitudes, such as ictal seizure events, or the phase and amplitude of specific continuous oscillations, such as theta oscillations. Signals to be manipulated are the signals detected at the recording sites or signals generated at distant areas, such as upstream or downstream brain regions, depending on the locations of stimulation (**Figure 2C**). This chapter summarizes recent studies employing these experimental challenges in rodents and discusses the possibility of further clinical applications. Other therapeutic strategies using pharmacological, behavioral, and psychological methods to alter brain oscillations (e.g., Leuchter et al., 2015) are beyond the scope of this paper.

Animal Models

Transient neuronal events within a short time window (hundreds of milliseconds) are widely utilized target signals for closed-loop systems. For instance, transcranial and intracranial closed-loop stimulation at the time of detection of large amplitude and high-frequency cortical seizure events have been shown to suppress subsequent seizures in epilepsy animal models (Berenyi et al., 2012; Takeuchi et al., 2021). This technique has also been applied to LFP oscillations under non-pathological conditions to test their causal roles in memory processing. For example, closed-loop amplification and disruption of hippocampal ripples (150–250 Hz), which represent transient neuronal synchronization within a short time window (∼100 ms), can improve (Fernandez-Ruiz et al., 2019) and inhibit (Jadhav et al., 2012; Oliva et al., 2020; Igata et al., 2021), respectively, subsequent memory processing. While targeting this type of transient signal is an excellent means to manipulate large short neuronal events, it appears inappropriate for modulating emotional states, as brain signals underlying emotion and stress-induced disease are much longer and oscillate in lower frequency bands, as described above.

Given the importance of theta-range (4–12 Hz) oscillations in the HPC-PFC-AMY circuit in emotional behavior and stress-induced psychiatric disorders, manipulation of neuronal activity that impact these theta-range oscillations might be effective in ameliorating psychiatric symptoms. Using open-loop systems, theta-range oscillations can be exogenously induced by injecting sinusoidal stimulation at the corresponding frequencies. In particular, optogenetic photostimulation is appropriate for creating sinusoidal stimulus patterns with particular rise and decay amplitudes to manipulate specific types of neurons. Padilla-Coreano et al. (2019) demonstrated that selective activation of mPFC-projecting neurons in the vHPC by optogenetic photostimulation with a theta (8-Hz) sinusoidal pattern evoked open arm avoidance in an EPM, suggesting increased anxiety. Interestingly, this effect was not observed when an 8-Hz pulsatile stimulation pattern was applied, suggesting the importance of oscillatory neuronal activity. Karalis et al. (2016) demonstrated that modulation of mPFC parvalbumin-expressing (PV) interneurons by 4-Hz, but not 8-Hz, sinusoidal photostimulation induced synchronized mPFC and BLA spikes and contextual fear behavior, suggesting a causal role of 4-Hz oscillations in the expression of aversive memories. Furthermore, using a similar strategy, Ozawa et al. (2020) showed that rhythmic stimulation of BLA PV interneurons with a sinusoidal waveform of light at 4 Hz or 8 Hz augmented or suppressed freezing behavior, respectively, specifically after a postextinction learning trial, demonstrating the bidirectional modulation of extinction memories by BLA PV interneurons depending on different oscillatory frequencies. In addition, they suggested that extinction learning with suppression of conditioned fear cell ensembles in the BLA-mPFC circuit was mediated by BLA PV interneurons via enhancement of a BLA 8-Hz (6–12 Hz) oscillation that interfered with a BLA-mPFC 4-Hz (3–6 Hz) oscillation for fear expression (Davis et al., 2017). Further causal relationships can be tested by a closed-loop system with higher temporal resolution in which stimulation is applied at a specific phase of each cycle of oscillations. Dejean et al. (2016) demonstrated that phase-targeting optogenetic activation of mPFC PV interneurons in the ascending or descending phases of mPFC 4-Hz oscillations decreases and increases conditioned freezing behavior, respectively, suggesting the importance of phase-specific mPFC cell ensemble activity for bidirectional control of fear behavior. Using similar experimental strategies, increased anxiety and impaired fear extinction by chronic stress might be restored by adjusting the intensity of theta-range oscillations and phase-specific modulation of neuronal activity on theta-range oscillations in the HPC-PFC-AMY circuit. Similar ideas that target theta-range oscillations have been recently applied to other animal models of Parkinson's disease and Alzheimer's disease (Cordon et al., 2018; Senova et al., 2018).

For more complex challenges regarding the understanding of functional connectivity and interregional information transfer underlying emotional behavior, manipulations of multiple brain regions at the same or different phases in oscillations may be more useful (**Figure 2C**), as demonstrated by Ozawa et al. (2020). Finally, animals' behavioral states (e.g., sleep states and attentional levels) are also crucial factors in interventions of neuronal activity. For example, Boyce et al. (2016) demonstrated that a reduction in HPC theta oscillations specifically during REM sleep eliminated conditioned fear memories, suggesting that applying interventions in the proper behavioral states may be important to maximize their outputs and avoid side effects.

Application to Clinical Studies

While it is not possible to simply extrapolate clinical applications based on insights from basic animal studies, interventions targeting brain oscillations may also be an effective therapeutic strategy in clinical studies if properly applied. Deep brain stimulation (DBS) is an invasive treatment approach for treatment-resistant depressions applied by electrodes implanted in brain tissue (Mayberg et al., 2005; Scangos et al., 2021). On the other hand, transcranial electric stimulation is a non-invasive

approach that is roughly divided into two types depending on stimulus patterns: transcranial direct current stimulation (tDCS) with non-oscillating static currents and transcranial alternating current stimulation (tACS) with oscillating currents. For more focal and intense stimulation, repetitive transcranial magnetic stimulation (rTMS) applies magnetic pulses to induce current flow in the brain. Accumulating clinical evidence suggests that restorations of brain oscillations by these interventions ameliorate pathological symptoms in depressive patients. For instance, rTMS on the frontal cortex increased gamma oscillations in patients showing improved depressive symptoms (Noda et al., 2017), consistent with a pharmacological effect of ketamine on gamma oscillations (Hong et al., 2010). Vagus nerve stimulation (VNS) is another intervention approach for treatment-resistant depression (Moeller et al., 2019). This method directly activates subcortical arousal-promoting nuclei through stimulation of the vagus nerve. Recently, a non-invasive transcutaneous auricular vagus nerve stimulation (taVNS) method has been developed (Hein et al., 2013; Rong et al., 2016; Trevizol et al., 2016), which can alter alpha EEG oscillations (Sharon et al., 2021).

Compared with simple pulsatile stimulation such as tDCS, resonance approaches using oscillatory stimulus patterns such as tACS may be more effective in entraining brain oscillations at the corresponding or other specific frequency bands [for more detail, see Hanslmayr et al. (2019)]. For instance, in healthy human subjects, intense tACS with a 1-Hz sinusoidal wave has been shown to induce alpha-band parietal cortical activity (Voroslakos et al., 2018). In older adults, tACS over the frontotemporal regions improves memory performance and cognitive functions (Reinhart and Nguyen, 2019). More specifically, a closed-loop system using DBS may be a promising strategy, in which brief stimulation is delivered in response to ongoing changes in the brain states of patients (Scangos and Ross, 2018). In addition, biofeedback methods in which individuals are provided with real-time information on brain activity have been proposed as another means to modify EEG signals and improve psychiatric states. For instance, restoring frontal alpha symmetry by biofeedback signals has been shown to reduce negative affect in human subjects that learned conscious control of their own alpha asymmetry signals (Mennella et al., 2017).

CONCLUSION AND FUTURE PERSPECTIVE

Recent advancements in electrophysiological recording techniques, optogenetic tools, and analytical methods such as machine learning algorithms unveiled emotion-related and stress-induced oscillations for complex coordination of multiple brain regions. This review specifically focused on theta-range oscillations, as a key oscillation, in the HPC-PFC-AMY circuit in rodents. Precisely timed interventions based on these oscillations by open-loop and closed-loop systems enable us to test a causal role of these target oscillatory signals in the expression of psychiatric symptoms. In the future, in addition to observing changes in behavioral phenotypes, it will be interesting to see how emotional memory-encoding and oscillatory phase-locked neuronal ensembles are recruited at single-neuron levels in response to these interventions. While the same experimental strategies may not be directly extrapolated to clinical studies, the ideas of interventions are adopted as effective therapeutic strategies for stress-induced mental illness. In both animal and clinical studies, a crucial issue is that there are a large number of combinations of technical parameters (e.g., stimulation regions, type, intensity, timing, and frequency band) for interventions. In addition, as the level of impairments in these brain signals and pathological symptoms considerably vary across individuals, interventions need to be ideally personalized based on their conditions, as previously demonstrated (Reinhart and Nguyen, 2019; Grover et al., 2021). Further oscillotherapeutic studies from both basic and clinical experiments are expected to identify more appropriate intervention strategies based on a precise understanding of cellular and circuit dynamics.

AUTHOR CONTRIBUTIONS

TO and TS prepared all the figures and wrote the main manuscript text. Both authors contributed to the article and approved the submitted version.

FUNDING

This work was supported by KAKENHI (19H04897 and 20H03545) from the Japan Society for the Promotion of Science (JSPS), a Precursory Research for Embryonic Science and Technology grant (JPMJPR1785) from the Japan Science and Technology Agency (JST), and a grant from the Advanced Research and Development Programs for Medical Innovation (1041630) of the Japan Agency for Medical Research and Development (AMED) to TS; and a JSPS Research Fellowship for Young Scientists to TO.

REFERENCES

Abe, R., Okada, S., Nakayama, R., Ikegaya, Y., and Sasaki, T. (2019). Social defeat stress causes selective attenuation of neuronal activity in the ventromedial prefrontal cortex. *Sci. Rep.* 9:9447. doi: 10.1038/s41598-019-45833-5

Adhikari, A., Topiwala, M. A., and Gordon, J. A. (2010). Synchronized activity between the ventral hippocampus and the medial prefrontal cortex during anxiety. *Neuron* 65, 257–269. doi: 10.1016/j.neuron.2009.12.002

Adhikari, A., Topiwala, M. A., and Gordon, J. A. (2011). Single units in the medial prefrontal cortex with anxiety-related firing patterns are preferentially influenced by ventral hippocampal activity. *Neuron* 71, 898–910.

Arnsten, A. F. (2015). Stress weakens prefrontal networks: molecular insults to higher cognition. *Nat. Neurosci.* 18, 1376–1385. doi: 10.1038/nn.4087

Baskaran, A., Milev, R., and McIntyre, R. S. (2012). The neurobiology of the EEG biomarker as a predictor of treatment response in depression. *Neuropharmacology* 63, 507–513. doi: 10.1016/j.neuropharm.2012.04.021

Berenyi, A., Belluscio, M., Mao, D., and Buzsaki, G. (2012). Closed-loop control of epilepsy by transcranial electrical stimulation. *Science* 337, 735–737. doi: 10.1126/science.1223154

Berton, O., McClung, C. A., Dileone, R. J., Krishnan, V., Renthal, W., Russo, S. J., et al. (2006). Essential role of BDNF in the mesolimbic dopamine pathway in social defeat stress. *Science* 311, 864–868. doi: 10.1126/science.1120972

Boyce, R., Glasgow, S. D., Williams, S., and Adamantidis, A. (2016). Causal evidence for the role of REM sleep theta rhythm in contextual memory consolidation. *Science* 352, 812–816. doi: 10.1126/science.aad5252

Burgos-Robles, A., Kimchi, E. Y., Izadmehr, E. M., Porzenheim, M. J., Ramos-Guasp, W. A., Nieh, E. H., et al. (2017). Amygdala inputs to prefrontal cortex guide behavior amid conflicting cues of reward and punishment. *Nat. Neurosci.* 20, 824–835. doi: 10.1038/nn.4553

Buzsaki, G. (2002). Theta oscillations in the hippocampus. *Neuron* 33, 325–340.

Buzsaki, G., Anastassiou, C. A., and Koch, C. (2012). The origin of extracellular fields and currents–EEG, ECoG, LFP and spikes. *Nat. Rev. Neurosci.* 13, 407–420. doi: 10.1038/nrn3241

Buzsaki, G., and Draguhn, A. (2004). Neuronal oscillations in cortical networks. *Science* 304, 1926–1929. doi: 10.1126/science.1099745

Buzsaki, G., and Watson, B. O. (2012). Brain rhythms and neural syntax: implications for efficient coding of cognitive content and neuropsychiatric disease. *Dialog, Clin. Neurosci.* 14, ,345–367.

Caliskan, G., and Stork, O. (2019). Hippocampal network oscillations at the interplay between innate anxiety and learned fear. *Psychopharmacology (Berl)* 236, 321–338. doi: 10.1007/s00213-018-5109-z

Ciocchi, S., Passecker, J., Malagon-Vina, H., Mikus, N., and Klausberger, T. (2015). Brain computation. Selective information routing by ventral hippocampal CA1 projection neurons. *Science* 348, 560–563. doi: 10.1126/science.aaa3245

Clancy, K., Ding, M., Bernat, E., Schmidt, N. B., and Li, W. (2017). Restless 'rest': intrinsic sensory hyperactivity and disinhibition in post-traumatic stress disorder. *Brain* 140, 2041–2050. doi: 10.1093/brain/awx116

Cordon, I., Nicolas, M. J., Arrieta, S., Alegre, M., Artieda, J., and Valencia, M. (2018). Theta-phase closed-loop stimulation induces motor paradoxical responses in the rat model of Parkinson disease. *Brain Stimul.* 11, 231–238. doi: 10.1016/j.brs.2017.10.004

Davis, P., Zaki, Y., Maguire, J., and Reijmers, L. G. (2017). Cellular and oscillatory substrates of fear extinction learning. *Nat. Neurosci.* 20, 1624–1633. doi: 10.1038/nn.4651

Dejean, C., Courtin, J., Karalis, N., Chaudun, F., Wurtz, H., Bienvenu, T. C., et al. (2016). Prefrontal neuronal assemblies temporally control fear behaviour. *Nature* 535, 420–424. doi: 10.1038/nature18630

Drysdale, A. T., Grosenick, L., Downar, J., Dunlop, K., Mansouri, F., Meng, Y., et al. (2017). Resting-state connectivity biomarkers define neurophysiological subtypes of depression. *Nat. Med.* 23, 28–38. doi: 10.1038/nm.4246

Fernandez-Ruiz, A., Oliva, A., Fermino de Oliveira, E., Rocha-Almeida, F., Tingley, D., and Buzsaki, G. (2019). Long-duration hippocampal sharp wave ripples improve memory. *Science* 364, 1082–1086. doi: 10.1126/science.aax0758

Fitzgerald, P. J., and Watson, B. O. (2018). Gamma oscillations as a biomarker for major depression: an emerging topic. *Transl. Psychiatry* 8:177. doi: 10.1038/s41398-018-0239-y

Golden, S. A., Covington, H. E. III, Berton, O., and Russo, S. J. (2011). A standardized protocol for repeated social defeat stress in mice. *Nat. Protoc.* 6, 1183–1191. doi: 10.1038/nprot.2011.361

Gordon, J. A., Lacefield, C. O., Kentros, C. G., and Hen, R. (2005). State-dependent alterations in hippocampal oscillations in serotonin 1A receptor-deficient mice. *J. Neurosci.* 25, 6509–6519. doi: 10.1523/JNEUROSCI.1211-05.2005

Greicius, M. D., Flores, B. H., Menon, V., Glover, G. H., Solvason, H. B., Kenna, H., et al. (2007). Resting-state functional connectivity in major depression: abnormally increased contributions from subgenual cingulate cortex and thalamus. *Biol. Psychiatry* 62, 429–437. doi: 10.1016/j.biopsych.2006.09.020

Grover, S., Nguyen, J. A., Viswanathan, V., and Reinhart, R. M. G. (2021). High-frequency neuromodulation improves obsessive-compulsive behavior. *Nat. Med.* 27, 232–238. doi: 10.1038/s41591-020-01173-w

Grunewald, B. D., Greimel, E., Trinkl, M., Bartling, J., Grossheinrich, N., and Schulte-Korne, G. (2018). Resting frontal EEG asymmetry patterns in adolescents with and without major depression. *Biol. Psychol.* 132, 212–216. doi: 10.1016/j.biopsycho.2018.01.003

Hanslmayr, S., Axmacher, N., and Inman, C. S. (2019). Modulating human memory via entrainment of brain oscillations. *Trends Neurosci.* 42, 485–499. doi: 10.1016/j.tins.2019.04.004

Hein, E., Nowak, M., Kiess, O., Biermann, T., Bayerlein, K., Kornhuber, J., et al. (2013). Auricular transcutaneous electrical nerve stimulation in depressed patients: a randomized controlled pilot study. *J. Neural. Transm. (Vienna.)* 120, 821–827. doi: 10.1007/s00702-012-0908-6

Hong, L. E., Summerfelt, A., Buchanan, R. W., O'Donnell, P., Thaker, G. K., Weiler, M. A., et al. (2010). Gamma and delta neural oscillations and association with clinical symptoms under subanesthetic ketamine. *Neuropsychopharmacology* 35, 632–640. doi: 10.1038/npp.2009.168

Huang, M. X., Yurgil, K. A., Robb, A., Angeles, A., Diwakar, M., Risbrough, V. B., et al. (2014). Voxel-wise resting-state MEG source magnitude imaging study reveals neurocircuitry abnormality in active-duty service members and veterans with PTSD. *Neuroimage Clin.* 5, 408–419. doi: 10.1016/j.nicl.2014.08.004

Hultman, R., Mague, S. D., Li, Q., Katz, B. M., Michel, N., Lin, L., et al. (2016). Dysregulation of prefrontal cortex-mediated slow-evolving limbic dynamics drives stress-induced emotional pathology. *Neuron* 91, 439–452. doi: 10.1016/j.neuron.2016.05.038

Hultman, R., Ulrich, K., Sachs, B. D., Blount, C., Carlson, D. E., Ndubuizu, N., et al. (2018). Brain-wide electrical spatiotemporal dynamics encode depression vulnerability. *Cell* 173, 166–180.e114. doi: 10.1016/j.cell.2018.02.012

Igata, H., Ikegaya, Y., and Sasaki, T. (2021). Prioritized experience replays on a hippocampal predictive map for learning. *Proc. Natl. Acad. Sci. U.S.A.* 118:e2011266118. doi: 10.1073/pnas.2011266118

Iosifescu, D. V. (2011). Electroencephalography-derived biomarkers of antidepressant response. *Harv. Rev. Psychiatry* 19, 144–154. doi: 10.3109/10673229.2011.586549

Ishikawa, A., and Nakamura, S. (2003). Convergence and interaction of hippocampal and amygdalar projections within the prefrontal cortex in the rat. *J. Neurosci.* 23, 9987–9995.

Iturra-Mena, A. M., Aguilar-Rivera, M., Arriagada-Solimano, M., Perez-Valenzuela, C., Fuentealba, P., and Dagnino-Subiabre, A. (2019). Impact of stress on Gamma oscillations in the rat nucleus accumbens during spontaneous social interaction. *Front. Behav. Neurosci.* 13:151. doi: 10.3389/fnbeh.2019.00151

Jacinto, L. R., Reis, J. S., Dias, N. S., Cerqueira, J. J., Correia, J. H., and Sousa, N. (2013). Stress affects theta activity in limbic networks and impairs novelty-induced exploration and familiarization. *Front. Behav. Neurosci.* 7:127. doi: 10.3389/fnbeh.2013.00127

Jadhav, S. P., Kemere, C., German, P. W., and Frank, L. M. (2012). Awake hippocampal sharp-wave ripples support spatial memory. *Science* 336, 1454–1458. doi: 10.1126/science.1217230

Jesulola, E., Sharpley, C. F., Bitsika, V., Agnew, L. L., and Wilson, P. (2015). Frontal alpha asymmetry as a pathway to behavioural withdrawal in depression: research findings and issues. *Behav. Brain Res.* 292, 56–67. doi: 10.1016/j.bbr.2015.05.058

Karalis, N., Dejean, C., Chaudun, F., Khoder, S., Rozeske, R. R., Wurtz, H., et al. (2016). 4-Hz oscillations synchronize prefrontal-amygdala circuits during fear behavior. *Nat. Neurosci.* 19, 605–612. doi: 10.1038/nn.4251

Kim, J., Pignatelli, M., Xu, S., Itohara, S., and Tonegawa, S. (2016). Antagonistic negative and positive neurons of the basolateral amygdala. *Nat. Neurosci.* 19, 1636–1646. doi: 10.1038/nn.4414

Konno, D., Nakayama, R., Tsunoda, M., Funatsu, T., Ikegaya, Y., and Sasaki, T. (2019). Collection of biochemical samples with brain-wide electrophysiological recordings from a freely moving rodent. *J. Pharmacol. Sci.* 139, 346–351. doi: 10.1016/j.jphs.2019.02.006

Krishnan, V., and Nestler, E. J. (2008). The molecular neurobiology of depression. *Nature* 455, 894–902. doi: 10.1038/nature07455

Kuga, N., Nakayama, R., Shikano, Y., Nishimura, Y., Okonogi, T., Ikegaya, Y., et al. (2019). Sniffing behaviour-related changes in cardiac and cortical activity in rats. *J. Physiol.* 597, 5295–5306. doi: 10.1113/JP278500

Kumar, S., Hultman, R., Hughes, D., Michel, N., Katz, B. M., and Dzirasa, K. (2014). Prefrontal cortex reactivity underlies trait vulnerability to chronic social defeat stress. *Nat. Commun.* 5:4537. doi: 10.1038/ncomms5537

Lesting, J., Narayanan, R. T., Kluge, C., Sangha, S., Seidenbecher, T., and Pape, H. C. (2011). Patterns of coupled theta activity in amygdala-hippocampal-prefrontal

cortical circuits during fear extinction. *PLoS One* 6:e21714. doi: 10.1371/journal.pone.0021714

Leuchter, A. F., Hunter, A. M., Krantz, D. E., and Cook, I. A. (2015). Rhythms and blues: modulation of oscillatory synchrony and the mechanism of action of antidepressant treatments. *Ann. N.Y. Acad. Sci.* 1344, 78–91. doi: 10.1111/nyas.12742

Likhtik, E., Stujenske, J. M., Topiwala, M. A., Harris, A. Z., and Gordon, J. A. (2014). Prefrontal entrainment of amygdala activity signals safety in learned fear and innate anxiety. *Nat. Neurosci.* 17, 106–113. doi: 10.1038/nn.3582

Martinez, D., Clement, M., Messaoudi, B., Gervasoni, D., Litaudon, P., and Buonviso, N. (2018). Adaptive quantization of local field potentials for wireless implants in freely moving animals: an open-source neural recording device. *J. Neural. Eng.* 15:025001. doi: 10.1088/1741-2552/aaa041

Mayberg, H. S., Lozano, A. M., Voon, V., McNeely, H. E., Seminowicz, D., Hamani, C., et al. (2005). Deep brain stimulation for treatment-resistant depression. *Neuron* 45, 651–660. doi: 10.1016/j.neuron.2005.02.014

McEwen, B. S., Bowles, N. P., Gray, J. D., Hill, M. N., Hunter, R. G., Karatsoreos, I. N., et al. (2015). Mechanisms of stress in the brain. *Nat. Neurosci.* 18, 1353–1363. doi: 10.1038/nn.4086

Mennella, R., Patron, E., and Palomba, D. (2017). Frontal alpha asymmetry neurofeedback for the reduction of negative affect and anxiety. *Behav. Res. Ther.* 92, 32–40. doi: 10.1016/j.brat.2017.02.002

Mikulovic, S., Restrepo, C. E., Siwani, S., Bauer, P., Pupe, S., Tort, A. B. L., et al. (2018). Ventral hippocampal OLM cells control type 2 theta oscillations and response to predator odor. *Nat. Commun.* 9, 3638. doi: 10.1038/s41467-018-05907-w

Moeller, S., Lucke, C., Heinen, C., Bewernick, B. H., Aydin, M., Lam, A. P., et al. (2019). Vagus nerve stimulation as an adjunctive neurostimulation tool in treatment-resistant depression. *J. Vis. Exp.* 143:e58264. doi: 10.3791/58264

Nakayama, R., Ikegaya, Y., and Sasaki, T. (2019). Cortical-wide functional correlations are associated with stress-induced cardiac dysfunctions in individual rats. *Sci. Rep.* 9:10581. doi: 10.1038/s41598-019-47171-y

Narayanan, V., Heiming, R. S., Jansen, F., Lesting, J., Sachser, N., Pape, H. C., et al. (2011). Social defeat: impact on fear extinction and amygdala-prefrontal cortical theta synchrony in 5-HTT deficient mice. *PLoS One* 6:e22600. doi: 10.1371/journal.pone.0022600

Noda, Y., Zomorrodi, R., Saeki, T., Rajji, T. K., Blumberger, D. M., Daskalakis, Z. J., et al. (2017). Resting-state EEG gamma power and theta-gamma coupling enhancement following high-frequency left dorsolateral prefrontal rTMS in patients with depression. *Clin. Neurophysiol.* 128, 424–432. doi: 10.1016/j.clinph.2016.12.023

Nugent, A. C., Robinson, S. E., Coppola, R., Furey, M. L., and Zarate, C. A. Jr. (2015). Group differences in MEG-ICA derived resting state networks: application to major depressive disorder. *Neuroimage* 118, 1–12. doi: 10.1016/j.neuroimage.2015.05.051

Ognjanovski, N., Maruyama, D., Lashner, N., Zochowski, M., and Aton, S. J. (2014). CA1 hippocampal network activity changes during sleep-dependent memory consolidation. *Front. Syst. Neurosci.* 8:61. doi: 10.3389/fnsys.2014.00061

Okada, S., Igata, H., Sakaguchi, T., Sasaki, T., and Ikegaya, Y. (2016). A new device for the simultaneous recording of cerebral, cardiac, and muscular electrical activity in freely moving rodents. *J. Pharmacol. Sci.* 132, 105–108. doi: 10.1016/j.jphs.2016.06.001

Okonogi, T., Nakayama, R., Sasaki, T., and Ikegaya, Y. (2018). Characterization of peripheral activity states and cortical local field potentials of mice in an elevated plus maze test. *Front. Behav. Neurosci.* 12:62. doi: 10.3389/fnbeh.2018.00062

Oliva, A., Fernandez-Ruiz, A., Leroy, F., and Siegelbaum, S. A. (2020). Hippocampal CA2 sharp-wave ripples reactivate and promote social memory. *Nature* 587, 264–269. doi: 10.1038/s41586-020-2758-y

Oliveira, J. F., Dias, N. S., Correia, M., Gama-Pereira, F., Sardinha, V. M., Lima, A., et al. (2013). Chronic stress disrupts neural coherence between cortico-limbic structures. *Front. Neural Circ.* 7:10. doi: 10.3389/fncir.2013.00010

Orsini, C. A., Kim, J. H., Knapska, E., and Maren, S. (2011). Hippocampal and prefrontal projections to the basal amygdala mediate contextual regulation of fear after extinction. *J. Neurosci.* 31, 17269–17277. doi: 10.1523/JNEUROSCI.4095-11.2011

Ozawa, M., Davis, P., Ni, J., Maguire, J., Papouin, T., and Reijmers, L. (2020). Experience-dependent resonance in amygdalo-cortical circuits supports fear memory retrieval following extinction. *Nat. Commun.* 11:4358. doi: 10.1038/s41467-020-18199-w

Padilla-Coreano, N., Canetta, S., Mikofsky, R. M., Alway, E., Passecker, J., Myroshnychenko, M. V., et al. (2019). Hippocampal-prefrontal theta transmission regulates avoidance behavior. *Neuron* 104, 601–610.e604. doi: 10.1016/j.neuron.2019.08.006

Popa, D., Duvarci, S., Popescu, A. T., Lena, C., and Pare, D. (2010). Coherent amygdalocortical theta promotes fear memory consolidation during paradoxical sleep. *Proc. Natl. Acad. Sci. U.S.A.* 107, 6516–6519. doi: 10.1073/pnas.0913016107

Reinhart, R. M. G., and Nguyen, J. A. (2019). Working memory revived in older adults by synchronizing rhythmic brain circuits. *Nat. Neurosci.* 22, 820–827. doi: 10.1038/s41593-019-0371-x

Rong, P., Liu, J., Wang, L., Liu, R., Fang, J., Zhao, J., et al. (2016). Effect of transcutaneous auricular vagus nerve stimulation on major depressive disorder: a nonrandomized controlled pilot study. *J. Affect. Disord.* 195, 172–179. doi: 10.1016/j.jad.2016.02.031

Scangos, K. W., Makhoul, G. S., Sugrue, L. P., Chang, E. F., and Krystal, A. D. (2021). State-dependent responses to intracranial brain stimulation in a patient with depression. *Nat. Med.* 27, 229–231. doi: 10.1038/s41591-020-01175-8

Scangos, K. W., and Ross, D. A. (2018). What We've got here is failure to communicate: improving interventional psychiatry with closed-loop stimulation. *Biol. Psychiatry* 84, e55–e57. doi: 10.1016/j.biopsych.2018.08.005

Seidenbecher, T., Laxmi, T. R., Stork, O., and Pape, H. C. (2003). Amygdalar and hippocampal theta rhythm synchronization during fear memory retrieval. *Science* 301, 846–850. doi: 10.1126/science.1085818

Senn, V., Wolff, S. B., Herry, C., Grenier, F., Ehrlich, I., Grundemann, J., et al. (2014). Long-range connectivity defines behavioral specificity of amygdala neurons. *Neuron* 81, 428–437. doi: 10.1016/j.neuron.2013.11.006

Senova, S., Chaillet, A., and Lozano, A. M. (2018). Fornical closed-loop stimulation for alzheimer's disease. *Trends Neurosci.* 41, 418–428. doi: 10.1016/j.tins.2018.03.015

Sharon, O., Fahoum, F., and Nir, Y. (2021). Transcutaneous vagus nerve stimulation in humans induces pupil dilation and attenuates alpha oscillations. *J. Neurosci.* 41, 320–330. doi: 10.1523/JNEUROSCI.1361-20.2020

Sheline, Y. I., Price, J. L., Yan, Z., and Mintun, M. A. (2010). Resting-state functional MRI in depression unmasks increased connectivity between networks via the dorsal nexus. *Proc. Natl. Acad. Sci. U.S.A.* 107, 11020–11025. doi: 10.1073/pnas.1000446107

Shikano, Y., Ikegaya, Y., and Sasaki, T. (2018). Monitoring brain neuronal activity with manipulation of cardiac events in a freely moving rat. *Neurosci. Res.* 136, 56–62. doi: 10.1016/j.neures.2018.02.004

Shikano, Y., Nishimura, Y., Okonogi, T., Ikegaya, Y., and Sasaki, T. (2019). Vagus nerve spiking activity associated with locomotion and cortical arousal states in a freely moving rat. *Eur. J. Neurosci.* 49, 1298–1312. doi: 10.1111/ejn.14275

Siegle, J. H., and Wilson, M. A. (2014). Enhancement of encoding and retrieval functions through theta phase-specific manipulation of hippocampus. *eLife* 3:e03061. doi: 10.7554/eLife.03061

Stujenske, J. M., Likhtik, E., Topiwala, M. A., and Gordon, J. A. (2014). Fear and safety engage competing patterns of theta-gamma coupling in the basolateral amygdala. *Neuron* 83, 919–933. doi: 10.1016/j.neuron.2014.07.026

Takeuchi, Y., and Berenyi, A. (2020). Oscillotherapeutics – Time-targeted interventions in epilepsy and beyond. *Neurosci. Res.* 152, 87–107. doi: 10.1016/j.neures.2020.01.002

Takeuchi, Y., Harangozo, M., Pedraza, L., Foldi, T., Kozak, G., Li, Q., et al. (2021). Closed-loop stimulation of the medial septum terminates epileptic seizures. *Brain* 144, 885–908. doi: 10.1093/brain/awaa450

Totty, M. S., Chesney, L. A., Geist, P. A., and Datta, S. (2017). Sleep-dependent oscillatory synchronization: a role in fear memory consolidation. *Front. Neural. Circ.* 11:49. doi: 10.3389/fncir.2017.00049

Tovote, P., Fadok, J. P., and Luthi, A. (2015). Neuronal circuits for fear and anxiety. *Nat. Rev. Neurosci.* 16, 317–331. doi: 10.1038/nrn3945

Trevizol, A. P., Shiozawa, P., Taiar, I., Soares, A., Gomes, J. S., Barros, M. D., et al. (2016). Transcutaneous vagus nerve stimulation (taVNS) for major depressive disorder: an open label proof-of-concept trial. *Brain Stimul.* 9, 453–454. doi: 10.1016/j.brs.2016.02.001

Voroslakos, M., Takeuchi, Y., Brinyiczki, K., Zombori, T., Oliva, A., Fernandez-Ruiz, A., et al. (2018). Direct effects of transcranial electric stimulation on brain

circuits in rats and humans. *Nat. Commun.* 9, 483. doi: 10.1038/s41467-018-02928-3

Yehuda, R., and LeDoux, J. (2007). Response variation following trauma: a translational neuroscience approach to understanding PTSD. *Neuron* 56, 19–32. doi: 10.1016/j.neuron.2007.09.006

Zhu, X. O., and McNaughton, N. (1995). Minimal changes with long-term administration of anxiolytics on septal driving of hippocampal rhythmical slow activity. *Psychopharmacology (Berl)* 118, 93–100. doi: 10.1007/BF02245254

Zuo, C., Yang, X., Wang, Y., Hagains, C. E., Li, A. L., Peng, Y. B., et al. (2012). A digital wireless system for closed-loop inhibition of nociceptive signals. *J. Neural. Eng.* 9:056010. doi: 10.1088/1741-2560/9/5/056010

Conflict of Interest: The authors declare that the research was conducted in the absence of any commercial or financial relationships that could be construed as a potential conflict of interest.

frontiers in Behavioral Neuroscience

ORIGINAL RESEARCH
published: 10 June 2021
doi: 10.3389/fnbeh.2021.680206

Task-Related c-Fos Expression in the Posterior Parietal Cortex During the "Rubber Tail Task" Is Diminished in Ca^{2+}-Dependent Activator Protein for Secretion 2 (*Caps2*)-Knockout Mice

Makoto Wada[1], Kouji Takano[2], Masakazu Ide[1], Yoshitake Sano[3], Yo Shinoda[3,4], Teiichi Furuichi[3] and Kenji Kansaku[2,5,6]*

[1] Developmental Disorders Section, Department of Rehabilitation for Brain Functions, Research Institute of National Rehabilitation Center for Persons with Disabilities, Tokorozawa, Japan, [2] Systems Neuroscience Section, Department of Rehabilitation for Brain Functions, Research Institute of National Rehabilitation Center for Persons with Disabilities, Tokorozawa, Japan, [3] Department of Applied Biological Science, Tokyo University of Science, Noda, Japan, [4] Department of Environmental Health, School of Pharmacy, Tokyo University of Pharmacy and Life Sciences, Hachioji, Japan, [5] Department of Physiology, School of Medicine, Dokkyo Medical University, Mibu, Japan, [6] Center for Neuroscience and Biomedical Engineering, The University of Electro-Communications, Chofu, Japan

OPEN ACCESS

Edited by:
Yuichi Takeuchi, Osaka City University, Japan

Reviewed by:
H. Henrik Ehrsson, Karolinska Institutet (KI), Sweden
Jakub Limanowski, Technische Universität Dresden, Germany

***Correspondence:**
Makoto Wada
wada-makoto@rehab.go.jp

Specialty section:
This article was submitted to Pathological Conditions, a section of the journal Frontiers in Behavioral Neuroscience

Received: *13 March 2021*
Accepted: *14 May 2021*
Published: *10 June 2021*

Citation:
Wada M, Takano K, Ide M, Sano Y, Shinoda Y, Furuichi T and Kansaku K (2021) Task-Related c-Fos Expression in the Posterior Parietal Cortex During the "Rubber Tail Task" Is Diminished in Ca^{2+}-Dependent Activator Protein for Secretion 2 (Caps2)-Knockout Mice. Front. Behav. Neurosci. 15:680206. doi: 10.3389/fnbeh.2021.680206

Rubber hand illusion (RHI), a kind of body ownership illusion, is sometimes atypical in individuals with autism spectrum disorder; however, the brain regions associated with the illusion are still unclear. We previously reported that mice responded as if their own tails were being touched when rubber tails were grasped following synchronous stroking to rubber tails and their tails (a "rubber tail illusion", RTI), which is a task based on the human RHI; furthermore, we reported that the RTI response was diminished in *Ca^{2+}-dependent activator protein for secretion 2*-knockout (*Caps2*-KO) mice that exhibit autistic-like phenotypes. Importance of the posterior parietal cortex in the formation of illusory perception has previously been reported in human imaging studies. However, the local neural circuits and cell properties associated with this process are not clear. Therefore, we aimed to elucidate the neural basis of the RTI response and its impairment by investigating the c-Fos expression in both wild-type (WT) and *Caps2*-KO mice during the task since the c-Fos expression occurred soon after the neural activation. Immediately following the delivery of the synchronous stroking to both rubber tails and actual tails, the mice were perfused. Subsequently, whole brains were cryo-sectioned, and each section was immunostained with anti-c-Fos antibody; finally, c-Fos positive cell densities among the groups were compared. The c-Fos expression in the posterior parietal cortex was significantly lower in the *Caps2*-KO mice than in the WT mice. Additionally, we compared the c-Fos expression in the WT mice between synchronous and asynchronous conditions and found that the c-Fos-positive cell densities were

significantly higher in the claustrum and primary somatosensory cortex of the WT mice exposed to the synchronous condition than those exposed to the asynchronous condition. Hence, the results suggest that decreased c-Fos expression in the posterior parietal cortex may be related to impaired multisensory integrations in *Caps2*-KO mice.

Keywords: body image, autism model mouse, body ownership illusion, c-Fos imaging, autism

INTRODUCTION

In the rubber hand illusion (RHI) task, a human participant feels as if a rubber hand becomes one's own hand when the rubber hand and the participant's hand are stroked synchronously with two brushes (Botvinick and Cohen, 1998; Armel and Ramachandran, 2003; Tsakiris and Haggard, 2005). In the task, visual (i.e., stroking of the rubber hand) and tactile stimuli (i.e., stroking brush of the unseen participant's own hand) are simultaneously delivered, and perception of tactile stimuli by the brush gradually moves to the rubber hand by the integration of visual and tactile stimuli; illusory body ownership of the rubber hand subsequently occurs.

This kind of illusory body ownership is sometimes atypical in individuals with autism spectrum disorder (ASD). For example, Paton et al. (2012) reported that participants with ASD showed lesser proprioceptive drifts, which are used as a major indicator for the human RHI task, than did the controls. Furthermore, Cascio et al. (2012) reported that children with ASD initially showed lesser proprioceptive drifts than did the controls; however, the former group showed the effects of the illusion after 6 min. They discussed that the delayed occurrence of the RHI may have resulted from atypical multisensory temporal integration.

Several neuroimaging studies with neurotypical human participants have suggested that multisensory temporal integration in the posterior parietal cortex (PPC) is critical for the occurrence of the RHI and that the activation of the ventral premotor cortex is related to the illusory body ownership of the rubber hand (Ehrsson et al., 2004, 2005). Modulation of the fronto-parietal connections during the RHI was examined by transcranial magnetic stimulation (TMS) (Karabanov et al., 2017). In addition, a human electrophysiological study using intracranial electrodes has now suggested that increased high-γ (70–200 Hz) activity in the premotor cortex and PPC is related to the illusory body ownership of the rubber hand (Guterstam et al., 2019). These human studies have suggested the importance of the PPC in the formation of illusory perception of the rubber hand at the premotor regions. To investigate the neural basis of the body ownership further, in terms of local neural circuits, cell properties, etc., it becomes necessary to perform invasive measurements in animal models.

Several studies have suggested that the RHI also occurs in macaque monkey (Shokur et al., 2013; Fang et al., 2019). Shokur et al. (2013) have suggested that synchronous visual and tactile stimuli to an avatar's and a monkey's hand caused neural activation in the somatosensory cortex when the avatar's hand is "touched" thorough a virtual reality system. Moreover, Fang et al. (2019) have developed primate version of the RHI using a video-based system. We previously found that even mice show RHI-like response (a "rubber tail illusion", RTI) (Wada et al., 2016). In the experiment, synchronous stroking of an artificial tail (rubber tail) and the real tail of a mouse was performed using two small brushes (a "rubber tail task" in mice). After >1 min of synchronous stroking, the mice responded (e.g., orienting or retracting the head) as if their own tails were being touched when the rubber tails were grasped. Using the rubber tail task, we also found that the response was weakened in the Ca^{2+}-*dependent activator protein for secretion 2*-knockout (*Caps2*-KO) mice (Wada et al., 2019), which are known as ASD model mice (Sadakata et al., 2007a,b; Shinoda et al., 2011). This result is consistent with those of other studies, that is, the occurrence of the RHI is atypical in individuals with ASD or higher autistic traits (Cascio et al., 2012; Paton et al., 2012; Palmer et al., 2013; Ide and Wada, 2017). To clarify the neural basis of the atypical response, we attempted to investigate neural circuits related to the RTI phenomenon.

c-Fos, which encodes a 62 kDa protein, is found as a proto-oncogene, and it responds immediately to extracellular signals (immediate early gene) (Sheng and Greenberg, 1990). In neuronal cells, the expression of c-Fos is induced by an inflow of calcium ions that is accompanied with action potentials, and it is used as one of the activity dependent markers (Morgan et al., 1987; Guzowski et al., 1999). By conducting functional histological studies with immediate-early genes (e.g., c-fos, arc) that are expressed immediately following neural activations (Hirokawa et al., 2008; Wada et al., 2010), we can detect task-related regions at whole section levels. Moreover, after such screening tests, we can identify cell properties and related local neural circuits using double staining.

The previous behavioral study suggests that a large difference in response rate of the synchronous stroking condition was observed between in *Caps2*-KO and wild-type (WT) mice in the rubber tail task (Wada et al., 2019). Therefore, in this study, we investigated c-Fos expression in *Caps2*-KO and WT mice following synchronous stroking, which would cause the RTI response in the WT mice, to investigate the brain regions that are related to the weakened responses in the KO mice. In addition, we also compared the c-Fos expression between WT mice exposed to synchronous and asynchronous stroking to investigate the brain regions that would be related to the RTI response.

MATERIALS AND METHODS

Subjects

Wild-type mice (n = 12) and *Caps2*-KO mice (n = 8) were used in this study. The mice were derived from our previous study

(Wada et al., 2016, 2019). All the WT mice were C57BL/6NCrj (Charles River Laboratories Japan Inc., Yokohama, Japan). All the *Caps2*-KO mice were derived from Tokyo University of Science. Details regarding the production and phenotypes of the KO mice were reported previously, and the mice were characterized based on their autistic behaviors (Sadakata et al., 2007a,b; Shinoda et al., 2011). All the mice in the present study experienced the rubber tail task, and the behavioral results were previously reported (Wada et al., 2016, 2019). Thus, exactly same mice that previously behavioral tested were used in the study. The mice were provided *ad libitum* access to water and food, and were housed in groups of two to four littermates in a room with a 12 h light/dark cycle. The experiment was conducted during the light cycle. Prior to the experiment, the mice had no history of drug administration or surgery, and had experienced the rubber tail tasks that were reported previously (Wada et al., 2016, 2019). The experiments were approved by the institutional committee for animal experimentation (Research Institute of the National Rehabilitation Center for Persons with Disabilities).

Apparatus

The mice were trained in a stainless-steel tube that was designed for the rubber-tail task (O'Hara, Tokyo, Japan). One side of the tube was open, and the other side of the tube was connected to a transparent plastic cone. A rubber tail was placed on either the right or the left side of the cone. In the control experiment in the previous study (Wada et al., 2016), when the rubber tail was occluded by an opaque plastic plate, the response measured as head movements significantly decreased, suggesting that the mice can see the rubber tail from the cone. Thus, visuotactile integration seems to be important for the RTI phenomenon. The mice were not fixed during the behavioral tasks. The apparatus was essentially identical to those used in our previous study (Wada et al., 2016, 2019).

Visuotactile Stimulation Before Perfusion (Synchronous or Asynchronous Condition)

All mice underwent the rubber tail task, and the results were previously reported (Wada et al., 2016, 2019). Four WT mice were derived from the first study (Wada et al., 2016), while eight WT mice and all KO mice were derived from the latter study (Wada et al., 2019). Since all the mice experienced the rubber tail task, the mice were accustomed to receiving synchronous or asynchronous stroking of their tails and the neighboring rubber tails in the small tube (**Figure 1A**). More than 3 days following the rubber tail task, in the visuotactile stimulation preceding the perfusion (**Figure 1B**), the mice were placed in the tube for 20 min, and their tail and the rubber tail were brush stroked. Eight KO mice and six WT mice underwent synchronous stroking of their tails (synchronous condition), and the other six WT mice underwent asynchronous stroking of the tails (asynchronous condition). Unlike in the rubber tail task, neither the rubber tail nor the actual tail was grasped by the experimenter before the perfusion to prevent brain activities that could have resulted from the motor responses related to tail grasping.

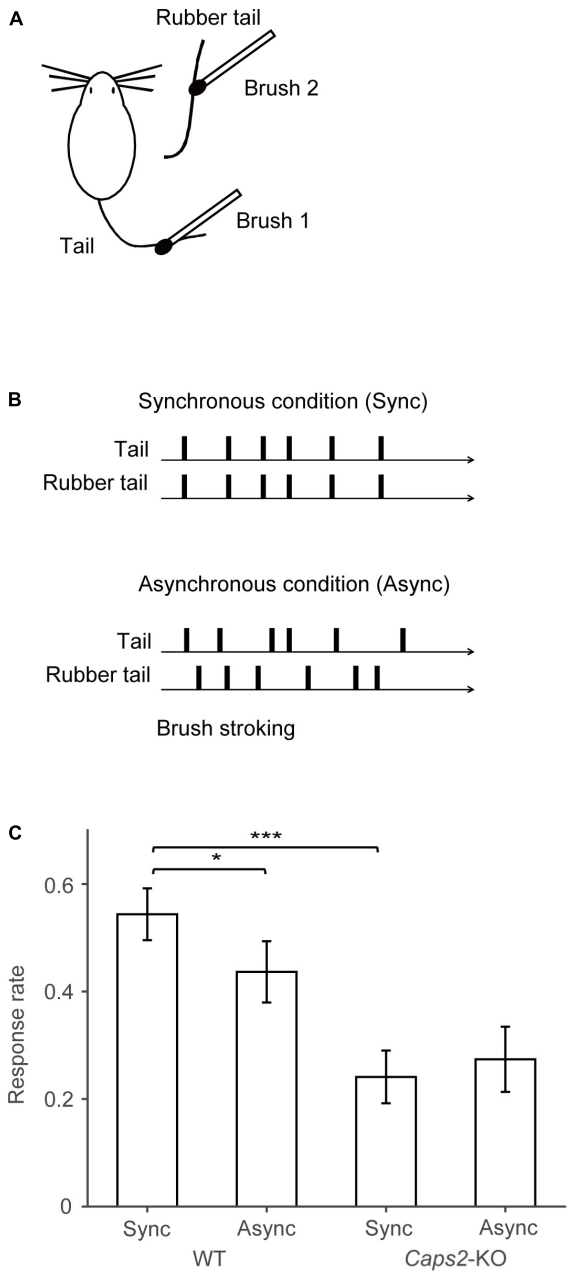

FIGURE 1 | Behavioral task. **(A)** Task set-up: Synchronous or asynchronous stroking of real tails of mice and the rubber tails was performed by using two small brushes. **(B)** Behavioral task: Under the synchronous condition, synchronous stroking of an actual tail and a rubber tail was performed by using two small brushes. In contrast, under the asynchronous condition, mice received asynchronous stroking. Details of the apparatus are essentially identical to those used in our previous study (Wada et al., 2016, 2019). **(C)** Result of the rubber tail task: As reported previously (Wada et al., 2019), in the rubber tail task, the mice were received to 10-min daily tests under two conditions: (1) synchronous stroking of the real tail and a rubber tail (synchronous condition, Sync), and (2) asynchronous stroking of both tails (asynchronous condition, Async). After the tails were stroked for approximately 1 min, an experimenter who was blinded to experimental conditions grasped the rubber tail. The behavioral test consisting 8–10 trials/condition was conducted more than 10 days. Movements of the mice

(Continued)

FIGURE 1 | *(Continued)*
were evaluated by technical staffs who were blinded to experimental conditions using recorded movies. If the mouse's head immediately turned toward the rubber tail or retracted into the tube, the response was considered a full response with a full score (1.0). If the response was small or delayed (∼1 s), the response was considered as an intermediate response with a partial score (0.5). Moreover, trials in a case, in which the mouse did not respond, were given a score of zero (0). For calculating the response rate of the mice, the moving averages before and after 10 trials (every 21 trials) of the response were calculated. We subsequently extracted the time point at which the difference between the response rates of the synchronous and asynchronous conditions was maximized for each mouse (minimum *p*-values between conditions, one-sample *t*-test) for the response rate in the rubber tail task. Bar graphs indicate averaged response rates from 12 wild-type (WT) mice and 8 *Caps2*-KO mice that were used in the present experiment. The behavioral data and analysis were derived from the previous studies (Wada et al., 2016, 2019). $*p < 0.05$, $***p < 0.001$.

Histology

After the 20-min behavioral test, the mice were immediately anesthetized, administered an overdose of pentobarbital intraperitoneally, and perfused intracardially with 60 ml of saline followed by 30 ml of 4% paraformaldehyde in 0.1 M phosphate buffer (Wako Junyaku, Osaka, Japan). The brains were removed and stored overnight in 4% paraformaldehyde at 4°C overnight. Subsequently, the brains were first transferred to 20% sucrose in 0.1 M phosphate buffer and then to 30% sucrose in 0.1 M phosphate buffer at 4°C until they sank. The brain blocks were mounted in OCT compound (Miles Inc., Elkhart, IN, United States), rapidly frozen in a bath (UT-2000F, Tokyo Rikakikai Co, Ltd, Tokyo, Japan) filled with pentane and hexane (1:1) at −100°C, and then stored at −80°C until dissection. Coronal brain sections (7 μm) were sliced on a freezing microtome (CM3050S, Leica, Nussloch, Germany). The sections were mounted on pre-coated slides (MAS-coated slide, Matsunami Glass Ind., Ltd., Osaka, Japan).

Immunostaining of c-Fos

For the labeling of cells that expressed c-Fos protein, the avidin-biotin peroxidase (ABC) method was used with a polyclonal rabbit antibody specific to c-Fos (SC-52; Santa Cruz Biotechnology, Santa Cruz, CA, United States). The sections were first treated with 0.3% H_2O_2 in methanol for 30 min to destroy endogenous peroxidases and then incubated for 20 min with diluted normal blocking serum in phosphate-buffered saline to minimize nonspecific labeling. Subsequently, the tissue sections were incubated for 30 min at room temperature in anti-c-Fos antibody (SC-52) diluted to 1:500 with Da Vinci Green Diluent (Biocare Medical, LLC, Pacheco, CA, United States). The sections were washed, placed in biotinylated goat anti-rabbit antibody diluted to 1:200 for 30 min (Vectastain, ABC Elite kit, Vector Laboratories, Burlingame, CA, United States), washed again, and then placed for 30 min in avidin–biotin complex diluted to 1:200 (Vectastain, ABC Elite kit). The peroxidase activity was visualized with a coloring solution (Histofine DAB Substrate, NICHIREI Bioscience Inc., Tokyo, Japan). After washing with distilled water, the sections were dehydrated through mixtures of ethanol, methanol, and 2-propanol for four washes, transferred to xylene for four washes, and then covered with coverslips. This immunostaining process was conducted on contract (Genetic lab, Sapporo, Japan). The specificity of the antibody (SC-52) had been confirmed in the previous study (Wada et al., 2010).

c-Fos Imaging

For quantitative analysis, we calculated the densities of c-Fos-positive cells and compared them among the groups according to the previously reported methods (Wada et al., 2016, 2019). The level from the bregma point of each coronal section was determined by using a mouse brain atlas (Paxinos and Franklin, 2001).

Images of each section were acquired using a slide scanner with a bright-field microscope (×20, Nippon Roper, Tokyo, Japan), adjusted such that 1 pixel was equal to 2.5 μm. Scanning of the images was conducted on contract (Genetic lab). For each mouse, neighboring sections were captured at six levels from bregma (+2, +1, −1, −2, −3, and −4 ± 0.2 mm).

The adjusted image of a whole section was fast Fourier transform (FFT) band-pass filtered with an NIH image-J program (NIH, Bethesda, MD, United States) to eliminate low-frequency drifts (>20 pixels = 50 μm) and high frequency noises (<1 pixel = 2.5 μm). The filtered image was further analyzed with a homemade program that was developed on MATLAB with image processing and statistics toolboxes (Mathworks Inc., Natick, MA, United States). As described previously (Wada et al., 2006, 2010), a density map of c-Fos positive cells was prepared for each section by detecting c-Fos positive cells and by calculating the number of immunostained cells in each compartment sized 100 μm × 100 μm, and the map was resized and normalized to a standard section (150 × 200 pixels, 1 pixel ≒ 50 μm). For each mouse, we created c-fos-positive cell density maps (PCDM) at the six levels. A medial–lateral axis of the PCDMs was aligned according to the side on which the rubber tail was placed. Subsequently, we created matrices by piling the maps of each group.

Statistical Parametric Mapping of the c-Fos-PCDM

Using the matrices, we carried out a pixel-by-pixel between-group comparison of c-Fos-positive cell densities in each matrix of PCDMs. *T*-test was repeatedly applied to each block, after spatially smoothing each map with a Gaussian filter (SD = 8 pixels ≒ 400 μm). We first calculated if the regions where the WT mice were exposed to the synchronous condition ($n = 6$) showed a greater (or lesser) c-Fos cell density than did the *Caps2*-KO mice exposed to the synchronous condition ($n = 8$). The *p*-value of the *t*-test at each point ($p < 0.001$) was mapped to show areas that would reflect the differences between the groups.

Then, we applied the cluster extent threshold to avoid false-positive activities. In this study, we used a two-dimensional cluster because the slice gap (approximately 1 mm) was sufficiently large to ignore effects of other clusters. Thus, from a formula of the cluster extent threshold for the 3-dimensional clustering (Kawaguchi, 2017), we transformed this formula for

2-dimensional clustering by using Euler characteristic densities two-dimensionally. Then, a cluster size, S, for the threshold was calculated as follows by using MATLAB:

$$S = \frac{\mathrm{FWHM}^2 \cdot \log p}{A \cdot T_{inv}\left(1 - \frac{p}{2},\ n_1 + n_2 - 2\right)^2 \cdot \Gamma(2)}, \quad (1)$$

Where p is the corrected p-value for multiple comparisons ($p = 0.05$), FWHM is the full width at half maximum (eight pixel), n_1 and n_2 are sample size of each group, and A is the constant number, calculated as follows:

$$A = \frac{4 \log 2}{2\pi}$$

We further examined the regions where the WT mice exposed to the synchronous condition ($n = 6$) showed a greater (or lesser) c-Fos cell density than did those exposed to the asynchronous condition ($n = 6$) in the same way.

In addition, we carried out a pixel-by-pixel calculation of the Pearson correlation coefficient between the response rate of the synchronous condition in the rubber tail task and c-Fos-positive cell densities in each matrix of PCDMs, using the matrices of the WT and *Caps2*-KO mice exposed to the synchronous condition ($n = 14$). The correlation coefficients (r) were displayed with a pseudo-color map (**Supplementary Figure 1**), while the results of pixels that could not confirm the normality of the dataset using the Kolmogorov-Smironov test ($p < 0.05$) were omitted (colored with black).

RESULTS

The mice were derived from the previous studies, and all of them experienced the rubber tail task (Wada et al., 2016, 2019). In the rubber tail task, the mice were received to daily tests under two conditions: (1) synchronous stroking of the real tail and a rubber tail (synchronous condition), and (2) asynchronous stroking of both tails (asynchronous condition). As previously reported, in the *Caps2*-KO mice, a strain of the ASD model mice, the RTI response by the rubber tail task was weak (Wada et al., 2019). Considering the mice that were used the present study, the response rates (0.24 ± 0.049, mean $\pm$ sem) of the *Caps2*-KO mice [from the previous study (Wada et al., 2019)] were also significantly smaller than those (0.54 ± 0.048) of the WT mice [from the previous study (Wada et al., 2016, 2019)] in the synchronous condition of the rubber tail task (**Figure 1C**, $t_{17.0} = -4.40$, $p = 0.00039$, Welch's t-test, 95% *confidence interval* = [−0.45, −0.16], $d = 1.97$), while the difference in the response rates (*Caps2*-KO: 0.27 ± 0.060, WT: 0.44 ± 0.057, respectively) were marginal but not significant in the asynchronous condition ($t_{16.6} = -1.95$, $p = 0.068$, Welch's t-test, 95% *confidence interval* = [−0.34, 0.013], $d = 0.88$). In addition, as previously reported (Wada et al., 2016, 2019), the WT mice showed significantly higher response rates under the synchronous condition than under the asynchronous condition (**Figure 1C**, $t_{11} = 2.38$, $p = 0.037$, one-sample t-test, 95% *confidence interval* = [0.0079, 0.21], $d = 0.69$), while there were no significant differences in the response rates under the conditions ($t_7 = 0.55$, $p = 0.60$, one-sample t-test, 95% *confidence interval* = [−0.17, 0.11], $d = -0.19$) in the *Caps2*-KO mice.

From the behavioral results, a large difference in response rate of the synchronous stroking condition was observed between in *Caps2*-KO and WT mice. Therefore, we investigated c-Fos expression in *Caps2*-KO and WT mice following synchronous stroking. In addition, we also compared the c-Fos expression between WT mice exposed to synchronous and asynchronous stroking. More than 3 days after the rubber tail task, synchronous or asynchronous visuotactile stimulation (**Figure 1B**) and the perfusion were conducted.

c-Fos-PCDM

Figure 2 shows c-Fos-PCDMs at the six levels for the WT mice exposed to the synchronous and asynchronous conditions and the *Caps2*-KO mice exposed to the synchronous condition. A medial–lateral axis of the PCDMs was aligned according to the side on which the rubber tail was placed. In the figure, red color indicates regions where c-Fos-positive cell densities were high (e.g., the primary visual cortex in all three groups).

Statistical Parametric Mapping of c-Fos-PCDM

We compared the densities of c-Fos-positive cells among the groups by using statistical parametric mapping of immuno-positive cell density. **Figures 3**, **4** show the differences among the groups in detail, because the statistical parametric mapping can detect even small differences in cell densities (Wada et al., 2006).

As shown in a left column of **Figure 3** ("WT Sync > *Caps2*-KO Sync"), the WT mice exposed to the synchronous condition showed significantly higher densities of c-Fos-positive cells than did the *Caps2*-KO mice exposed to the synchronous condition in several regions after correcting for multiple comparisons at the cluster-level threshold ($p < 0.05$). Significantly higher densities of c-Fos-positive cells in the ipsilateral posterior parietal association cortex (LPtA, lateral parietal association cortex, bregma −2 mm level) and the ipsilateral retrosplenial agranular cortex (RSA, bregma −2 mm, −3 mm level) were observed in the WT mice than in the *Caps2*-KO mice (**Table 1A**). Regarding the ipsilateral posterior LPtA cortex (bregma −2 mm level), a small cluster was also observed at the comparison between the synchronous and asynchronous conditions in the WT mice ("WT Sync > WT Async," $p < 0.001$, uncorrected) in the WT mice, although the cluster size was not reached the cluster-level threshold.

On the contrary, as shown in a right column of **Figure 3** ("*Caps2*-KO Sync > WT Sync"), the *Caps2*-KO mice exposed to the synchronous condition showed significantly higher densities of c-Fos-positive cells than did the WT mice exposed to the synchronous condition in the contralateral hippocampus (**Table 1B**).

As shown in a left column of **Figure 4** ("WT Sync > WT Async"), at bregma 1 mm level, densities of c-Fos-positive cells were significantly higher in the ipsilateral claustrum (cl) and dorsal endopiriform nucleus (DEn) in the WT mice exposed to the synchronous condition than those exposed to

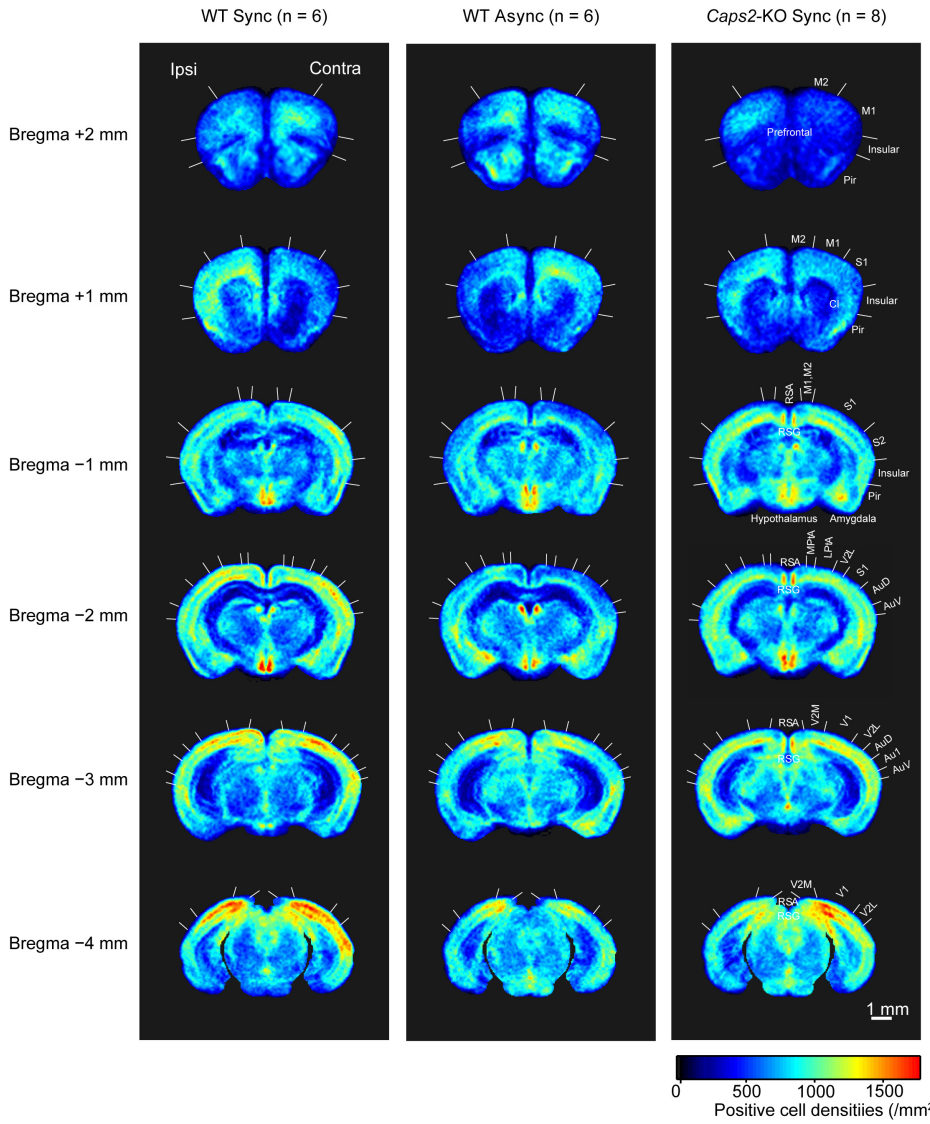

FIGURE 2 | c-Fos-positive cell density maps (PCDM). PCDMs corresponding to six different levels (bregma +2, +1, −1, −2, −3, and −4 mm) are shown in rows for each group (columns: WT with Asynchronous condition, WT with Synchronous condition, *Caps2*-KO with Synchronous condition). Each PCDM map was aligned according to the side of the rubber tail and combined. Boundaries between regions were determined by reference to the brain atlas (Paxinos and Franklin, 2001). M2, secondary motor cortex; M1, primary motor cortex; Pir, Piriform cortex, SI, primary somatosensory cortex; S2, secondary somatosensory cortex; RSA, retrosplenial agranular cortex; RSG, retrosplenial granular cortex; MPtA, medial parietal association cortex; LPtA, lateral parietal association cortex; Au1, primary auditory cortex; AuD, secondary auditory cortex dorsal area; AuV, secondary auditory cortex ventral area; V1, primary visual cortex; V2M, medial secondary visual cortex; V2L, lateral secondary visual cortex. Scale bar: 1 mm.

the asynchronous condition (**Table 1C**). At bregma −1 mm and −2 mm levels, significantly higher densities of c-Fos-positive cells were observed in the primary somatosensory cortex (SI) in the contralateral side that the rubber tail were presented. According to previous studies (Woolsey, 1967; Krubitzer et al., 2011), the tail region of the SI is located in an anteromedial part (an arrow in **Figure 4**) adjacent to the motor cortex. There was no significant cluster that reached the cluster-level threshold in the surrounding region.

Furthermore, as shown in a right column of **Figure 4** ("WT Async > WT Sync"), densities of c-Fos-positive cells in the WT mice exposed to asynchronous condition were significantly higher than those exposed to the synchronous condition only in the contralateral basal amygdaloid nucleus at bregma −3 mm (**Table 1D**).

Additionally, with regards to the WT and *Caps2*-KO mice exposed to the synchronous condition, we calculated the Pearson correlation coefficient between the response rate of the synchronous condition in the rubber tail task and c-Fos-positive cell densities in each matrix of PCDMs (**Supplementary Figure 1**). In addition to the contralateral SI cortex (bregma −1 mm level), ipsilateral LPtA cortex (bregma −2 mm level),

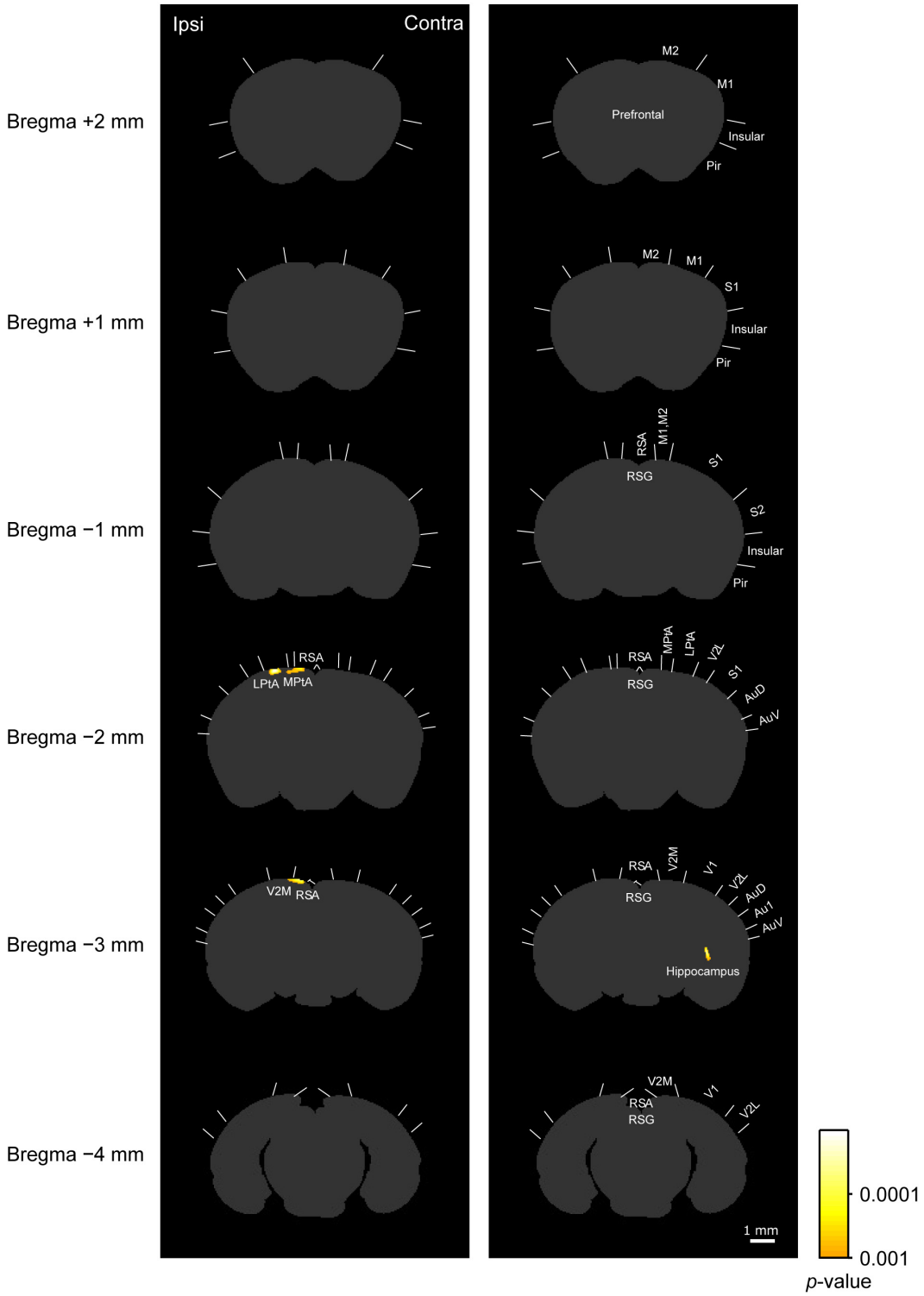

FIGURE 3 | c-Fos imaging (statistical parametric mapping): Comparison between WT and *Caps2*-KO mice exposed to synchronous stroking. **(A)** Areas that showed significantly higher densities of c-Fos-positive cells in the WT mice exposed to the synchronous condition than in the *Caps2*-KO mice exposed to the synchronous condition after correcting for multiple comparisons at the cluster-level threshold ($p < 0.05$). Pixel-by-pixel *t*-tests were applied between two groups. **(B)** Areas that showed significantly higher densities of c-Fos-positive cells densities in the *Caps2*-KO mice exposed to the synchronous condition than in the WT mice exposed to the synchronous condition after the cluster level control. Boundaries between regions were determined by reference to the brain atlas (Paxinos and Franklin, 2001). Scale bar: 1 mm.

TABLE 1 | Regions that have significant difference in c-Fos imaging among groups.

Bregma	Region	Minimum *p*	Area (pixel^2)
(A) WT Sync > *Caps2*-KO Sync			
−2 mm	LPtA	0.000011	49
−2 mm	RSA, MPtA	0.00018	56
−3 mm	RSA, V2M	0.000014	68
(B) *Caps2*-KO Sync > WT Sync			
−3 mm	Hippocampus	0.000026	31
(C) WT Sync > WT Async			
+1 mm	DEn	0.0001	49
+1 mm	Cl	0.00033	41
−1 mm	Sl, S2	0.000021	136
−2 mm	Sl	0.000048	52
−2 mm	Sl	0.0002	36
(D) WT Async > WT Sync			
−3 mm	Amygdala	0.00024	34

Regions that had larger area than the cluster-level threshold (A,B) larger than 28 pixel^2, (C,D) larger than 25 pixel^2) are listed.
LPtA, lateral parietal association cortex; MPtA, medial parietal association cortex; RSA, retrosplenial agranular cortex; AuD, secondary auditory cortex dorsal area; AuV, secondary auditory cortex ventral area; V2M, medial secondary visual cortex; Cl, Claustrum; DEn, dorsal endopiriform nucleus; Sl, primary somatosensory cortex.

higher correlations ($r > 0.7$) were observed at the ipsilateral motor cortex (M1, primary motor cortex; M2, secondary motor cortex; bregma 1 mm level) and contralateral DEn (bregma 2 mm level).

DISCUSSION

In this study, we found that the c-Fos-positive cell densities in the ipsilateral PPC and adjacent regions under the synchronous conditions were significantly lower in the *Caps2*-KO mice than in the WT mice, and densities of c-Fos-positive cells in the regions were generally higher in the WT mice exposed to the synchronous condition than those exposed to the asynchronous condition, although the difference did not reach a significant level.

In human imaging studies, activations of the PPC, ventral premotor cortex (PMv), lateral occipitotemporal cortex, and extrastriate cortex have been reported to be associated with the RHI (Ehrsson et al., 2004, 2005; Limanowski and Blankenburg, 2015, 2016). Functional connections between the frontal and parietal areas may play an important role in the occurrence of the illusion (Limanowski and Blankenburg, 2015; Arizono et al., 2016; Karabanov et al., 2017). In particular, in humans, the PPC is thought to be important for multisensory integration, which may be involved in the occurrence of RHI (Ehrsson et al., 2005), and attenuation of the illusion was reported after TMS over the PPC (Kammers et al., 2009). In the present study, a significant decrease in the density of c-Fos positive cells in the PPC was observed in the *Caps2*-KO mice that showed impairment of the RTI response (Wada et al., 2019). In addition, the c-Fos-positive cell densities in the motor cortex (M1 and M2) were also correlated with the response rates in the synchronous condition in the rubber tail task, while there was no significant difference in the statistical parametric mapping due to individual variation. The correlation in the higher motor cortex might reflect the illusion related activity like human imaging studies (Ehrsson et al., 2004; Gentile et al., 2013), though it is also possible that the correlation in the M1 simply reflects the motor response of the mice. Based on these results, we speculate that simultaneous visuotactile stimuli by two brushes causes synchronized activities and integration of information in the PPC, and the information would be conveyed to the higher motor cortex. This step is important for the occurrence of the RTI. The decreased c-Fos expression in the PPC under the synchronous condition may be related to impaired multisensory integrations in the *Caps2*-KO mice, although sensory dysfunctions was not reported in this strain (Sadakata et al., 2007a; Shinoda et al., 2011). This might cause weakened RTI responses (Wada et al., 2019). In individuals with ASD, atypical occurrence of the RHI (Cascio et al., 2012; Paton et al., 2012) and atypical multisensory integrations (Stevenson et al., 2014) have been reported. Moreover, previous human imaging studies suggest that multisensory integration in PPC is important for the occurrence of RHI (Ehrsson et al., 2004, 2005; Ehrsson, 2012). The lower activation of PPC by simultaneous visuotactile stimuli in the present study indicates that there is insufficient multisensory integration in this case, and then would relate atypical occurrence of RTI in the ASD model. However, in this study, we examined just one strain (*Caps2*-KO) of ASD model mice, and so evaluations using other ASD models are needed in future studies.

An increase in the density of c-Fos positive cells in the ipsilateral claustrum and adjacent regions were also observed in the WT mice exposed to the synchronous condition. The claustrum is a region of the brain that is a characteristic feature of mammals and is a thin gray matter that is located between the insular cortex and the striatum; it extends in the anterior-posterior and dorsoventral directions (Mathur, 2014). Surprisingly, the claustrum has bidirectional connections with almost all cerebral regions and basolateral amygdala (White et al., 2017). Although the involvement of claustrum in the RHI has not been reported so far, the region has been suggested to be involved in multimodal sensory integration, saliency detection, attentional load allocation, and switch-on/off of consciousness (Calvert, 2001; Crick and Koch, 2005; Mathur, 2014; Dillingham et al., 2017; Smith et al., 2019). These broad connections indicate the possibility that the claustrum might be related to the visuotactile integration for the modulation of body consciousness. However, density of c-Fos positive cells in the claustrum was not significantly different between in the WT mice and *Caps2*-KO mice. This result indicates that this region is not critical for the weakening of RTI response in *Caps2*-KO mice.

In addition, an increase in the densities of c-Fos positive cells were observed in the contralateral primary somatosensory (SI) cortex of the WT mice exposed to the synchronous condition. One possibility is that synchronous presentation of visual and tactile stimuli amplified the response of the SI, because activity of the SI cortex would be modulated by visual inputs via the

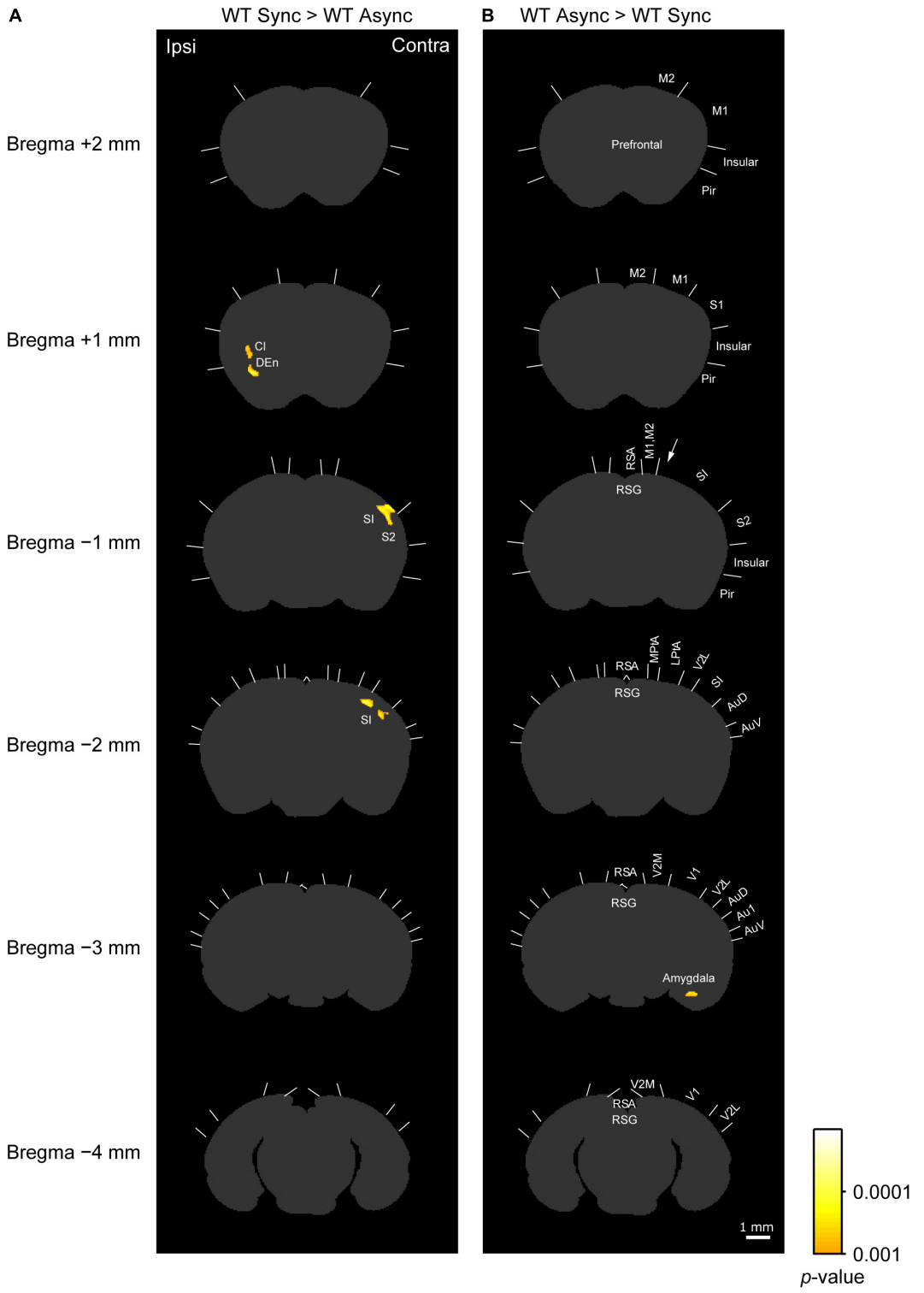

FIGURE 4 | c-Fos imaging (statistical parametric mapping): Comparison between Synchronous and Asynchronous conditions in WT mice. **(A)** Areas that showed significantly higher densities of c-Fos-positive cells in the WT mice exposed to the synchronous condition (WT Sync) than in those exposed to the asynchronous condition (WT Async) after the cluster level control. Pixel-by-pixel t-tests were applied between two groups. **(B)** Areas that showed significantly higher c-Fos-positive cell densities in the WT mice exposed to the asynchronous condition (WT Async) than in those exposed to the synchronous condition (WT Sync) after the cluster level control. Boundaries between regions were determined by reference to the brain atlas (Paxinos and Franklin, 2001). Cl, claustrum; DEn, dorsal endopiriform nucleus. Scale bar: 1 mm.

thalamus or direct connections from the visual cortex (Allen et al., 2017; Masse et al., 2017). Therefore, there is a possibility that grasping of the rubber tail might cause the activation of the SI cortex. As previously mentioned, in monkeys, neurons in the SI and primary motor cortices respond to virtual touches alone after they occurred synchronously with physical brushes to monkeys' arms (Shokur et al., 2013). However, this was not the case in the present experiment, because c-Fos expression in the tail region of SI of the WT mice exposed to the synchronous condition was not significantly high. Consistently, human neuroimaging studies have not reported activations in the hand region of SI during the RHI (Ehrsson et al., 2004, 2005; Gentile et al., 2013; Guterstam et al., 2019). Thus, another possibility is rather plausible. For example, an increase in spatial attention by the RTI would cause whisking behavior to the side of the rubber tail, because whiskers are important for exploratory behavior (Deschenes et al., 2012). In the present study, an increase in the density of c-Fos positive cells on the SI cortex was widely observed on the barrel field of SI. To clarify the reason of SI activation during the RTI, further observation of the behavior (i.e., observation of whisking behavior during the task) and acquisition of physiological measurements for time course and receptive field of each neuron (i.e., electrophysiological or optical imaging experiments) are needed in future studies.

The present study also suggests higher densities of c-Fos-positive cells in the contralateral hippocampus of the *Caps2*-KO mice. A previous study suggests that the number of GABAergic inhibitory neurons and their synapses are decreased in the hippocampus of the *Caps2*-KO mice, while excitatory neurons in the hippocampus are largely unaffected (Shinoda et al., 2011). This might cause overactivation in the hippocampus in specific situations. In addition, higher densities of c-Fos-positive cells in the contralateral amygdala in the asynchronous condition of the WT mice was observed, compared to that in the synchronous condition. We speculate that unpredictable stimuli compared to the synchronous stroking might cause this activation (Herry et al., 2007). Because a recent study suggests that the amygdala reduces susceptibility to the RHI (Spengler et al., 2019), the activation of amygdala in the asynchronous condition might contribute inhibition of occurrence of the RHI.

We compared the c-Fos expression in both the WT and the *Caps2*-KO mice that experienced the synchronous stroking of rubber and actual tails, since a greater difference in the response rates of the RTI response was observed in this condition. Moreover, this enabled to control the amount of brush stroking during the rubber tail task. Because of the limited number of samples, we used this type of comparison instead of measuring interactions between synchronous and asynchronous conditions among the groups. Thus, the present results could potentially include general differences between *Caps2*-KO and WT mice. To investigate the precise interactions, measuring the interaction using the factorial design is needed in future studies.

In this study, we investigated the c-Fos expression in both WT and the *Caps2*-KO mice during the rubber tail task to elucidate the neural basis of the RTI response and its impairment. After comparing densities of c-Fos positive cells of each section among the groups, we found that the c-Fos expression in the PPC cortex was diminished in the *Caps2*-KO mice exposed to synchronous stroking. The decrease in the c-Fos expression in the PPC may suggest that the synchronized activity from visual and tactile inputs was diminished, and it may be related to impaired multisensory integrations in the *Caps2*-KO mice.

DATA AVAILABILITY STATEMENT

The raw data supporting the conclusions of this article will be made available by the authors, without undue reservation.

ETHICS STATEMENT

The animal study was reviewed and approved by institutional committee for animal experimentation (Research Institute of National Rehabilitation Center for Persons with Disabilities). Written informed consent was obtained from the owners for the participation of their animals in this study.

AUTHOR CONTRIBUTIONS

MW and KK conceived the research. MW and MI conducted the experiments. YSh, YSa, and TF provided the mice. MW and KT analysed the data. MW wrote first draft of the manuscript. All authors read and approved the final manuscript.

FUNDING

This study was supported by a Grant-in-Aid from JSPS (JP26700012, JP26290026, JP15H03126, JP17H03563, JP17H01757, and JP21H03786).

ACKNOWLEDGMENTS

We would like to thank Toru Ogata, Yasuhiro Sawada, Motoshi Nagao, and Takahiro Maekawa for use of facilities; Naoko Kume, Taemi Nawa, and Takeshi Atsumi for technical assistance; and Yasoichi Nakajima and Reiko Fukatsu for their continuous encouragement.

SUPPLEMENTARY MATERIAL

The Supplementary Material for this article can be found online at: https://www.frontiersin.org/articles/10.3389/fnbeh.2021.680206/full#supplementary-material

Supplementary Figure 1 | Correlation mapping between c-Fos-positive cell densities and response rates in the synchronous condition of the rubber tail task. With regards to the WT and *Caps2*-KO mice exposed to the synchronous condition (WT Sync + *Caps2*-KO Sync), the Pearson correlation coefficient between the response rate of the synchronous condition in the rubber tail task and c-Fos-positive cell densities were calculated in each matrix of PCDMs. Scale bar: 1 mm.

REFERENCES

Armel, K. C., and Ramachandran, V. S. (2003). Projecting sensations to external objects: evidence from skin conductance response. *Proc Biol Sci* 270, 1499–1506. doi: 10.1098/rspb.2003.2364

Botvinick, M., and Cohen, J. (1998). Rubber hands 'feel' touch that eyes see. *Nature* 391, 756. doi: 10.1038/35784

Tsakiris, M., and Haggard, P. (2005). The rubber hand illusion revisited: visuotactile integration and self-attribution. *J Exp Psychol Hum Percept Perform* 31, 80–91. doi: 10.1037/0096-1523.31.1.80

Paton, B., Hohwy, J., and Enticott, P. G. (2012). The rubber hand illusion reveals proprioceptive and sensorimotor differences in autism spectrum disorders. *J Autism Dev Disord* 42, 1870–1883. doi: 10.1007/s10803-011-1430-7

Cascio, C. J., Foss-Feig, J. H., Burnette, C. P., Heacock, J. L., and Cosby, A. A. (2012). The rubber hand illusion in children with autism spectrum disorders: delayed influence of combined tactile and visual input on proprioception. *Autism* 16, 406–419. doi: 10.1177/1362361311430404

Ehrsson, H. H., Holmes, N. P., and Passingham, R. E. (2005). Touching a rubber hand: feeling of body ownership is associated with activity in multisensory brain areas. *J Neurosci* 25, 10564–10573. doi: 10.1523/jneurosci.0800-05.2005

Ehrsson, H. H., Spence, C., and Passingham, R. E. (2004). That's my hand! Activity in premotor cortex reflects feeling of ownership of a limb. *Science* 305, 875–877. doi: 10.1126/science.1097011

Karabanov, A. N., Ritterband-Rosenbaum, A., Christensen, M. S., Siebner, H. R., and Nielsen, J. B. (2017). Modulation of fronto-parietal connections during the rubber hand illusion. *Eur J Neurosci* 45, 964–974. doi: 10.1111/ejn.13538

Guterstam, A., Collins, K. L., Cronin, J. A., Zeberg, H., Darvas, F., Weaver, K. E., et al. (2019). Direct Electrophysiological Correlates of Body Ownership in Human Cerebral Cortex. *Cereb Cortex* 29, 1328–1341. doi: 10.1093/cercor/bhy285

Fang, W., Li, J., Qi, G., Li, S., Sigman, M., and Wang, L. (2019). Statistical inference of body representation in the macaque brain. *Proc. Natl. Acad. Sci. U.S.A.* 116, 20151–20157. doi: 10.1073/pnas.1902334116

Shokur, S., O'Doherty, J. E., Winans, J. A., Bleuler, H., Lebedev, M. A., and Nicolelis, M. A. (2013). Expanding the primate body schema in sensorimotor cortex by virtual touches of an avatar. *Proc. Natl. Acad. Sci. U.S.A.* 110, 15121–15126. doi: 10.1073/pnas.1308459110

Wada, M., Takano, K., Ora, H., Ide, M., and Kansaku, K. (2016). The Rubber Tail Illusion as Evidence of Body Ownership in Mice. *J Neurosci* 36, 11133–11137. doi: 10.1523/jneurosci.3006-15.2016

Wada, M., Ide, M., Atsumi, T., Sano, Y., Shinoda, Y., Furuichi, T., et al. (2019). Rubber tail illusion is weakened in Ca^{2+}-dependent activator protein for secretion 2 (Caps2)-knockout mice. *Sci Rep* 9, 7552.

Sadakata, T., Kakegawa, W., Mizoguchi, A., Washida, M., Katoh-Semba, R., Shutoh, F., et al. (2007a). Impaired cerebellar development and function in mice lacking CAPS2, a protein involved in neurotrophin release. *J Neurosci* 27, 2472–2482. doi: 10.1523/jneurosci.2279-06.2007

Sadakata, T., Washida, M., Iwayama, Y., Shoji, S., Sato, Y., Ohkura, T., et al. (2007b). Autistic-like phenotypes in Cadps2-knockout mice and aberrant CADPS2 splicing in autistic patients. *J Clin Invest* 117, 931–943. doi: 10.1172/jci29031

Shinoda, Y., Sadakata, T., Nakao, K., Katoh-Semba, R., Kinameri, E., Furuya, A., et al. (2011). Calcium-dependent activator protein for secretion 2 (CAPS2) promotes BDNF secretion and is critical for the development of GABAergic interneuron network. *Proc. Natl. Acad. Sci. U.S.A.* 108, 373–378. doi: 10.1073/pnas.1012220108

Ide, M., and Wada, M. (2017). Salivary Oxytocin Concentration Associates with the Subjective Feeling of Body Ownership during the Rubber Hand Illusion. *Front Hum Neurosci* 11:166.

Palmer, C. J., Paton, B., Hohwy, J., and Enticott, P. G. (2013). Movement under uncertainty: the effects of the rubber-hand illusion vary along the nonclinical autism spectrum. *Neuropsychologia* 51, 1942–1951. doi: 10.1016/j.neuropsychologia.2013.06.020

Sheng, M., and Greenberg, M. E. (1990). The regulation and function of c-fos and other immediate early genes in the nervous system. *Neuron* 4, 477–485. doi: 10.1016/0896-6273(90)90106-p

Morgan, J. I., Cohen, D. R., Hempstead, J. L., and Curran, T. (1987). Mapping patterns of c-fos expression in the central nervous system after seizure. *Science* 237, 192–197. doi: 10.1126/science.3037702

Guzowski, J. F., McNaughton, B. L., Barnes, C. A., and Worley, P. F. (1999). Environment-specific expression of the immediate-early gene Arc in hippocampal neuronal ensembles. *Nat Neurosci* 2, 1120–1124. doi: 10.1038/16046

Hirokawa, J., Bosch, M., Sakata, S., Sakurai, Y., and Yamamori, T. (2008). Functional role of the secondary visual cortex in multisensory facilitation in rats. *Neuroscience* 153, 1402–1417. doi: 10.1016/j.neuroscience.2008.01.011

Wada, M., Higo, N., Moizumi, S., and Kitazawa, S. (2010). c-Fos expression during temporal order judgment in mice. *PLoS One* 5:e10483. doi: 10.1371/journal.pone.0010483

Paxinos, G., and Franklin, K. B. J. (2001). *The Mouse Brain in Stereotaxic Coordinates*. San Diego, CA: Academic Press.

Wada, M., Yoshimi, K., Higo, N., Ren, Y. R., Mochizuki, H., Mizuno, Y., et al. (2006). Statistical parametric mapping of immunopositive cell density. *Neurosci Res* 56, 96–102. doi: 10.1016/j.neures.2006.05.013

Kawaguchi, A. (2017). Statistical Cluster Inference in Brain Imaging Analysis. *Japanese J. Magn. Reson. Med.* 37, 39–49. doi: 10.1016/j.jspi.2015.03.004

Krubitzer, L., Campi, K. L., and Cooke, D. F. (2011). All rodents are not the same: a modern synthesis of cortical organization. *Brain Behav Evol* 78, 51–93. doi: 10.1159/000327320

Woolsey, T. A. (1967). Somatosensory, auditory and visual cortical areas of the mouse. *Johns Hopkins Med J* 121, 91–112.

Limanowski, J., and Blankenburg, F. (2015). Network activity underlying the illusory self-attribution of a dummy arm. *Hum Brain Mapp* 36, 2284–2304. doi: 10.1002/hbm.22770

Limanowski, J., and Blankenburg, F. (2016). That's not quite me: limb ownership encoding in the brain. *Soc Cogn Affect Neurosci* 11, 1130–1140. doi: 10.1093/scan/nsv079

Arizono, N., Ohmura, Y., Yano, S., and Kondo, T. (2016). Functional Connectivity Analysis of NIRS Data under Rubber Hand Illusion to Find a Biomarker of Sense of Ownership. *Neural Plast* 2016, 6726238.

Kammers, M. P., Verhagen, L., Dijkerman, H. C., Hogendoorn, H., De Vignemont, F., and Schutter, D. J. (2009). Is this hand for real? Attenuation of the rubber hand illusion by transcranial magnetic stimulation over the inferior parietal lobule. *J Cogn Neurosci* 21, 1311–1320. doi: 10.1162/jocn.2009.21095

Gentile, G., Guterstam, A., Brozzoli, C., and Ehrsson, H. H. (2013). Disintegration of multisensory signals from the real hand reduces default limb self-attribution: an fMRI study. *J Neurosci* 33, 13350–13366. doi: 10.1523/jneurosci.1363-13.2013

Stevenson, R. A., Siemann, J. K., Schneider, B. C., Eberly, H. E., Woynaroski, T. G., Camarata, S. M., et al. (2014). Multisensory temporal integration in autism spectrum disorders. *J Neurosci* 34, 691–697.

Ehrsson, H. H. (2012). "The Concept of Body Ownership and Its Relation to Multisensory Integration," in *The New Handbook of Multisensory Processes*, ed. B. E. Stein (Cambridge, MA: MIT Press).

Mathur, B. N. (2014). The claustrum in review. *Front Syst Neurosci* 8:48.

White, M. G., Cody, P. A., Bubser, M., Wang, H. D., Deutch, A. Y., and Mathur, B. N. (2017). Cortical hierarchy governs rat claustrocortical circuit organization. *J Comp Neurol* 525, 1347–1362. doi: 10.1002/cne.23970

Calvert, G. A. (2001). Crossmodal processing in the human brain: insights from functional neuroimaging studies. *Cereb Cortex* 11, 1110–1123. doi: 10.1093/cercor/11.12.1110

Crick, F. C., and Koch, C. (2005). What is the function of the claustrum? *Philos Trans R Soc Lond B Biol Sci* 360, 1271–1279. doi: 10.1098/rstb.2005.1661

Dillingham, C. M., Jankowski, M. M., Chandra, R., Frost, B. E., and O'Mara, S. M. (2017). The claustrum: Considerations regarding its anatomy, functions and a programme for research. *Brain Neurosci Adv* 1, 2398212817718962.

Smith, J. B., Watson, G. D. R., Liang, Z., Liu, Y., Zhang, N., Alloway, K. D., et al. (2019). A Role for the Claustrum in Salience Processing? *Front Neuroanat* 13:64.

Allen, A. E., Procyk, C. A., Brown, T. M., and Lucas, R. J. (2017). Convergence of visual and whisker responses in the primary somatosensory thalamus (ventral posterior medial region) of the mouse. *J Physiol* 595, 865–881. doi: 10.1113/jp272791

Masse, I. O., Ross, S., Bronchti, G., and Boire, D. (2017). Asymmetric Direct Reciprocal Connections Between Primary Visual and Somatosensory Cortices of the Mouse. *Cereb Cortex* 27, 4361–4378.

Deschenes, M., Moore, J., and Kleinfeld, D. (2012). Sniffing and whisking in rodents. *Curr Opin Neurobiol* 22, 243–250. doi: 10.1016/j.conb.2011.11.013

Herry, C., Bach, D. R., Esposito, F., Di Salle, F., Perrig, W. J., Scheffler, K., et al. (2007). Processing of temporal unpredictability in human and animal amygdala. *J Neurosci* 27, 5958–5966. doi: 10.1523/jneurosci.5218-06.2007

Spengler, F. B., Scheele, D., Kaiser, S., Heinrichs, M., and Hurlemann, R. (2019). A Protective Mechanism against Illusory Perceptions Is Amygdala-Dependent. *J Neurosci* 39, 3301–3308. doi: 10.1523/jneurosci.2577-18.2019

Conflict of Interest: The authors declare that the research was conducted in the absence of any commercial or financial relationships that could be construed as a potential conflict of interest.

frontiers in Behavioral Neuroscience

ORIGINAL RESEARCH
published: 20 July 2021
doi: 10.3389/fnbeh.2021.710725

Differential Impact of Acute and Chronic Stress on CA1 Spatial Coding and Gamma Oscillations

Anupratap Tomar†, Denis Polygalov and Thomas J. McHugh**

Laboratory for Circuit and Behavioral Physiology, RIKEN Center for Brain Science, Saitama, Japan

Chronic and acute stress differentially affect behavior as well as the structural integrity of the hippocampus, a key brain region involved in cognition and memory. However, it remains unclear if and how the facilitatory effects of acute stress on hippocampal information coding are disrupted as the stress becomes chronic. To examine this, we compared the impact of acute and chronic stress on neural activity in the CA1 subregion of male mice subjected to a chronic immobilization stress (CIS) paradigm. We observed that following first exposure to stress (acute stress), the spatial information encoded in the hippocampus sharpened, and the neurons became increasingly tuned to the underlying theta oscillations in the local field potential (LFP). However, following repeated exposure to the same stress (chronic stress), spatial tuning was poorer and the power of both the slow-gamma (30–50 Hz) and fast-gamma (55–90 Hz) oscillations, which correlate with excitatory inputs into the region, decreased. These results support the idea that acute and chronic stress differentially affect neural computations carried out by hippocampal circuits and suggest that acute stress may improve cognitive processing.

Keywords: hippocampus, acute stress, chronic stress, place cells, theta, slow gamma, fast gamma, phase-locking

OPEN ACCESS

Edited by:
Yuichi Takeuchi,
Osaka City University, Japan

Reviewed by:
Chenguang Zheng,
Tianjin University, China
Qun Li,
University of Szeged, Hungary

***Correspondence:**
Anupratap Tomar
anupratap.tomar@bristol.ac.uk
Thomas J. McHugh
thomas.mchugh@riken.jp

†***Present address:***
Anupratap Tomar,
Center for Synaptic Plasticity, School of Physiology, Pharmacology and Neuroscience, University of Bristol, University Walk, Bristol, United Kingdom

Specialty section:
This article was submitted to Pathological Conditions, a section of the journal Frontiers in Behavioral Neuroscience

Received: *17 May 2021*
Accepted: *28 June 2021*
Published: *20 July 2021*

Citation:
Tomar A, Polygalov D and McHugh TJ (2021) Differential Impact of Acute and Chronic Stress on CA1 Spatial Coding and Gamma Oscillations. Front. Behav. Neurosci. 15:710725. doi: 10.3389/fnbeh.2021.710725

INTRODUCTION

It is generally accepted that while mild or acute stress can be beneficial for cognition and learning, repeated exposure to stressors (chronic stress) disrupts these processes (Luksys and Sandi, 2011). This dichotomy in the impact of acute and chronic stress has also been observed in the hippocampus, a brain region crucial for the acquisition and consolidation of declarative memory. At the cellular level, chronic, but not acute stress, causes dendritic shrinkage and debranching (Watanabe et al., 1992; Sousa et al., 2000) and decreases the number of synaptic contacts (spines) on principal hippocampal pyramidal neurons (Magariños et al., 1997; Sandi et al., 2003). Further, earlier studies employing both *ex vivo* electrophysiology and *in vivo* tetrode recordings report that chronic stress also alters the functionality of hippocampal pyramidal cells. For example, chronic stress disrupts synaptic plasticity in hippocampal slices (Alfarez et al., 2003). Similarly, the spatial map or internal representation of the surroundings (O'Keefe and Nadel, 1978), evident in the location-specific increase in average firing rate of hippocampal pyramidal "place" cells (O'Keefe and Dostrovsky, 1971; O'Keefe, 1976) is altered in chronically stressed rodents (Kim et al., 2007; Passecker et al., 2011; Tomar et al., 2015). However, the interpretation of acute stress effects on hippocampal synaptic plasticity is more complex (Joëls and Krugers, 2007; MacDougall and Howland, 2013) and consequently, the impact of acute stress on the neural computations carried out by hippocampal circuits in the intact brain remains unclear.

In addition to the rate code (i.e., location-specific spiking), place cells also use temporal coding to signal spatial aspects of the animal's location or behavior (O'Keefe and Recce, 1993). Temporal coding involves place cells spiking at a specific phase of ongoing oscillations in the local field potential (LFP), such as theta (6–12 Hz) and gamma (30–90 Hz), during exploratory behavior. These oscillations, as well as the more transient coupling of the theta-gamma oscillations themselves, are thought to provide temporal precision to the activity of hippocampal cell assemblies and to facilitate phenomena including synaptic plasticity and retrospective and prospective coding (Harris et al., 2003; Lisman, 2005; Buzsáki, 2010; Fries, 2015). Interestingly, temporal coding, as well as theta and gamma coupling, have been shown to be altered in neurodegenerative disorders (Goutagny et al., 2013; Booth et al., 2016; Mably et al., 2017), for which stress is a risk factor (Bisht et al., 2018). Thus, it is likely that both acute and chronic stress may impact these oscillatory patterns in unique ways.

To address these gaps in our knowledge we employed tetrode recordings in the dorsal CA1 of male mice. Recordings were made while mice explored a linear track before and after experiencing chronic immobilization stress (CIS; Suvrathan et al., 2010), a protocol that has been previously shown to reduce hippocampal volume, spatial memory (Rahman et al., 2016), and context discrimination (Tomar et al., 2015). Specifically, we examined alterations in both rate and temporal coding of CA1 pyramidal cells, as well as changes in the hippocampal oscillatory activity, following acute and chronic stress.

MATERIALS AND METHODS

Animals

All experiments were performed using male C57BL/6J mice. A total of five mice, aged between 3 and 6 months, were used for this study. The data related to the physiology during the stress exposure from these mice was previously reported (Tomar et al., 2021). Mice were maintained on a 12-h light-dark cycle with *ad libitum* access to food and water. All procedures were approved by the RIKEN Institutional Animal Care and Use Committee and complied with the National Institutes of Health guide for the care and use of laboratory animals (NIH Publications No. 8023, revised 1978). All efforts were made to minimize animal suffering and to reduce the number of animals used.

Experimental Design and Stress Protocol

Mice were habituated to the small sleep-box as well as a linear track daily, and after surgery, mice were again habituated to the sleep-box in which later all "rest" data was collected. Thus, mice were completely habituated to the experimenter, room, sleep box, etc., minimizing the contribution of other (non-stress) repetitive factors/experiences to the changes we observed in the physiology of the hippocampus. Mice underwent the same CIS protocol as described previously (Tomar et al., 2015). Briefly, mice experienced complete immobilization (2 h/day for 10 consecutive days: **Figure 1A**) in rodent immobilization bags, without access to either food or water. During the actual experiment, all mice experienced a familiar track twice, the first before (PRE) and second after the stress exposure (POST), on the first day (Acute) and the last day (Chronic) of a CIS paradigm thus providing us with four conditions: (i) PRE-Acute; (ii) POST-Acute; (iii) PRE-Chronic; and (iv) POST-Chronic. Each track (RUN) epoch was bracketed by Rest-state (REST) epochs and each epoch was $\sim$ 30 min.

Surgery, Recordings, and Histology

Mice were anesthetized using Avertin (2,2,2-tribromoethanol; Sigma-Aldrich, 476 mg/kg, i.p.) and were surgically implanted with a microdrive (manufactured with the assistance of the Advanced Manufacturing Support Team, RIKEN Center for Advanced Photonics, Japan). The microdrive housed eight independently movable tetrodes (14 μm diameter, nichrome) and was placed above the right dorsal hippocampus (coordinates from Bregma: AP −1.8 mm; ML + (1.2 mm). Prior to surgery, tetrodes were gold plated to lower impedance down to a range of 100–250 kΩ. Tetrodes were gradually lowered over the course of several days, such that by the start of the experiment they reached the CA1 stratum pyramidale. Data were acquired using a 32-channel Digital Lynx 4S acquisition system (Neuralynx, Bozeman, MT, USA). Signals were sampled at 32,556 Hz and spike waveforms were filtered between 600 Hz and 6 kHz. Skull screws located above the cerebellum served as a ground, and a tetrode positioned in the superficial layers of the neocortex, and devoid of spiking activity, was used for reference. Three to four weeks after surgery, when all tetrodes reached the CA1 stratum pyramidale, evident by multiple large amplitude spikes and SPW-Rs, the experiment was initiated. During REST epochs, the mice were located in a small circular sleep box (15-cm diameter). At the conclusion of the experiment, mice underwent terminal anesthesia (Avertin), and electric current (30 μA, for 8 s) was administered through each electrode to mark their locations. Transcardial perfusion was carried out using saline followed by 4% paraformaldehyde (PFA) followed by a further 24-h fixation in 4% PFA. Brains were sliced using a vibratome (Leica) to prepare coronal slices (50 μm thick) and inspected by standard light microscopy to confirm electrode placement.

Unit Isolation and Spike Analysis

Spike sorting was performed by an automatic spike sorting program [KlustaKwik (Harris et al., 2000)], followed by manual adjustments of the cluster boundaries using SpikeSort3D software (Neuralynx). Candidate clusters with $<$0.5% of spikes displaying an inter-spike-interval shorter than 2 ms, a total number of spikes exceeding 50, having a cluster isolation distance value (Schmitzer-Torbert et al., 2005) $\geq$10, spike halfwidth (peak-to-trough $>$170 μs and complex spike index (CSI; McHugh et al., 1996) $>$5 were considered as pyramidal cells and were used for further analysis.

Place Cell Properties

Pyramidal cells that were active during the period of exploration (RUN) with a speed $>$2 cm/s on the linear track, had field size $\geq$6 bins and covered less than 50% of the track were considered place cells. Peak firing rate was defined as the firing rate in the spatial bin containing the maximal value within each

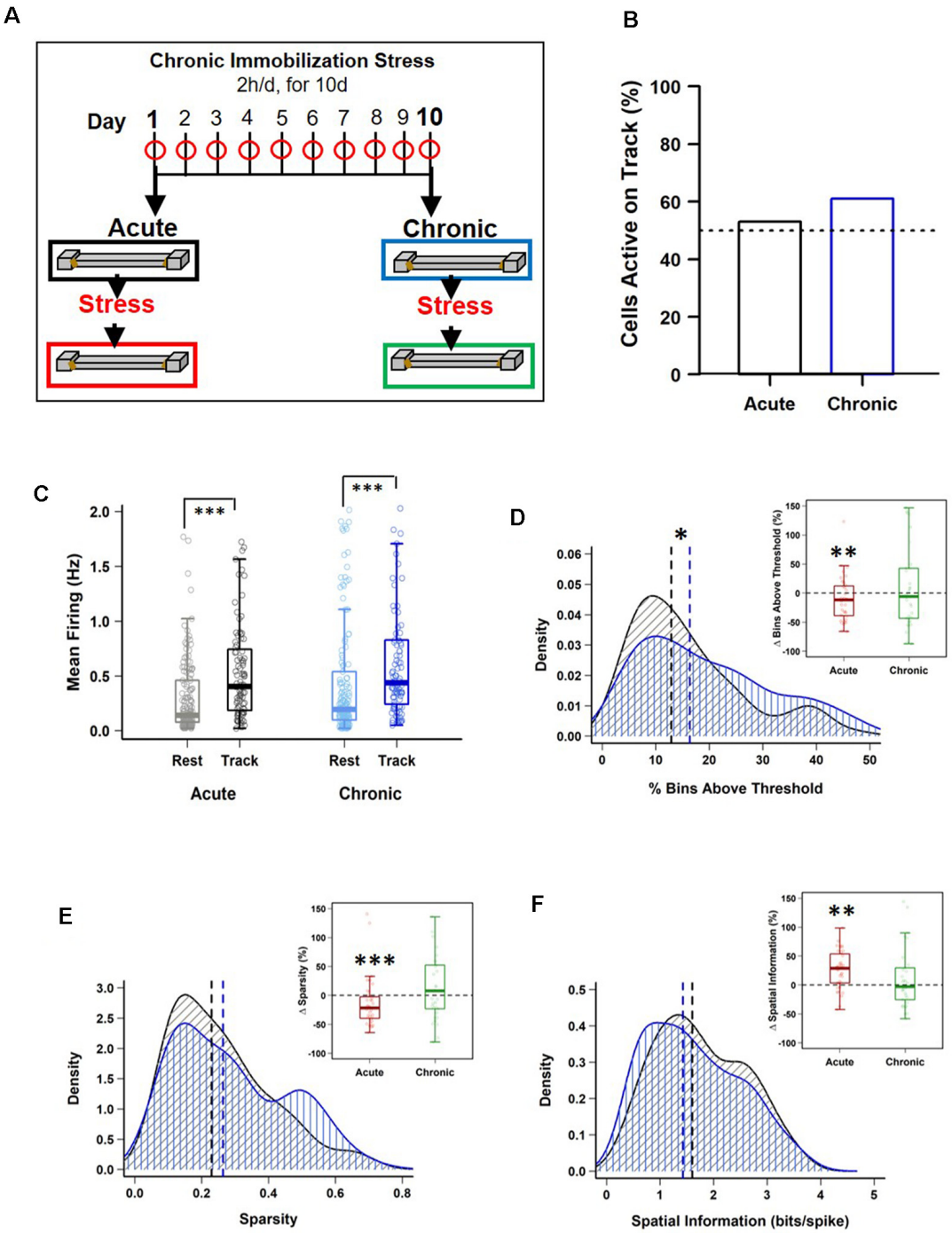

FIGURE 1 | Impact of stress on CA1 place cell activity. **(A)** Schematic representation of the chronic immobilization stress (CIS) protocol and experimental design. **(B)** Percentage of pyramidal cells active during exploration (RUN) compared to quiet wakefulness/sleep (REST) period, before stress administration (Pre-stress), on day-1 (black) and day-10 (blue), [day-1: 95/180 (53%) vs. day-10: 101/166 (61%), $p = 0.164$, chi-square test]. Dotted line represents 50%. **(C)** Pre-stress mean firing rates between REST and RUN on day-1 and day-10 [LMMs: main effect of day, $F_{(1,538)} = 3.988$, $p = 0.046$; main effect of session, $F_{(1,538)} = 64.02$, $p = 7.708 \times 10^{-15}$; interaction, $F_{(1,538)} = 0.018$, $p = 0.892$; *post hoc* Tukey's test, day-1: REST ($n = 180$) vs. RUN ($n = 95$), $p < 0.0001$, day-10: REST ($n = 166$) vs. RUN ($n = 101$), $p < 0.0001$]. **(D)** Pre-stress place field size density distribution differs between day-1 and day-10 (PRE-Acute ($n = 95$) vs. PRE-Chronic ($n = 101$), $p = 0.049$, KS-test). However, place cells active during RUN, before and after stress exposure, display a decrease in field size on day-1 (PRE-Acute 13.89 ± 1.46 vs. POST-Acute, 11.25 ± 0.96, $V = 280$, $p = 0.009$, Wilcoxon signed-rank test, $n = 36$) but not on day-10 (PRE-Chronic, 19.71 ± 2.39 vs. POST-Chronic, 17.81 ± 1.99, $V = 186$, $p = 0.316$, Wilcoxon signed-rank test, $n = 34$). **(E)** Pre-stress sparsity of place fields does not differ between

(*Continued*)

FIGURE 1 | Continued
day-1 and day-10 (PRE-Acute (n = 95) vs. PRE-Chronic (n = 101), $p > 0.05$, KS-test). However, place cells active during RUN, before and after stress exposure, display a decrease in sparsity-index on day-1 (PRE-Acute, 0.22 ± 0.02 vs. POST-Acute, 0.18 ± 0.02, V = 307, $p = 1.47 \times 10^{-4}$, Wilcoxon signed-rank test, n = 36) but not on day-10 (PRE-Chronic, 0.27 ± 0.03 vs. POST-Chronic, 0.28 ± 0.02, V = 145, p = 0.90, Wilcoxon signed-rank test, n = 34). **(F)** Pre-stress information content (bits/spike) of place fields does not differ between day-1 and day-10 [PRE-Acute (n = 95) vs. PRE-Chronic (n = 101), $p > 0.05$, KS-test]. However, place cells active during RUN, before and after stress exposure, display a significant increase on day-1 (PRE-Acute, 1.96 ± 0.16 vs. POST-Acute, 2.22 ± 0.14, V = 91, p = 0.002, Wilcoxon signed-rank test, n = 36) but not on day-10 (PRE-Chronic, 1.68 ± 0.17 vs. POST-Chronic, 1.59 ± 0.15, V = 167 p = 0.643, Wilcoxon signed-rank test, n = 34). All box plots represent interquartile range (IQR, 25th–75th percentiles), median is the thick line in the box and whiskers extend to 1.5 times the IQR. The black and red dotted lines on density plots display median values. $^{*}p < 0.05$, $^{**}p < 0.01$, $^{***}p < 0.001$, N = 5 mice.

firing rate map. The place field size was defined as the number of spatial bins where place cell field firing exceeded 20% of the peak firing rate. The mean firing rate was calculated by dividing the number of spikes which occurred within periods when velocity exceeded 2 cm/s by that period's duration and then these values were averaged. CSI is defined as CSI = 100 *(pos − neg), where "pos" is the number of inter-spike intervals positively contributing to CSI, that is, preceding spikes with larger amplitudes and following spikes with smaller amplitudes (complex bursts) occurring within 3 ms (refractory period) and 15 ms (maximum inter-spike interval defining a burst); "neg" is the number of inter-spike intervals that contribute negatively to CSI, i.e., violating either or both these rules. A "burst" was defined as at least two spikes occurring within a 10 ms time bin. The burst detection and analysis were performed using MATLAB scripts previously described in Bakkum et al. (2014). Place field "sparsity" was computed as previously described in Resnik et al. (2012). Briefly, "sparsity" was defined as a number ranging from 0 to 1, where 0 corresponds to a firing rate map which consists of equal firing rate values in every visited spatial bin. The firing rate map with sparsity value 1 corresponds to the case when all the spikes generated by any given cell occurred in a single spatial bin. Spatial Information (SI, bits/spike) was calculated as previously reported (Skaggs et al., 1993); Briefly SI = sum{$P_{spk}(i)$ * log2 [$P_{spk}(i)/P_{occ}(i)$]}, where $P_{spk}(i)$ is the probability of spiking in bin "i" and "$P_{occ}(i)$" is the occupancy probability in bin "i". The "P_{spk}" and "P_{occ}" values were computed from the rate and occupancy maps respectively.

Power Spectral Density

The Power Spectral Density (PSD) during exploratory behavior was calculated by using Welch's averaged modified periodogram method with a 2,048-sample (1.26 s) window size, 50% overlap and 4,096 FFT points (2.52 s) resulting in a time-varying spectrogram. The PSD curves corresponding to time bins when the animal's velocity was above 6 cm/s were averaged yielding a single PSD curve for each of the four experimental conditions. In order to account for power fluctuations caused by differences in position/impedance of the electrodes and make PSD values comparable across mice, we normalized each PSD curve by its own mean power within the 0–3 Hz band.

Quantification of Modulation of Firing Rate and Gamma Oscillations by Animal's Running Speed

Instantaneous running speed curves were obtained by element-wise division of relative changes in the animal's position between video frames by correspondent inter-frame timestamps. The resulting signal was then smoothed with a 2.5-SD gaussian kernel. For every place cell, all the spikes fired by the cell when the animal was running along the track were binned, using the camera's frame rate (1/30 s as the bin size, yielding an instantaneous firing rate curve. Instantaneous running speed values were then binned using logarithmically distributed velocity values. The resulting index matrix (second return value of the MATLAB histc() function) was then used to calculate the mean firing rate of the cell within each running speed bin. Modulation of LFP power in gamma frequency bands by the animal's running speed was assessed by first down-sampling the LFP signal to 400 Hz and up-sampling the previously calculated instantaneous velocity curve using linear interpolation method to the same sampling frequency value as the down-sampled LFP. The resulting LFP signal was then filtered in the target frequency bands (slow and fast gamma) and converted into instantaneous power values by calculating the absolute value of the Hilbert transform of the filtered LFP trace. The up-sampled running speed curve was then binned using the same logarithmically distributed velocity values, and corresponding mean fast and slow gamma power was calculated by using the method described above for each velocity bin.

Theta/Gamma Phase-Locking to Spikes

The phase relationship between spikes and theta LFP was calculated as previously described (Siapas et al., 2005). Briefly, the instantaneous theta phase was derived from the Hilbert-transformed LFP trace filtered in the theta band (6–12 Hz). Peaks and troughs were assigned 0- and 180° phases respectively, with spike phase calculated using interpolation, a method not sensitive to theta wave asymmetry. The resultant phases were converted to firing probability histograms (10° bin size) while limiting spikes to time periods when the animal's velocity exceeded 6 cm/s. Significance of the phase locking, preferred firing phase, strength of modulation, and statistical comparison of phase values were calculated using functions from the Circular Statistics Toolbox (Berens, 2009). Gamma/spikes modulation was computed in a similar manner; the calculation was performed using LFP traces filtered in slow gamma (30–50 Hz) and fast gamma (55–90 Hz) frequency bands. Due to the transient nature of gamma oscillations, additional gamma "bursts" detection was performed by calculating time periods when instantaneous power (absolute value of Hilbert transform) of gamma-band filtered LFP trace exceeded various threshold values (in Standard Deviations, 0.5 SD, 1 SD, 2 SD) above mean value of the trace.

Cross-Frequency Coupling Between Theta and Gamma Oscillations

Cross-Frequency Coupling (CFC) was calculated as described previously (Tort et al., 2010). To reliably detect the phenomena, relatively long chunks of LFP representing a consistent behavior state are necessary, thus time periods when the mouse was running along the track were used in this analysis. LFP data of each lap was first down-sampled to 800 Hz, z-scored and converted to time-varying power over multiple frequency bands matrices by using wavelet transform (mother wavelet function: Morlet, wavelet parameter: 5). Then modulation index (MI) values were calculated for each pair of low (4–20 Hz) and high (30–300 Hz) frequency bands. The significance of the MI values was assessed by using the permutation method ($N_{perm} = 200$), for details see Tort et al. (2010).

Statistical Analysis

All statistical analyses were performed in R software (3.3.2). The normality of distributions was not assumed, so comparisons were made using non-parametric statistics. For between-group comparisons, Wilcoxon rank-sum tests were used, while for cells matched between two epochs, Wilcoxon signed-rank tests were used to test the equality of medians. Two-way ANOVAs (aov function, stats package) followed by Tukey's honestly significant difference (HSD) test (TukeyHSD function, stats package) was used to test for differences between treatments. Overall differences in place cell properties were assessed using linear mixed effects models (LMMs), where mouse identity was specified as a random factor and day and behavior state were specified as fixed factors. The output of the *lmer* function was summarized as an ANOVA table (*anova* function, stats package). Similarly, comparisons for power distributions across various frequency bands in LFP signals were assessed using LMMs, where mouse identity was specified as a random factor and frequency bands as categorical variables were specified as fixed factors. Correlation between parameters was calculated using Pearson's correlation coefficient analysis (base package). The dependence of a parameter on another was calculated by employing standardized major axis (SMA) regression (*sma* function, smatr package). Comparisons between regression lines were made by likelihood ratio tests (*sma* function, smatr package). For density curve analysis, the Kolmogorov-Smirnov test was employed (*ks.test*, stats package). For phase-locking analysis, statistical analyses were performed on 10° binned data however for visualization purposes data is presented in 30° bins. Boxplots represent Interquartile Range (IQR, 25th–75th percentiles), the median is the thick line housed in the box and whiskers extend to 1.5 times the IQR. No data points were removed as outliers either for making boxplots or for statistical analysis, however for visualization purposes, axes of graphs were readjusted. All statistical tests used were two-sided, and unless otherwise stated, the significance threshold for all tests was set at $p < 0.05$ and p-values are shown as follows: $^{*}p < 0.05$; $^{**}p < 0.01$; $^{***}p < 0.001$.

RESULTS

The main aim of this study was to examine the differential impact of acute and chronic stress on CA1 spatial coding and hippocampal physiology. To this end, we employed a longitudinal design similar to that employed in previous studies that contrasted neural activity from the same rodents before and after they received exposure to stress (Kim et al., 2007; Ghosh et al., 2013; Tomar et al., 2021). Specifically, we monitored CA1 place cell activity and theta (6–12 Hz) and gamma oscillations (30–90 Hz) during two track exploration sessions: one occurring before (PRE) and second after (POST) the stress exposure, on the first day (Acute) and the last day (Chronic) of a CIS paradigm (**Figure 1A**; see "Materials and Methods" section), thus providing us with four

TABLE 1 | Pyramidal cell properties during baseline activity and exploratory states on day-1 and day-10.

Parameters	First-day (REST; *n* = 180 cells)	Last-day (REST; *n* = 166 cell)	Statistics
Peak firing (Hz)	4.60 ± 0.69	5.68 ± 0.59	W = 12,556, $^{*}p = 0.01$
Mean firing (Hz)	0.49 ± 0.07	0.53 ± 0.06	W = 13,316, $p = 0.08$
Complex Spike Index	22.21 ± 0.95	23.48 ± 1.11	W = 14,384, $p = 0.55$
Burst duration	7.72 ± 0.19	7.96 ± 0.22	W = 12,189, $^{*}p = 0.0108$
Burst ratio	0.32 ± 0.01	0.36 ± 0.01	W = 13,306, $p = 0.08$
Spikes per burst (n)	2.25 ± 0.01	2.32 ± 0.02	W = 12,267, $^{**}p = 0.0051$
Place cell properties			
	First-day (RUN; *n* = 95 cells)	**Last-day (RUN; *n* = 101 cell)**	**Statistics**
Peak firing (Hz)	4.33 ± 0.30	4.94 ± 0.39	W = 4,339, $p = 0.248$
Mean firing (Hz)	0.56 ± 0.06	0.76 ± 0.09	W = 4,289, $p = 0.201$
Complex Spike Index	20.31 ± 1.16	21.39 ± 1.11	W = 4,505, $p = 0.463$
Burst duration	7.40 ± 0.10	7.23 ± 0.16	W = 6,824, $p = 0.128$
Burst ratio	0.34 ± 0.01	0.36 ± 0.01	W = 5,870, $p = 0.477$
Spikes per burst (n)	2.26 ± 0.02	2.27 ± 0.02	W = 5,869, $p = 0.546$

Impact of stress on CA1 pyramidal cells during baseline activity (REST) and exploration (RUN). Top: comparisons of spiking and bursting properties of pyramidal cells during quiet wakefulness/sleep (REST) between day-1 and day-10. Bottom: comparisons of spiking and bursting properties of pyramidal "place" cells during pre-stress track exploration (RUN) between day-1 and day-10. Data is presented as Mean ± SEM, Wilcoxon rank-sum test, $^{*}p < 0.05$, $^{**}p < 0.01$, N = 5 mice.

conditions: (i) PRE-Acute; (ii) POST-Acute; (iii) PRE-Chronic; and (iv) POST-Chronic.

Differential Impact of Acute and Chronic Stress on Spatial Tuning of CA1 Place Cells

Our recordings from the dorsal CA1 region of the hippocampus (**Supplementary Figure 1A**) during baseline activity state (REST) yielded a total of 180 pyramidal cells on day-1 (Acute) and 166 pyramidal cells on day-10 (Chronic). No major differences in firing rates was observed, although bursting activity showed a small, but significant, increase at the chronic time point (**Table 1**). Next, we assessed the impact of stress on mouse behavior during track exploration (RUN) by employing ANOVA statistics where the "main effect of day" signifies the comparisons made between day-1 and day-10 (i.e., after a single exposure and repeated stress) while the "main effect of session" means comparisons made before and after exposure to stress. We observed no discernible change in behavior as the total number of laps traveled by mice did not differ between sessions across days (2-way repeated measures ANOVA: main effect of day, $F_{(1,4)} = 0.564$, $p = 0.467$; main effect of session, $F_{(1,4)} = 1.459$, $p = 0.250$; interaction, $F_{(1,4)} = 0.001$, $p = 0.974$, $N = 5$ mice). Similarly, distance traveled on the track did not differ between days and sessions (2-way repeated measures ANOVA: main effect of day, $F_{(1,4)} = 1.873$, $p = 0.243$; main effect of session, $F_{(1,4)} = 6.699$, $p = 0.061$; interaction, $F_{(1,4)} = 0.465$, $p = 0.533$, $N = 5$ mice). These data demonstrated that neither acute nor chronic stress strongly affected mouse locomotor behavior.

Next, we examined the impact of stress on the location-specific activation of CA1 pyramidal "place" cells during linear track exploration (O'Keefe and Dostrovsky, 1971). The fraction of neurons that passed place cell criteria during RUN (see "Materials and Methods" section) was similar on the first and the last day of CIS (**Figure 1B**; day-1: 95/180 (53%) vs. day-10: 101/166 (61%), $p = 0.164$, χ^2 test, $N = 5$ mice), indicating that chronic stress did not alter activation of place cell ensembles. As expected, the mean firing of cells was significantly higher during RUN compared to the baseline REST session (**Figure 1C**), with no discernible effect of repeated stress exposure (averaged firing; LMMs: main effect of day, $F_{(1,538)} = 3.988$, $p = 0.046$; main effect of session, $F_{(1,538)} = 64.02$, $p = 7.708 \times 10^{-15}$; interaction, $F_{(1,538)} = 0.018$, $p = 0.892$, $n = 542$ cells, $N = 5$ mice). Thus, pyramidal cells increased their discharge rate during spatial coding and neither acute nor chronic stress affected this property of pyramidal cells.

We then performed detailed analysis of place cell properties. Place field size, defined as the proportion of the track that a place cell was active on, showed a main effect of day (**Figure 1D**; size; LMMs: main effect of day, $F_{(1,369)} = 8.660$, $p = 0.0035$; main effect of session, $F_{(1,369)} = 1.201$, $p = 0.274$; interaction, $F_{(1,369)} = 0.019$, $p = 0.890$, $n = 373$ cells, $N = 5$ mice). Further, density distribution of field size during PRE-stress sessions changed after repeated stress such that compared to day-1, on day-10, a greater fraction of cells had larger place fields [day-1 ($n = 95$ cells) vs. day-10, ($n = 101$ cells); KS-test, $p = 0.049$, $N = 5$ mice]. Moreover, neurons, that were active during both PRE and POST stress sessions, displayed a decrease in field size after stress exposure on day-1 (PRE-Acute, 13.89 ± 1.46 vs. POST-Acute, 11.25 ± 0.96, $p = 0.009$, Wilcoxon signed-rank test, $n = 36$ cells, $N = 5$ mice) but not on day-10 (PRE-Chronic, 19.71 ± 2.39 vs. POST-Chronic, 17.81 ± 1.99, $p = 0.316$, Wilcoxon signed-rank test, $n = 34$ cells, $N = 5$ mice). Thus, place fields decreased in size after the acute stress, but expanded after repeated exposure to stress.

Altered place field size alone fails to capture all changes in spatial coding, as previous studies have reported that bigger place fields can be suggestive of both improved spatial coding (Hussaini et al., 2011) and a loss of spatial specificity (McHugh et al., 1996). Thus, we next assessed the impact of stress on spatial tuning by measuring the sparsity-index, a metric of spatial selectivity (Jung et al., 1994). The sparsity-index of individual place cells was also impacted by stress (**Figure 1E**; sparsity; LMMs: main effect of day, $F_{(1,369)} = 8.931$, $p = 0.003$; main effect of session, $F_{(1,369)} = 1.929$, $p = 0.166$; interaction, $F_{(1,369)} = 2.017$, $p = 0.156$, $n = 373$ cells, $N = 5$ mice). A further analysis of cells that were active before and after exposure to stress confirmed this result, as significantly lower sparsity-index was noticed after acute stress (PRE-Acute, 0.22 ± 0.02 vs. POST-Acute, 0.18 ± 0.02, $p = 1.47 \times 10^{-4}$, Wilcoxon signed-rank test, $n = 36$ cells, $N = 5$ mice), but not after repeated stress (PRE-Chronic, 0.27 ± 0.03 vs. POST-Chronic, 0.28 ± 0.02, $p = 0.90$, Wilcoxon signed-rank test, $n = 34$ cells, $N = 5$ mice). Further, spatial information content (bits/spike), a parameter which quantifies how much information about the mouse's location is contained within the activity of a place cell (Skaggs et al., 1993), was also impacted by stress (**Figure 1F**; information; LMMs: main effect of day, $F_{(1,369)} = 10.969$, $p = 0.001$; main effect of session, $F_{(1,369)} = 2.586$, $p = 0.109$; interaction, $F_{(1,369)} = 5.414$, $p = 0.0205$, $n = 373$ cells, $N = 5$ mice). This was further confirmed as place cells active on the track before and after the exposure to stress also showed a significant increase in information content on day-1 (PRE-Acute, 1.96 ± 0.16 vs. POST-Acute, 2.22 ± 0.14, $p = 0.002$, Wilcoxon signed-rank test, $n = 36$ cells, $N = 5$ mice) but not on day-10 (PRE-Chronic, 1.68 ± 0.17 vs. POST-Chronic, 1.59 ± 0.15, $p = 0.643$, Wilcoxon signed-rank test, $n = 34$ cells, $N = 5$ mice) of the CIS protocol.

Sharpening of place coding after acute stress was not caused by altered firing rate. However, a main effect of day on firing rate was observed (mean firing; LMMs: main effect of day, $F_{(1,369)} = 13.014$, $p = 3.518 \times 10^{-4}$; main effect of session, $F_{(1,369)} = 0.381$, $p = 0.537$; interaction, $F_{(1,369)} = 1.362$, $p = 0.244$, $n = 373$ cells, $N = 5$ mice, Tukey's *post hoc*, POST-Acute vs. POST-Chronic, $p = 0.005$). In view of reports that firing rate increases along with running speed of freely behaving rodents (McNaughton et al., 1983), we next asked if differential impact of acute and chronic stress on place coding was result of difference in exploration speed across days or session but found no significant difference (2-way repeated measures ANOVA: main effect of day, $F_{(1,4)} = 3.106$, $p = 0.103$; main effect of session, $F_{(1,4)} = 1.318$, $p = 0.273$; interaction, $F_{(1,4)} = 0.08$, $p = 0.782$, $N = 5$ mice). Further, when we compared firing rate of each place cell across different speed bins (**Supplementary Figure 1B**) by using speed as a repeated variable and each recording session as non-repeated variable, we noticed a clear pattern of increase in firing rate as the speed increased [2-way mixed ANOVA:

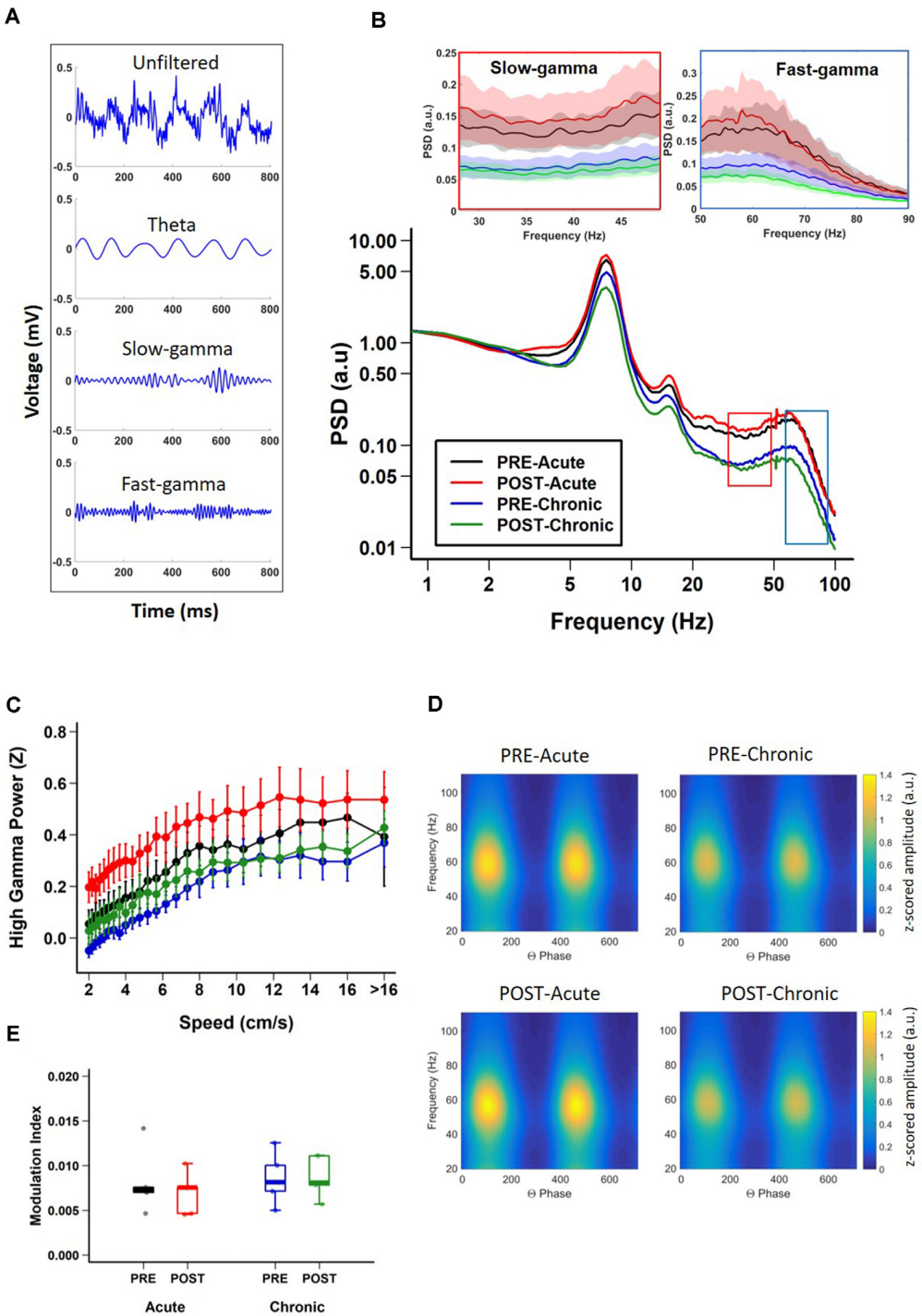

FIGURE 2 | Impact of stress on CA1 oscillatory activity. **(A)** Representative examples of unfiltered (top) and filtered (bottom) local field potentials (LFPs) during track exploration for theta, slow-gamma, and fast-gamma. **(B)** Power spectral density (PSD) curves of CA1 LFPs during linear track exploration (RUN) show no significant differences for theta (6–12 Hz; Theta, 2-way repeated measure ANOVA: day, main effect of day $F_{(1,19)} = 2.7018$, $p = 0.1262$; main effect of session, $F_{(1,19)} = 0.0427$, $p = 0.8398$; interaction, $F_{(1,19)} = 0.4823$, $p = 0.501$). Fast-gamma (55–90 Hz) showed an effect of day but not of session (FG, *right inset*; 2-way repeated measure ANOVA: main effect of day, $F_{(1,19)} = 6.7062$, $p = 0.0237$; main effect of session, $F_{(1,19)} = 0.1047$, $p = 0.752$ interaction, $F_{(1,19)} = 0.2074$, $p = 0.657$). Slow-gamma (30–50 Hz) showed an effect of day but not of session (SG, *left inset*, 2-way repeated measure ANOVA: main effect of day, $F_{(1,19)} = 8.3668$, $p = 0.0135$; main effect of session, $F_{(1,19)} = 0.0634$, $p = 0.805$; interaction, $F_{(1,19)} = 0.3754$, $p = 0.551$). **(C)** Relationship between FG power and running speed on the track (FG; 2-way repeated measure ANOVA : main effect of speed, $F_{(1,36)} = 471.385$, $p < 2.22 \times 10^{-16}$, main effect of group, $F_{(3,36)} = 5.306$,

(*Continued*)

FIGURE 2 | Continued
$p = 0.015$; interaction, $F_{(3,36)} = 10.033$, $p = 2.261 \times 10^{-6}$, $N = 5$ mice). **(D)** Representative examples of modulation of gamma amplitude by theta phase in dorsal CA1 pyramidal cell layer before (top) and after (bottom) stress exposure on day-1 (left) and day-10 (right). The colorbar represents the z-scored gamma power in arbitrary units (a.u.) for both left and right-side graphs. **(E)** Theta-FG phase-amplitude coupling (top) did not differ across days and sessions (2-way repeated measures ANOVA: day, main effect of day, $F_{(1,4)} = 0.839$, $p = 0.411$; main effect of session, $F_{(1,4)} = 3.399$, $p = 0.139$; interaction, $F_{(1,4)} = 4.953$, $p = 0.09$). Similarly, theta-SG coupling (bottom) was not affected by either acute or chronic stress (2-way repeated measures ANOVA: day, main effect of day, $F_{(1,4)} = 0.592$, $p = 0.484$; main effect of session, $F_{(1,4)} = 1.756$, $p = 0.256$; interaction, $F_{(1,4)} = 1.02$, $p = 0.370$). $N = 5$ mice.

main effect of speed, $F_{(1,369)} = 1{,}424.752$, $p < 2.22 \times 10^{-16}$, main effect of group, $F_{(3,369)} = 16.666$, $p = 3.546 \times 10^{-10}$; interaction, $F_{(3,369)} = 37.866$, $p < 2.22 \times 10^{-16}$, $N = 5$ mice; PRE-Acute ($n = 95$) cells vs. POST-Acute ($n = 89$ cells), $p = 0.012$, PRE-Chronic ($n = 101$ cells) vs. POST-Chronic ($n = 88$ cells), $p < 0.0001$, PRE-Acute ($n = 95$ cells) vs. PRE-Chronic ($n = 101$ cells), $p = 0.003$, Tukey's *post hoc* test]. Overall, the above data indicate that smaller place fields and enhanced spatial tuning, following acute stress, was not caused by altered speed or relationship between firing rate and speed. However, same was not true for chronic stress.

Differential Impact of Acute and Chronic Stress on Exploration-Associated Theta and Gamma Oscillations

Having established the differential impact of acute and chronic stress on place cell activity, next we asked if the same was true for hippocampal LFPs (**Figure 2A**) which provides a measure of average synaptic input to a local region (Buzsáki et al., 2012) and to some extent also reflects slow dynamics of spiking in a local region (Rasch et al., 2008). During exploratory behavior, the hippocampal LFP is dominated by prominent large-amplitude theta (6–12 Hz) oscillations (Vanderwolf, 1969; O'Keefe and Dostrovsky, 1971), which play a crucial role in the temporal organization of hippocampal activity (Buzsáki and Moser, 2013). Thus, we examined the impact of acute and chronic stress on theta oscillations. A comparison of the PSD of the LFPs, across sessions (**Figure 2B**) revealed that theta oscillations were robustly present and power in the theta band was not affected by either acute or chronic stress, as no effect of day or session was observed (theta; 2-way repeated measures ANOVA: day, main effect of day $F_{(1,19)} = 2.7018$, $p = 0.1262$; main effect of session, $F_{(1,19)} = 0.0427$, $p = 0.8398$; interaction, $F_{(1,19)} = 0.4823$, $p = 0.501$, $N = 5$ mice).

In addition to theta, the hippocampus displays occasional low-amplitude, high frequency gamma (30–90 Hz) oscillations (Bragin et al., 1995; Buzsáki et al., 2003; Colgin, 2016). Gamma oscillations consist of distinct subtypes with non-overlapping frequency ranges, slow (SG: 30–50 Hz) and fast (FG: 55–90 Hz) gamma (Schomburg et al., 2014; Colgin, 2016; Middleton and McHugh, 2016; Alexander et al., 2018), and enhanced gamma oscillatory activity has been suggested to reflect dynamic changes in excitatory input into CA1 (Buzsáki and Moser, 2013; Fries, 2015). Thus, we next assessed the impact of stress on these individual gamma bands. Significant decreases in fast-gamma power were evident on day-10 (**Figure 2B**; FG; 2-way repeated measures ANOVA: main effect of day, $F_{(1,19)} = 6.7062$, $p = 0.0237$; main effect of session, $F_{(1,19)} = 0.1047$, $p = 0.752$; interaction, $F_{(1,19)} = 0.2074$, $p = 0.657$, $N = 5$ mice). Similarly, chronic stress also led to similar decreases in slow-gamma power (**Figure 2B**; SG; 2-way repeated measures ANOVA: main effect of day, $F_{(1,19)} = 8.3668$, $p = 0.0135$; main effect of session, $F_{(1,19)} = 0.0634$, $p = 0.805$; interaction, $F_{(1,19)} = 0.3754$, $p = 0.551$, $N = 5$ mice). In agreement with a previous report (Chen et al., 2011), the power of gamma oscillations consistently increased across the range of speeds for FG (**Figure 2C**; 2-way repeated measure ANOVA: main effect of speed, $F_{(1,36)} = 471.385$, $p < 2.22 \times 10^{-16}$, main effect of group, $F_{(3,36)} = 5.306$, $p = 0.015$; interaction, $F_{(3,36)} = 10.033$, $p = 2.261 \times 10^{-6}$, $N = 5$ mice). However, the increase in slow gamma power as the speed increased was subtler (SG; 2-way repeated measure ANOVA: main effect of speed, $F_{(1,36)} = 42.562$, $p = 1.485 \times 10^{-9}$, main effect of group, $F_{(3,36)} = 5.774$, $p = 0.011$; interaction, $F_{(3,36)} = 5.124$, $p = 0.002$, $N = 5$ mice).

The amplitude of gamma oscillations has also been shown to be modulated by the phase of slower underlying theta rhythm (Bragin et al., 1995; Chrobak and Buzsáki, 1998; Canolty et al., 2006) and this theta-phase gamma-amplitude coupling has been suggested to reflect local information processing in hippocampal circuits (Tort et al., 2009; Buzsáki and Wang, 2012). Thus, we next determined the impact of stress on theta-gamma coupling during periods when mice ran along the linear track linear (i.e., when prominent theta oscillations are known to be present) by calculating modulation index (MI), a measure of the strength of coupling between gamma-amplitude and theta phase (Tort et al., 2010). We found no changes in the strength of theta-gamma coupling (**Figures 2D,E**; theta-gamma; 2-way repeated measures ANOVA: day, main effect of day, $F_{(1,4)} = 0.839$, $p = 0.411$; main effect of session, $F_{(1,4)} = 3.399$, $p = 0.139$; interaction, $F_{(1,4)} = 4.953$, $p = 0.09$, $N = 5$ mice). Further no significant difference was observed either between theta-fast gamma coupling (theta-FG; 2-way repeated measures ANOVA: day, main effect of day, $F_{(1,4)} = 0.839$, $p = 0.411$; main effect of session, $F_{(1,4)} = 3.399$, $p = 0.139$; interaction, $F_{(1,4)} = 4.953$, $p = 0.09$, $N = 5$ mice) or theta-slow gamma coupling (theta-SG; 2-way repeated measures ANOVA: day, main effect of day, $F_{(1,4)} = 0.592$, $p = 0.484$; main effect of session, $F_{(1,4)} = 1.756$, $p = 0.256$; interaction, $F_{(1,4)} = 1.02$, $p = 0.370$, $N = 5$ mice).

Thus, LFP power analysis indicated that while the first exposure to stress did not alter theta and gamma oscillatory activity, repeated stress led to suppression of SG and FG power, but had no impact on CFC between theta and gamma.

Impact of Acute and Chronic Stress on Temporal Coding (LFP-Spike Interactions)

In addition to rate coding (location-specific spiking), place cells also display temporal coding, reflecting their preference for spiking at specific phases of the concurrent oscillations (O'Keefe, 1976; Fox et al., 1986; Csicsvari et al., 1999). It has been hypothesized that temporal coding supports transient

TABLE 2 | Distribution of place cells phase-locked to theta and gamma oscillations on day-1 and day-10.

Rhythm	PRE-Acute	POST-Acute	PRE-Chronic	POST-Chronic	Statistics
Theta	35/48 (73%)	26/38 (68%)	53/73 (73%)	45/68 (66%)	$p = 0.814$, χ^2 test
Fast-gamma	30/66 (45%)	26/63 (41%)	34/78 (44%)	30/74 (40%)	$p = 0.935$, χ^2 test
Slow-gamma	27/74 (36%)	30/87 (34%)	29/91 (32%)	31/87 (36%)	$p = 0.928$, χ^2 test

activation of place cell ensembles, a phenomenon central to spatial information processing (Harris et al., 2003; O'Keefe and Burgess, 2005; Buzsáki, 2010; Lever et al., 2014). Knowing that acute and chronic stress differentially alter the place cell rate code, we next asked if they differentially impact temporal coding by assessing the strength and phase preference of CA1 place cell spiking to theta and gamma oscillations. Similar to a previous report (Jones and Wilson, 2005), the majority (66–73%) of CA1 place cells demonstrated significant modulation by theta (Rayleigh test of uniformity $p < 0.05$) and neither acute nor chronic stress affected this distribution (**Table 2**; $p = 0.814$, χ^2 test). Further, as expected based on earlier studies (Csicsvari et al., 1999; Jones and Wilson, 2005; Jadhav et al., 2016), the majority of neurons displayed a preference to spike near the trough of the theta oscillation (**Figure 3A**) and this mean preferred phase for theta-modulated cells was not affected by stress (**Supplementary Figure 1C**; phase; Circular ANOVA, $F_{(3,155)} = 1.305$, $p = 0.274$, $n = 159$ cells, $N = 5$ mice). Interestingly, however, the strength of theta-phase locking (**Figure 3B**) was significantly increased specifically after acute stress (MI; LMMs: main effect of day, $F_{(1,155)} = 1.892$, $p = 0.171$; main effect of session, $F_{(1,155)} = 5.425$, $p = 0.022$; interaction, $F_{(1,155)} = 5.702$, $p = 0.018$, $n = 159$ cells, $N = 5$ mice); *post hoc* Tukey's test, PRE-Acute ($n = 35$ cells) vs. POST-Acute ($n = 26$ cells), $p = 0.006$, POST-Acute ($n = 26$ cells) vs. POST-Chronic ($n = 45$ cells), $p = 0.038$.

Similar to the modulation of spiking by theta, the precise timing of pyramidal cell firing can also be entrained by gamma oscillations (Csicsvari et al., 2003). Thus, we next performed the spike phase-locking analysis of gamma oscillations during high velocity periods (speed > 6 cm/s) on the track. A large fraction (40–45%; Rayleigh test of uniformity $p < 0.05$) of CA1 place cell population displayed a significant phase preference during FG and neither acute nor chronic stress affected this distribution (**Table 2**; $p = 0.935$, χ^2 test). Moreover, stress did not alter the preferred phase (phase; Circular ANOVA, $F_{(3,108)} = 1.932$, $p = 0.129$, $n = 112$ cells, $N = 5$ mice, **Supplementary Figure 1D**) or strength (MI; LMMs: main effect of day, $F_{(1,108)} = 1.499$, $p = 0.224$; main effect of session, $F_{(1,108)} = 1.292$, $p = 0.258$; interaction, $F_{(1,108)} = 0.055$, $p = 0.815$, $n = 112$ cells, $N = 5$ mice) of the phase-locking of CA1 pyramidal cells. As gamma oscillations are more transient than theta during locomotion, we next focused on periods of strong FG on the track regardless of animal's speed or position on the track (see "Materials and Methods" section), and again observed that stress did not alter either the preferred phase (**Figure 3C**; phase: Circular ANOVA, $F_{(3,62)} = 0.919$, $p = 0.437$, $n = 66$ cells, $N = 5$ mice) or the strength of FG phase-locking (**Figure 3D**; MI: LMMs: main effect of day, $F_{(1,62)} = 0.986$, $p = 0.325$; main effect of session, $F_{(1,62)} = 0.801$, $p = 0.374$; interaction, $F_{(1,62)} = 1.936$, $p = 0.169$, $n = 66$ cells, $N = 5$ mice).

Unlike FG, the preferred phase of the cells modulated by SG was more variable across the population during high velocity periods on the track. The proportion of CA1 place cells with a significant SG phase preference was ∼32–36%; (Rayleigh test of uniformity $p < 0.05$) and showed no differences across four sessions (**Table 2**; $p = 0.928$, χ^2 test). Nonetheless, following chronic stress we did observe a small, yet significant change in the mean preferred phase (**Supplementary Figure 1E**; phase: Circular ANOVA, $F_{(3,113)} = 6.862$, $p = 2.74 \times 10^{-4}$, $n = 117$ cells, $N = 5$ mice), but noticed no change in the strength of modulation (MI: LMMs: main effect of day, $F_{(1,113)} = 0.182$, $p = 0.671$; main effect of session, 0.035, $p = 0.852$; interaction, $F_{(1,113)} = 2.358$, $p = 0.127$, $n = 117$ cells, $N = 5$ mice). Finally, when we focused on the phase-locking of place cells specifically during periods of strong SG regardless of the animal's speed or position on the track, we found that chronic stress led place cells to fire at the later phase of SG (**Figure 3E**-phase; Circular ANOVA, $F_{(3,37)} = 5.057$, $p = 0.005$, $n = 41$ cells, $N = 5$ mice; *post hoc* Watson-Wheeler test, PRE-Acute ($n = 13$ cells) vs. PRE-Chronic ($n = 11$ cells), $p = 0.036$). Chronic stress showed a trend that it affected the strength of SG-phase locking but it was not significant (**Figure 3F**; MI: LMMs: main effect of day, $F_{(1,37)} = 3.747$, $p = 0.063$; main effect of session, $F_{(1,37)} = 1.063$, $p = 0.309$; interaction, $F_{(1,37)} = 0.115$, $p = 0.737$, $n = 41$ cells, $N = 5$ mice).

Thus, while first exposure to stress increased the strength of theta phase-locking demonstrating the facilitatory effects of acute stress on temporal coding, chronic stress disrupted temporal coding as the mean phase and the strength of phase-locking of place cells to slow-gamma oscillations was altered on day-10.

DISCUSSION

Despite reports that acute stress positively impacts cognition, including hippocampal information processing (Henckens et al., 2009; Yuen et al., 2009; Kirby et al., 2013), it is not yet clear how this is reflected in hippocampal place cell activity and LFP-spike interactions, two neural processes involved in spatial coding (O'Keefe and Dostrovsky, 1971; Buzsáki, 2010; Lever et al., 2014). Here, we show that while after the first exposure to stress (Acute stress) or the last exposure to stress (Chronic stress) the averaged speed and distance covered on the track were not affected. However, after acute stress, CA1 place cells displayed refined spatial coding (**Figure 1D**), increased information content (**Figure 1F**) and decreased sparsity-index (**Figure 1E**). Further, chronic, but not acute stress, led to decreased LFP power in the slow-gamma (SG; 30–50 Hz) and fast-gamma (FG 55–90 Hz) bands (**Figure 2B**) along with an increase in place field size.

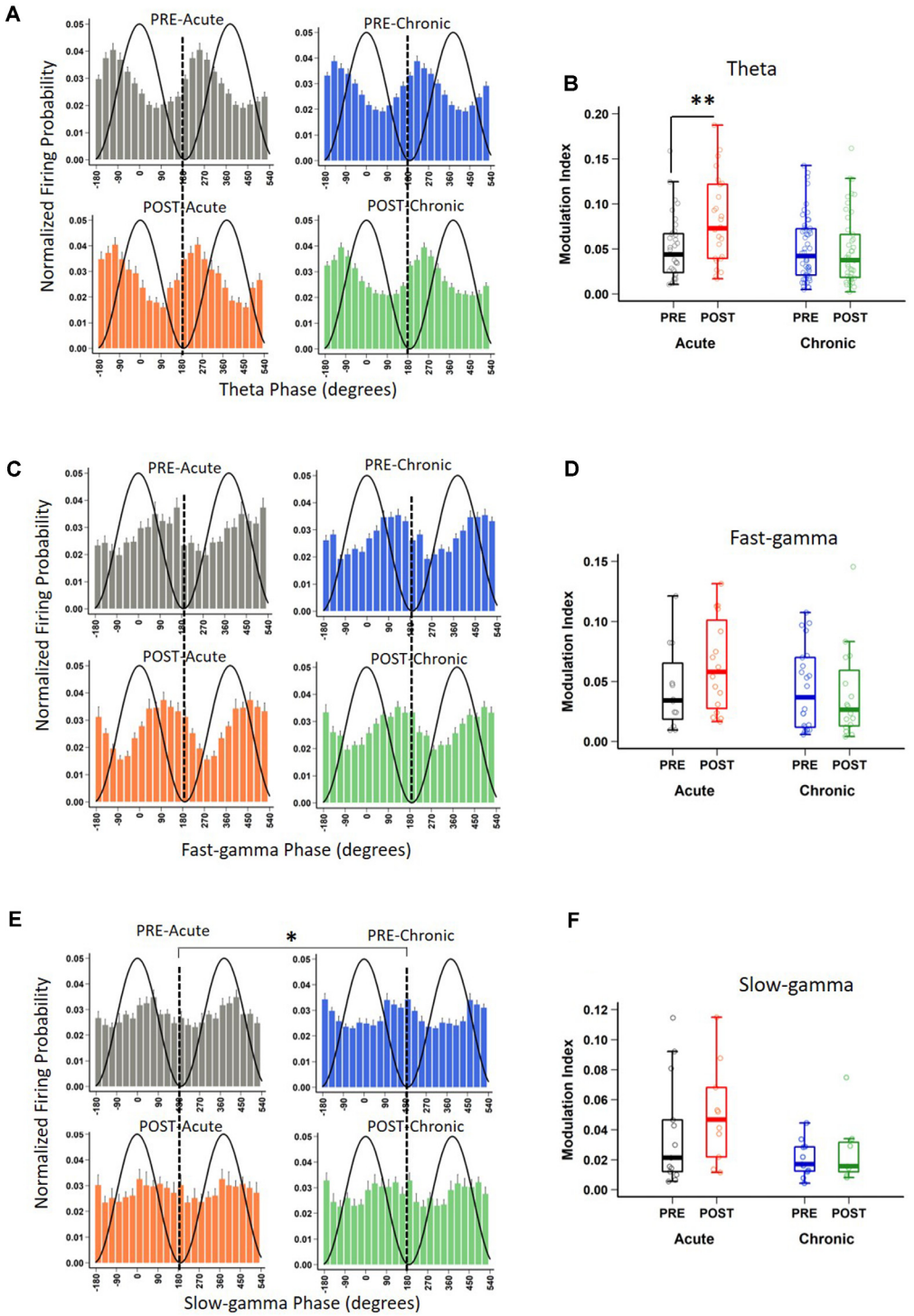

FIGURE 3 | Impact of stress on phase-locking properties of CA1 place cells to theta and gamma oscillations. **(A)** The spiking probability plotted as a function of the phase of theta for significantly theta-modulated place cell populations (Rayleigh $p < 0.05$). Population spiking probability is elevated around the trough and ascending phase of theta (0/360° set for theta peak, 180° for theta trough). **(B)** The strength of theta-phase locking (Modulation index, MI) is altered by stress [LMMs: main effect of day, $F_{(1,155)} = 1.892$, $p = 0.171$; main effect of session, $F_{(1,155)} = 5.425$, $p = 0.022$; interaction, $F_{(1,155)} = 5.702$, $p = 0.018$); *post hoc* Tukey's test, PRE-Acute ($n = 35$) vs. POST-Acute ($n = 26$), $p = 0.006$, POST-Acute ($n = 26$) vs. POST-Chronic ($n = 45$), $p = 0.038$]. **(C)** The spiking probability plotted as a function of the phase of fast-gamma (FG) for significantly FG-modulated place cell populations (Rayleigh $p < 0.05$) is elevated around the trough and descending phase of FG (0/360° set for FG peak, 180° for FG trough) but stress did not affect this phase relationship: (FG, Circular ANOVA, $F_{(3,62)} = 0.919$, $p = 0.437$). **(D)** The

(*Continued*)

FIGURE 3 | Continued
strength of FG phase-locking (MI) remains unaltered by stress (FG; LMMs: main effect of day, $F_{(1,62)} = 0.986$, $p = 0.325$; main effect of session, $F_{(1,62)} = 0.801$, $p = 0.374$; interaction, $F_{(1,62)} = 1.936$, $p = 0.169$). **(E)** The spiking probability plotted as a function of the phase of slow-gamma (SG) for significantly SG-modulated place cell populations (Rayleigh $p < 0.05$). Population spiking probability is elevated around the descending phase of SG (0/360° set for SG peak, 180° for SG trough). **(F)** The strength of SG-phase locking (MI) was not significantly altered by stress (SG; LMMs: main effect of day, $F_{(1,37)} = 3.747$, $p = 0.063$; main effect of session, $F_{(1,37)} = 1.063$, $p = 0.309$; interaction, $F_{(1,37)} = 0.115$, $p = 0.737$). Boxplots represent interquartile range (IQR, 25th–75th percentiles), median is the thick line in the box and whiskers extend to 1.5 times the IQR., $^{*}p < 0.05$, $^{**}p < 0.01$, $N = 5$ mice.

Furthermore, the strength of theta phase-locking to CA1 place cells increased after acute stress (**Figures 3A,B**), however, the mean phase of slow-gamma phase-locking was altered as stress became chronic (**Figure 3E**). Together, these results indicate that acute stress has a facilitatory impact on hippocampal information coding, while chronic stress impairs it.

Stress impacts on hippocampal functionality have been hypothesized to follow a U-shaped curve, where exposure to acute stress facilitates, while chronic stress disrupts, hippocampal function (Salehi et al., 2010; McEwen et al., 2016). Our results of enhanced spatial information content and increased strength of phase-locking after acute stress, as well as broader place fields and suppressed gamma power after repeated stress are consistent with stress exerting a U-shaped impact on hippocampal function in the intact brain. Rate and temporal coding of CA1 pyramidal cells aid spatial information processing (O'Keefe, 1976; O'Keefe and Recce, 1993; O'Keefe and Burgess, 2005). Since acute stress facilitated both types of coding (i.e., improved spatial tuning and strength of theta phase-locking), the idea that acute stress effects on hippocampal spatial coding are indeed facilitatory in nature is not far-fetched. Mechanistically, the facilitatory effects of acute stress on hippocampal coding are likely brought about by the combined action of a cocktail of neuromodulators released by stress-induced activation of sympatho-adrenal medullary (SAM)-pathways (Cadle and Zoladz, 2015; Gunn and Baram, 2017). Future studies are needed to further investigate the role of SAM-activated neuromodulation on CA1 spatial coding.

Instantaneous coupling between theta and gamma oscillations in hippocampal networks is thought to represent dynamic processing in hippocampal circuits (Buzsáki and Wang, 2012). A previous study using evoked auditory potentials also noted a decrease in gamma power following CIS and concluded that chronic stress disrupts functional connectivity within the hippocampal circuitry (Ghosh et al., 2013). The same conclusion was also reached by Passecker et al. (2011) who studied the impact of repeated exposure to photic stress on hippocampal spatial coding. Gamma oscillations route information flow in hippocampal circuits including slow CA1 gamma which reflects interactions between CA3-CA1 neuronal networks (Montgomery and Buzsáki, 2007), while fast CA1 gamma indicates CA1-MEC interactions (Colgin et al., 2009; Colgin, 2016). Our observation of decreased slow and fast gamma power following chronic, but not acute stress reflects the poor functional connectivity in hippocampal-entorhinal circuits in chronically stressed subjects. Importantly, functional connectivity was not altered after acute stress, as place maps were more informative of animal's location in space.

What factors may lead to weakened functional connectivity in hippocampal circuits in response to repeated stress? Earlier studies have reported that chronic, but not acute stress, causes dendritic shortening and debranching and synaptic loss on apical branches of pyramidal cells in areas CA3 and CA1 (Magariños and McEwen, 1995; Conrad et al., 1999; Sousa et al., 2000; Sandi et al., 2003). Hitherto, the functional consequences of these structural changes have not been well understood. Since apical dendritic branches of CA1 pyramidal cells are the loci of Schaffer collateral inputs (from CA3) and temporoammonic pathways (from the medial entorhinal cortex; MEC), chronic stress-induced CA1 dendritic shrinkage likely reflects poor information flow into CA1 circuits (Colgin et al., 2009). Knowing that CA1 SG oscillations reflect interactions between CA1 and CA3/CA2 circuitry (Colgin et al., 2009; Middleton and McHugh, 2016; Alexander et al., 2018), while FG represents the interactions between area CA1 and medial entorhinal cortical circuits (Colgin et al., 2009; Kemere et al., 2013), it is not surprising that chronic (but not acute stress) causes a decrease in SG and FG power. In addition, AMPA-dependent synaptic plasticity is implicated in modulating gamma phase-locking of pyramidal cells by altering inhibitory-excitatory balance in area CA1 (Kitanishi et al., 2015). Knowing that chronic stress alters hippocampal synaptic plasticity (Alfarez et al., 2003) and AMPA-dependent synaptic transmission in the temporoammonic-CA1 pathway (Kallarackal et al., 2013), it is likely that chronic stress-induced altered synaptic plasticity is another potential candidate underlying chronic stress phenotypes noticed in this study. Further, inhibitory neuronal activity plays a key role in the generation of gamma oscillations, as well as the phase-locking of pyramidal cells to gamma oscillations (Bartos et al., 2002; Buzsáki and Wang, 2012). Reports that chronic stress causes decreases in hippocampal PV^{+} inhibitory neuronal density by ∼20–25% (Zaletel et al., 2016; Csabai et al., 2017) suggests that decreased gamma power and altered gamma phase-locking of CA1 place cells, observed in this study, are contributed by CIS-induced weakening of inhibition. Future studies will have to assess the differential contributions of chronic stress-induced altered inhibition, synaptic plasticity and dendritic atrophy to altered place cell activity, gamma oscillations and phase-locking phenotypes observed in this study.

Inescapability along with repeatability are two key components of modern-day life stress. Therefore, the majority of animal models of chronic stress have inescapability and repeatability built into them (Chattarji et al., 2015). The immobilization stress (and the closely related restraint stress) models are particularly popular in experimental stress neurobiology research as in addition to psychological stress (involving inescapability and repeatability aspects), these stress models also exert physical stress on the subject (McEwen, 1999).

Since this study only employed immobilization stress, it is not yet clear if the changes observed in this study would be elicited by other models of stress. Thus, future studies employing two or more different animal models of chronic stress are needed to clarify if only the immobilization-related physical model of stress or any stress could differentially alter spatial coding and gamma oscillations when applied either once or repeatedly.

A decrease in gamma (30–90 Hz) power and broadening of place field size after repeated stress exposure indicates that acute and chronic stress differentially alter information coding in the CA1 subregion. In view of reports that hippocampal phase-locking is altered in neurodegenerative disease models (Booth et al., 2016; Mably et al., 2017), for which stress is a risk factor (Bisht et al., 2018), it is not surprising that we observed altered phase-locking in response to CIS. These data further add to accumulating evidence that repeated stress negatively impacts spatial coding (Kim et al., 2007; Chattarji et al., 2015; Tomar et al., 2015). Spike-LFP interactions are responsible for not only local computations within a circuit but also coordinate activity across distant but connected circuits (Buzsáki and Freeman, 2015; Harris and Gordon, 2015; Colgin, 2016; Shin and Jadhav, 2016; Makino et al., 2019). Thus, our results of altered oscillatory and place cell activity have implications for neural computations across various memory-related circuits connected to the hippocampus.

In conclusion, our results of acute stress-induced increased information content of place cells and strengthening of phase-locking to theta oscillations further support the idea that acute stress facilitates hippocampal neural computations. Based on these findings, we propose that acute and chronic stress differentially, likely opposingly, influence hippocampal information processing.

DATA AVAILABILITY STATEMENT

The raw data supporting the conclusions of this article will be made available by the authors, without undue reservation.

ETHICS STATEMENT

The animal study was reviewed and approved by RIKEN Institutional Animal Care and Use Committee.

AUTHOR CONTRIBUTIONS

AT and TM conceived the study. AT performed all experiments. AT, DP, and TM analyzed the data. AT and TM wrote the manuscript with inputs from DP. Funding provided by TM. All authors contributed to the article and approved the submitted version.

FUNDING

This work was supported by Grant-in-Aid for Scientific Research from MEXT (19H05646; TM), Grant-in-Aid for Scientific Research on Innovative Areas from MEXT (19H05233; TM), and RIKEN BSI and CBS (TM).

ACKNOWLEDGMENTS

We thank all members of the CBP laboratory for their support, the Advanced Manufacturing Support Team, RIKEN Center for Advanced Photonics for their assistance in microdrive production and Lalitha Krishnan for assistance with figure generation.

SUPPLEMENTARY MATERIAL

The Supplementary Material for this article can be found online at: https://www.frontiersin.org/articles/10.3389/fnbeh.2021.710725/full#supplementary-material.

SUPPLEMENTARY FIGURE 1 | The impact of stress on the relationship between CA1 place cell spiking vs. running speed and LFP oscillatory phase. **(A)** Coronal section of the hippocampus showing the tetrode locations (black arrows) at the CA1 pyramidal layer. **(B)** Dependence of firing rate on the speed was affected by stress (2-way mixed ANOVA: main effect of speed, $F_{(1,370)} = 1{,}424.752$, $p < 2.22 \times 10^{-16}$, main effect of group, $F_{(3,370)} = 16.666$, $p = 3.546 \times 10^{-10}$; interaction, $F_{(3,370)} = 37.866$, $p < 2.22 \times 10^{-16}$, $N = 5$ mice). On day-1, after acute stress, place cells displayed lower firing over the range of speed bins examined (PRE-Acute ($n = 95$) cells vs. POST-Acute ($n = 89$ cells), $p < 0.012$, *post hoc* Tukey's test). However, after repeated stress, the firing rate of place cells increased over the range of speed bins examined (PRE-Acute ($n = 95$ cells) vs. PRE-Chronic ($n = 101$ cells) $p < 0.003$, *post hoc* Tukey's test) and this relationship further increased after experiencing the stress on day-10 (PRE-Chronic ($n = 101$ cells). vs. POST-Chronic ($n = 88$ cells), $p < 0.0001$, *post hoc* Tukey's test). Circular histograms display the preferred phase of all place cells during theta **(C)**, FG **(D)**, and SG **(E)**. The thick line in each circular histogram depicts averaged phase across all cells.

REFERENCES

Alexander, G. M., Brown, L. Y., Farris, S., Lustberg, D., Pantazis, C., Gloss, B., et al. (2018). CA2 neuronal activity controls hippocampal low gamma and ripple oscillations. *eLife* 7:e38052. doi: 10.7554/eLife.38052

Alfarez, D. N., Joëls, M., and Krugers, H. J. (2003). Chronic unpredictable stress impairs long-term potentiation in rat hippocampal CA1 area and dentate gyrus *in vitro*. *Eur. J. Neurosci* 17, 1928–1934. doi: 10.1046/j.1460-9568.2003.02622.x

Bakkum, D. J., Radivojevic, M., Frey, U., Franke, F., Hierlemann, A., and Takahashi, H. (2014). Parameters for burst detection. *Front. Comput. Neurosci.* 7:193. doi: 10.3389/fncom.2013.00193

Bartos, M., Vida, I., Frotscher, M., Meyer, A., Monyer, H., Geiger, J. R. P., et al. (2002). Fast synaptic inhibition promotes synchronized gamma oscillations in hippocampal interneuron networks. *Proc. Natl. Acad. Sci. U S A* 99, 13222–13227. doi: 10.1073/pnas.192233099

Berens, P. (2009). CircStat: a MATLAB toolbox for circular statistics. *J. Stat. Softw.* 31, 1–21. doi: 10.18637/jss.v031.i10

Bisht, K., Sharma, K., and Tremblay, M.-È. (2018). Chronic stress as a risk factor for Alzheimer's disease: roles of microglia-mediated synaptic remodeling, inflammation and oxidative stress. *Neurobiol. Stress* 9, 9–21. doi: 10.1016/j.ynstr.2018.05.003

Booth, C. A., Witton, J., Nowacki, J., Tsaneva-Atanasova, K., Jones, M. W., Randall, A. D., et al. (2016). Altered intrinsic pyramidal neuron properties and pathway-specific synaptic dysfunction underlie aberrant hippocampal network function in a mouse model of tauopathy. *J. Neurosci.* 36, 350–363. doi: 10.1523/JNEUROSCI.2151-15.2016

Bragin, A., Jandó, G., Nádasdy, Z., Hetke, J., Wise, K., and Buzsáki, G. (1995). Gamma (40–100 Hz) oscillation in the hippocampus of the behaving rat. *J. Neurosci.* 15, 47–60. doi: 10.1523/JNEUROSCI.15-01-00047.1995

Buzsáki, G. (2010). Neural syntax: cell assemblies, synapsembles and readers. *Neuron* 68, 362–385. doi: 10.1016/j.neuron.2010.09.023

Buzsáki, G., Anastassiou, C. A., and Koch, C. (2012). The origin of extracellular fields and currents — EEG, ECoG, LFP and spikes. *Nat. Rev. Neurosci.* 13, 407–420. doi: 10.1038/nrn3241

Buzsáki, G., and Freeman, W. (2015). Editorial overview: brain rhythms and dynamic coordination. *Curr. Opin. Neurobiol.* 31, v–ix. doi: 10.1016/j.conb.2015.01.016

Buzsáki, G., and Moser, E. I. (2013). Memory, navigation and theta rhythm in the hippocampal-entorhinal system. *Nat. Neurosci.* 16, 130–138. doi: 10.1038/nn.3304

Buzsáki, G., and Wang, X.-J. (2012). Mechanisms of gamma oscillations. *Annu. Rev. Neurosci.* 35, 203–225. doi: 10.1146/annurev-neuro-062111-150444

Buzsáki, G., Buhl, D. L., Harris, K. D., Csicsvari, J., Czéh, B., and Morozov, A. (2003). Hippocampal network patterns of activity in the mouse. *Neuroscience* 116, 201–211. doi: 10.1016/s0306-4522(02)00669-3

Cadle, C. E., and Zoladz, P. R. (2015). Stress time-dependently influences the acquisition and retrieval of unrelated information by producing a memory of its own. *Front. Psychol.* 6:910. doi: 10.3389/fpsyg.2015.00910

Canolty, R. T., Edwards, E., Dalal, S. S., Soltani, M., Nagarajan, S. S., Kirsch, H. E., et al. (2006). High gamma power is phase-locked to theta oscillations in human neocortex. *Science* 313, 1626–1628. doi: 10.1126/science.1128115

Chattarji, S., Tomar, A., Suvrathan, A., Ghosh, S., and Rahman, M. M. (2015). Neighborhood matters: divergent patterns of stress-induced plasticity across the brain. *Nat. Neurosci.* 18, 1364–1375. doi: 10.1038/nn.4115

Chen, Z., Resnik, E., McFarland, J. M., Sakmann, B., and Mehta, M. R. (2011). Speed controls the amplitude and timing of the hippocampal gamma rhythm. *PLoS One* 6:e21408. doi: 10.1371/journal.pone.0021408

Chrobak, J. J., and Buzsáki, G. (1998). Gamma oscillations in the entorhinal cortex of the freely behaving rat. *J. Neurosci.* 18, 388–398. doi: 10.1523/JNEUROSCI.18-01-00388.1998

Colgin, L. L. (2016). Rhythms of the hippocampal network. *Nat. Rev. Neurosci.* 17, 239–249. doi: 10.1038/nrn.2016.21

Colgin, L. L., Denninger, T., Fyhn, M., Hafting, T., Bonnevie, T., Jensen, O., et al. (2009). Frequency of gamma oscillations routes flow of information in the hippocampus. *Nature* 462, 353–357. doi: 10.1038/nature08573

Conrad, C. D., LeDoux, J. E., Magariños, A. M., and McEwen, B. S. (1999). Repeated restraint stress facilitates fear conditioning independently of causing hippocampal CA3 dendritic atrophy. *Behav. Neurosci.* 113, 902–913. doi: 10.1037//0735-7044.113.5.902

Csabai, D., Seress, L., Varga, Z., Ábrahám, H., Miseta, A., Wiborg, O., et al. (2017). Electron microscopic analysis of hippocampal axo-somatic synapses in a chronic stress model for depression. *Hippocampus* 27, 17–27. doi: 10.1002/hipo.22650

Csicsvari, J., Hirase, H., Czurkó, A., Mamiya, A., and Buzsáki, G. (1999). Oscillatory coupling of hippocampal pyramidal cells and interneurons in the behaving Rat. *J. Neurosci.* 19, 274–287. doi: 10.1523/JNEUROSCI.19-01-00274.1999

Csicsvari, J., Jamieson, B., Wise, K. D., and Buzsáki, G. (2003). Mechanisms of gamma oscillations in the hippocampus of the behaving rat. *Neuron* 37, 311–322. doi: 10.1016/s0896-6273(02)01169-8

Fox, S. E., Wolfson, S., and Ranck, J. B., Jr (1986). Hippocampal theta rhythm and the firing of neurons in walking and urethane anesthetized rats. *Exp. Brain Res. Exp.* 62, 495–508. doi: 10.1007/BF00236028

Fries, P. (2015). Rhythms for cognition: communication through coherence. *Neuron* 88, 220–235. doi: 10.1016/j.neuron.2015.09.034

Ghosh, S., Laxmi, T. R., and Chattarji, S. (2013). Functional connectivity from the amygdala to the hippocampus grows stronger after stress. *J. Neurosci.* 33, 7234–7244. doi: 10.1523/JNEUROSCI.0638-13.2013

Goutagny, R., Gu, N., Cavanagh, C., Jackson, J., Chabot, J.-G., Quirion, R., et al. (2013). Alterations in hippocampal network oscillations and theta-gamma coupling arise before Aβ overproduction in a mouse model of Alzheimer's disease. *Eur. J. Neurosci.* 37, 1896–1902. doi: 10.1111/ejn.12233

Gunn, B. G., and Baram, T. Z. (2017). Stress and Seizures: Space, Time and Hippocampal Circuits. *Trends Neurosci.* 40, 667–679. doi: 10.1016/j.tins.2017.08.004

Harris, A. Z., and Gordon, J. A. (2015). Long-range neural synchrony in behavior. *Annu. Rev. Neurosci.* 38, 171–194. doi: 10.1146/annurev-neuro-071714-034111

Harris, K. D., Csicsvari, J., Hirase, H., Dragoi, G., and Buzsáki, G. (2003). Organization of cell assemblies in the hippocampus. *Nature* 424, 552–556. doi: 10.1038/nature01834

Harris, K. D., Henze, D. A., Csicsvari, J., Hirase, H., and Buzsáki, G. (2000). Accuracy of tetrode spike separation as determined by simultaneous intracellular and extracellular measurements. *J. Neurophysiol.* 84, 401–414. doi: 10.1152/jn.2000.84.1.401

Henckens, M. J. A. G., Hermans, E. J., Pu, Z., Joëls, M., and Fernández, G. (2009). Stressed memories: how acute stress affects memory formation in humans. *J. Neurosci.* 29, 10111–10119. doi: 10.1523/JNEUROSCI.1184-09.2009

Hussaini, S. A., Kempadoo, K. A., Thuault, S. J., Siegelbaum, S. A., and Kandel, E. R. (2011). Increased size and stability of CA1 and CA3 place fields in HCN1 knockout mice. *Neuron* 72, 643–653. doi: 10.1016/j.neuron.2011.09.007

Jadhav, S. P., Rothschild, G., Roumis, D. K., and Frank, L. M. (2016). Coordinated excitation and inhibition of prefrontal ensembles during awake hippocampal sharp-wave ripple events. *Neuron* 90, 113–127. doi: 10.1016/j.neuron.2016.02.010

Joëls, M., and Krugers, H. J. (2007). LTP after stress: up or down. *Neural Plast.* 2007:93202. doi: 10.1155/2007/93202

Jones, M. W., and Wilson, M. A. (2005). Theta rhythms coordinate hippocampal-prefrontal interactions in a spatial memory task. *PLoS Biol.* 3:e402. doi: 10.1371/journal.pbio.0030402

Jung, M. W., Wiener, S. I., and McNaughton, B. L. (1994). Comparison of spatial firing characteristics of units in dorsal and ventral hippocampus of the rat. *J. Neurosci.* 14, 7347–7356. doi: 10.1523/JNEUROSCI.14-12-07347.1994

Kallarackal, A. J., Kvarta, M. D., Cammarata, E., Jaberi, L., Cai, X., Bailey, A. M., et al. (2013). Chronic stress induces a selective decrease in AMPA receptor-mediated synaptic excitation at hippocampal temporoammonic-CA1 synapses. *J. Neurosci.* 33, 15669–15674. doi: 10.1523/JNEUROSCI.2588-13.2013

Kemere, C., Carr, M. F., Karlsson, M. P., and Frank, L. M. (2013). Rapid and continuous modulation of hippocampal network state during exploration of new places. *PLoS One* 8:e73114. doi: 10.1371/journal.pone.0073114

Kim, J. J., Lee, H. J., Welday, A. C., Song, E., Cho, J., Sharp, P. E., et al. (2007). Stress-induced alterations in hippocampal plasticity, place cells and spatial memory. *Proc. Natl. Acad. Sci. U S A* 104, 18297–18302. doi: 10.1073/pnas.0708644104

Kirby, E. D., Muroy, S. E., Sun, W. G., Covarrubias, D., Leong, M. J., Barchas, L. A., et al. (2013). Acute stress enhances adult rat hippocampal neurogenesis and activation of newborn neurons via secreted astrocytic FGF2. *eLife* 2:e00362. doi: 10.7554/eLife.00362

Kitanishi, T., Ujita, S., Fallahnezhad, M., Kitanishi, N., Ikegaya, Y., and Tashiro, A. (2015). Novelty-induced phase-locked firing to slow gamma oscillations in the hippocampus: requirement of synaptic plasticity. *Neuron* 86, 1265–1276. doi: 10.1016/j.neuron.2015.05.012

Lever, C., Kaplan, R., and Burgess, N. (2014). "The Function of Oscillations in the Hippocampal Formation," in *Space,Time and Memory in the Hippocampal Formation*, ed D. Derdikman and J. J. Knierim (Vienna: Springer), 303–350.

Lisman, J. (2005). The theta/gamma discrete phase code occuring during the hippocampal phase precession may be a more general brain coding scheme. *Hippocampus* 15, 913–922. doi: 10.1002/hipo.20121

Luksys, G., and Sandi, C. (2011). Neural mechanisms and computations underlying stress effects on learning and memory. *Curr. Opin. Neurobiol.* 21, 502–508. doi: 10.1016/j.conb.2011.03.003

Mably, A. J., Gereke, B. J., Jones, D. T., and Colgin, L. L. (2017). Impairments in spatial representations and rhythmic coordination of place cells in the 3xTg mouse model of Alzheimer's disease. *Hippocampus* 27, 378–392. doi: 10.1002/hipo.22697

MacDougall, M. J., and Howland, J. G. (2013). Acute stress and hippocampal output: exploring dorsal CA1 and subicular synaptic plasticity simultaneously in anesthetized rats. *Physiol. Rep.* 1:e00035. doi: 10.1002/phy2.35

Magariños, A. M., and McEwen, B. S. (1995). Stress-induced atrophy of apical dendrites of hippocampal CA3c neurons: involvement of glucocorticoid

secretion and excitatory amino acid receptors. *Neuroscience* 69, 89–98. doi: 10.1016/j.ceca.2021.102404

Magariños, A. M., Verdugo, J. M. G., and McEwen, B. S. (1997). Chronic stress alters synaptic terminal structure in hippocampus. *Proc. Natl. Acad. Sci. U S A* 94, 14002–14008. doi: 10.1016/j.ceca.2021.102404

Makino, Y., Polygalov, D., Bolaños, F., Benucci, A., and McHugh, T. J. (2019). Physiological signature of memory age in the prefrontal-hippocampal circuit. *Cell Rep.* 29, 3835.e5–3846.e5. doi: 10.1016/j.celrep.2019.11.075

McEwen, B. S. (1999). Stress and hippocampal plasticity. *Annu. Rev. Neurosci.* 22, 105–122. doi: 10.1146/annurev.neuro.22.1.105

McEwen, B. S., Nasca, C., and Gray, J. D. (2016). Stress effects on neuronal structure: hippocampus, amygdala and prefrontal cortex. *Neuropsychopharmacology* 41, 3–23. doi: 10.1038/npp.2015.171

McHugh, T. J., Blum, K. I., Tsien, J. Z., Tonegawa, S., and Wilson, M. A. (1996). Impaired hippocampal representation of space in CA1-specific NMDAR1 knockout mice. *Cell* 87, 1339–1349. doi: 10.1016/s0092-8674(00)81828-0

McNaughton, B. L., Barnes, C. A., and O'Keefe, J. (1983). The contributions of position, direction and velocity to single unit activity in the hippocampus of freely-moving rats. *Exp. Brain Res.* 52, 41–49. doi: 10.1007/BF00237147

Middleton, S. J., and McHugh, T. J. (2016). Silencing CA3 disrupts temporal coding in the CA1 ensemble. *Nat. Neurosci.* 19, 945–951. doi: 10.1038/nn.4311

Montgomery, S. M., and Buzsáki, G. (2007). Gamma oscillations dynamically couple hippocampal CA3 and CA1 regions during memory task performance. *Proc. Natl. Acad. Sci. U S A* 104, 14495–14500. doi: 10.1073/pnas.0701826104

O'Keefe, J. (1976). Place units in the hippocampus of the freely moving rat. *Exp. Neurol.* 51, 78–109. doi: 10.24875/ACM.21000011

O'Keefe, J., and Burgess, N. (2005). Dual phase and rate coding in hippocampal place cells: theoretical significance and relationship to entorhinal grid cells. *Hippocampus* 15, 853–866. doi: 10.24875/ACM.21000011

O'Keefe, J., and Dostrovsky, J. (1971). The hippocampus as a spatial map. Preliminary evidence from unit activity in the freely-moving rat. *Brain Res.* 34, 171–175. doi: 10.24875/ACM.21000011

O'Keefe, J., and Nadel, L. (1978). *The Hippocampus as a Cognitive Map*. Oxford: Oxford University Press.

O'Keefe, J., and Recce, M. L. (1993). Phase relationship between hippocampal place units and the EEG theta rhythm. *Hippocampus* 3, 317–330. doi: 10.24875/ACM.21000011

Passecker, J., Hok, V., Della-Chiesa, A., Chah, E., and O'Mara, S. M. (2011). Dissociation of dorsal hippocampal regional activation under the influence of stress in freely behaving rats. *Front. Behav. Neurosci.* 5:66. doi: 10.3389/fnbeh.2011.00066

Rahman, M. M., Callaghan, C. K., Kerskens, C. M., Chattarji, S., and O'Mara, S. M. (2016). Early hippocampal volume loss as a marker of eventual memory deficits caused by repeated stress. *Sci. Rep.* 6:29127. doi: 10.1038/srep29127

Rasch, M. J., Gretton, A., Murayama, Y., Maass, W., and Logothetis, N. K. (2008). Inferring spike trains from local field potentials. *J. Neurophysiol.* 99, 1461–1476. doi: 10.1152/jn.00919.2007

Resnik, E., McFarland, J. M., Sprengel, R., Sakmann, B., and Mehta, M. R. (2012). The effects of GluA1 deletion on the hippocampal population code for position. *J. Neurosci.* 32, 8952–8968. doi: 10.1523/JNEUROSCI.6460-11.2012

Salehi, B., Cordero, M. I., and Sandi, C. (2010). Learning under stress: the inverted-U-shape function revisited. *Learn. Mem.* 17, 522–530. doi: 10.1101/lm.1914110

Sandi, C., Davies, H. A., Cordero, M. I., Rodriguez, J. J., Popov, V. I., and Stewart, M. G. (2003). Rapid reversal of stress induced loss of synapses in CA3 of rat hippocampus following water maze training. *Eur. J. Neurosci.* 17, 2447–2456. doi: 10.1046/j.1460-9568.2003.02675.x

Schmitzer-Torbert, N., Jackson, J., Henze, D., Harris, K., and Redish, A. D. (2005). Quantitative measures of cluster quality for use in extracellular recordings. *Neuroscience* 131, 1–11. doi: 10.1016/j.neuroscience.2004.09.066

Schomburg, E. W., Fernández-Ruiz, A., Mizuseki, K., Berényi, A., Anastassiou, C. A., Koch, C., et al. (2014). Theta phase segregation of input-specific gamma patterns in entorhinal-hippocampal networks. *Neuron* 84, 470–485. doi: 10.1016/j.neuron.2014.08.051

Shin, J. D., and Jadhav, S. P. (2016). Multiple modes of hippocampal-prefrontal interactions in memory-guided behavior. *Curr. Opin. Neurobiol.* 40, 161–169. doi: 10.1016/j.conb.2016.07.015

Siapas, A. G., Lubenov, E. V., and Wilson, M. A. (2005). Prefrontal phase locking to hippocampal theta oscillations. *Neuron* 46, 141–151. doi: 10.1016/j.neuron.2005.02.028

Skaggs, W. E., McNaughton, B. L., Gothard, K. M., and Markus, E. J. (1993). "An information-theoretic approach to deciphering the hippocampal code," in *Advances in Neural Information Processing System*, Vol. 5, eds S. J. Hanson, J. D. Cowan, and C. L. Giles (San Mateo, CA: Morgan Kaufmann), 1030–1037.

Sousa, N., Lukoyanov, N. V., Madeira, M. D., Almeida, O. F., and Paula-Barbosa, M. M. (2000). Reorganization of the morphology of hippocampal neurites and synapses after stress-induced damage correlates with behavioral improvement. *Neuroscience* 97, 253–266. doi: 10.1016/s0306-4522(00)00050-6

Suvrathan, A., Tomar, A., and Chattarji, S. (2010). Effects of chronic and acute stress on rat behavior in the forced-swim test. *Stress* 13, 533–540. doi: 10.3109/10253890.2010.489978

Tomar, A., Polygalov, D., Chattarji, S., and McHugh, T. J. (2015). The dynamic impact of repeated stress on the hippocampal spatial map. *Hippocampus* 25, 38–50. doi: 10.1002/hipo.22348

Tomar, A., Polygalov, D., Chattarji, S., and McHugh, T. J. (2021). Stress enhances hippocampal neuronal synchrony and alters ripple-spike interaction. *Neurobiol. Stress* 14:100327. doi: 10.1016/j.ynstr.2021.100327

Tort, A. B. L., Komorowski, R., Eichenbaum, H., and Kopell, N. (2010). Measuring phase-amplitude coupling between neuronal oscillations of different frequencies. *J. Neurophysiol.* 104, 1195–1210. doi: 10.1152/jn.00106.2010

Tort, A. B. L., Komorowski, R. W., Manns, J. R., Kopell, N. J., and Eichenbaum, H. (2009). Theta-gamma coupling increases during the learning of item-context associations. *Proc. Natl. Acad. Sci. U S A* 106, 20942–20947. doi: 10.1073/pnas.0911331106

Vanderwolf, C. H. (1969). Hippocampal electrical activity and voluntary movement in the rat. *Electroencephalogr. Clin. Neurophysiol.* 26, 407–418. doi: 10.1016/0013-4694(69)90092-3

Watanabe, Y., Gould, E., and McEwen, B. S. (1992). Stress induces atrophy of apical dendrites of hippocampal CA3 pyramidal neurons. *Brain Res.* 588, 341–345. doi: 10.1016/0006-8993(92)91597-8

Yuen, E. Y., Liu, W., Karatsoreos, I. N., Feng, J., McEwen, B. S., and Yan, Z. (2009). Acute stress enhances glutamatergic transmission in prefrontal cortex and facilitates working memory. *Proc. Natl. Acad. Sci. U S A* 106, 14075–14079. doi: 10.1073/pnas.0906791106

Zaletel, I., Filipović, D., and Puškaš, N. (2016). Chronic stress, hippocampus and parvalbumin-positive interneurons: what do we know so far. *Rev. Neurosci.* 27, 397–409. doi: 10.1515/revneuro-2015-0042

Conflict of Interest: The authors declare that the research was conducted in the absence of any commercial or financial relationships that could be construed as a potential conflict of interest.

frontiers in Human Neuroscience

CASE REPORT
published: 13 August 2021
doi: 10.3389/fnhum.2021.702961

Case Report: Chronic Adaptive Deep Brain Stimulation Personalizing Therapy Based on Parkinsonian State

Asuka Nakajima[1], Yasushi Shimo[1,2], Atsuhito Fuse[1], Joji Tokugawa[3], Makoto Hishii[3], Hirokazu Iwamuro[2,4], Atsushi Umemura[2,4] and Nobutaka Hattori[5]*

[1] Department of Neurology, Juntendo University Nerima Hospital, Tokyo, Japan, [2] Department of Research and Therapeutics for Movement Disorders, School of Medicine, Juntendo University, Tokyo, Japan, [3] Department of Neurosurgery, Juntendo University Nerima Hospital, Tokyo, Japan, [4] Department of Neurosurgery, School of Medicine, Juntendo University, Tokyo, Japan, [5] Department of Neurology, School of Medicine, Juntendo University, Tokyo, Japan

We describe the case of a 51-year-old man with Parkinson's disease (PD) presenting with motor fluctuations, who received bilateral subthalamic deep brain stimulation (DBS) with an adaptive DBS (aDBS) device, Percept™ PC (Medtronic, Inc. , Minneapolis, MN). This device can deliver electrical stimulations based on fluctuations of neural oscillations of the local field potential (LFP) at the target structure. We observed that the LFP fluctuations were less evident inside the hospital than outside, while the stimulation successfully adapted to beta oscillation fluctuations during the aDBS phase without any stimulation-induced side effects. Thus, this new device facilitates condition-dependent stimulation; this new stimulation method is feasible and provides new insights into the pathophysiological mechanisms of PD.

Keywords: Parkinson's disease, adaptive deep brain stimulation, beta oscillation, local field potential, physiological biomarker

OPEN ACCESS

Edited by:
Yuichi Takeuchi,
Osaka City University, Japan

Reviewed by:
Martijn Beudel,
Amsterdam University Medical Center, Netherlands
Atsushi Nambu,
National Institute for Physiological Sciences (NIPS), Japan

***Correspondence:**
Yasushi Shimo
yshimo@juntendo.ac.jp

Specialty section:
This article was submitted to Brain Imaging and Stimulation, a section of the journal Frontiers in Human Neuroscience

Received: *30 April 2021*
Accepted: *19 July 2021*
Published: *13 August 2021*

Citation:
Nakajima A, Shimo Y, Fuse A, Tokugawa J, Hishii M, Iwamuro H, Umemura A and Hattori N (2021) Case Report: Chronic Adaptive Deep Brain Stimulation Personalizing Therapy Based on Parkinsonian State. Front. Hum. Neurosci. 15:702961. doi: 10.3389/fnhum.2021.702961

INTRODUCTION

Deep brain stimulation (DBS) is widely used to treat advanced Parkinson's disease (PD). To adapt to the stimulation parameters, adaptive DBS (aDBS) uses the local field potential (LFP) of the target structure recorded through the implanted electrodes that deliver stimulation (Little and Brown, 2014). An abnormal LFP oscillation (beta band oscillation [13–30 Hz]) is observed in the subthalamic nucleus (STN) and is modulated by levodopa (Kuhn et al., 2006) or movement (Androulidakis et al., 2008). Furthermore, the power of these beta band oscillations is correlated with the akinesia and rigidity of parkinsonism (Kuhn et al., 2006) and is considered the most promising biomarker for aDBS in PD (Bouthour et al., 2019). The aDBS system can change the current depending on the strength of the beta band oscillation, and can, therefore, overcome conventional DBS (cDBS) therapy limitations, including stimulation-induced long term side effects, such as dyskinesia (Arlotti et al., 2018) or speech deterioration (Little et al., 2016). However, to date, no studies have assessed oscillations based on the patients' conditions, such as inside or outside the hospital, for a long period. Herein, we report the differences in beta band oscillations based on the patient's circumstances.

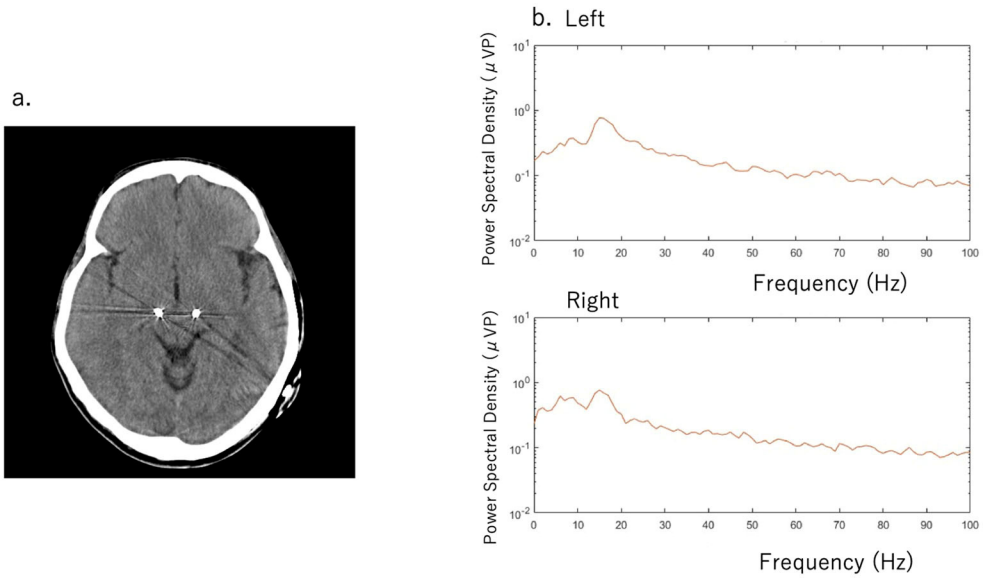

FIGURE 1 | (a) Computed tomography scan with deep brain stimulation (DBS) electrodes **(b)** Beta band oscillation was detected in the left subthalamic nucleus (STN) (16.6 Hz with 1.20 μVp) and in the right STN (1.72 μVp) during the med-off/stim-off phase. The Movement Disorder Society revision of the United Parkinson's Rating Scale (MDS-UPDRS) score was 27 points.

CASE DESCRIPTION

A 51-year-old man with a 16-year history of PD was admitted to our hospital with an indication for STN-DBS. He presented with severe motor fluctuations and off symptoms for more than 2 h a day. His routine medications included levodopa/carbidopa (800 mg, 8 times), pramipexole (1.5 mg), zonisamide (25 mg), and istradefylline (20 mg). He showed no cognitive decline according to the Japanese version of the Montreal Cognitive Assessment (26 points) and Frontal Assessment Battery (17 points) and no psychiatric symptoms (Neuropsychiatric Inventory: 10 points, Beck depression Inventory: 29 points). His Movement Disorder Society revision of the Unified Parkinson's Disease Rating Scale (MDS-UPDRS) motor score was 38 in the off-state (withdrawal of anti-parkinsonian drugs for >12 h) and four in the on-state (1 h following the administration of 1.5 times higher than usual morning levodopa dose; 150 mg/50 mg of levodopa/decarboxylase inhibitor following the drug-off phase). After these evaluations, he consented to undergo STN-DBS with Percept PC (Medtronic, Inc., Minneapolis, MN) (**Figure 1a**). Four days after surgery, we recorded the bipolar LFP activity from contacts 1–3 and 9–11 of the electrodes (contacts 0 and 8 were the most ventral contacts of the left-sided and right-sided electrodes, respectively) in the STN. The contact selected for stimulation was situated between the bipolar contact selected for recording (contact 2 or 10). We could confirm the specific beta oscillation (16.6 Hz, 1.07 μVp) in the off-state before applying the stimulation. Following a manual assessment of rigidity, finger tapping, and pronation-supination movements with DBS off, the current was increased by 1.0-mA increments starting from 0 mA to the point of reducing parkinsonian symptoms, inducing side effects, or reaching the safety limit (5 mA). Contacts that had a wider therapeutic window and improved motor outcome were selected as active contacts, after which, the stimulation was set at 0.8 mA, 60 μs, and 130 Hz, and the current was increased by 0.2–0.4 mA each day. The final cDBS was set at 2 (–) C (+), 130 Hz, 60 μs, and 2.2 mA in both hemispheres, and his levodopa equivalent daily dose was reduced from 950 mg to 550 mg (levodopa/carbidopa 400 mg, four times, pramipexole 1.5 mg). One month post-surgery, we re-evaluated his motor symptoms. The MDS-UPDRS motor score was 27 points during med-off/stim-off, and the LFP intensity values were 1.20 μVp and 1.72 μVp in the left and right STN, respectively (**Figure 1b**). The improvement observed during the off-state following surgery may be attributed to the micro lesioning effect compared to that before surgery. During the med-off /stim-on phase, the MDS-UPDRS score was 22 points while the LFP intensity was 1.24 μVp (left) and 1.00 μVp (right). After a few weeks, the patient was hospitalized with adjustments to the aDBS setting. Prior to the start of the aDBS session, we verified the presence of a significant beta peak (16.6 Hz), and initiated aDBS to establish effective stimulation parameters. We defined the stimulation threshold of aDBS as the stimulation range between the current that elicits the minimum detectable effect (minimum stimulation) on cardinal symptoms and the current that elicits side effects (maximum stimulation). The aDBS stimulation was finally set with the upper stimulation at 3.5 mA on both sides and the lower stimulations at 0.7 mA and 1.2 mA on the left and right sides, respectively. The strength of the beta oscillations that was detected at the minimum and maximum stimulations was set as "upper strength of LFP" and "lower strength of LFP," respectively. If LFP reached the upper

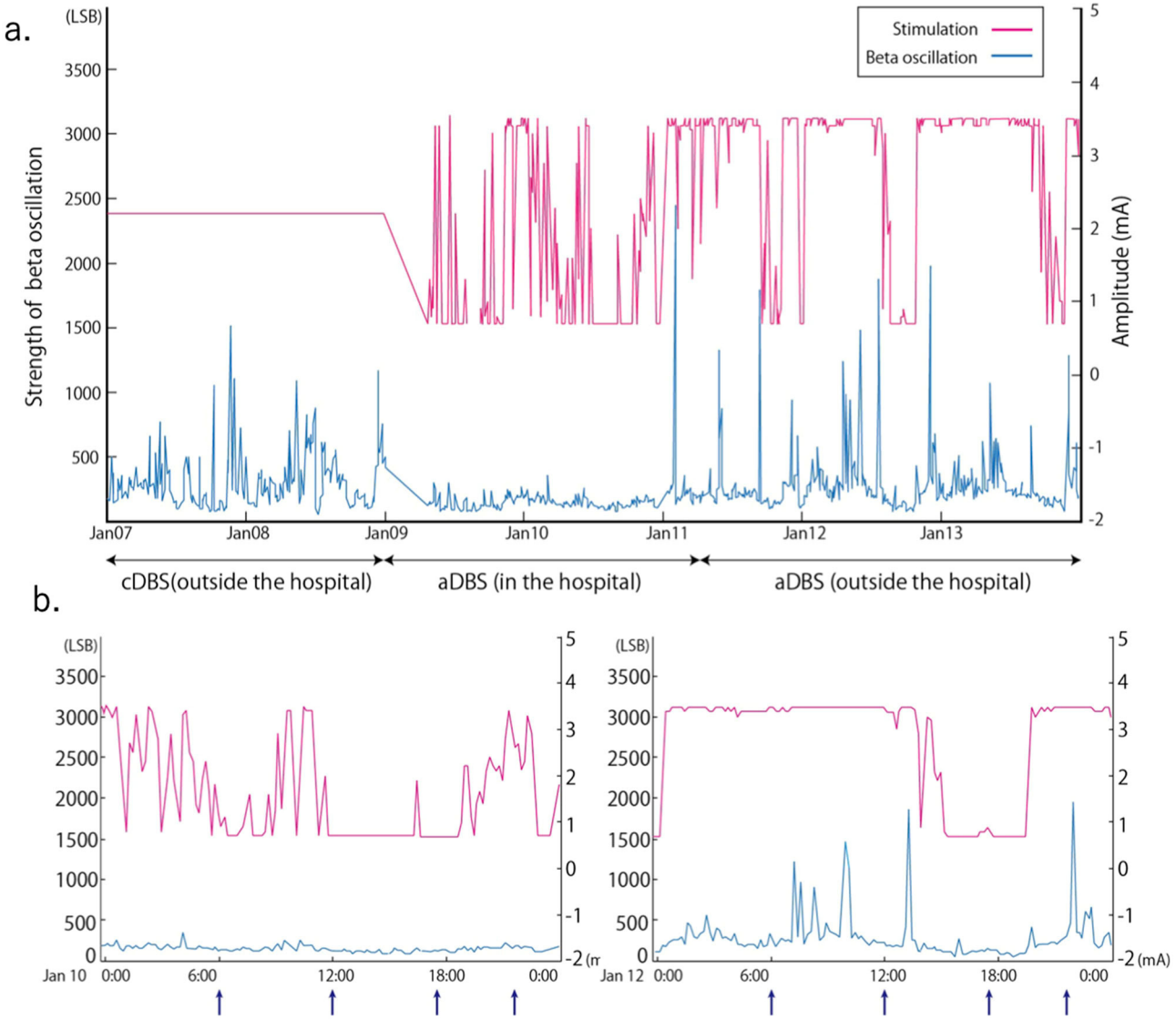

FIGURE 2 | Stimulation amplitude of adaptive deep brain stimulation (aDBS) and fluctuations in the beta band (16.60 ± 2.5 Hz) oscillation of the local field potential (LFP) over time for a long period **(a)** and a short period **(b)**. Arrow in **(b)** indicates the timing of levodopa 100 mg /carbidopa 25 mg intake. Conventional DBS (cDBS) (outside the hospital): Stimulation was set at 2.2 mA. aDBS (inside and outside the hospital): Upper stimulation was set at 3.5 mA and lower at 0.7 mA. Strength of beta oscillation = Vin (v) * Gain * 16 (LSB) / 1.2 (v) Vin: input voltage to the analog to digital convertor, Gain = 250, LSB of an analog-to-digital convertor is 16 least significant bits, The analog-to-digital convertor has a voltage range of 1.2 v.

strength of LFP, stimulation was gradually increased toward the maximum stimulation. If LFP reached the lower strength of LFP, stimulation was gradually decreased toward the minimum stimulation. The stimulation frequency and duration were set at 130 Hz and 60 μs, respectively. The patient returned to work the day following discharge. During the aDBS/outside the hospital phase, the MDS-UPDRS dyskinesia score was 0 points and 0 points during the cDBS/outside the hospital phase. The motor fluctuation score was 0 points during the aDBS phase/outside hospital phase and 3 points during the cDBS/outside the hospital phase. During the cDBS mode (outside the hospital), the mean strength of the beta band oscillation and stimulation were 291 least significant bits (LSB) and 2.2 mA, respectively. During the aDBS mode, the mean strength of the beta band oscillation and stimulation amplitude were less evident in the hospital setting (mean strength of beta oscillation: 144.6 LSB; mean amplitude of stimulation: 1.61 mA) than in the non-hospital setting (mean strength of beta oscillation: 280 LSB; mean amplitude of stimulation: 2.93 mA). The percentage exceeding the beta upper threshold was 12%, that below the threshold was 41%, and that between the threshold was 47% inside the hospital setting. Conversely, the percentage exceeding the beta upper threshold was 73%, that below the threshold was 15%, and that between the threshold was 12% in the non-hospital setting,

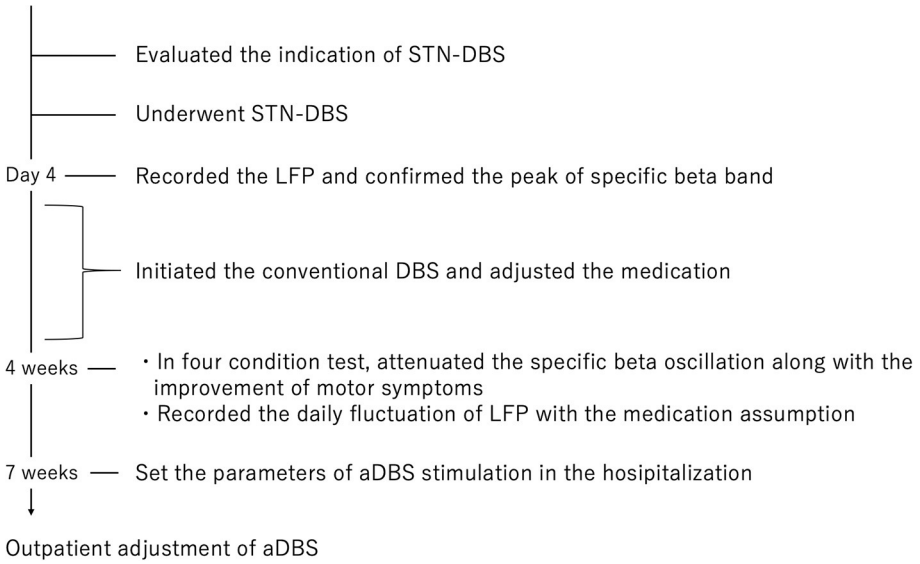

FIGURE 3 | Clinical course of the patient.

while the stimulation successfully adapted to the fluctuations of LFP during the aDBS phase (**Figure 2**). The clinical course is summarized in **Figure 3**.

DISCUSSION

Previous reports have demonstrated the feasibility of aDBS in comparison to cDBS, which continuously delivers electrical stimulation regardless of beta band oscillation fluctuations (Little et al., 2016; Arlotti et al., 2018). Previous reports have also illustrated the effectiveness of aDBS over shorter periods (Little et al., 2013; Rosa et al., 2015; Gilron et al., 2021). To the best of our knowledge, this is the first report to demonstrate that the power or fluctuation of the beta band oscillation depends on the long-term living conditions. Furthermore, beta power and stimulation amplitude were higher outside the hospital than inside, suggesting that the aDBS successfully adapted its stimulation strength based on the beta power. In our case, beta band oscillations fluctuated more while the strength of the oscillation was higher outside the hospital than inside. A high beta band oscillation strength in the STN of patients with PD is correlated with the severity of motor symptoms, especially rigidity and bradykinesia (Kuhn et al., 2006). The strength of the beta band oscillation is influenced not only by movement (Feingold et al., 2015) or dopaminergic drugs (Weinberger et al., 2006), but also by several other factors (Urrestarazu et al., 2009; Duprez et al., 2019; Benis et al., 2020). A previous study has suggested that PD motor symptoms worsened when patients were subjected to stress (van der Heide et al., 2021), while training and relaxation programs mitigated motor symptoms of PD (Reuter et al., 2011). These factors would therefore differ between in-hospital and non-hospital conditions, and may attribute to the variation in the power of beta oscillations, which ultimately affects the fluctuation and mean strength of the stimulation amplitude. No reports have demonstrated the change in beta band oscillation throughout the day and the adaptation of DBS to the change in power of the beta band oscillation. The LFP may provide important information regarding the patient's daily condition, which may serve as a biomarker of PD.

In conclusion, these findings provide new insights into the development of new generation implantable aDBS devices for the treatment of PD.

DATA AVAILABILITY STATEMENT

All datasets presented in this study are included in the article.

ETHICS STATEMENT

The patient gave written informed consent for the publication of any potentially identifiable images or data included in this article.

AUTHOR CONTRIBUTIONS

AN and YS made substantial contributions to the study concept and design, acquisition of the data, and manuscript for intellectual content. AF, JT, MH, HI, AU, and NH participated in drafting the article or critically revising it for important intellectual content. All authors gave final approval of the version to be submitted and any revised version.

FUNDING

This work was supported by the Japan Society for the Promotion of Science [YS, grant number 21K07282].

ACKNOWLEDGMENTS

The authors would like to acknowledge the contributions of specific colleagues, institutions, or agencies that aided the efforts of the authors.

REFERENCES

Androulidakis, A. G., Brucke, C., Kempf, F., Kupsch, A., Aziz, T., Ashkan, K., et al. (2008). Amplitude modulation of oscillatory activity in the subthalamic nucleus during movement. *Eur. J. Neurosci.* 27, 1277–1284. doi: 10.1111/j.1460-9568.2008.06085.x

Arlotti, M., Marceglia, S., Foffani, G., Volkmann, J., Lozano, A. M., Moro, E., et al. (2018). Eight-hours adaptive deep brain stimulation in patients with Parkinson disease. *Neurology* 90, e971–e976. doi: 10.1212/WNL.0000000000005121

Benis, D., Haegelen, C., Voruz, P., Pierce, J., Milesi, V., Houvenaghel, J. F., et al. (2020). Subthalamic nucleus oscillations during vocal emotion processing are dependent of the motor asymmetry of Parkinson's disease. *Neuroimage* 222:117215. doi: 10.1016/j.neuroimage.2020.117215

Bouthour, W., Megevand, P., Donoghue, J., Luscher, C., Birbaumer, N., and Krack, P. (2019). Biomarkers for closed-loop deep brain stimulation in Parkinson disease and beyond. *Nat. Rev. Neurol.* 15, 343–352. doi: 10.1038/s41582-019-0166-4

Duprez, J., Houvenaghel, J. F., Dondaine, T., Peron, J., Haegelen, C., Drapier, S., et al. (2019). Subthalamic nucleus local field potentials recordings reveal subtle effects of promised reward during conflict resolution in Parkinson's disease. *Neuroimage* 197, 232–242. doi: 10.1016/j.neuroimage.2019.04.071

Feingold, J., Gibson, D. J., DePasquale, B., and Graybiel, A. M. (2015). Bursts of beta oscillation differentiate post-performance activity in the striatum and motor cortex of monkeys performing movement tasks. *Proc. Natl. Acad. Sci. U. S. A.* 112, 13687–13689. doi: 10.1073/pnas.1517629112

Gilron, R., Little, S., Perrone, R., Wilt, R., de Hemptinne, C., Yaroshinsky, M. S., et al. (2021). Long-term wireless streaming of neural recordings for circuit discovery and adaptive stimulation in individuals with Parkinson's disease. *Nat. Biotechnol.* doi: 10.1038/s41587-021-00897-5. [Epub ahead of print].

Kuhn, A. A., Kupsch, A., Schneider, G. H., and Brown, P. (2006). Reduction in subthalamic 8–35 Hz oscillatory activity correlates with clinical improvement in Parkinson's disease. *Eur. J. Neurosci.* 23, 1956–1960. doi: 10.1111/j.1460-9568.2006.04717.x

Little, S., and Brown, P. (2014). The functional role of beta oscillations in Parkinson's disease. *Parkinsonism Relat. Disord.* 20, S44–S48. doi: 10.1016/S1353-8020(13)70013-0

Little, S., Pogosyan, A., Neal, S., Zavala, B., Zrinzo, L., Hariz, M., et al. (2013). Adaptive deep brain stimulation in advanced Parkinson disease. *Ann. Neurol.* 74, 449–457. doi: 10.1002/ana.23951

Little, S., Tripoliti, E., Beudel, M., Pogosyan, A., Cagnan, H., Herz, D., et al. (2016). Adaptive deep brain stimulation for Parkinson's disease demonstrates reduced speech side effects compared to conventional stimulation in the acute setting. *J. Neurol. Neurosurg. Psychiatry* 87, 1388–1389. doi: 10.1136/jnnp-2016-313518

Reuter, I., Mehnert, S., Leone, P., Kaps, M., Oechsner, M., and Engelhardt, M. (2011). Effects of a flexibility and relaxation programme, walking, and nordic walking on Parkinson's disease. *J. Aging Res.* 2011:232473. doi: 10.4061/2011/232473

Rosa, M., Arlotti, M., Ardolino, G., Cogiamanian, F., and Marceglia, S., Di Fonzo, A., et al. (2015). Adaptive deep brain stimulation in a freely moving Parkinsonian patient. *Mov. Disord.* 30, 1003–1005. doi: 10.1002/mds.26241

Urrestarazu, E., Iriarte, J., Alegre, M., Clavero, P., Rodriguez-Oroz, M. C., Guridi, J., et al. (2009). Beta activity in the subthalamic nucleus during sleep in patients with Parkinson's disease. *Mov. Disord.* 24, 254–260. doi: 10.1002/mds.22351

van der Heide, A., Speckens, A. E. M., Meinders, M. J., Rosenthal, L. S., Bloem, B. R., and Helmich, R. C. (2021). Stress and mindfulness in Parkinson's disease - a survey in 5000 patients. *NPJ Parkinsons Dis.* 7:7. doi: 10.1038/s41531-020-00152-9

Weinberger, M., Mahant, N., Hutchison, W. D., Lozano, A. M., Moro, E., Hodaie, M., et al. (2006). Beta oscillatory activity in the subthalamic nucleus and its relation to dopaminergic response in Parkinson's disease. *J. Neurophysiol.* 96, 3248–3256. doi: 10.1152/jn.00697.2006

Conflict of Interest: The authors declare that the research was conducted in the absence of any commercial or financial relationships that could be construed as a potential conflict of interest.

Publisher's Note: All claims expressed in this article are solely those of the authors and do not necessarily represent those of their affiliated organizations, or those of the publisher, the editors and the reviewers. Any product that may be evaluated in this article, or claim that may be made by its manufacturer, is not guaranteed or endorsed by the publisher.

frontiers in Computational Neuroscience

ORIGINAL RESEARCH
published: 01 September 2021
doi: 10.3389/fncom.2021.726641

An Approach for Stabilizing Abnormal Neural Activity in ADHD Using Chaotic Resonance

Sou Nobukawa[1*], *Nobuhiko Wagatsuma*[2], *Haruhiko Nishimura*[3], *Hirotaka Doho*[3,4] *and Tetsuya Takahashi*[5,6,7]

[1] Department of Computer Science, Chiba Institute of Technology, Chiba, Japan, [2] Department of Information Science, Faculty of Science, Toho University, Chiba, Japan, [3] Graduate School of Applied Informatics, University of Hyogo, Kobe, Japan, [4] Faculty of Education, Teacher Training Division, Kochi University, Kochi, Japan, [5] Research Center for Child Mental Development, Kanazawa University, Kanazawa, Japan, [6] Department of Neuropsychiatry, University of Fukui, Fukui, Japan, [7] Uozu Shinkei Sanatorium, Uozu, Japan

Reduced integrity of neural pathways from frontal to sensory cortices has been suggested as a potential neurobiological basis of attention-deficit hyperactivity disorder. Neurofeedback has been widely applied to enhance reduced neural pathways in attention-deficit hyperactivity disorder by repeated training on a daily temporal scale. Clinical and model-based studies have demonstrated that fluctuations in neural activity underpin sustained attention deficits in attention-deficit hyperactivity disorder. These aberrant neural fluctuations may be caused by the chaos–chaos intermittency state in frontal-sensory neural systems. Therefore, shifting the neural state from an aberrant chaos–chaos intermittency state to a normal stable state with an optimal external sensory stimulus, termed chaotic resonance, may be applied in neurofeedback for attention-deficit hyperactivity disorder. In this study, we applied a neurofeedback method based on chaotic resonance induced by "reduced region of orbit" feedback signals in the Baghdadi model for attention-deficit hyperactivity disorder. We evaluated the stabilizing effect of reduced region of orbit feedback and its robustness against noise from errors in estimation of neural activity. The effect of chaotic resonance successfully shifted the abnormal chaos-chaos intermittency of neural activity to the intended stable activity. Additionally, evaluation of the influence of noise due to measurement errors revealed that the efficiency of chaotic resonance induced by reduced region of orbit feedback signals was maintained over a range of certain noise strengths. In conclusion, applying chaotic resonance induced by reduced region of orbit feedback signals to neurofeedback methods may provide a promising treatment option for attention-deficit hyperactivity disorder.

Keywords: attention-deficit hyperactivity disorder, neural network, feedback control, chaos-chaos intermittency, neurofeedback

OPEN ACCESS

Edited by:
Qun Li,
University of Szeged, Hungary

Reviewed by:
Adam Ponzi,
Okinawa Institute of Science and Technology Graduate University, Japan
Ergin Yilmaz,
Bulent Ecevit University, Turkey

***Correspondence:**
Sou Nobukawa
nobukawa@cs.it-chiba.ac.jp

Received: *17 June 2021*
Accepted: *09 August 2021*
Published: *01 September 2021*

Citation:
Nobukawa S, Wagatsuma N, Nishimura H, Doho H and Takahashi T (2021) An Approach for Stabilizing Abnormal Neural Activity in ADHD Using Chaotic Resonance. Front. Comput. Neurosci. 15:726641. doi: 10.3389/fncom.2021.726641

1. INTRODUCTION

Attention-deficit hyperactivity disorder (ADHD) is a behavioral disorder underscored by inattention, impulsivity, and hyperactivity. ADHD is one of the most common neurobehavioral disorders presenting for treatment in both children and adolescents (DuPaul et al., 1998; American Psychiatric Association, 2013). ADHD symptoms may cause serious psychological and social effects on patients' quality of life (Sonuga-Barke et al., 2013). During development in particular, impulsivity and hyperactivity become less apparent, whereas attention deficits persist in most patients (Achenbach et al., 1995; Hart et al., 1995; Mick et al., 2004; Mullane et al., 2011). Therefore, efficacious treatments to ameliorate attention deficits in ADHD are a critical unmet need.

Dysfunction in dopaminergic (Tripp and Wickens, 2008; Volkow et al., 2009; Wu et al., 2012) and noradrenergic neural systems (Rowe et al., 2005; Konrad et al., 2006; van Dongen-Boomsma et al., 2010) across extensive brain regions has been well-described as a biological basis of ADHD. In particular, deficits in attention function are associated with the reduced integrity of these neural pathways (Rowe et al., 2005; Konrad et al., 2006; van Dongen-Boomsma et al., 2010) (reviewed in Swanson et al., 2007; Mueller et al., 2017). To ameliorate attention deficits in ADHD, medications that block dopamine and norepinephrine reuptake such as methylphenidate and atomoxetine are widely used (Gibbins and Weiss, 2007; Wolraich et al., 2019) and have been demonstrated to significantly improve symptoms (Stevens et al., 2013). Nevertheless, their long-term effects have not been confirmed (Molina et al., 2009; Cunill et al., 2016).

Neurofeedback is a type of biofeedback involving self-regulation of brain function. Neurofeedback involves the detection and measurement of neural activity and the generation of a recurrent signal to enable enhancement of neural pathways (Bluschke et al., 2016; Bussalb et al., 2019; Rubia et al., 2019; Van Doren et al., 2019). Based on the theory of reduced integrity of neural pathways in ADHD (Rowe et al., 2005; Konrad et al., 2006; van Dongen-Boomsma et al., 2010) (reviewed in Swanson et al., 2007; Mueller et al., 2017), neurofeedback techniques have gained increasing interest as a non-pharmacological treatment (reviewed in Hammond, 2007; Sitaram et al., 2017; Hampson et al., 2019) and have been successfully applied to chronically enhance the reduced integrity of neural pathways in ADHD (Strehl et al., 2006; Gevensleben et al., 2010; Van Doren et al., 2019).

In addition to the theory of reduced neural pathway integrity in ADHD, both clinical and model-based studies have demonstrated that fluctuations in neural activity contribute to sustained attention deficits in ADHD (Baghdadi et al., 2015; Gonen-Yaacovi et al., 2016; Michelini et al., 2018). In clinical studies, large temporal fluctuations in neural activity were observed in ADHD patients in conditions both with and without sensory stimuli (Gonen-Yaacovi et al., 2016); these fluctuations reflect sustained attention deficits in ADHD (Michelini et al., 2018). A model-based study by Baghdadi et al. showed that the temporal fluctuate behaviors in neural activity corresponded to abnormal temporal profiles of attention levels in ADHD in a neural network model consisting of excitatory and inhibitory neural populations in frontal and sensory cortices (Baghdadi et al., 2015) (this model is termed the Baghdadi model in this study). Using their model, Baghdadi et al. further ascertained that these aberrant neural fluctuations arose from chaos-chaos intermittency (CCI) (reviewed in Anishchenko et al., 2007), in which an orbit with chaotic behaviors hops among separated attractor regions (Baghdadi et al., 2015). In particular, in the case that the feedback of neural pathway from the frontal cortex and sensory cortex becomes weak, this abnormal CCI neural activity easily appears (Baghdadi et al., 2015).

According to the non-linear feedback control theory, appropriate external feedback signals permit the transition of a system state with abnormal behaviors to a stable state, typified as chaos-controlling methods (reviewed in Schöll and Schuster, 2008; Nobukawa and Nishimura, 2020). Furthermore, it is well-established that neural activity underpinning attention-related functions can be activated by external sensory stimuli (Moore et al., 2003; Perrin et al., 2004; Vandewalle et al., 2006; Newman et al., 2016). Therefore, directly stabilizing abnormal CCI with external sensory stimuli based on non-linear feedback control may serve as another approach to already established neurofeedback methods that reinforce neural pathways in ADHD (Hammond, 2007; Sitaram et al., 2017; Hampson et al., 2019). To stabilize abnormal CCI, the synchronization of CCI against an external stimulus, termed chaotic resonance (Nishimura et al., 2000) (review in Anishchenko et al. (2007); Rajasekar and Sanjuán (2016); Nobukawa and Nishimura (2020)), is a plausible solution (Nobukawa et al., 2018, 2019b, 2020a; Nobukawa and Shibata, 2019; Doho et al., 2020). This is because synchronization against an external stimulus as the intended reference of neural activity may induce the transition of dysfunctional neural activity to healthy neural activity.

As a feedback control method to induce chaotic resonance by external signals, we previously proposed the "reduced region of orbit" (RRO) feedback method, which reduces the absolute local maximum and minimum values of non-linear map functions in dynamical systems to induce attractor-merging bifurcation where chaotic resonance emerges (Nobukawa et al., 2018). This method enables the control of chaotic resonance without the need to adjust internal neural parameters (Nobukawa et al., 2018). Therefore, by broadening the scope of application of chaotic resonance, this method opened novel avenues for utilizing chaotic resonance in neural systems (Nobukawa and Shibata, 2019; Nobukawa et al., 2019b; Doho et al., 2020) (reviewed in Nobukawa and Nishimura, 2020). In particular, the RRO feedback method achieves the transition of abnormal neural activity of bipolar disorder due to imbalance of excitatory and inhibitory neural populations (E/I imbalance) to healthy state (Doho et al., 2020).

In this context, we hypothesized that the chaotic resonance produced by the RRO feedback method would promote an efficacious neurofeedback method to improve dysfunctional neural activity in ADHD under pathological impairment of neural pathway from the sensory cortex to frontal cortex as well as E/I imbalance. To verify this hypothesis, we applied

the RRO feedback method to induce chaotic resonance in the Baghdadi model for ADHD. We then evaluated the stabilizing effect of RRO feedback and its robustness against noise due to measurement errors.

2. MATERIALS AND METHODS

2.1. Frontal and Sensory Neural System Composed of Excitatory and Inhibitory Neural Populations

The pathology of ADHD involves multiple complicated neural pathways associated with dopamine (Tripp and Wickens, 2008; Volkow et al., 2009; Wu et al., 2012) and noradrenaline neural systems, which project to widespread brain regions (Rowe et al., 2005; Konrad et al., 2006; van Dongen-Boomsma et al., 2010). In particular, abnormal frontal cortical activity has been reported to cause attention dysfunction (Murias et al., 2007; Cubillo et al., 2012). The abnormal frontal activity in ADHD patients is associated with reduced inhibitory neural activity and dopaminergic activity (Barkley, 1997; Nigg, 2001; Spronk et al., 2008; Volkow et al., 2009; Loskutova et al., 2010; Fisher et al., 2011). The Baghdadi model (Baghdadi et al., 2015) is a neural network model that reproduces the abnormal temporal behavior of attention levels, focusing on the pathological imbalance between excitatory (glutamatergic) and inhibitory (GABAergic) neural populations in the frontal cortex (Barkley, 1997; Nigg, 2001; Spronk et al., 2008; Volkow et al., 2009; Loskutova et al., 2010) and dysfunction of feedback loops from the sensory cortex to the frontal cortex (Mazaheri et al., 2010; Moriyama et al., 2012).

An overview of the Baghdadi model is presented in **Figure 1**. The temporal behavior of neural activity in the frontal cortex $x(n)$ ($n = 1, 2, \cdots$) is regulated by the competition between excitatory and inhibitory neural populations (Baghdadi et al., 2015):

$$x(n+1) = F(x(n)), \tag{1}$$

$$F(x(n)) = K\left(B\tanh(w_2 x(n)) - A\tanh(w_1 x(n))\right). \tag{2}$$

Here, $F(x(n))$ represents the map function for $x(n)$. w_1 and A indicate the synaptic weights of input and output for inhibitory neural populations, respectively. w_2 and B represent the synaptic weights of input and output for excitatory neural populations, respectively. The positive and negative values of $x(n)$ correspond to neural activities in the activate and resting state for neural population, respectively. K is an attenuation coefficient of frontal neural activity. In the Baghdadi model, frontal neural dynamics $x(n)$ is determined by output from the frontal cortex: $B\tanh(w_2 x(n)) - A\tanh(w_1 x(n))$ and its feedback through sensory cortex with attenuation K in Equation (2) (Baghdadi et al., 2015). Therefore, the output term from frontal cortex is multiplied by K. The setting of $K < 1.0$ corresponds to the case of the loss of information of brain activity due to lower attention (Baghdadi et al., 2015). In this study, we used the parameter set ($w_1 = 0.2223, w_2 = 1.487$) (Baghdadi et al., 2015).

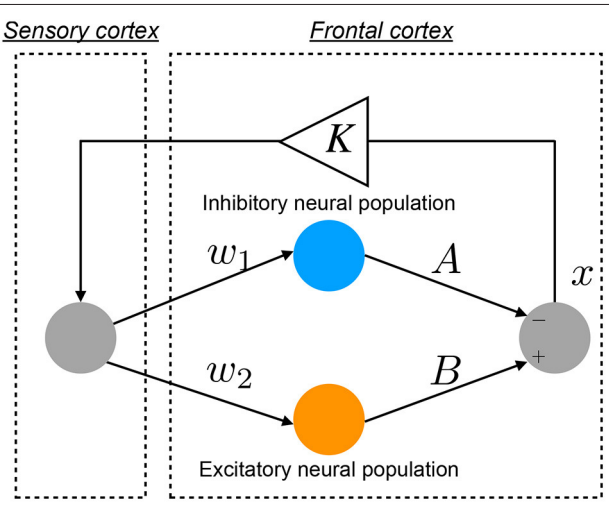

FIGURE 1 | Neural network model to reproduce the abnormal temporal behavior of attention levels, focusing on the pathological imbalance between excitatory (glutamatergic) and inhibitory (GABAergic) neural populations in the frontal cortex and dysfunction in the feedback loop from the sensory cortex to frontal cortex (Baghdadi et al., 2015).

2.2. Neural System With External Periodic Signals and RRO Feedback Signals

The conventional neurofeedback methods enhance the neural pathway by the repeated daily-temporal-scale training (Strehl et al., 2006; Gevensleben et al., 2010; Van Doren et al., 2019), which corresponds to increasing the strength of neural pathway K from the sensory cortex to the frontal cortex in the Baghdadi model. In this study, as another approach to directly stabilizing abnormal CCI, we applied the RRO feedback signals to the Baghdadi model to induce chaotic resonance for the transition of the CCI of $x(n)$ to the periodic state. A methodological chart of the system for this control method is shown in **Figure 2**. The frontal cortical neural activity $x(n)$ is controlled by RRO feedback signals $Cu(x)$ and a periodic input signal $S(n) = \alpha\sin(2\pi n/p)$, as follows:

$$x(n+1) = F(x(n)) + Cu(x(n)) + S(n), \tag{3}$$

$$u(x) = -(x - x_d)\exp(-(x - x_d)^2/(2\sigma^2)). \tag{4}$$

Here, C, x_d, and σ denote the strength of RRO feedback, the merging point of two chaotic attractors, and a parameter to regulate the region of the RRO feedback effect, respectively. $S(n)$ is an example reference of the desired neural activity corresponding to the healthy condition, i.e., the neural activity observed as lower temporal fluctuation in electroencephalogram (EEG) (Gonen-Yaacovi et al., 2016). We assumed that RRO feedback signal $Cu(x(n))$ and periodic input signal $S(n)$ are implemented by an external sensory stimulus. In this study, we utilized $x_d = 0$ and $\sigma = 1.0$, because the structure of return-map of Equation (1) has a point symmetry at around $x = 0$ with local maximum and minimum values of the map function located within the region $-\sigma < x < \sigma$ ($\sigma = 1.0$) (Nobukawa et al., 2018). For input signal $S(n)$, we used the four p periods: 4, 8, 16, and 32.

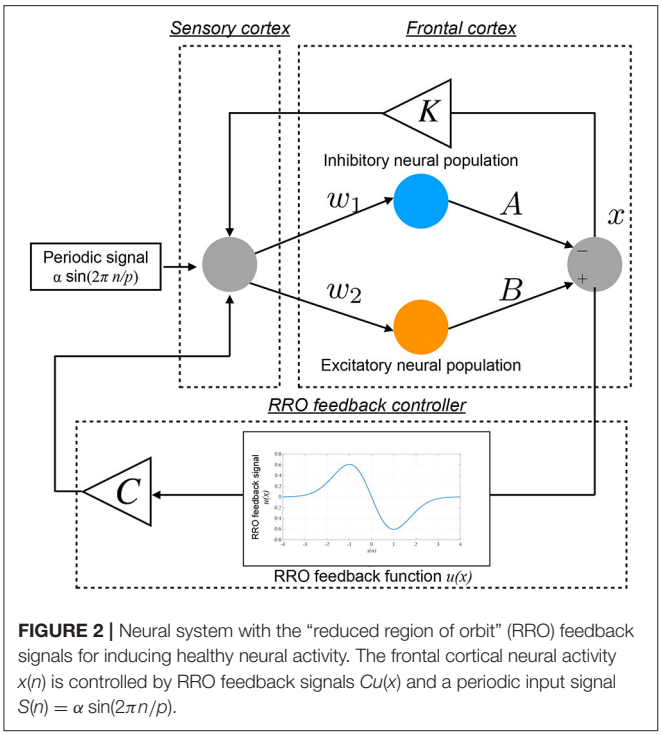

FIGURE 2 | Neural system with the "reduced region of orbit" (RRO) feedback signals for inducing healthy neural activity. The frontal cortical neural activity $x(n)$ is controlled by RRO feedback signals $Cu(x)$ and a periodic input signal $S(n) = \alpha \sin(2\pi n/p)$.

To develop the RRO feedback signals based on actual frontal neural activity, the influence of measurement errors on RRO feedback signals must be evaluated. Therefore, in addition to the noise-free condition, we evaluated the influence of measurement errors on RRO feedback signals using Gaussian white noise $\xi(n)$ (mean, 0; standard deviation, 1.0):

$$u_e(x) = -((x + D\xi(n)) - x_d)\exp(-((x + D\xi(n)) - x_d)^2/(2\sigma^2)). \quad (5)$$

Here, D exhibits the noise strength.

2.3. Evaluation Indexes

To investigate neural activity, the bifurcation diagram of $x(n)$ was used. To evaluate the chaotic state of the Baghdadi model, the Lyapunov exponent was measured by the following (Parker and Chua, 2012):

$$\lambda = \frac{1}{\tau M}\sum_{k=1}^{M}\ln\left(\frac{d^k(t_l = \tau)}{d^k(t_l = 0)}\right). \quad (6)$$

Here, $d^k(t_l = 0) = d_0$ $(k = 1, 2, \cdots, M)$ indicates M perturbed initial conditions to the orbit of $x(n)$ applied at $n = n_0 + (k-1)\tau$. The temporal development during $t_l \in [0:\tau]$ is $d^k(t_l = \tau) = (x(n) - x'(n))|_{n=n_0+k\tau}$. $x'(n)$ is an orbit-applied perturbation. The chaotic and periodic state of $x(n)$ correspond to $\lambda > 0$ and $\lambda < 0$, respectively.

The CCI of $x(n)$ is induced by attractor-merging bifurcation. To detect this bifurcation, the conditions $F(f_{\max}) + Cu(f_{\max})$ and $F(f_{\min}) + Cu(f_{\min})$ were utilized. $F(f_{\max,\min}) + Cu(f_{\max,\min}) = 0$ corresponds to the attractor-merging bifurcation point; in the attractor-merging condition, $F(f_{\max}) + Cu(f_{\max}) < 0$ and $F(f_{\min}) + Cu(f_{\min}) > 0$ are satisfied (Nobukawa et al., 2018).

To evaluate the synchronization between $x(n)$ and $S(n)$, we utilized their correlation coefficients with considering time delay τ:

$$\mathrm{Corr}(\tau) = \frac{C_{sx}(\tau)}{\sqrt{C_{ss}C_{xx}}}, \quad (7)$$

$$C_{sx}(\tau) = \langle (S(n+\tau) - \langle S\rangle)(X(n) - \langle X\rangle)\rangle, \quad (8)$$

$$C_{ss} = \langle (S(n) - \langle S\rangle)^2\rangle, \quad (9)$$

$$C_{xx} = \langle (X(n) - \langle X\rangle)^2\rangle, \quad (10)$$

where $\langle\cdot\rangle$ denotes the average in n. X represents the binarized $x(n)$ value, i.e., $X(n) = 1$ in $x(n) \geq 0$ case and $X(n) = -1$ in $x(n) < 0$ to focus on the CCI behavior. In this study, τ was set to the value for $\arg\max_\tau \mathrm{Corr}(\tau)$ in each time series of $x(n)$. $\arg\max_\tau \mathrm{Corr}(\tau)$ was assessed among ten trials using different initial conditions of $x(0)$.

To evaluate the amount of perturbation for the applied signals consisting of input periodic signal $S(n)$ and RRO feedback signal $Cu(x)$, the following perturbation was used:

$$\Theta = < S(n)^2 + (Cu(x(n)))^2 >, \quad (11)$$

where $< \cdot >$ is the average in n (Doho et al., 2020). Θ was assessed among ten trials using different initial conditions of $x(0)$.

3. RESULTS

3.1. System Behavior in Neural Network Composed of Excitatory and Inhibitory Neural Populations

ADHD is characterized by an imbalance of the reduction in inhibitory neural activity caused by dysfunction in the dopaminergic neural system (Barkley, 1997; Nigg, 2001; Spronk et al., 2008; Volkow et al., 2009; Loskutova et al., 2010) and reduced feedback strength from the sensory cortex to frontal cortex (Moriyama et al., 2012). The neural activity of ADHD detected by EEG represents larger fluctuation in comparison with healthy condition (Gonen-Yaacovi et al., 2016). Baghdadi et al. demonstrated that this larger temporal fluctuation in ADHD and smaller temporal fluctuation in healthy condition might correspond to CCI and periodic behaviors in their proposed model (Baghdadi et al., 2015). First, we demonstrated the dependence of system behavior on inhibitory synaptic strength A and attenuation coefficient of frontal neural activity K in the Baghdadi model. **Figure 3A** shows the Lyapunov exponent λ as a function of A and K and attractor-merging condition $F(f_{\max,\min}) = 0$ in the case of $(B = 5.821, w_1 = 0.2223, w_2 = 1.487)$. In the region for breaking the attractor-merging condition, i.e., $F(f_{\max}) < 0, F(f_{\min}) > 0$ and arising chaotic activity $\lambda > 0$, CCI, which corresponds to abnormal neural activity in ADHD, emerges. The system behavior under the conditions of fixed K or A values is depicted in **Figure 3B**. The left and right panels of **Figure 3B** show the dependence of system behavior on A at $K = 1.0$ and dependence on

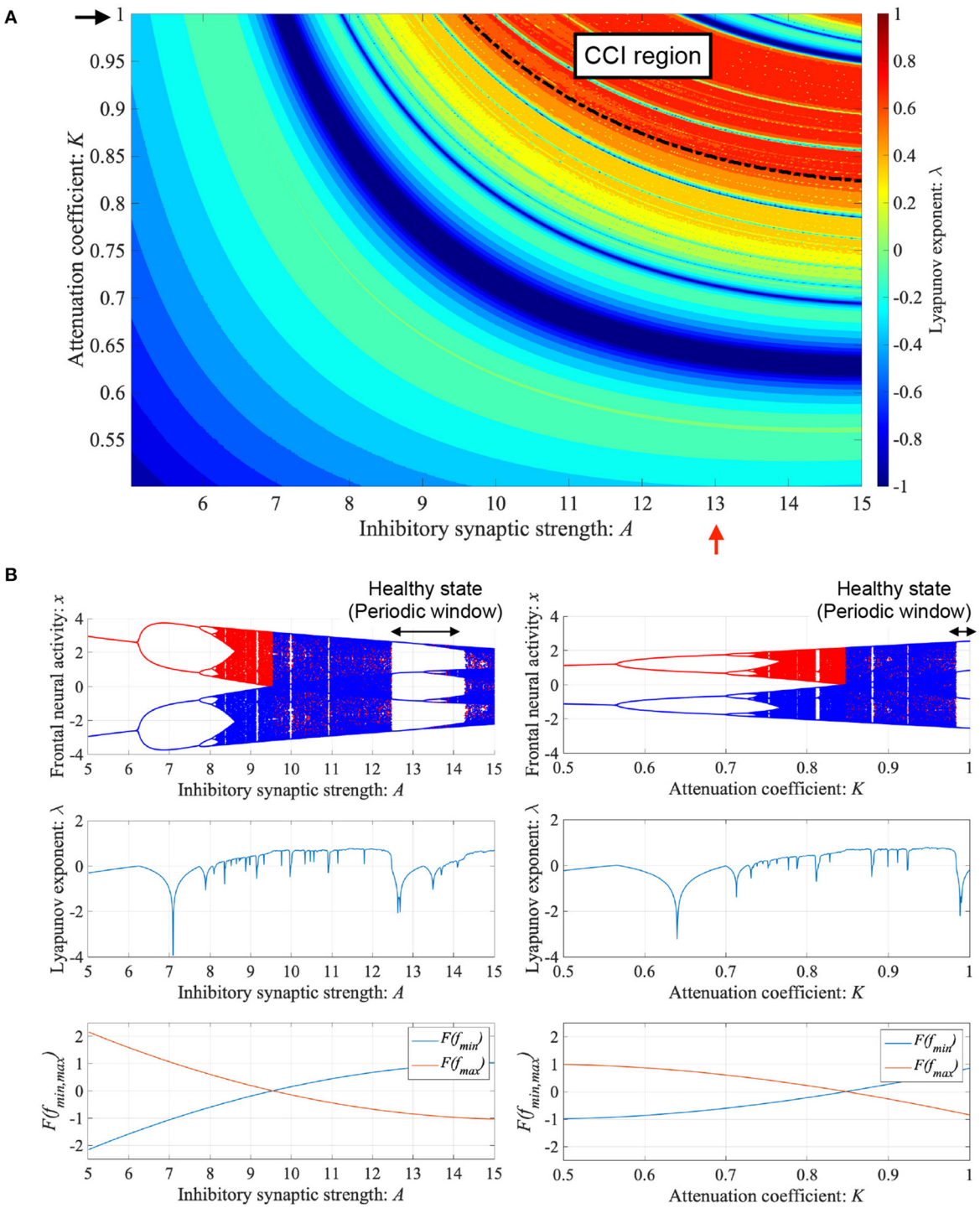

FIGURE 3 | Dependence of system behavior on inhibitory synaptic strength A and attenuation coefficient of frontal neural activity K in the Baghdadi model. **(A)** Lyapunov exponent λ as a function of A and K ($B = 5.821, w_1 = 0.2223, w_2 = 1.487$). Black dashed line indicates attractor-merging condition $F(f_{\max,\min}) = 0$. In $\lambda > 0$ in the upper region of the dashed black line satisfying the breaking attractor-merging condition, i.e., $F(f_{\max}) < 0, F(f_{\min}) > 0$, chaos-chaos intermittency (CCI), which corresponds to abnormal neural activity in ADHD, is noted. **(B)** (Left) Dependence of system behavior on A at $K = 1.0$ corresponding to K value indicated by black arrow in **(A)**. Bifurcation diagram of frontal neural activity x (top). Lyapunov exponent λ (middle). Attractor-merging condition $F(f_{\max,\min})$ (bottom). (Right) Dependence of system behavior on K at $A = 13.0$ corresponding to A value indicated by red arrow in **(A)**. Bifurcation diagram of frontal neural activity x (top). The blue and red dots indicate the cases with positive and negative initial values $x(0)$, respectively. Lyapunov exponent λ (middle). Attractor-merging condition $F(f_{\max,\min})$ (bottom). Periodic windows in $12.2 \lesssim A \lesssim 14.3$ (left panel of figure) and $0.87 \lesssim K \leq 1.0$ (right panel of figure) correspond to the regions of healthy neural activity.

K at $A = 13.0$, respectively, by the bifurcation diagram of frontal neural activity x, Lyapunov exponent λ, and attractor-merging condition $F(f_{\max,\min})$. The results demonstrate that CCI ($F(f_{\max}) < 0, F(f_{\min}) > 0, \lambda > 0$) corresponding to abnormal neural activity in ADHD, which was demonstrated by Baghdadi et al. (2015), arises in the region $9.8 \lesssim A \lesssim 12.3$ and $A \gtrsim 14.3$ in the dependence on A and $0.85 \lesssim K \lesssim 0.98$ in the dependence on K. Furthermore, in the adjacent CCI regions, periodic windows in $12.2 \lesssim A \lesssim 14.3$ and $0.87 \lesssim K \leq 1.0$, corresponding to the regions for healthy neural activity (Baghdadi et al., 2015), exist.

3.2. Controlling Abnormal Neural Activity Using the RRO Feedback Method

To control CCI behaviors caused by the abnormal imbalance in excitatory and inhibitory neural activity and the weaker feedback of neural pathways from the frontal and sensory cortices shown in **Figure 3**, RRO feedback signals were applied to the Baghdadi model according to Equations (3) and (4). **Figure 4** shows the map function of the Baghdadi model with RRO feedback signals and its orbits (see **Figure 4A**), the time-series of $x(n)$ (see **Figure 4B**) in the case with feedback strength

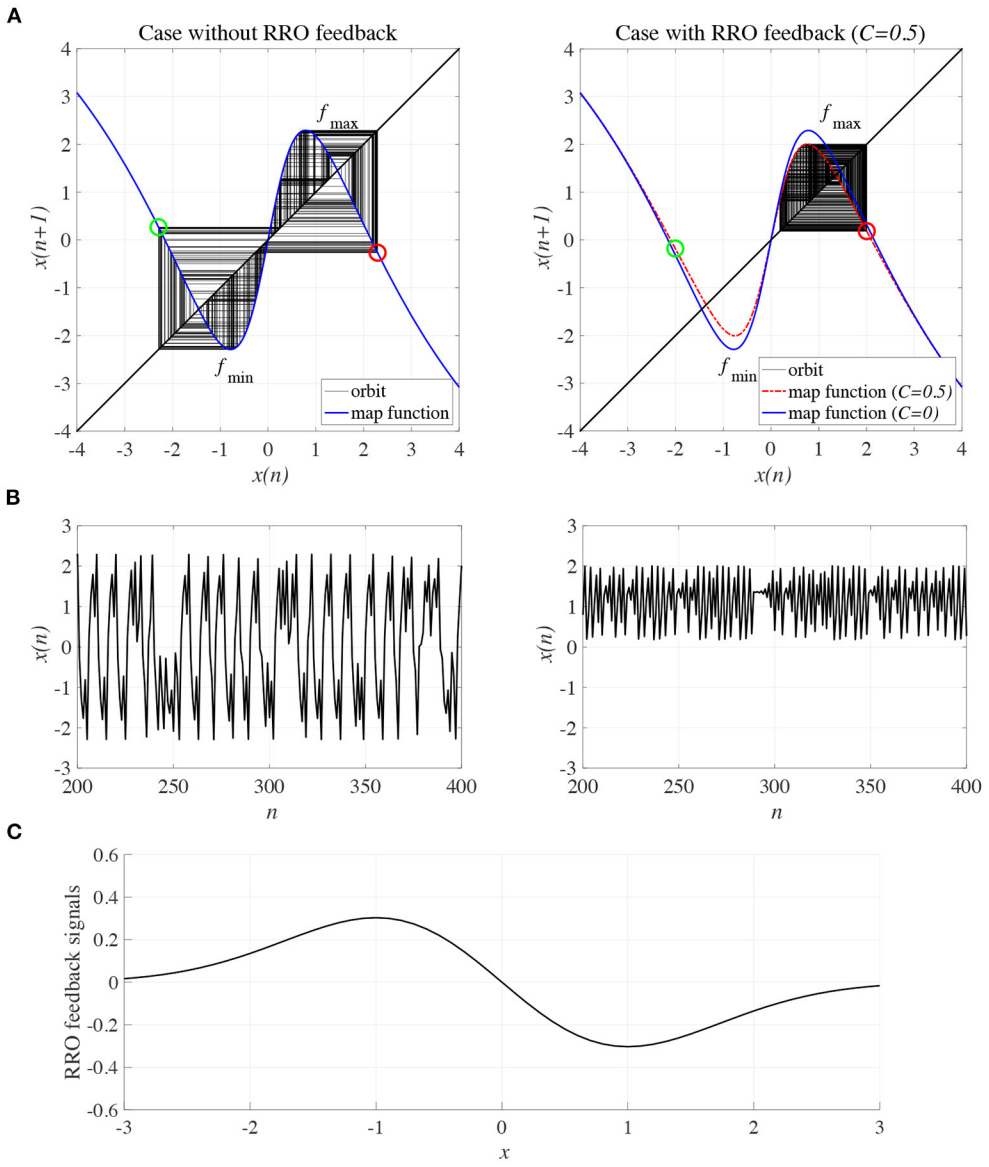

FIGURE 4 | Controlling CCI by "reduced region of orbit" (RRO) feedback signals in the Baghdadi model ($A = 13.0, B = 5.821, w_1 = 0.2223, w_2 = 1.487, K = 0.9$). **(A)** Map function of the Baghdadi model with RRO feedback signals given by Equations (3) and (4) and its orbits in the case with feedback strength $C = 0$ (left panel) and 0.5 (right panel). Red and green open circles indicate attractor-merging conditions $F(f_{\max,\min}) + Cu(f_{\max,\min})$ (red: $f_{\max}$ case, green: $f_{\min}$ case). In $C = 0$ case, the attractor-merging conditions: $F(f_{\max}) + Cu(f_{\max}) < 0$ and $F(f_{\min}) + Cu(f_{\min}) > 0$ is satisfied. While, in $C = 0.5$ case, the attractor is separated due to $F(f_{\max}) + Cu(f_{\max}) > 0$ and $F(f_{\min}) + Cu(f_{\min}) < 0$. **(B)** Time series of $x(n)$ corresponding to the orbits given by **(A)** in the case with feedback strength $C = 0$ (left panel) and 0.8 (right panel). **(C)** Profile of RRO feedback signals in the case with $C = 0.5$. CCI in the temporal behavior of $x(n)$ is restricted, and the orbit is confined to either the negative or positive regions of $x(n)$, depending on the initial value of $x(0)$.

$C = 0, 0.5$, and the profile of RRO feedback signals with its strength $C = 0.5$ (see **Figure 4C**). In the $C = 0.5$ case, the absolute local maximum/minimum values of map functions $f_{\max,\min}$ were reduced by the effect of RRO feedback signals. By this reduction, the attractor-merging condition was broken, i.e., $F(f_{\max}) + Cu(f_{\max}) > 0$ and $F(f_{\min}) + Cu(f_{\min}) < 0$; consequently, $x(n)$ stayed in either the positive or negative region of $x(n)$. The dependence of the system behavior on RRO feedback strength C was evaluated in more detail. **Figure 5** shows the bifurcation diagram of x, Lyapunov exponent λ, and attractor-merging condition $F(f_{\max,\min}) + Cu(f_{\max,\min})$ in attenuation $K = 0.89, 0.9, 0.91$. CCI behavior between positive and negative x regions ($F(f_{\max}) + Cu(f_{\max}) < 0, F(f_{\min}) + Cu(f_{\min}) > 0, \lambda > 0$) was suppressed ($F(f_{\max}) + Cu(f_{\max}) > 0, F(f_{\min}) + Cu(f_{\min}) < 0$) in the region of feedback strength $C \gtrsim 0.23, 0.28, 0.34$ in the cases with $K = 0.89, 0.9, 0.91$, respectively. Additionally, the periodic windows appear at around $C = 0.05, 0.1, 0.15$, in the cases with $K = 0.89, 0.9, 0.91$. However, the RRO feedback signal does not always produce these periodic windows with lower temporal fluctuation corresponding to healthy condition. Therefore, the external periodic input $S(n)$ is needed for the transition to the lower temporal fluctuation, which is dealt in section 3.3.

3.3. Transition of Abnormal Neural Activity to Healthy State by Synchronization

We investigated synchronization against external periodic input $S(n)$ induced by RRO feedback signals. The top panel of **Figure 6** shows the dependence of correlation coefficient $\arg\max_\tau \mathrm{Corr}(\tau)$ between $x(n)$ and a periodic input signal $S(n)$ on the strength of RRO feedback signals C ($A = 13.0, B = 5.821, w_1 = 0.2223, w_2 = 1.487, K = 0.9$) in cases of input signal strength $\alpha = 0.01, 0.15$. In $\alpha = 0.15$ and relatively long periods, such as $p = 16, 32$, the high synchronization ($\arg\max_\tau \mathrm{Corr}(\tau) \approx 0.3, 0.5$ in $p = 16, 32$, respectively) was produced by RRO feedback signals at its appropriate strength $C = 0.2$. This strength $C = 0.2$ corresponded to one for slightly weaker strength of attractor-merging bifurcation $F(f_{\max,\min}) + Cu(f_{\max,\min}) = 0$ at $C = 0.28$ under condition without the external periodic stimulus $S(n)$ (see **Figure 5**). Here, by the additional effect of $S(n)$, the attractor-merging bifurcation appears at its appropriate strength $C = 0.2$. That is, chaotic resonance was interpreted as being induced by RRO feedback signals and external stimulus $S(n)$ (Nobukawa et al., 2018, 2019b; Nobukawa and Shibata, 2019). The dependence of perturbation Θ of $S(n)$ and $Cu(x(n))$ on the strength of RRO feedback signals C is shown in the bottom panels of **Figure 6**. The results indicated that Θ to achieve the high synchronization state was significantly smaller ($\Theta \approx 0.02$) than the temporal variation in $x(n)$ shown in **Figure 5**. As the typical time-series of $x(n)$, **Figure 7** shows the time-series of $x(n)$ under RRO feedback signals $Ku(x)$ and periodic input signal $S(n)$ corresponding to the case of $\alpha = 0.15, p = 32$ in **Figure 6**. Under small RRO feedback signals ($C = 0.05$), the frequency of CCI was too high; subsequently, CCI did not synchronize to $S(n)$ (correlation coefficient $\arg\max_\tau \mathrm{Corr}(\tau) \approx 0.23$). In contrast, under the appropriate RRO feedback strength $C = 0.2$, the frequency of CCI was reduced. Using the appropriate CCI frequency, high synchronization was achieved ($\arg\max_\tau \mathrm{Corr}(\tau) \approx 0.46$). Under stronger RRO feedback strength ($C = 0.4$), CCI did not respond to $S(n)$ ($\arg\max_\tau \mathrm{Corr}(\tau) \approx 0.06$) due to the CCI frequency being too low. In addition, at $C = 0.4$ under condition without $S(n)$, the CCI does not appear (see $K = 0.9$ case in **Figure 5**), while the effect of the external stimulus $S(n)$ leads CCI, although its frequency is low in $C = 0.4$ case of **Figure 7**.

In addition to attenuation $K = 0.9$, the dependences of $\arg\max_\tau \mathrm{Corr}(\tau)$ and Θ at different levels of attenuation $K = 0.89, 0.91$ were evaluated under the same setting for $S(n)$ ($p = 32, \alpha = 0.15$ corresponding to **Figure 6B**) as shown in **Figure 8**. As the result, with increasing K, attractor merging bifurcation point shifts to smaller C values (see **Figure 5**); subsequently, the peak of $\arg\max_\tau \mathrm{Corr}(\tau)$ shifts to smaller C region. At these attenuation levels, the perturbation Θ to induce peak of $\arg\max_\tau \mathrm{Corr}(\tau)$ is significantly smaller ($\Theta \approx 0.02$) than the temporal variation in $x(n)$ shown in **Figure 5**.

When determining the RRO feedback signals estimated from actual frontal neural activity, measurement errors may affect the accuracy of producing RRO feedback signals. Therefore, we evaluated synchronization against external periodic input induced by RRO feedback signals under Gaussian white noise $D\xi(n)$ given by Equation (5). Here, RRO feedback strength C is fixed $C = 0.2$ where $\arg\max_\tau \mathrm{Corr}(\tau)$ exhibits a peak in **Figure 6B**. **Figure 9** shows the dependences of correlation coefficient $\arg\max_\tau \mathrm{Corr}(\tau)$ and perturbation Θ on noise strength D ($A = 13.0, B = 5.821, w_1 = 0.2223, w_2 = 1.487, K = 0.9, \alpha = 0.15$). The results indicated that $\arg\max_\tau \mathrm{Corr}(\tau)$ decreased with increasing noise strength D, maintaining $\Theta \approx 0.02$.

4. DISCUSSION AND CONCLUSIONS

In this study, we developed an efficacious neurofeedback method based on chaotic resonance produced by RRO feedback signals in the Baghdadi model for abnormal neural activity in ADHD with E/I imbalance and impairment of neural pathway from the sensory cortex to the frontal cortex. We confirmed that the effect of chaotic resonance shifted aberrant neural activity caused by abnormal CCI of neural activity to healthy neural activity when the frequency of reference signals was relatively low. Moreover, we evaluated the influence of noise due to measurement errors and observed that the efficiency of chaotic resonance produced by RRO feedback signals was maintained over a certain range of noise strengths.

First, we discuss why the synchronization of CCI against the external reference signal is enhanced at attractor-merging bifurcation induced by RRO feedback signals, i.e., why chaotic resonance arises. Near the attractor-merging bifurcation, the frequency of autonomous CCI is low. In this condition, the external signal plays a perturbative role and switches neural activity between positive and negative attractor regions even if its strength is weak. Therefore, the CCI induced by the external signal becomes dominant among all CCIs; subsequently, high CCI synchronization with the external signal is realized. This

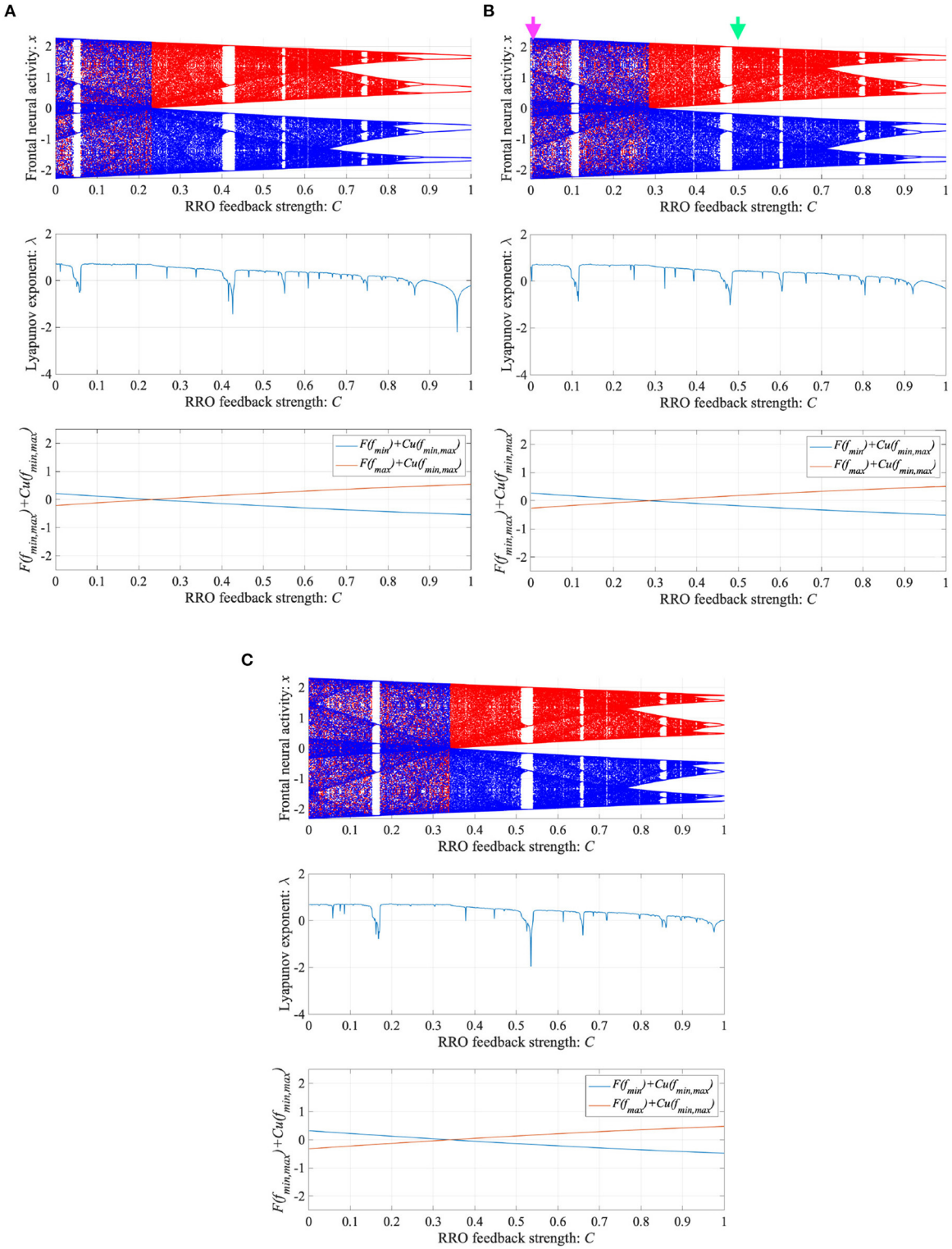

FIGURE 5 | Dependence of system behavior on RRO feedback strength C in the Baghdadi model. ($A = 13.0, B = 5.821, w_1 = 0.2223, w_2 = 1.487, K = 0.9$). Bifurcation diagram of frontal neural activity x (top). Lyapunov exponent λ (middle). Attractor-merging condition $F(f_{\max,\min}) + Cu(f_{\max,\min})$ (bottom). **(A)** Attenuation $K = 0.89$. **(B)** $K = 0.9$. Here, magenta and green arrows correspond to the parameter sets for attractor merging ($C = 0$) and separated ($C = 0.5$) conditions in **Figure 4**. **(C)** $K = 0.91$. CCI behavior between positive and negative x regions ($F(f_{\max}) + Cu(f_{\max}) < 0, F(f_{\min}) + Cu(f_{\min}) > 0, \lambda > 0$) is suppressed ($F(f_{\max}) + Cu(f_{\max}) > 0, F(f_{\min}) + Cu(f_{\min}) < 0$) in the region of feedback strength $C \gtrsim 0.23, 0.28, 0.34$ in the cases with $K = 0.89, 0.9, 0.91$, respectively.

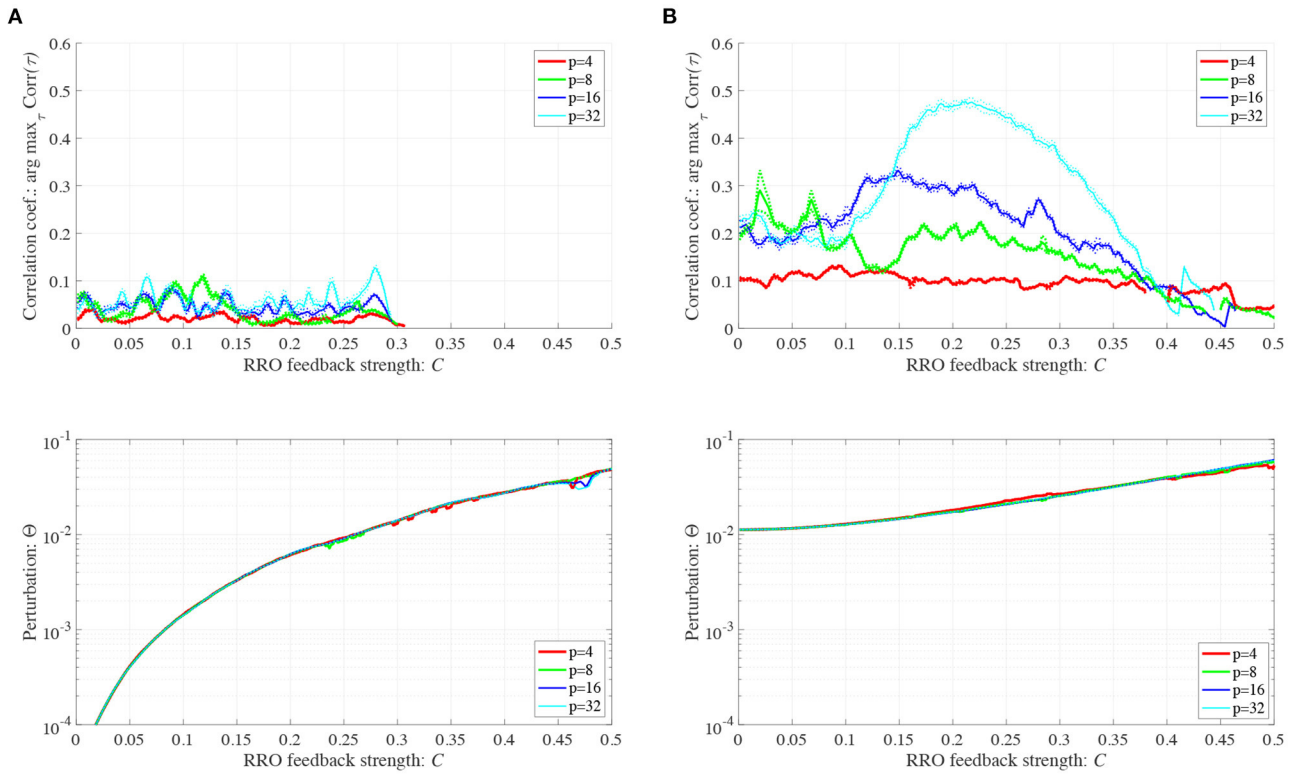

FIGURE 6 | Synchronization against external periodic input induced by RRO feedback signals. Dependence of correlation coefficient arg $\max_\tau \mathrm{Corr}(\tau)$ between $x(n)$ and a periodic input signal $S(n) = \alpha \sin(2\pi n/p)$ on the strength of RRO feedback signals C (top). Dependence of perturbation Θ on the strength of RRO feedback signals C (bottom). ($A = 13.0, B = 5.821, w_1 = 0.2223, w_2 = 1.487, K = 0.9$). **(A)** Case for the input signal strength $\alpha = 0.01$. **(B)** Case for the input signal strength $\alpha = 0.15$. Here, solid and dotted lines indicate mean and standard deviation, respectively. In $\alpha = 0.15$ and relatively long periods such as $p = 16, 32$, the high synchronization (arg $\max_\tau \mathrm{Corr}(\tau) \approx 0.3, 0.5$ in $p = 16, 32$, respectively) is produced by RRO feedback signals at its appropriate strength $C = 0.2$, where its perturbation Θ is significantly smaller ($\Theta \approx 0.02$) than the temporal variation in $x(n)$ shown in **Figure 5**.

tendency is congruent with our previous findings on chaotic resonance induced by RRO feedback signals (Nobukawa et al., 2018; Nobukawa and Shibata, 2019; Doho et al., 2020).

Then, we compare the current approach with conventional neurofeedback methods. The attractor-merging bifurcation induced by changing the synaptic weights as internal neural system parameters (see **Figure 3**) may correspond to the enhancement of neural pathways induced by the repeated daily-temporal-scale training used in conventional neurofeedback (Hammond, 2007; Baghdadi et al., 2015; Sitaram et al., 2017; Hampson et al., 2019). This is because abnormal CCI of neural activity is significantly suppressed under the condition of enhanced synaptic weights of the neural pathway from the frontal and sensory cortices, as reported in the model-based study by Baghdadi et al. (2015). In contrast, in our proposed method, the attractor-merging bifurcation produced by RRO feedback signals is realized by the external stimulus, instead of reinforcement through repeated training. Therefore, the neurofeedback method based on RRO feedback signals may facilitate the development of promising neurofeedback methods for ADHD which immediately induce the enhancement of attention in a single trial of feedback signal application.

The actual external stimulus consisting of the reference signal for intended neural activity $S(n)$ and RRO feedback signals $Cu(n)$ to the frontal and sensory cortices must be considered. Abnormal neural activity of dopaminergic neural networks in the frontal eye field (FEF) and visual area 4 (V4) are known to cause dysfunction in covert spatial attention and selective attention in ADHD (Mason et al., 2003) (reviewed in Noudoost and Moore, 2011). Moreover, microstimulation to the FEF and V4 can induce control of covert spatial attention and selective attention (reviewed in Moore et al., 2003). This microstimulation may be considered an effective candidate for the actual external stimulus in the RRO feedback method. However, from the viewpoint of neurofeedback, the application of stimuli using invasive methods is unsuitable. In this regard, the presentation of a blue-light stimulus to the eyes has been reported to affect neural activity in the brainstem, including the locus coeruleus and noradrenergic neural networks (González and Aston-Jones, 2006; Vandewalle et al., 2007). Moreover, the use of a blue-light stimulus reportedly enhances neural activity in right-hemisphere attention networks (Perrin et al., 2004; Vandewalle et al., 2006) and directivity of spatial attention (Newman et al., 2016). Therefore, the application of a blue-light stimulus

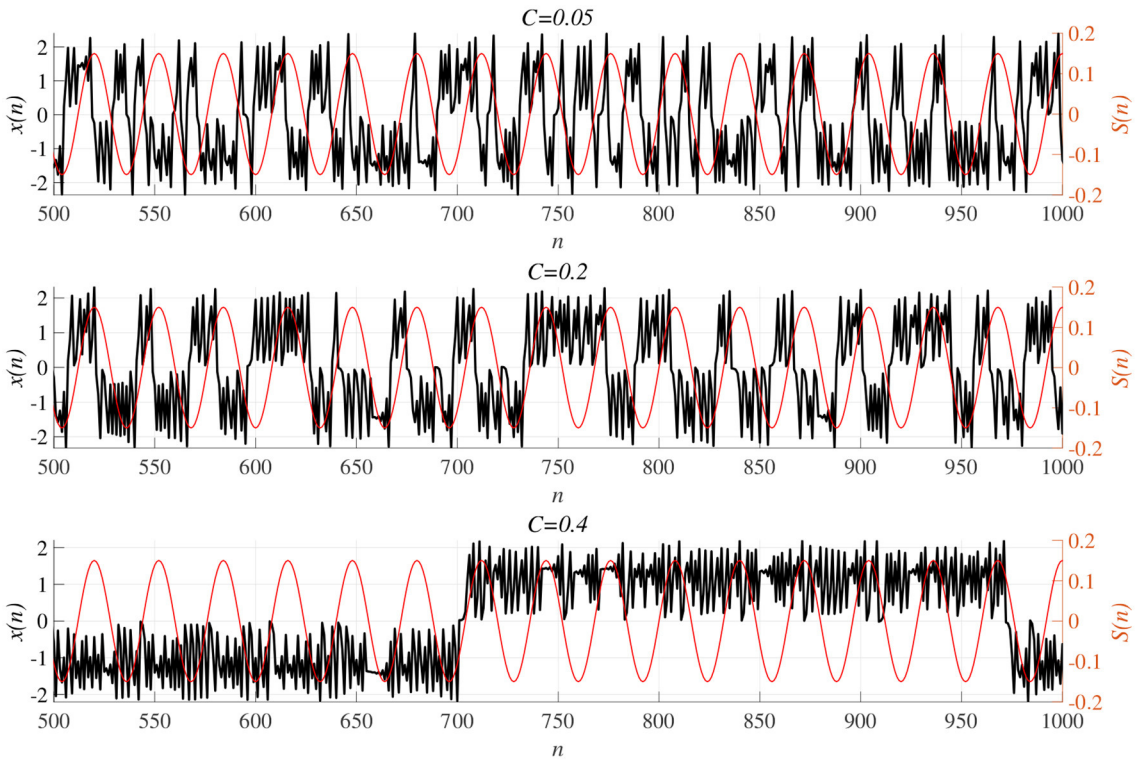

FIGURE 7 | Time-series of $x(n)$ (black line) under RRO feedback signals $Cu(x)$ and periodic input signal $S(n)$ (red line) corresponding to the case of $\alpha = 0.15, p = 32$ in **Figure 6**. **(Top)** A case of strength of RRO feedback signals $C = 0.05$. (middle) $C = 0.2$ case. **(Bottom)** $C = 0.4$ case. Under small RRO feedback signals ($C = 0.05$), the frequency of CCI is too high; subsequently, CCI does not synchronize to $S(n)$ (correlation coefficient $\arg\max_\tau \mathrm{Corr}(\tau) \approx 0.23$). In contrast, under the appropriate RRO feedback strength $C = 0.2$, the frequency of CCI is reduced. Using the appropriate CCI frequency enables high synchronization to be achieved ($\arg\max_\tau \mathrm{Corr}(\tau) \approx 0.46$). Under stronger RRO feedback strength, CCI does not respond to $S(n)$ ($\arg\max_\tau \mathrm{Corr}(\tau) \approx 0.06$) due to CCI frequency being too low.

may be a practical and effective candidate for implementing reference signals and RRO feedback signals in neurofeedback. Additionally, under the appropriate strength of RRO feedback signal, the synchronization to the reference signal can be achieved despite weak perturbation where the synchronization cannot be induced by only input of external stimulus (see **Figures 6**, **8**). Consequently, RRO feedback signals might lead the lower invasive neurofeedback method in comparison with the case using only periodic stimulation.

To reduce abnormal CCI of neural activity, a synchronization mechanism was utilized through chaotic resonance produced by the RRO feedback method in this study. In addition to this approach, alternative methods to stabilize chaotic frontal neural activity should be discussed. Studies on non-linear feedback control theory have proposed various chaos-controlling methods, typified as the Ott–Grebogi–Yorke method (Ott et al., 1990), delayed feedback method (Pyragas, 1992; Nakajima, 1997), and H_∞ control (Jiang et al., 2005) (reviewed in Schöll and Schuster, 2008). In particular, the delayed feedback method was utilized in neural systems because this method is realized by feedback terms based on previous targeted periodic p states (Rosenblum and Pikovsky, 2004; Nobukawa et al., 2020b). However, the stabilization cannot be realized under conditions of odd numbers of real characteristics of map functions multipliers, i.e., $F^p(x(n))$ where p is an odd number and F corresponds to the map functions for neural activity observed in the experimental condition (Ushio, 1996; Nakajima, 1997). To determine whether this condition is to be avoided, an estimation of the detailed profile of map multipliers is necessary (Ushio, 1996; Nakajima, 1997); generally, estimating this profile from actual neural activity is challenging. In our proposed method utilizing chaotic resonance, the estimation of map multipliers is not required.

Several limitations of this study should be considered. First, comparison of the results of model-based studies, such as this study, with empirical studies is crucial to validate the proposed method. However, in this study, we used a simple neural system consisting of frontal and sensory cortices. To reproduce the neural activity in ADHD underpinned by complex neural bases, more precise and realistic neural network models are required for comparison and validation. For these evaluations, the use of spiking neural networks to reproduce realistic neural activity (Nobukawa et al., 2019a, 2020c) enhances the physiological validity of RRO feedback methods. Additionally, the model-based study with high physiological validity is critical to develop RRO feedback signals corresponding to actual sensory stimulus. In addition to modeling studies, developing physiological external stimuli to control neural activity for attention-related functions, such as the aforementioned blue-light (González and

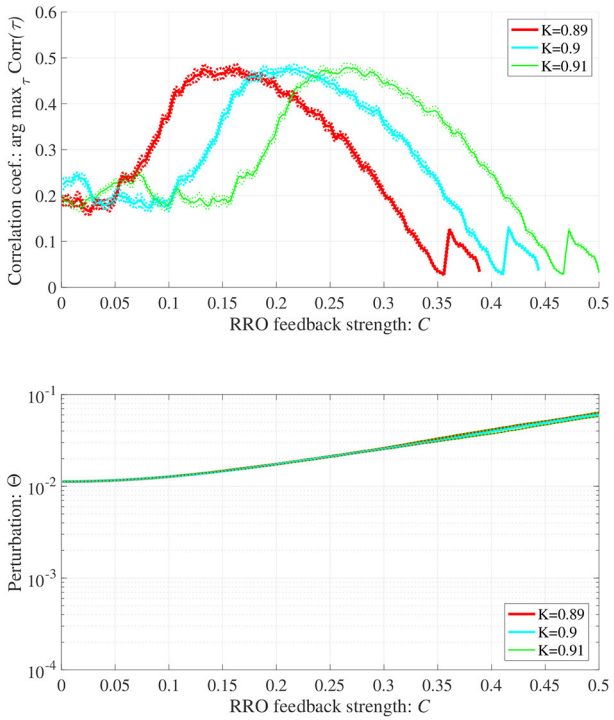

FIGURE 8 | Synchronization against external periodic input induced by RRO feedback signals in cases with attenuation $K = 0.89, 0.9, 0.91$. Dependence of correlation coefficient arg $\max_\tau \mathrm{Corr}(\tau)$ between $x(n)$ and a periodic input signal $S(n) = \alpha \sin(2\pi n/p)$ on the strength of RRO feedback signals C **(top)**. Dependence of perturbation Θ on the strength of RRO feedback signals C **(bottom)** ($A = 13.0, B = 5.821, w_1 = 0.2223, w_2 = 1.487, alpha = 0.15$, $p = 32$). Here, the solid and dotted lines indicate mean and standard deviation, respectively. With increasing K, attractor merging bifurcation point shifts to smaller C values (see **Figure 5**); subsequently, the peak of arg $\max_\tau \mathrm{Corr}(\tau)$ shifts to smaller C region. At the different attenuation levels, the perturbation Θ to induce peak of arg $\max_\tau \mathrm{Corr}(\tau)$ is significantly smaller ($\Theta \approx 0.02$) than the temporal variation in $x(n)$ shown in **Figure 5**.

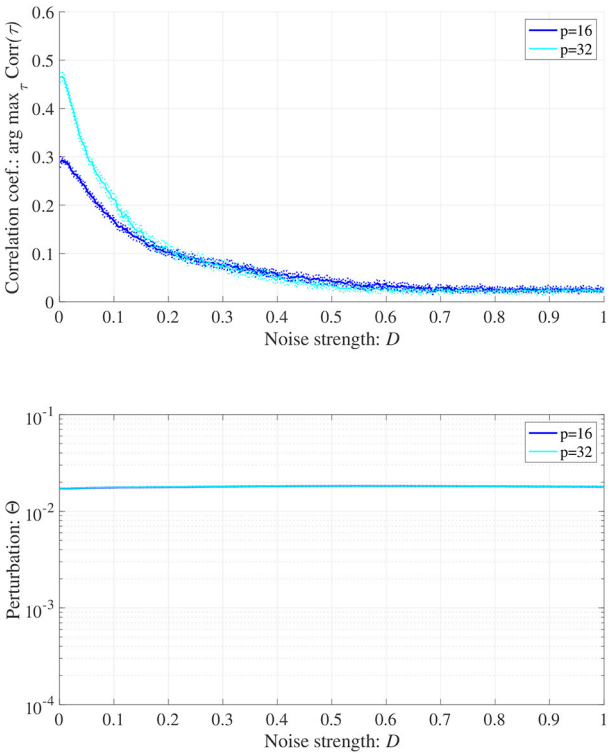

FIGURE 9 | Synchronization against external periodic input induced by RRO feedback signals under Gaussian white noise $D\xi(n)$. Here, RRO feedback strength C is fixed $C = 0.2$, where arg $\max_\tau \mathrm{Corr}(\tau)$ exhibits a peak in **Figure 6**. Dependence of correlation coefficient arg $\max_\tau \mathrm{Corr}(\tau)$ between $x(n)$ and a periodic input signal $S(n) = \alpha \sin(2\pi n/p)$ on noise strength D **(top)**. Dependence of perturbation Θ on noise strength D **(bottom)**. Here, the solid and dotted lines indicate mean and standard deviation, respectively. arg $\max_\tau \mathrm{Corr}(\tau)$ decreases with increasing noise strength D, maintaining $\Theta \approx 0.02$. ($A = 13.0, B = 5.821, w_1 = 0.2223, w_2 = 1.487, K = 0.9$, $\alpha = 0.15$).

Aston-Jones, 2006; Vandewalle et al., 2007; Newman et al., 2016), is needed to implement signals to induce chaotic resonance. Moreover, the clarification of validate range of the measurement error and its influence to the RRO feedback method in the actual experimental environment regarding the modeling results shown in **Figure 9** are relevant. In addition to measurement error, evaluation against delay in the process for producing RRO feedback signals is a crucial issue in the empirical conditions, because this delay might affect the ability of chaotic resonance. For these evaluations, the experimental studies using EEG are needed. Future research should pursue these avenues.

In conclusion, this model-based study demonstrated that chaotic resonance controlled by the RRO feedback method induced the transition of dysfunctional frontal cortical neural activity underscoring attention deficits to approximate intended healthy activity. Although several limitations exist, our proposed neurofeedback method utilizing the mechanism of chaotic resonance produced by RRO feedback signals can be practically applied as a promising treatment option for ADHD.

DATA AVAILABILITY STATEMENT

The raw data supporting the conclusions of this article will be made available by the authors, without undue reservation.

AUTHOR CONTRIBUTIONS

SN, NW, HN, and TT conceived the methods. SN analyzed the results, wrote the main manuscript text, and prepared all the figures. SN and HD conducted the experiments. All authors reviewed the manuscript.

FUNDING

This work were supported by JSPS KAKENHI for Scientific Research (C) (grant number 20K11976) to HN and Scientific Research (C) (grant number 20K07964) to TT. It was partially supported by JST CREST (grant number JPMJCR17A4).

REFERENCES

Achenbach, T. M., Howell, C. T., McConaughy, S. H., and Stanger, C. (1995). Six-year predictors of problems in a national sample of children and youth: I. Cross-informant syndromes. *J. Am. Acad. Child Adolesc. Psychiatry* 34, 336–347.

American Psychiatric Association (2013). *Diagnostic and Statistical Manual of Mental Disorders: DSM-5*.

Anishchenko, V. S., Astakhov, V., Neiman, A., Vadivasova, T., and Schimansky-Geier, L. (2007). *Nonlinear Dynamics of Chaotic and Stochastic Systems: Tutorial and Modern Developments*. Berlin; Heidelberg: Springer Science & Business Media.

Baghdadi, G., Jafari, S., Sprott, J., Towhidkhah, F., and Golpayegani, M. H. (2015). A chaotic model of sustaining attention problem in attention deficit disorder. *Commun. Nonlinear Sci. Num. Simul.* 20, 174–185. doi: 10.1016/j.cnsns.2014.05.015

Barkley, R. A. (1997). Behavioral inhibition, sustained attention, and executive functions: constructing a unifying theory of ADHD. *Psychol. Bull.* 121:65.

Bluschke, A., Broschwitz, F., Kohl, S., Roessner, V., and Beste, C. (2016). The neuronal mechanisms underlying improvement of impulsivity in ADHD by theta/beta neurofeedback. *Sci. Rep.* 6, 1–9. doi: 10.1038/srep31178

Bussalb, A., Congedo, M., Barthélemy, Q., Ojeda, D., Acquaviva, E., Delorme, R., et al. (2019). Clinical and experimental factors influencing the efficacy of neurofeedback in ADHD: a meta-analysis. *Front. Psychiatry* 10:35. doi: 10.3389/fpsyt.2019.00035

Cubillo, A., Halari, R., Smith, A., Taylor, E., and Rubia, K. (2012). A review of fronto-striatal and fronto-cortical brain abnormalities in children and adults with attention deficit hyperactivity disorder (ADHD) and new evidence for dysfunction in adults with ADHD during motivation and attention. *Cortex* 48, 194–215. doi: 10.1016/j.cortex.2011.04.007

Cunill, R., Castells, X., Tobias, A., and Capellá, D. (2016). Efficacy, safety and variability in pharmacotherapy for adults with attention deficit hyperactivity disorder: a meta-analysis and meta-regression in over 9000 patients. *Psychopharmacology* 233, 187–197. doi: 10.1007/s00213-015-4099-3

Doho, H., Nobukawa, S., Nishimura, H., Wagatsuma, N., and Takahashi, T. (2020). Transition of neural activity from the chaotic bipolar-disorder state to the periodic healthy state using external feedback signals. *Front. Comput. Neurosci.* 14:76. doi: 10.3389/fncom.2020.00076

DuPaul, G. J., Power, T. J., Anastopoulos, A. D., and Reid, R. (1998). *ADHD Rating Scale-IV: Checklists, Norms, and Clinical Interpretation*. Philadelphia, PA: Guilford Press.

Fisher, T., Aharon-Peretz, J., and Pratt, H. (2011). Dis-regulation of response inhibition in adult attention deficit hyperactivity disorder (ADHD): an ERP study. *Clin. Neurophysiol.* 122, 2390–2399. doi: 10.1016/j.clinph.2011.05.010

Gevensleben, H., Holl, B., Albrecht, B., Schlamp, D., Kratz, O., Studer, P., et al. (2010). Neurofeedback training in children with ADHD: 6-month follow-up of a randomised controlled trial. *Eur. Child Adolesc. Psychiatry* 19, 715–724. doi: 10.1007/s00787-010-0109-5

Gibbins, C., and Weiss, M. (2007). Clinical recommendations in current practice guidelines for diagnosis and treatment of ADHD in adults. *Curr. Psychiatry Rep.* 9, 420–426. doi: 10.1007/s11920-007-0055-1

Gonen-Yaacovi, G., Arazi, A., Shahar, N., Karmon, A., Haar, S., Meiran, N., et al. (2016). Increased ongoing neural variability in ADHD. *Cortex* 81, 50–63. doi: 10.1016/j.cortex.2016.04.010

González, M. M., and Aston-Jones, G. (2006). Circadian regulation of arousal: role of the noradrenergic locus coeruleus system and light exposure. *Sleep* 29, 1327–1336. doi: 10.1093/sleep/29.10.1327

Hammond, D. C. (2007). What is neurofeedback? *J. Neurother.* 10, 25–36. doi: 10.1300/J184v10n04_04

Hampson, M., Ruiz, S., and Ushiba, J. (2019). Neurofeedback. *Neuroimage* 2019:116473. doi: 10.1016/j.neuroimage.2019.116473

Hart, E. L., Lahey, B. B., Loeber, R., Applegate, B., and Frick, P. J. (1995). Developmental change in attention-deficit hyperactivity disorder in boys: a four-year longitudinal study. *J. Abnormal Child Psychol.* 23, 729–749.

Jiang, W., Guo-Dong, Q., and Bin, D. (2005). H variable universe adaptive fuzzy control for chaotic system. *Chaos Solitons Fractals* 24, 1075–1086. doi: 10.1016/j.chaos.2004.09.056

Konrad, K., Neufang, S., Hanisch, C., Fink, G. R., and Herpertz-Dahlmann, B. (2006). Dysfunctional attentional networks in children with attention deficit/hyperactivity disorder: evidence from an event-related functional magnetic resonance imaging study. *Biol. Psychiatry* 59, 643–651. doi: 10.1016/j.biopsych.2005.08.013

Loskutova, L., Kostyunina, N., and Dubrovina, N. (2010). Involvement of different types of dopamine receptors in the formation of latent inhibition of a conditioned passive avoidance reaction in rats. *Neurosci. Behav. Physiol.* 40, 483–487. doi: 10.1007/s11055-010-9285-5

Mason, D. J., Humphreys, G. W., and Kent, L. S. (2003). Exploring selective attention in ADHD: visual search through space and time. *J. Child Psychol. Psychiatry* 44, 1158–1176. doi: 10.1111/1469-7610.00204

Mazaheri, A., Coffey-Corina, S., Mangun, G. R., Bekker, E. M., Berry, A. S., and Corbett, B. A. (2010). Functional disconnection of frontal cortex and visual cortex in attention-deficit/hyperactivity disorder. *Biol. Psychiatry* 67, 617–623. doi: 10.1016/j.biopsych.2009

Michelini, G., Kitsune, V., Vainieri, I., Hosang, G. M., Brandeis, D., Asherson, P., et al. (2018). Shared and disorder-specific event-related brain oscillatory markers of attentional dysfunction in ADHD and bipolar disorder. *Brain Topogr.* 31, 672–689. doi: 10.1007/s10548-018-0625-z

Mick, E., Faraone, S. V., and Biederman, J. (2004). Age-dependent expression of attention-deficit/hyperactivity disorder symptoms. *Psychiatr. Clin.* 27, 215–224. doi: 10.1016/j.psc.2004.01.003

Molina, B. S., Hinshaw, S. P., Swanson, J. M., Arnold, L. E., Vitiello, B., Jensen, P. S., et al. (2009). The MTA at 8 years: prospective follow-up of children treated for combined-type ADHD in a multisite study. *J. Am. Acad. Child Adolesc. Psychiatry* 48, 484–500. doi: 10.1097/CHI.0b013e31819c23d0

Moore, T., Armstrong, K. M., and Fallah, M. (2003). Visuomotor origins of covert spatial attention. *Neuron* 40, 671–683. doi: 10.1016/s0896-6273(03)00716-5

Moriyama, T. S., Polanczyk, G., Caye, A., Banaschewski, T., Brandeis, D., and Rohde, L. A. (2012). Evidence-based information on the clinical use of neurofeedback for ADHD. *Neurotherapeutics* 9, 588–598. doi: 10.1007/s13311-012-0136-7

Mueller, A., Hong, D. S., Shepard, S., and Moore, T. (2017). Linking ADHD to the neural circuitry of attention. *Trends Cogn. Sci.* 21, 474–488. doi: 10.1016/j.tics.2017.03.009

Mullane, J. C., Corkum, P. V., Klein, R. M., McLaughlin, E. N., and Lawrence, M. A. (2011). Alerting, orienting, and executive attention in children with ADHD. *J. Attent. Disord.* 15, 310–320. doi: 10.1177/1087054710366384

Murias, M., Swanson, J. M., and Srinivasan, R. (2007). Functional connectivity of frontal cortex in healthy and ADHD children reflected in EEG coherence. *Cereb. Cortex* 17, 1788–1799. doi: 10.1093/cercor/bhl089

Nakajima, H. (1997). On analytical properties of delayed feedback control of chaos. *Phys. Lett. A* 232, 207–210.

Newman, D. P., Lockley, S. W., Loughnane, G. M., Martins, A. C. P., Abe, R., Zoratti, M. T., et al. (2016). Ocular exposure to blue-enriched light has an asymmetric influence on neural activity and spatial attention. *Sci. Rep.* 6:27754. doi: 10.1038/srep27754

Nigg, J. T. (2001). Is ADHD a disinhibitory disorder? *Psychol. Bull.* 127:571. doi: 10.1037/0033-2909.127.5.571

Nishimura, H., Katada, N., and Aihara, K. (2000). Coherent response in a chaotic neural network. *Neural Process. Lett.* 12, 49–58. doi: 10.1023/A:1009626028831

Nobukawa, S., Doho, H., Shibata, N., Nishimura, H., and Yamanishi, T. (2020a). Chaos-chaos intermittency synchronization controlled by external feedback signals in Chua's circuits. *IEICE Trans. Fundament. Electron. Commun. Comput. Sci.* 103, 303–312. doi: 10.1587/transfun.2019EAP1081

Nobukawa, S., and Nishimura, H. (2020). Synchronization of chaos in neural systems. *Front. Appl. Math. Stat.* 6:19. doi: 10.3389/fams.2020.00019

Nobukawa, S., Nishimura, H., Doho, H., and Takahashi, T. (2020b). Stabilizing circadian rhythms in bipolar disorder by chaos control methods. *Front. Appl. Math. Stat.* 6:562929. doi: 10.3389/fams.2020.562929

Nobukawa, S., Nishimura, H., Wagatsuma, N., Ando, S., and Yamanishi, T. (2020c). Long-tailed characteristic of spiking pattern alternation induced by log-normal excitatory synaptic distribution. *IEEE Trans. Neural Netw. Learn. Syst.* (2021) 32, 3525–3537. doi: 10.1109/TNNLS.2020.3015208

Nobukawa, S., Nishimura, H., and Yamanishi, T. (2019a). Temporal-specific complexity of spiking patterns in spontaneous activity induced by a dual complex network structure. *Sci. Rep.* 9:12749. doi: 10.1038/s41598-019-49286-8

Nobukawa, S., Nishimura, H., Yamanishi, T., and Doho, H. (2018). Controlling chaotic resonance in systems with chaos-chaos intermittency using external feedback. *IEICE Trans. Fundament. Electron. Commun. Comput. Sci.* 101, 1900–1906. doi: 10.1587/transfun.E101.A.1900

Nobukawa, S., and Shibata, N. (2019). Controlling chaotic resonance using external feedback signals in neural systems. *Sci. Rep*. 9:4990. doi: 10.1038/s41598-019-41535-0

Nobukawa, S., Shibata, N., Nishimura, H., Doho, H., Wagatsuma, N., and Yamanishi, T. (2019b). Resonance phenomena controlled by external feedback signals and additive noise in neural systems. *Sci. Rep*. 9, 1–15. doi: 10.1038/s41598-019-48950-3

Noudoost, B., and Moore, T. (2011). The role of neuromodulators in selective attention. *Trends Cogn. Sci*. 15, 585–591. doi: 10.1016/j.tics.2011.10.006

Ott, E., Grebogi, C., and Yorke, J. A. (1990). Controlling chaos. *Phys. Rev. Lett*. 64:1196.

Parker, T. S., and Chua, L. (2012). *Practical Numerical Algorithms for Chaotic Systems*. New York, NY: Springer Science & Business Media.

Perrin, F., Peigneux, P., Fuchs, S., Verhaeghe, S., Laureys, S., Middleton, B., et al. (2004). Nonvisual responses to light exposure in the human brain during the circadian night. *Curr. Biol*. 14, 1842–1846. doi: 10.1016/j.cub.2004.09.082

Pyragas, K. (1992). Continuous control of chaos by self-controlling feedback. *Phys. Lett. A* 170, 421–428.

Rajasekar, S., and Sanjuán, M. A. F. (2016). *Nonlinear Resonances*. Cham: Springer. doi: 10.1007/978-3-319-24886-8

Rosenblum, M., and Pikovsky, A. (2004). Delayed feedback control of collective synchrony: an approach to suppression of pathological brain rhythms. *Phys. Rev. E* 70:041904. doi: 10.1103/PhysRevE.70.041904

Rowe, D. L., Robinson, P., Lazzaro, I., Powles, R., Gordon, E., and Williams, L. (2005). Biophysical modeling of tonic cortical electrical activity in attention deficit hyperactivity disorder. *Int. J. Neurosci*. 115, 1273–1305. doi: 10.1080/00207450590934499

Rubia, K., Criaud, M., Wulff, M., Alegria, A., Brinson, H., Barker, G., et al. (2019). Functional connectivity changes associated with fMRI neurofeedback of right inferior frontal cortex in adolescents with ADHD. *Neuroimage* 188, 43–58. doi: 10.1016/j.neuroimage.2018.11.055

Schöll, E., and Schuster, H. G. (2008). *Handbook of Chaos Control*, Vol. 2. Weinheim: Wiley Online Library.

Sitaram, R., Ros, T., Stoeckel, L., Haller, S., Scharnowski, F., Lewis-Peacock, J., et al. (2017). Closed-loop brain training: the science of neurofeedback. *Nat. Rev. Neurosci*. 18, 86–100. doi: 10.1038/nrn.2016.164

Sonuga-Barke, E. J., Brandeis, D., Cortese, S., Daley, D., Ferrin, M., Holtmann, M., et al. (2013). Nonpharmacological interventions for ADHD: systematic review and meta-analyses of randomized controlled trials of dietary and psychological treatments. *Am. J. Psychiatry* 170, 275–289. doi: 10.1176/appi.ajp.2012.12070991

Spronk, M., Jonkman, L., and Kemner, C. (2008). Response inhibition and attention processing in 5-to 7-year-old children with and without symptoms of ADHD: an ERP study. *Clin. Neurophysiol*. 119, 2738–2752. doi: 10.1016/j.clinph.2008.09.010

Stevens, J. R., Wilens, T. E., and Stern, T. A. (2013). Using stimulants for attention-deficit/hyperactivity disorder: clinical approaches and challenges. *Primary Care Companion CNS Disord*. 15:12f01472. doi: 10.4088/PCC.12f01472

Strehl, U., Leins, U., Goth, G., Klinger, C., Hinterberger, T., and Birbaumer, N. (2006). Self-regulation of slow cortical potentials: a new treatment for children with attention-deficit/hyperactivity disorder. *Pediatrics* 118, e1530–e1540. doi: 10.1542/peds.2005-2478

Swanson, J. M., Kinsbourne, M., Nigg, J., Lanphear, B., Stefanatos, G. A., Volkow, N., et al. (2007). Etiologic subtypes of attention-deficit/hyperactivity disorder: brain imaging, molecular genetic and environmental factors and the dopamine hypothesis. *Neuropsychol. Rev*. 17, 39–59. doi: 10.1007/s11065-007-9019-9

Tripp, G., and Wickens, J. R. (2008). Research review: dopamine transfer deficit: a neurobiological theory of altered reinforcement mechanisms in ADHD. *J. Child Psychol. Psychiatry* 49, 691–704. doi: 10.1111/j.1469-7610.2007.01851.x

Ushio, T. (1996). Limitation of delayed feedback control in nonlinear discrete-time systems. *IEEE Trans. Circ. Syst. I Fundament. Theory Appl*. 43, 815–816.

van Dongen-Boomsma, M., Lansbergen, M. M., Bekker, E. M., Kooij, J. S., van der Molen, M., Kenemans, J. L., et al. (2010). Relation between resting EEG to cognitive performance and clinical symptoms in adults with attention-deficit/hyperactivity disorder. *Neurosci. Lett*. 469, 102–106. doi: 10.1016/j.neulet.2009.11.053

Van Doren, J., Arns, M., Heinrich, H., Vollebregt, M. A., Strehl, U., and Loo, S. K. (2019). Sustained effects of neurofeedback in ADHD: a systematic review and meta-analysis. *Eur. Child Adolesc. Psychiatry* 28, 293–305. doi: 10.1007/s00787-018-1121-4

Vandewalle, G., Balteau, E., Phillips, C., Degueldre, C., Moreau, V., Sterpenich, V., et al. (2006). Daytime light exposure dynamically enhances brain responses. *Curr. Biol*. 16, 1616–1621. doi: 10.1016/j.cub.2006.06.031

Vandewalle, G., Schmidt, C., Albouy, G., Sterpenich, V., Darsaud, A., Rauchs, G., et al. (2007). Brain responses to violet, blue, and green monochromatic light exposures in humans: prominent role of blue light and the brainstem. *PLoS ONE* 2:e1247. doi: 10.1371/journal.pone.0001247

Volkow, N. D., Wang, G.-J., Kollins, S. H., Wigal, T. L., Newcorn, J. H., Telang, F., et al. (2009). Evaluating dopamine reward pathway in ADHD: clinical implications. *JAMA* 302, 1084–1091. doi: 10.1001/jama.2009.1308

Wolraich, M. L., Chan, E., Froehlich, T., Lynch, R. L., Bax, A., Redwine, S. T., et al. (2019). ADHD diagnosis and treatment guidelines: a historical perspective. *Pediatrics* 144:e20191682. doi: 10.1542/peds.2019-1682

Wu, J., Xiao, H., Sun, H., Zou, L., and Zhu, L.-Q. (2012). Role of dopamine receptors in ADHD: a systematic meta-analysis. *Mol. Neurobiol*. 45, 605–620. doi: 10.1007/s12035-012-8278-5

Conflict of Interest: The authors declare that the research was conducted in the absence of any commercial or financial relationships that could be construed as a potential conflict of interest.

Publisher's Note: All claims expressed in this article are solely those of the authors and do not necessarily represent those of their affiliated organizations, or those of the publisher, the editors and the reviewers. Any product that may be evaluated in this article, or claim that may be made by its manufacturer, is not guaranteed or endorsed by the publisher.

frontiers in Systems Neuroscience

ORIGINAL RESEARCH
published: 24 September 2021
doi: 10.3389/fnsys.2021.746859

Sensory-Evoked 40-Hz Gamma Oscillation Improves Sleep and Daily Living Activities in Alzheimer's Disease Patients

Aylin Cimenser[1], Evan Hempel[1], Taylor Travers[1], Nathan Strozewski[1], Karen Martin[1], Zach Malchano[1] and Mihály Hajós[1,2]**

[1] Cognito Therapeutics, Inc., Cambridge, MA, United States, [2] Department of Comparative Medicine, Yale University School of Medicine, New Haven, CT, United States

Pathological proteins contributing to Alzheimer's disease (AD) are known to disrupt normal neuronal functions in the brain, leading to unbalanced neuronal excitatory-inhibitory tone, distorted neuronal synchrony, and network oscillations. However, it has been proposed that abnormalities in neuronal activity directly contribute to the pathogenesis of the disease, and in fact it has been demonstrated that induction of synchronized 40 Hz gamma oscillation of neuronal networks by sensory stimulation reverses AD-related pathological markers in transgenic mice carrying AD-related human pathological genes. Based on these findings, the current study evaluated whether non-invasive sensory stimulation inducing cortical 40 Hz gamma oscillation is clinically beneficial for AD patients. Patients with mild to moderate AD (n = 22) were randomized to active treatment group (n = 14; gamma sensory stimulation therapy) or to sham group (n = 8). Participants in the active treatment group received precisely timed, 40 Hz visual and auditory stimulations during eye-closed condition to induce cortical 40 Hz steady-state oscillations in 1-h daily sessions over a 6-month period. Participants in the sham group were exposed to similar sensory stimulation designed to not evoke cortical 40 Hz steady-state oscillations that are observed in the active treatment patients. During the trial, nighttime activities of the patients were monitored with continuous actigraphy recordings, and their functional abilities were measured by Alzheimer's Disease Cooperative Study – Activities of Daily Living (ADCS-ADL) scale. Results of this study demonstrated that 1-h daily therapy was well tolerated throughout the 6-month treatment period by all subjects. Patients receiving gamma sensory stimulation showed significantly reduced nighttime active periods, in contrast, to deterioration in sleep quality in sham group patients. Patients in the sham group also showed the expected, significant decline in ADCS-ADL scores, whereas patients in the gamma sensory stimulation group fully maintained their functional abilities over the 6-month period. These findings confirm the safe application of 40 Hz sensory stimulation in AD

OPEN ACCESS

Edited by:
Tatsuya Mima, Ritsumeikan University, Japan

Reviewed by:
Sumiya Shibata, Niigata University of Health and Welfare, Japan
Yu Liu, University of Tennessee Health Science Center (UTHSC), United States

***Correspondence:**
Aylin Cimenser
acimenser@cognitotx.com
Mihály Hajós
mihaly.hajos@yale.edu

Received: *25 July 2021*
Accepted: *30 August 2021*
Published: *24 September 2021*

Citation:
Cimenser A, Hempel E, Travers T, Strozewski N, Martin K, Malchano Z and Hajós M (2021) Sensory-Evoked 40-Hz Gamma Oscillation Improves Sleep and Daily Living Activities in Alzheimer's Disease Patients. Front. Syst. Neurosci. 15:746859. doi: 10.3389/fnsys.2021.746859

patients and demonstrate a high adherence to daily treatment. Furthermore, this is the first time that beneficial clinical effects of the therapy are reported, justifying expanded and longer trials to explore additional clinical benefits and disease-modifying properties of gamma sensory stimulation therapy.

Clinical Trial Registration: clinicaltrials.gov, identifier: NCT03556280.

Keywords: Alzheimer's disease, sleep, actigraphy, sensory-evoked gamma oscillation, activities of daily living

INTRODUCTION

Despite significant advances in our understanding of pathological mechanisms involved in Alzheimer's disease (AD), treatment options are still limited. AD is a progressive neurodegenerative illness with long preclinical and prodromal phases, resulting in cognitive dysfunction, behavioral abnormalities, and impaired performance of activity of daily living (Masters et al., 2015). It has been well-established that hallmarks of AD-related pathological proteins, including amyloid-β (Aβ) oligomers and hyperphosphorylated tau, disrupt normal neuronal functions in the brain, leading to unbalanced neuronal excitatory-inhibitory tone, distorted neuronal synchrony, and network oscillations (Mucke and Selkoe, 2012; Das et al., 2018). However, the probability that abnormal neuronal activity, such as hyperexcitability directly contributes to the pathogenesis of AD has recently been proposed (Canter et al., 2016; Hijazi et al., 2020). Remarkably, it has been recently demonstrated that induction of synchronized gamma oscillation of neuronal networks by optogenetic or sensory stimulation effectively halts or reverses AD-related pathology in transgenic mice carrying AD-related human pathological genes (Iaccarino et al., 2016; Adaikkan et al., 2019; Martorell et al., 2019; Zhang et al., 2020). Several mechanisms downstream to gamma-oscillations have been identified, such as activation of brain innate immune system leading to increased phagocytic activity of microglia, together with augmented vasodilation and transcytosis across the brain endothelium contributing to the removal of pathological proteins. Transgenic animals sub-chronically exposed to 40 Hz sensory stimulation also showed reduced neurodegeneration and brain atrophy, increased synaptic density, improved cognitive function, and normalized circadian rhythm (Adaikkan et al., 2019; Martorell et al., 2019; Yao et al., 2020).

Based on these experimental findings, current clinical trials are evaluating the safety and efficacy of 40 Hz audio-visual stimulation in AD patients. The present study analyzed clinical results of participants of the clinical trial Overture (NCT03556280) who received treatment during eye-closed conditions and completed the 6-month trial period (**Figure 1**). We report here safety and adherence findings together with results of nighttime activities obtained by continuous monitoring with actigraphy, and functional abilities assessed by Alzheimer's Disease Cooperative Study Activities of Daily Living (ADCS-ADL) scale (Galasko et al., 1997).

Analysis of nighttime activities has been a key importance of this study. Recent experimental findings demonstrated that 40 Hz light stimulation over 30 days period significantly reduced abnormally high activity in Aβ overproducing transgenic (APP/PS1) mice during their rest phase and normalized hypothalamic central clock function (Yao et al., 2020). Sleep disorders are more frequent and more severe in mild cognitive impairment (MCI) and AD patients compared to cognitively normal older adults (Mander et al., 2015). A cardinal complaint about sleep of these patients is excessive nocturnal awakenings. Therefore, one of the aims of our trial was to evaluate the applicability of actigraphy recordings of nighttime activities of AD patients over a long-time period, monitoring potential benefits of therapeutic intervention on sleep quality. Establishing a relatively easy and practical method for monitoring nighttime activity can be highly valuable, since accumulating clinical data demonstrate a strong, bidirectional connection between sleep disorders and disease progression in AD, indicating a vicious circle contributing to AD progression (Bubu et al., 2020; Wang and Holtzman, 2020).

In the present study, nighttime activity has been monitored daily throughout the entire 6-month study period with a wrist-worn actigraphy watch, using this data, we identified and measured durations of active periods in sleep. Although actigraphy can detect rest and active periods, cross-validation with polysomnography sleep studies has led to the generally accepted interpretation that periods of nighttime restfulness are considered a reasonable measure of sleep (Tachikawa et al., 2017; Smith et al., 2018). Furthermore, previous studies have demonstrated that for AD patients, assessment of sleep by actigraphy is more accurate and reliable than a subjective report of sleep quality due to the ease of use, passive effort, and continuous measurement (Canazei et al., 2019) and has been more directly linked to cognitive impairment (Cabanel et al., 2020). In line with these observations, recent experimental and epidemiological findings demonstrate that sleep disorders represent a risk for developing AD, and a close correlation exists between sleep abnormalities and decline in activities of daily living of AD patients (Macedo et al., 2017; Hennawy et al., 2019; Bubu et al., 2020). Therefore, in addition of monitoring nighttime activities, functional abilities of patients were assessed by the (ADCS-ADL) scale (Galasko et al., 1997).

MATERIALS AND METHODS

Patients and Study Design

The objective of the present study was to evaluate the effects of daily, 1-h 40 Hz sensory stimulation over a 6-month period on sleep quality and daily living activities in mild to moderate AD

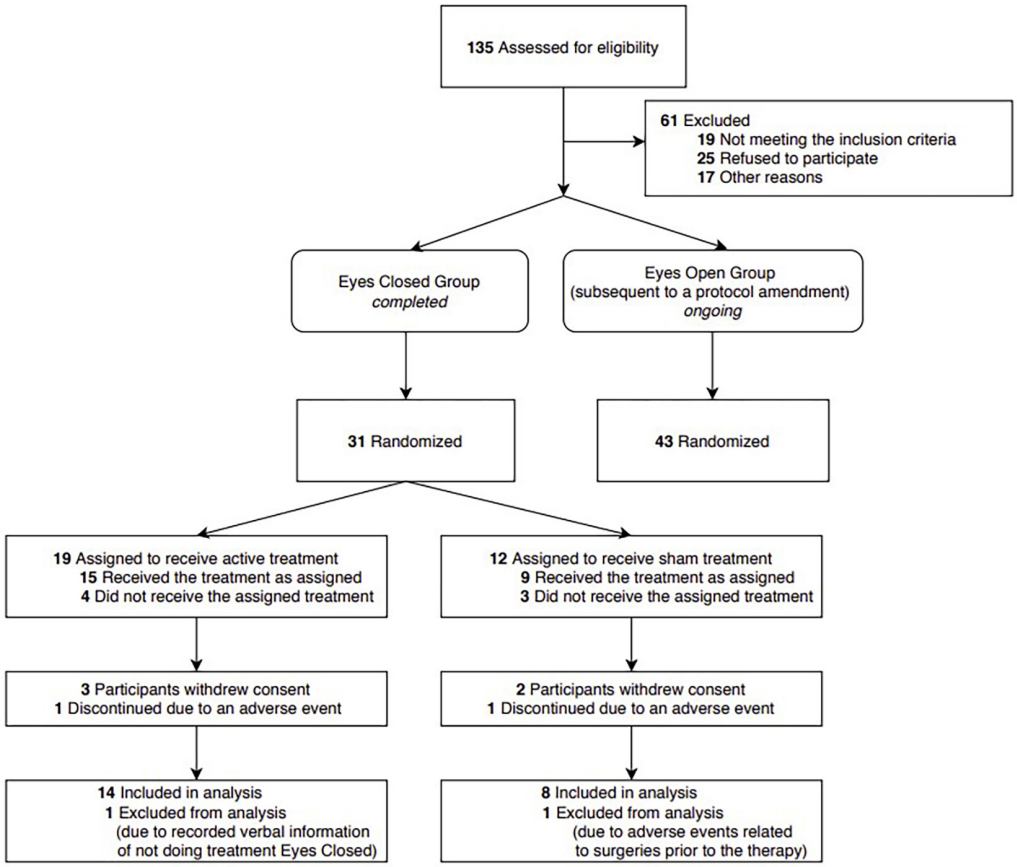

FIGURE 1 | CONSORT flow diagram and study design. Current analysis included patients receiving treatment during eyes-closed condition and completed the 6-month trial, including all patients in the treatment and sham groups. Patients not included in this report are currently receiving therapy during the eyes-open condition in the on-going trial.

patients. Patients included in this analysis formed a subgroup of patients enrolled in, and completed an ongoing Phase I/II randomized, controlled single-blind clinical trial[1]. Patients gave written informed consent, and they were randomized to treatment or sham groups (**Figure 1**, CONSORT Flow Diagram and Study Design).

Patients included in the present analysis (n = 22) were clinically diagnosed having mild to moderate AD and were under the care of their care neurologist. Inclusion criteria were age of 55 years or older, Mini-Mental State Examination (MMSE) score 14–26 and participation of a caregiver, whereas exclusion criteria included profound hearing or visual impairment, seizure disorder, or implantable, non-MR compatible devices. Patients on AD medication therapy with acetylcholine esterase inhibitors (donepezil, rivastigmine) could enroll, but their dosing were maintained the same during the trial. Use of memantine was not permitted during the study. Participants were asked about their medications every 4 weeks. In the treatment group 50% of participants and the sham group 75% of participants reported using donepezil during the study. One participant in the treatment group reported using rivastigmine. Among the participants who were studied in the sleep analysis, only one participant reported using sleep medication. This participant was in the sham group and reported using melatonin. Demographic and clinical characteristics of patients are given in **Table 1**. Patients in active treatment group (n = 14; Gamma sensory stimulation therapy) received precisely timed, 40 Hz visual and auditory stimulations during eye-closed condition to induce cortical 40 Hz steady-state oscillations in 1-h daily sessions over a 6-month period. Patients in the sham group (n = 8) were exposed to sensory stimulation at a high frequency that has been previously shown to not evoke cortical steady-state oscillations at stimulus frequency (Herrmann, 2001). Patients were not required to do the treatment at the same time but were encouraged to do it in the morning hours. All 22 patients completed the 6-month trial.

Gamma Sensory Stimulation Device

The gamma sensory stimulation device is a therapeutic system developed by Cognito Therapeutics, Inc., that includes a handheld controller, an eye-set for visual stimulation, and headphones for auditory stimulation, that work together to

[1]https://clinicaltrials.gov/ct2/show/NCT03556280

TABLE 1 | Demographic and clinical characteristics of patients at the initial assessment.

Characteristic	Treatment group (*N* = 14)	Sham group (*N* = 8)
Demographics		
Age in years, mean ± SD	66.5 ± 8.0	73.5 ± 6.6
Gender, no (%)		
Female	10 (71)	5 (63)
Male	4 (29)	3 (37)
Race and Ethnicity, no (%)		
White	14 (100)	8 (100)
Hispanic or Latino	1 (7)	0 (0)
APOE4 status, no (%)		
Non-carrier	5 (36)	3 (37.5)
Heterozygous	7 (50)	4 (50)
Homozygous	1 (7)	1 (12.5)
Ambiguous*	1 (7)	NONE
Cognitive assessment		
MMSE score†, mean ± SD	19.9 ± 2.8	18.5 ± 2.7
Functional assessment		
ADCS-ADL score‡, mean ± SD	61.8 ± 9.1	65.0 ± 10.4

**Gs270: [rs429358(C; T), rs7412(C; T)]. Likely lo be heterozygous (APOE E2/E4) but non-carrier (APOE4 E1/E3) possibility exits.*

†Mini-Mental State Examination (MMSE) scores range between 0 and 30, higher scores indicating better cognitive performance.

‡Alzheimer's Disease Cooperative Study – Activities of Daily Living (ADCS-ADL) scores range between 0 and 78, higher scores indicating better functioning.

deliver precisely timed, non-invasive 40 Hz stimulation to induce steady-state gamma brainwave activity. Stimulation output parameters are determined and verified by a physician based on both patient-reported comfort information and in-clinic electroencephalography (EEG) evaluation. The Gamma sensory stimulation device is then configured to the determined settings, and all subsequent use is within this predefined operating range. Once prescribed, the patient uses the device at home for daily sessions lasting 1 h. The on-off periods of the visual stimulation are perceivable by the patient but not disruptive; the patient remains aware of their surroundings and can converse with a care partner during use of the system. The patient can adjust the brightness of the visual stimulation and the volume of the auditory stimulation within this predefined operating range via push buttons on the controller, with assistance from a care partner as needed. The system logs device usage and stimulation output settings for adherence monitoring; this information is uploaded to a secure cloud server for remote monitoring.

Monitoring Sleep Restful and Active Periods With Actigraphy and Signal Processing

Effects of gamma sensory stimulation therapy on durations of restful and active periods during sleep were determined over a 6-month period by continuous monitoring activity of AD patients with a wrist worn actigraphy watch (ActiGraph GT9X), recording 3-axis acceleration at 30 Hz sampling rate.

Preprocessing of the Data

Accelerometer data from three orthogonal dimensions are filtered with a Butterworth bandpass (0.3–3.5 Hz) filter. At each time point, Euclidean norm of the accelerometer data vector was calculated. The resulting time-series data was down-sampled by a factor of 4. This process is done for all data collected from all patients over the 6 months period. Two representations of the data were made: (i) Binary representation: All data was pooled together and a histogram in the log scale was obtained. The resulting histogram had a bimodal distribution, one peak corresponding to higher values in acceleration and hence high activity periods, and the second peak corresponding to lower values in acceleration and hence rest periods. Taking the acceleration value of the minimum between the two peaks as a threshold, acceleration magnitudes higher than the threshold were represented by 1's and acceleration magnitudes smaller than the threshold were represented by 0's. (ii) Smooth representation: A median filter with length of 6 h was applied to the down-sampled data to get a smooth estimate of the activity levels.

Extracting Nighttime (Sleep Segment)

Individual 24-h data segments were extracted from 12:00 pm midday on a given day to the next day 12:00 pm midday. The data was labeled with the binary representation for an initial estimate of the active – 1's and rest – 0's periods during the given 24-h window. This window consisted of three segments: daytime (segment prior to sleep), nighttime (sleep segment), and daytime (segment after sleep). We proposed that the nighttime segment would consist of more 0's than 1's and daytime segments would consist of more 1's than 0's. Therefore, we defined an ideal nighttime model built with a function that takes a value 0 within continuous period of duration "L" centered at a time "T" with a value 1 outside this region. Given an initial estimate of L and T, the difference between the ideal nighttime model and the binary representation of movement was computed using a quadratic cost function. In this cost function each mismatch, occurring when the binary value is 1 during nighttime or 0 during daytime, contributes 1, and each match, occurring when the binary value is 0 during nighttime and 1 during daytime, contributes 0. The initial estimate for T was taken to be the time point corresponding to the minimum of the smooth representation mentioned above. Initial estimate for L is set to 8 h. We then minimized this cost function using unconstrained non-linear optimization. This led to the best model estimate for L, the nighttime length, and T, the nighttime mid-point, and allowed us to locate the borders for the three segments (daytime, nighttime, and daytime) from the 24-h window. We then extracted the nighttime segment to evaluate the micro-changes within. The optimization algorithm to find the night-time periods provides an estimate for the night-time duration and the mid-night point (see **Supplementary Figure 1**).

Identification of Rest and Active Durations During Nighttime and Relating Them to Sleep

Within the nighttime segments, periods with all 0's is attributable to lack of movement and periods with all 1's is attributable to movement. However, mapping these periods directly to sleep-wake periods faces the problem that the durations of these periods

can range from milliseconds to hours in actigraphy data, whereas analysis of sleep is carried out by classifying non-overlapping epochs of 30 s duration into awake and asleep. To link our actigraphy analysis to the analysis timescales used in sleep studies, we took all segments of length N = 30 s and replaced the values in those segments by the median value over a window of 3N duration centered on the segment. In order to resolve situations that were marginal (15 s is rest and 15 s is active) it was considered reasonable to utilize a more robust estimate obtained from utilizing the adjacent windows. This is analogous to use of additional information for ambiguities in polysomnography studies. For longer duration rest periods this step should not make any difference. But for very small windows it would use the information from the neighboring windows to provide a more robust estimate of the subject state. We chose N = 30 s, but, found that the results were not sensitive to this exact choice. After we repeat this process for all short segments, consecutive time points in the nighttime segments corresponding to 0's were identified as rest durations and those corresponding to 1's were identified as active durations.

Determining the Distributions of Rest and Active Durations

Rest durations across all participants were pooled and the quantity $P(t) \equiv \int_t^\infty p(w)\,dw$, where $p(w)$ is the probability density function of rest durations between w and $w + dw$, was examined. P(t) represents the fraction of rest durations that are greater than length t and is referred to as the cumulative distribution function. Similarly, the cumulative distribution of the active durations was also calculated, and distributions of both rest and active durations are displayed in **Figure 2**.

Assessment of Functional Ability

Activities of daily living were assessed at baseline and regular monthly intervals during the 24-week treatment period in the same study population of actigraphy recordings using the clinically established ADCS-ADL scale (Galasko et al., 1997). The ADCS-ADL assesses the competence of AD patients in basic and instrumental activities of daily living. The assessments were by a caregiver in questionnaire format or administered by a healthcare professional as a structured interview with the caregiver.

Statistics

All statistical comparisons were done using Kolmogorov–Smirnov test.

RESULTS

The current analysis includes results on 22 mild-to-moderate AD subjects who successfully completed the 6-month study.

Safety

The safety profile of the treatment was benign (**Table 2**). Adverse events related to the study device had been reported of 42% of the participants, and 41% of the total adverse events were related to the device. Most (36%) adverse events were mild, 2.5% of them were moderate and 2.5% of them were severe. One participant in the treatment group and one participant in the sham group had discontinued the study due to an adverse event.

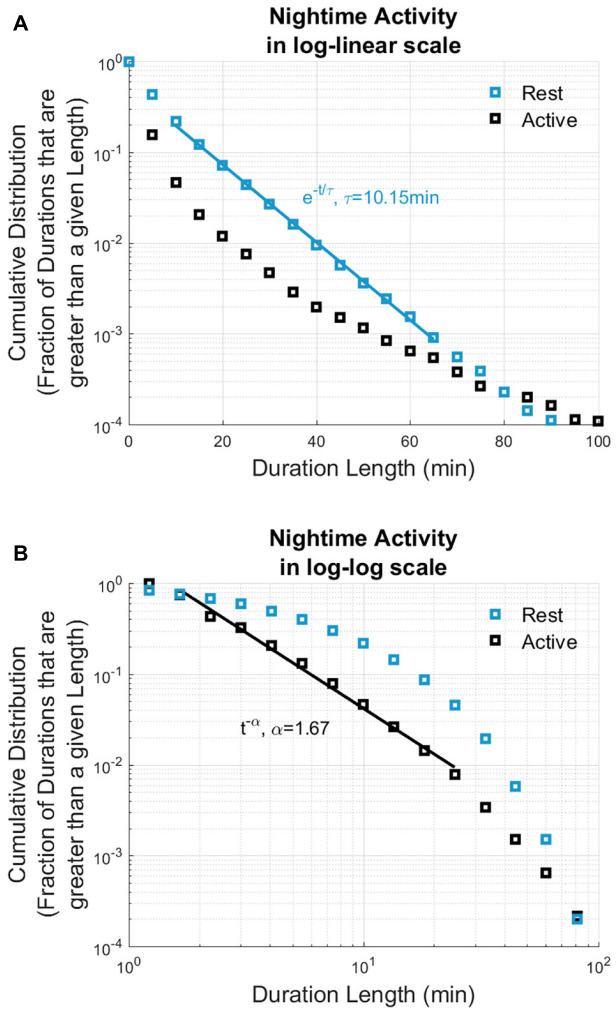

FIGURE 2 | Cumulative distribution of rest and active durations based on 14,736 h of nighttime actigraphy data recorded from all participated patients (n = 22). The cumulative distributions of nighttime rest periods (displayed in blue) show exponential distribution, whereas active periods (displayed in black) show power law distribution. Solid lines show the best straight-line fits: rest durations can be fitted by a straight line in log-linear scale **(A)**, and active durations can be fitted with a straight line in log-log scale **(B)**. *X* axis display the nighttime durations; *Y* axis show the cumulative distributions. The current actigraphy data analysis revealed similar nighttime rest/activity dynamics to nighttime sleep/wake dynamics based on polysomnography data analysis (Lo et al., 2013).

Adherence

We obtained the adherence rate from 21 out of 22 participants for the entire 6-month study period. The average adherence rate for these participants was 91%. For 1 participant, data was only available for the first 87 days; adherence rate for this participant was 92% during this period.

TABLE 2 | Safety analysis.

Adverse events	Treatment group (n = 19)		Sham group (n = 12)	
	Patients affected n (%)	Adverse events n (%)	Patients affected n (%)	Adverse events n (%)
Any adverse event	13 (68)	39 (100)	10 (83)	27 (100)
Adverse events unrelated to study device	10 (53)	23 (59)	8 (67)	18 (67)
Adverse events potentially related to study device	8 (42)	16 (41)	4 (33)	9 (33)
Mild Intensity	7 (37)	14 (36)	4 (33)	8 (30)
Anxiety	1 (5)	1 (3)	0	0
Benign positional vertigo	1 (5)	1 (3)	0	0
Confusion	0	0	1 (8)	1 (4)
Disorientation	0	0	1 (8)	1 (4)
Dizziness	1 (5)	1 (3)	1 (8)	1 (4)
Ear Irritation	1 (5)	1 (3)	0	0
Eye irritation	2 (11)	2 (5)	0	0
Fatigue	1 (5)	1 (3)	0	0
Hallucinations	0	0	1 (8)	1 (4)
Headache	5 (26)	5 (13)	2 (17)	2 (7)
Migraines	0	0	1 (8)	1 (4)
Nose irritation	1 (5)	1 (3)	0	0
Shoulder pain	1 (5)	1 (3)	0	0
Wandering	0	0	1 (8)	1 (4)
Moderate intensity	1 (5)	1 (3)	1 (8)	1 (4)
Agitation	0	0	1 (8)	1 (4)
Chest irritation	1 (5)	1 (3)	0	0
Severe intensity	1 (5)	1 (3)	0	0
Dementia exacerbation	1 (5)	1 (3)	0	0

Data are number of patients with an adverse event (percentage within study population; i.e., Treatment or Sham Group). Total number of adverse events (percentage of adverse events in the respective study population). Percentage values were rounded to the closest integer.

Sleep Evaluated by Continuous Actigraphy Recordings

An average of 100 days and nights of continuous actigraphy recordings were obtained from the 22 subjects in this subgroup of patients. Data from actigraphy recordings were processed for constructing a nighttime sleep model, which allowed to assess the durations of rest and active periods during sleep. All rest and active durations identified by actigraphy data processing were pulled and analyzed from each participant as described in "Materials and Methods" section, and the results were compared to published data of rest and active periods obtained by polysomnography-based sleep analysis. As evidenced by straight-line fits on a log-linear scale, the rest durations follow an exponential distribution, $e^{-t/\tau}$ with $\tau = 10.15\ min$. In contrast, active durations follow power law distribution (straight-line fit on a log-log scale), $t^{-\alpha}$ with $\alpha = 1.67$ (**Figure 2**). Such exponential and power law behaviors have been observed in sleep studies of healthy subjects (Lo et al., 2002, 2004, 2013). These authors analyzed nighttime sleep and awake states as obtained from polysomnographic (PSG) recordings of healthy subjects and found that cumulative distribution of sleep state durations is characterized by an exponential distribution whereas those of awake state durations were characterized with a power law distribution. Thus, the exponential decay constant as $\tau = 10.9\ min$ for light sleep, $\tau = 12.3\ min$ for deep sleep, $\tau = 9.9\ min$ for REM sleep durations, and the power law exponent as $\alpha = 1.1$ for awake durations were reported (Lo et al., 2013). We also found that the nighttime rest and active durations, estimated from actigraphy recordings of AD patients show exponential and power law behavior. Similarities in the form of the distributions between our results and previous work suggest that nighttime rest and active durations as assessed by actigraphy are analogous to sleep and awake states as assessed by polysomnography and that the effect of therapy on sleep may be indirectly assessed through its effect on active and rest durations.

Effects of Gamma Sensory Stimulation on Sleep Quality Determined by Continuous Actigraphy Recordings

Outcomes from gamma sensory stimulation therapy on sleep were evaluated from actigraphy data which allowed to assess the durations of rest and active periods during sleep. Results from this analysis of a single patient as shown in **Figure 3**, demonstrate nighttime active and rest periods; the level of continuous activity is determined and indicated by the black tracing. Furthermore, intervals were identified as sleep for each night (represented by

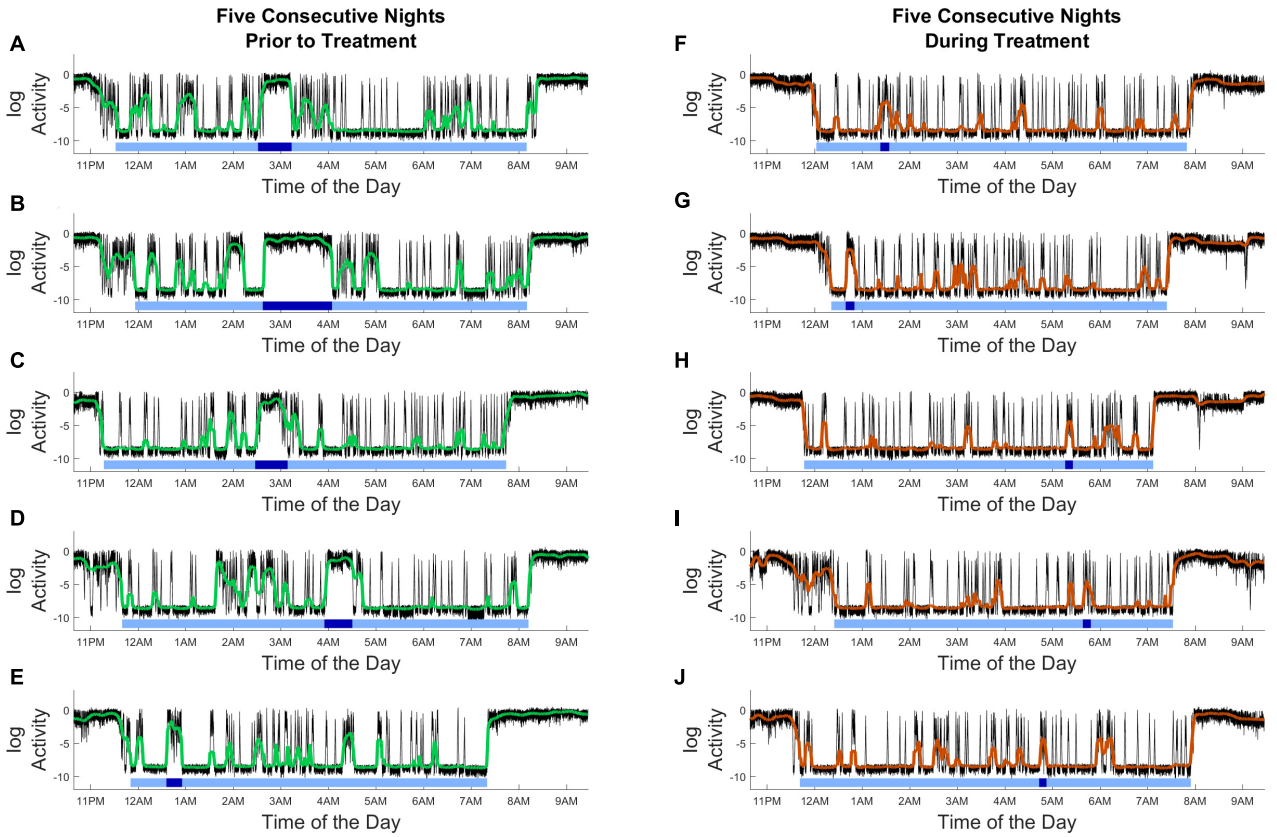

FIGURE 3 | Actigraphy recordings from a single patient demonstrating the effects of gamma sensory stimulation therapy on nighttime active and rest periods. **(A–E)** Five consecutive nights prior to treatment, **(F–J)** five consecutive nights during treatment period. Level of continuous activity is shown by the black tracing; median filtered activity levels are indicated by green **(A–E)** and brown **(F–J)** curves. The applied analysis identified nighttime active and rest periods: denoted sleep periods are marked by horizontal light blue bars, and the longest movement periods during nights are indicated by the dark blue bars. Compared to the pre-treatment period, fewer and shorter movement periods are observed. *X*-axis shows the time of day, *Y*-axis shows the activity level (in log scale).

horizontal light blue bars), and the longest movement periods are indicated by the dark blue bars. Effects of gamma sensory stimulation therapy on sleep were determined by comparing the distribution of the length of nighttime uninterrupted rest durations in the first and the second 12-week periods of the study. Although patients showed a high adherence to therapy, only subjects who wore the actigraphy device for at least 50% of the time during both the first and last 12-week periods were used for assessing efficacy of gamma sensory stimulation therapy on sleep ($n = 7$ Treatment, $n = 6$ Sham).

Compared to the first 12-week period, nighttime active durations were significantly ($p < 0.03$) reduced in the treatment group, whereas active durations were significantly ($p < 0.03$) increased in patients of the sham group. After active durations were normalized by dividing each active duration by the duration of the corresponding nighttime period of each patient, results further confirmed opposite changes in nighttime active durations between treatment and sham groups ($p < 0.001$, both groups; **Figure 4**). Furthermore, the average night-time period was 7.23 h for the treatment group, and 7.64 h for the sham group. The difference between the second 12-week period and the first 12-week period was in the order only of a couple of minutes. Specifically, the difference was −2.65 min for the treatment group and 2.07 min for the sham group. The present actigraphy findings demonstrate a reduction in nighttime active durations in response to gamma sensory stimulation therapy, leading to improvement in sleep quality, while the opposite can be assessed in the sham group.

Functional Ability as Assessed by Alzheimer's Disease Cooperative Study – Activities of Daily Living Was Maintained in Patients Treated With Gamma Sensory Stimulation

Effects of gamma sensory stimulation treatment on patients' ability to perform activities of daily living were evaluated by comparing average ADCS-ADL scores from the first 12-week and second 12-week periods in both treatment ($n = 14$) and sham ($n = 8$) groups (**Figure 5**). Each patient in the sham group showed a decline in ADCS-ADL scores, resulting in a significant decline ($P < 0.001$) of approximately three points in this patient group over the trial period. In contrast, nine out of 14 patients

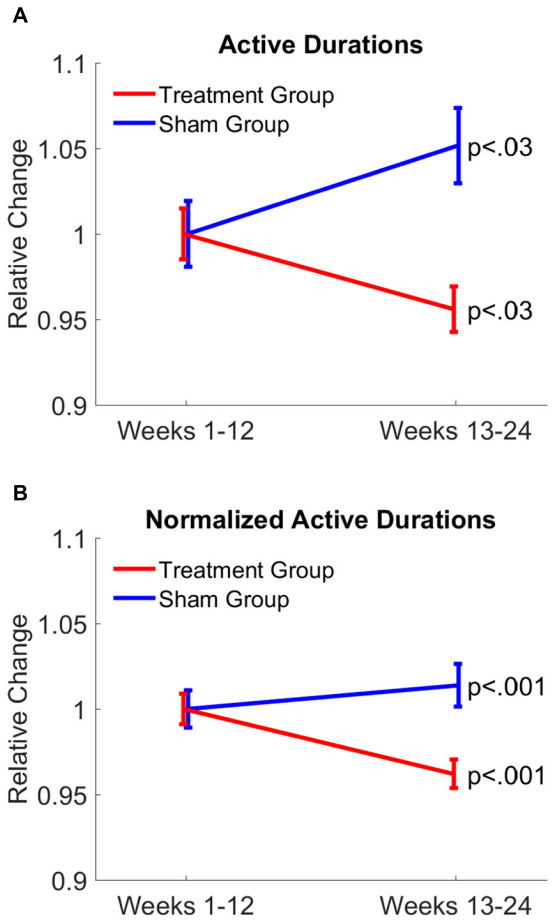

FIGURE 4 | Gamma sensory stimulation therapy reduced duration of active periods during nighttime. Changes in durations of active periods in treatment group is shown in red and sham group is shown in blue from the first 12 weeks to the last 12 weeks of the therapy **(A)**. Active durations were normalized by dividing duration of each active period by the duration of the corresponding nighttime period **(B)**. Changes observed in the treatment group (red) indicate a significant reduction in duration of active periods, indicating an improvement in sleep quality, while the opposite can be assessed in the sham group (blue).

in the treatment group maintained or improved their ADCS-ADL scores. Therefore, the average ADCS-ADL score in the treatment group significantly ($p < 0.035$) increased during the treatment period.

DISCUSSION

The present findings demonstrate that of 40 Hz audiovisual stimulation, eliciting 40 Hz gamma oscillation improves sleep quality and maintains functional abilities in mild to moderate AD patients and confirm a positive safety profile of the treatment with high patient adherence. The current findings are in line with a recent publication reporting that 4- or 8-weeks gamma sensory stimulation therapy is safe, tolerable, and feasible in subjects with mild cognitive impairment due to AD (He et al., 2021). The current results also provided evidence for applicability of continuous, long-term actigraphy recordings of nighttime activities in AD patients, suitable for assessing impact of potential therapeutics on sleep quality.

Sleep disorders in MCI and AD patients are well recognized, having a 35–60% prevalence of some form(s) of sleep abnormalities (Vitiello and Borson, 2001; Peter-Derex et al., 2015). Though early detection of sleep disorders has a particular significance given the established link between sleep disfunction and AD pathology, detecting these pathological changes in patients are challenging. The practicality of sleep questioners used in clinical practice for sleep disorders, such as the Pittsburgh sleep quality index or Athens insomnia scale provide limited value since patients frequently do not recognize their sleep disturbances (Most et al., 2012). Unquestionably, PSG studies are best suited to detect and monitor of sleep abnormalities, however, performing PSG recordings could be difficult for MCI or AD patients. Furthermore, monitoring sleep changes with PSG in response to therapeutic intervention over a longer period of time is impractical in MCI and AD patients. Recently, sleep monitoring with actigraphy in AD patients has become more frequent since a strong correlation between PSG and actigraphy data in sleep and wake time periods has been established (Ancoli-Israel et al., 2008). Our current findings show that wrist-worn actigraphy over 6 months is feasible and very well tolerated by participants. Longitudinal monitoring of sleep is a clear advantage when the onset of the treatment is unknown, like in our testing of gamma sensory stimulation therapy. Analysis of the current actigraphy data revealed identical nighttime rest/sleep – activity/awake dynamics to those which were based on PSG data analysis (Lo et al., 2013). This observation further validates the applicability of continuous monitoring of nighttime sleep-wake activity with actigraphy, and its suitability for AD patients.

Results, based on the collected actigraphy data over a 6-month period, demonstrate that gamma sensory stimulation therapy can significantly reduce active periods during night in mild to moderate AD patients. In contrast, patients in the sham group do not show improvement in sleep characteristics. These findings are in agreement with recent experimental finding demonstrating that a 40-Hz light stimulation alleviates abnormal circadian rhythm in Aβ overproducing transgenic APP/PS1 mice and significantly reduces abnormally high activity during their rest phase. These changes were accomplished by normalizing activity of suprachiasmatic neurons and the expression levels of proteins regulating the central circadian clock (Yao et al., 2020). The current findings demonstrating a beneficial effect of gamma sensory stimulation therapy in mild to moderate AD patients by prolonging nighttime undisturbed restful periods is considered as a translational biomarker demonstrating similar functional outcome in preclinical and clinical studies.

Pathomechanisms underlying sleep dysfunction in MCI and AD patients are mostly unknown, though AD-related pathological proteins, such as Aβ- and tau- oligomers are known to disrupt sleep but their mode of action is unknown. Brainstem ascending neurons considered playing a role in sleep-wake regulation, including cholinergic, serotoninergic and norepinephrine neurons show profound degeneration starting

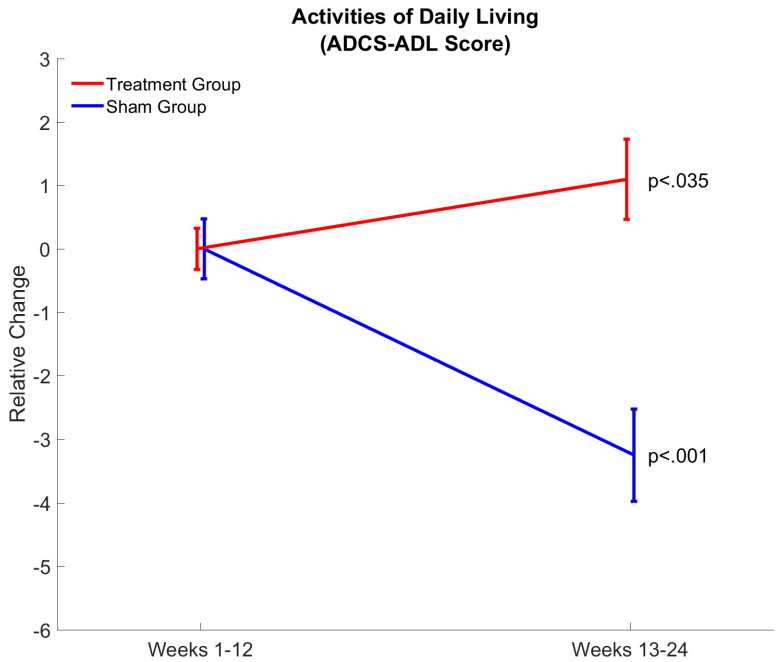

FIGURE 5 | Gamma sensory stimulation therapy results in maintenance of daytime activities assessed by Activities of Daily Living (ADCS-ADL) Score. Relative changes in daytime activities are shown between weeks 1–12 and weeks 13–24 in the treatment (red; $n = 14$) and sham (blue; $n = 8$) groups. Changes in daytime activities showed a significant ($p < 0.035$) improvement in the treatment group and a significant ($p < 0.001$) decline in the sham group.

from an early stage of the disease (Smith et al., 2018; Tiepolt et al., 2019; Kang et al., 2020). Similarly, suprachiasmatic nucleus containing neurons playing a key role in regulating circadian rhythms also shows neurodegeneration early in the disease (Van Erum et al., 2018). Whether similar mechanisms are involved in response to 40 Hz sensory stimulation in AD-related transgenic mice and AD patients is an open question at the moment.

There are only limited treatment options for sleep abnormalities in MCI and AD patients, and pharmacological treatments options include antidepressant, antihistamines, anxiolytics, and sedative-hypnotic drugs, some of them known to impair cognitive function and interference with motor behavior (Vitiello and Borson, 2001; Deschenes and McCurry, 2009; Ooms and Ju, 2016). Recently, suvorexant, an orexin receptor antagonist has been approved as a sleep medication for AD patients having clinically diagnosed insomnia. The main effects of suvorexant are a prolonged total sleep time and delayed wake after sleep onset, without impacting sleep fragmentation or altering sleep architecture (Herring et al., 2020). In the present trial evaluating gamma sensory stimulation, clinically diagnosed sleep abnormality such as insomnia has not been an including criteria requirement, consequently beneficial effects of gamma sensory stimulation are not limited to AD patients suffering from clinically recognized sleep problems.

Beneficial effect of gamma sensory stimulation on sleep quality in mild to moderate AD patients is particularly relevant, since scientific and clinical observations demonstrating a close relationship between sleep quality and activities of daily living (Zhou et al., 2019). It can be presumed that improving sleep quality in AD patients would provide multiple benefits: better sleep will enhance patients' daytime performance and reduce daytime sleepiness. In line with this hypothesis, patients on gamma sensory stimulation treatment maintained functional activity as reflected by their unchanged ADCS-ADL score over the 6-month treatment period. In contrast, ADCS scores of sham group patients dropped similarly to changes of placebo group patients observed previously in clinical trials (Doody et al., 2013, 2014). Even though the close relationship between sleep and daily activity is well documented, it is unknown at present whether improved sleep quality is the main factor contributing to the maintenance of ADCS-ADL scores in gamma sensory stimulation treated patients, or improvement in sleep and continuation of functional ability are unrelated positive outcomes from the therapy.

Currently, the underlying mechanisms of improved sleep and maintained functional ability of AD patients in response to gamma sensory stimulation are not known. Preclinical studies indicate that 40 Hz sensory stimulation reverses Aβ and tau pathologies, improves synaptic function leading to improved cognitive function in transgenic mice (Iaccarino et al., 2016; Adaikkan et al., 2019; Martorell et al., 2019). Although human AD-related biomarker studies are in progress, at the moment it is unknown if the same biochemical and neuroimmunology mechanisms are activated in AD patients as identified in mice. The bidirectional interaction between sleep and disease progression (Wang and Holtzman, 2020) supports the notion that improved sleep in response to gamma sensory stimulation treatment could also slow down disease progression.

DATA AVAILABILITY STATEMENT

The raw data supporting the conclusions of this article will be made available by the authors, without undue reservation.

ETHICS STATEMENT

The studies involving human participants were reviewed and approved by the Advarra IRB Research Ethics Board. The patients/participants provided their written informed consent to participate in this study.

AUTHOR CONTRIBUTIONS

AC had full access to all the data in the study, takes responsibility for the integrity of the data and the accuracy of the data analysis, and contributed to analysis and conceptualization of analysis approach. ZM and EH conceived and designed the study. EH, KM, and TT executed the study. AC, MH, and ZM interpreted the data. MH and AC drafted the manuscript. ZM, EH, TT, NS, KM, and AC provided administrative, technical, or material support. All authors contributed to the article and approved the submitted version.

FUNDING

The authors declare that this study received funding from Cognito Therapeutics, Inc. The funder was not involved in the study design, collection, analysis, interpretation of data, the writing of this article or the decision to submit it for publication.

ACKNOWLEDGMENTS

We would like to thank the subjects who volunteered for this research as well as investigators Paul Solomon, Michele Papka, and Mark Brody for their collaboration. In addition, we thank Alexandra Konisky and Nadia Myrthil for data collection and management in this project.

SUPPLEMENTARY MATERIAL

The Supplementary Material for this article can be found online at: https://www.frontiersin.org/articles/10.3389/fnsys.2021.746859/full#supplementary-material

REFERENCES

Adaikkan, C., Middleton, S. J., Marco, A., Pao, P. C., Mathys, H., Kim, D. N., et al. (2019). Gamma entrainment binds higher-order brain regions and offers neuroprotection. *Neuron* 102 92:e928. doi: 10.1016/j.neuron.2019.04.011

Ancoli-Israel, S., Palmer, B. W., Cooke, J. R., Corey-Bloom, J., Fiorentino, L., Natarajan, L., et al. (2008). Cognitive effects of treating obstructive sleep apnea in Alzheimer's disease: a randomized controlled study. *J. Am. Geriatr. Soc.* 56, 2076–2081. doi: 10.1111/j.1532-5415.2008.01934.x

Bubu, O. M., Andrade, A. G., Umasabor-Bubu, O. Q., Hogan, M. M., Turner, A. D., de Leon, M. J., et al. (2020). Obstructive sleep apnea, cognition and Alzheimer's disease: a systematic review integrating three decades of multidisciplinary research. *Sleep Med. Rev.* 50:101250. doi: 10.1016/j.smrv.2019.101250

Cabanel, N., Speier, C., Muller, M. J., and Kundermann, B. (2020). Actigraphic, but not subjective, sleep measures are associated with cognitive impairment in memory clinic patients. *Psychogeriatrics* 20, 133–139. doi: 10.1111/psyg.12474

Canazei, M., Turiaux, J., Huber, S. E., Marksteiner, J., Papousek, I., and Weiss, E. M. (2019). Actigraphy for assessing light effects on sleep and circadian activity rhythm in Alzheimer's dementia: a narrative review. *Curr. Alzheimer Res.* 16, 1084–1107. doi: 10.2174/1567205016666191010124011

Canter, R. G., Penney, J., and Tsai, L. H. (2016). The road to restoring neural circuits for the treatment of Alzheimer's disease. *Nature* 539, 187–196. doi: 10.1038/nature20412

Das, M., Maeda, S., Hu, B., Yu, G. Q., Guo, W., Lopez, I., et al. (2018). Neuronal levels and sequence of tau modulate the power of brain rhythms. *Neurobiol. Dis.* 117, 181–188. doi: 10.1016/j.nbd.2018.05.020

Deschenes, C. L., and McCurry, S. M. (2009). Current treatments for sleep disturbances in individuals with dementia. *Curr. Psychiatry Rep.* 11, 20–26. doi: 10.1007/s11920-009-0004-2

Doody, R. S., Raman, R., Farlow, M., Iwatsubo, T., Vellas, B., Joffe, S., et al. (2013). A phase 3 trial of semagacestat for treatment of Alzheimer's disease. *N. Engl. J. Med.* 369, 341–350. doi: 10.1056/NEJMoa1210951

Doody, R. S., Thomas, R. G., Farlow, M., Iwatsubo, T., Vellas, B., Joffe, S., et al. (2014). Phase 3 trials of solanezumab for mild-to-moderate Alzheimer's disease. *N. Engl. J. Med.* 370, 311–321. doi: 10.1056/NEJMoa1312889

Galasko, D., Bennett, D., Sano, M., Ernesto, C., Thomas, R., Grundman, M., et al. (1997). An inventory to assess activities of daily living for clinical trials in Alzheimer's disease. the Alzheimer's disease cooperative study. *Alzheimer Dis. Assoc. Disord.* 11(Suppl. 2), S33–S39.

He, Q., Colon-Motas, K. M., Pybus, A. F., Piendel, L., Seppa, J. K., Walker, M. L., et al. (2021). A feasibility trial of gamma sensory flicker for patients with prodromal Alzheimer's disease. *Alzheimers Dement (N Y)* 7:e12178. doi: 10.1002/trc2.12178

Hennawy, M., Sabovich, S., Liu, C. S., Herrmann, N., and Lanctot, K. L. (2019). Sleep and attention in Alzheimer's disease. *Yale J. Biol. Med.* 92, 53–61.

Herring, W. J., Ceesay, P., Snyder, E., Bliwise, D., Budd, K., Hutzelmann, J., et al. (2020). Polysomnographic assessment of suvorexant in patients with probable Alzheimer's disease dementia and insomnia: a randomized trial. *Alzheimers Dement* 16, 541–551. doi: 10.1002/alz.12035

Herrmann, C. S. (2001). Human EEG responses to 1-100 Hz flicker: resonance phenomena in visual cortex and their potential correlation to cognitive phenomena. *Exp. Brain Res.* 137, 346–353. doi: 10.1007/s002210100682

Hijazi, S., Heistek, T. S., van der Loo, R., Mansvelder, H. D., Smit, A. B., and van Kesteren, R. E. (2020). Hyperexcitable parvalbumin interneurons render hippocampal circuitry vulnerable to amyloid beta. *iScience* 23:101271. doi: 10.1016/j.isci.2020.101271

Iaccarino, H. F., Singer, A. C., Martorell, A. J., Rudenko, A., Gao, F., Gillingham, T. Z., et al. (2016). Gamma frequency entrainment attenuates amyloid load and modifies microglia. *Nature* 540, 230–235. doi: 10.1038/nature20587

Kang, S. S., Liu, X., Ahn, E. H., Xiang, J., Manfredsson, F. P., Yang, X., et al. (2020). Norepinephrine metabolite DOPEGAL activates AEP and pathological Tau aggregation in locus coeruleus. *J. Clin. Invest.* 130, 422–437.

Lo, C. C., Bartsch, R. P., and Ivanov, P. C. (2013). Asymmetry and basic pathways in sleep-stage transitions. *Europhys. Lett.* 102:10008. doi: 10.1209/0295-5075/102/10008

Lo, C. C., Chou, T., Penzel, T., Scammell, T. E., Strecker, R. E., Stanley, H.-E., et al. (2004). Common scale-invariant patterns of sleep–wake transitions across mammalian species. *PNAS* 101, 17545–17548.

Lo, C. C., Nunes Amaral, L. A., Havlin, S., Ivanov, P. C., Penzel, T., Peter, J. H., et al. (2002). Dynamics of sleep-wake transitions during sleep. *Europhys. Lett.* 57, 625–631.

Macedo, A. C., Balouch, S., and Tabet, N. (2017). Is sleep disruption a risk factor for Alzheimer's disease? *J. Alzheimers Dis.* 58, 993–1002. doi: 10.3233/JAD-161287

Mander, B. A., Marks, S. M., Vogel, J. W., Rao, V., Lu, B., Saletin, J. M., et al. (2015). beta-amyloid disrupts human NREM slow waves and related hippocampus-dependent memory consolidation. *Nat. Neurosci.* 18, 1051–1057. doi: 10.1038/nn.4035

Martorell, A. J., Paulson, A. L., Suk, H. J., Abdurrob, F., Drummond, G. T., Guan, W., et al. (2019). Multi-sensory gamma stimulation ameliorates Alzheimer's-Associated pathology and improves cognition. *Cell* 177, 256–271.e22. doi: 10.1016/j.cell.2019.02.014

Masters, C. L., Bateman, R., Blennow, K., Rowe, C. C., Sperling, R. A., and Cummings, J. L. (2015). Alzheimer's disease. *Nat. Rev. Dis. Primers* 1:15056. doi: 10.1038/nrdp.2015.56

Most, E. I., Aboudan, S., Scheltens, P., and Van Someren, E. J. (2012). Discrepancy between subjective and objective sleep disturbances in early- and moderate-stage Alzheimer disease. *Am. J. Geriatr. Psychiatry* 20, 460–467. doi: 10.1097/JGP.0b013e318252e3ff

Mucke, L., and Selkoe, D. J. (2012). Neurotoxicity of amyloid beta-protein: synaptic and network dysfunction. *Cold Spring Harb. Perspect. Med.* 2:a006338. doi: 10.1101/cshperspect.a006338

Ooms, S., and Ju, Y. E. (2016). Treatment of sleep disorders in dementia. *Curr. Treat Options Neurol* 18:40. doi: 10.1007/s11940-016-0424-423

Peter-Derex, L., Yammine, P., Bastuji, H., and Croisile, B. (2015). Sleep and Alzheimer's disease. *Sleep Med. Rev.* 19, 29–38. doi: 10.1016/j.smrv.2014.03.007

Smith, M. T., McCrae, C. S., Cheung, J., Martin, J. L., Harrod, C. G., Heald, J. L., et al. (2018). Use of actigraphy for the evaluation of sleep disorders and circadian rhythm sleep-wake disorders: an american academy of sleep medicine systematic review, meta-analysis, and GRADE assessment. *J. Clin. Sleep Med.* 14, 1209–1230. doi: 10.5664/jcsm.7228

Tachikawa, R., Minami, T., Matsumoto, T., Murase, K., Tanizawa, K., Inouchi, M., et al. (2017). Changes in habitual sleep duration after continuous positive airway pressure for obstructive sleep apnea. *Ann. Am. Thorac. Soc.* 14, 986–993. doi: 10.1513/AnnalsATS.201610-816OC

Tiepolt, S., Patt, M., Aghakhanyan, G., Meyer, P. M., Hesse, S., Barthel, H., et al. (2019). Current radiotracers to image neurodegenerative diseases. *EJNMMI Radiopharm. Chem.* 4:17. doi: 10.1186/s41181-019-0070-77

Van Erum, J., Van Dam, D., and De Deyn, P. P. (2018). Sleep and Alzheimer's disease: a pivotal role for the suprachiasmatic nucleus. *Sleep Med. Rev.* 40, 17–27. doi: 10.1016/j.smrv.2017.07.005

Vitiello, M. V., and Borson, S. (2001). Sleep disturbances in patients with Alzheimer's disease: epidemiology, pathophysiology and treatment. *CNS Drugs* 15, 777–796. doi: 10.2165/00023210-200115100-20011 5104

Wang, C., and Holtzman, D. M. (2020). Bidirectional relationship between sleep and Alzheimer's disease: role of amyloid, tau, and other factors. *Neuropsychopharmacology* 45, 104–120. doi: 10.1038/s41386-019-0478-475

Yao, Y., Ying, Y., Deng, Q., Zhang, W., Zhu, H., Lin, Z., et al. (2020). Non-invasive 40-Hz light flicker ameliorates Alzheimer's-Associated rhythm disorder via regulating central circadian clock in mice. *Front. Physiol.* 11:294. doi: 10.3389/fphys.2020.00294

Zhang, Z., Jing, Y., Ma, Y., Duan, D., Li, B., Holscher, C., et al. (2020). Driving GABAergic neurons optogenetically improves learning, reduces amyloid load and enhances autophagy in a mouse model of Alzheimer's disease. *Biochem. Biophys. Res. Commun.* 525, 928–935. doi: 10.1016/j.bbrc.2020.03.004

Zhou, G., Liu, S., Yu, X., Zhao, X., Ma, L., and Shan, P. (2019). High prevalence of sleep disorders and behavioral and psychological symptoms of dementia in late-onset Alzheimer disease: a study in Eastern China. *Medicine (Baltimore)* 98:e18405. doi: 10.1097/MD.0000000000018405

Conflict of Interest: All authors were employed by Cognito Therapeutics, Inc. at the time of this study.

Publisher's Note: All claims expressed in this article are solely those of the authors and do not necessarily represent those of their affiliated organizations, or those of the publisher, the editors and the reviewers. Any product that may be evaluated in this article, or claim that may be made by its manufacturer, is not guaranteed or endorsed by the publisher.

frontiers in Behavioral Neuroscience

MINI REVIEW
published: 25 November 2021
doi: 10.3389/fnbeh.2021.785328

Characterizing Hippocampal Oscillatory Signatures Underlying Seizures in Temporal Lobe Epilepsy

Thato Mary Mokhothu and Kazumasa Zen Tanaka**

Okinawa Institute of Science and Technology Graduate University, Okinawa, Japan

Temporal Lobe Epilepsy (TLE) is a neurological condition characterized by focal brain hyperexcitability, resulting in abnormal neuronal discharge and uncontrollable seizures. The hippocampus, with its inherently highly synchronized firing patterns and relatively high excitability, is prone to epileptic seizures, and it is usually the focus of TLE. Researchers have identified hippocampal high-frequency oscillations (HFOs) as a salient feature in people with TLE and animal models of this disease, arising before or at the onset of the epileptic event. To a certain extent, these pathological HFOs have served as a marker and a potential target for seizure attenuation using electrical or optogenetic interventions. However, many questions remain about whether we can reliably distinguish pathological from non-pathological HFOs and whether they can tell us about the development of the disease. While this would be an arduous task to perform in humans, animal models of TLE provide an excellent opportunity to study the characteristics of HFOs in predicting how epilepsy evolves. This minireview will (1) summarize what we know about the oscillatory disruption in TLE, (2) summarize knowledge about oscillatory changes in the latent period and their role in predicting seizures, and (3) propose future studies essential to uncovering potential treatments based on early detection of pathological HFOs.

Keywords: seizures, hippocampus, biomarkers, temporal lobe epilepsy, latent period, pathological oscillations, high-frequency oscillations

OPEN ACCESS

Edited by:
Yuichi Takeuchi,
Hokkaido University, Japan

Reviewed by:
Manuel Valero,
New York University, United States
Gabriele Deidda,
Italian Institute of Technology (IIT), Italy

****Correspondence:***
Thato Mary Mokhothu
thato.mokhothu@oist.jp
Kazumasa Zen Tanaka
kazumasa.tanaka@oist.jp

Specialty section:
This article was submitted to Pathological Conditions, a section of the journal Frontiers in Behavioral Neuroscience

Received: *29 September 2021*
Accepted: *29 October 2021*
Published: *25 November 2021*

Citation:
Mokhothu TM and Tanaka KZ (2021) Characterizing Hippocampal Oscillatory Signatures Underlying Seizures in Temporal Lobe Epilepsy. Front. Behav. Neurosci. 15:785328. doi: 10.3389/fnbeh.2021.785328

INTRODUCTION

Temporal Lobe Epilepsy (TLE) is the most commonly medically refractive focal epilepsy (Engel, 2014). It mainly begins in the limbic areas and could be secondarily generalized, resulting in tonic-clonic seizures (Shibley and Smith, 2002; Bone et al., 2012). Studies using electrical recordings and expression of immediate early genes to identify the cellular activations during seizures have found that this secondary generalization plays a role in the increased frequency of seizure episodes in the chronic stage (Kiernan, 2012; Sinel'Nikova et al., 2013) and is one of the risk factors for the phenomenon called sudden unexpected death in epilepsy (SUDEP), one of the leading causes of death for people with epilepsy (Bone et al., 2012). During epileptogenesis, there are numerous changes within the brain: epileptic discharges emerge, altered neural firing patterns due in part to altered neurotransmitter releases, the connection of and communication between cells (Janz et al., 2017; Ren and Curia, 2021), neural death and the aberrant migration of granule cells (Henderson et al., 2014; Cho et al., 2015; Kim and Cho, 2018). In animal models which use chemoconvulsants

for induction, these disease features are elicited similarly to the human condition (Curia et al., 2014; Paschen et al., 2020).

The hippocampus is one of the main foci of TLE and, simultaneously, a key area involved in various types of memory, including contextual memory and spatial navigation. Therefore, its pathology can lead to many cognitive deficits, including learning and memory (Andersen, 2007). The above features, which facilitate TLE progression, also correlate to higher cases of cognitive decline in both humans and animal models (Cho et al., 2015).

The distinctive three phases of TLE are (1) Acute phase: in which there is a prolonged seizure due to a brain insult, (2) Latent phase: is a period between the initial precipitating (IPI) and the chronic stage without any exhibition of behavioral seizures, and (3) The chronic phase: is marked by spontaneous recurrent seizures (SRS) (Panayiotopoulos, 2005; Curia et al., 2008; Kandratavicius et al., 2014; Janz et al., 2017). These are seemingly unprovoked seizures in the people with epilepsy, which occur weeks, months, or even years after the first incident (Maguire, 2016). In human cases, epilepsy is usually diagnosed at the chronic state, although the consensus is that many neurological changes occur long before the start of observable recurrent seizures (Cho et al., 2015; Maguire, 2016). The IPI itself is traced back using self and caretaker reports during consultation. In modern studies, animal models of TLE can distinctly depict these three stages, making them good models for studying TLE.

Sir William Gowers first described these stages and have been kept as a standard definition throughout the decades (Gowers, 1901). However, the latent period is the least understood. There is a high variability of its duration (making it challenging to define temporally), and there is no typical behavioral output (making it difficult to detect). For example, if seizures begin after 3 days after an IPI, we may be better able to link the two events, but there is a question about whether this can be regarded as latency at all vs. a series of seizures occurring 6 years after an IPI, in which a precise latency can be defined, but the details of the IPI may be less accurate due to time lapse (Löscher et al., 2015). The question about what latency constitutes and its role in developing TLE has been open for a long time. It is pressing even more now that we have better tools to assess the mechanisms underlying progression (Cai et al., 2021). Insights about brain activity during the so-called "latent period" may lead to better targeting procedures for interventions in TLE, possibly through earlier therapeutic windows.

THE LATENCY CONTROVERSY

There is currently an exciting debate in the epilepsy field: One school of thought is that the IPI presents all the necessary features to elicit SRS, and even without a latent period, the chronic seizures will begin (Rattka et al., 2011; Löscher et al., 2015). This view is based on observing varied results from some human and animal studies in which some seizures began almost immediately after the IPI (Löscher et al., 2015). Another thought is that latency is a prerequisite process in epileptogenesis during which changes occurring in the brain, including circuit rewiring, will culminate in the seizures elicited in chronic periods (Panayiotopoulos, 2005; Lee et al., 2017). This is based on a traditional view of the stages of epilepsy, whose central gap is the lack of explicit knowledge about brain activity in the absence of seizures. Maguire (2016) suggests that many cellular and molecular changes occur in the brain, making the emergence of SRSs more likely. It is now appreciated that dubbing the latent period as the "silent period" may be misleading: While behaviorally, there are no seizures, the brain activity may show a different picture. At this juncture, the presence of a latent period seems more likely as it is reported in more cases than not (Lévesque and Avoli, 2013), but what is still unclear is what happens during this time. To answer that, we need to evaluate differences between a latent epileptic brain and a healthy brain, and one of the ways to characterize neural population activity is through brain oscillations.

NON-PATHOLOGICAL OSCILLATIONS

Brain oscillations are local field potentials generated by microcircuits of specific cell types due to internal influences or external or cognitive demands (Menendez de la Prida and Huberfeld, 2019). Hippocampal theta oscillations (4–12 Hz) are very prominent in rodents, typically observed when the animal attends to a novel object or when it is paying attention or performing a task (Başar and Güntekin, 2008; Belchior et al., 2014), although their expression and characterization in human studies are still controversial (please see Herweg et al., 2020). These oscillations have been found persistently in the CA1, CA3, and DG of rodents during voluntary, preparatory, or exploratory movements, as well as during rapid eye movement (REM) sleep (Buzsáki, 2002), associated with a replay of memories and dreaming (Louie and Wilson, 2001). For example, during a contextual fear conditioning task, the theta oscillations were observed in both the hippocampus CA1 and the lateral amygdala, and their synchronization increased during retrieval of fear memories (Seidenbecher et al., 2003). Researchers further found that synchronization of neuronal activity in addition to theta bursts is correlated with both learning and retrieval of contextual fear memory (Zhou et al., 2020). Potentiation is most efficient during theta band oscillation: In 2009, a study showed that low-frequency stimulation on the perforant pathway induced theta rhythms in the dentate gyrus, which increased EPSPs and Ca^{2+} influx (Tsanov and Manahan-Vaughan, 2009). Theta oscillations are therefore conducive to synaptic plasticity. The same has been found in other regions, such as the medial prefrontal cortex (mPFC), where learning depends on theta oscillations. The theta-dependant neuronal synchrony is said to underlie memory transfer (Paz et al., 2008).

Gamma oscillations are high-frequency oscillations (30–80 Hz) observed in many brain parts, including the hippocampus (Buzsáki and Schomburg, 2015). Gamma oscillations have brief durations and arise from the interplay of excitation and inhibition in local cell assemblies, with the drive from PV^{+} inhibitory neurons playing an essential role (Buzsáki and Wang, 2012).

Gamma oscillations are frequently observed alongside theta waves. Theta-gamma coupling is highly regulated, and any disturbances in this system may lead to abnormalities and pathology in the brain (Zhang et al., 2016).

In the hippocampus, another type of physiological oscillation is called sharp waves (SPW). They are high amplitude, low-frequency patterns in the LFPs (Sullivan et al., 2011). They are often accompanied by a higher frequency of activity (ripple), and this phenomenon, where both waveforms co-occur (sharp-wave ripples, SWRs), is observed in various animals, including humans (Buzsáki, 2015). It tends to dominate the brain during the awake phase but immobile moments or non-REM sleep and has been linked to processes that support memory consolidation (Sullivan et al., 2011; Buzsáki, 2015; Oliva et al., 2018). In a study using a spatial discrimination task in rats, it was found that trained rats had a more sustained sharp-wave ripple activity following the task and during the non-REM stage of their sleep. Compared to the non-trained rats, the experimental group showed an increase in ripple density with increasing performance accuracy (Ramadan et al., 2009). During these SWRs in non-REM sleep, neurons active during a task are re-activated with the identical spike sequences but in a shorter timescale replay (Wilson and McNaughton, 1994; Skaggs and McNaughton, 1996; Lee and Wilson, 2002). Moreover, selective interruption of SWRs during awake causes a deficit in spatial learning (Jadhav et al., 2012). Because of these properties, the SWR was then considered the neural substrate of memory consolidation (Wilson and McNaughton, 1994; Ramadan et al., 2009; Buzsáki, 2015).

Oscillations whose spectral power goes beyond the limits of the gamma band are known as high-frequency oscillations (HFOs) (125–250 Hz) and very high-frequency oscillations (vHFOs) (250–500 Hz) (Kucewicz et al., 2014). In other studies, the former are referred to as ripples and the latter as fast ripples (Bragin et al., 1999). In a study on the visual cortex in humans, a visual HFS paradigm enhanced plasticity in the visual cortex by raising the phase synchrony of theta oscillations (Hamilton et al., 2020). These results imply that HFOs too facilitate neural plasticity and network rewiring in healthy animals for learning and memory. However, aberrant oscillations may lead to aberrant types of plasticity: for instance, the higher the HFO frequencies, the higher the likelihood of a disease, specifically above 300 Hz, the proposed physiological oscillatory frequency boundary (Pail et al., 2020). Therefore, we need to examine changes leading to pathological oscillations carefully.

PATHOLOGICAL OSCILLATIONS

Pathological oscillations are fast oscillations occurring at higher frequencies than the average observed in healthy brains (Engel et al., 2009; Ewell et al., 2019). Bragin et al. (1999) observed that in normal and in kindled rat brains, field recordings did not exceed 200 Hz, while in the kainate acid (KA)-treated animals, recordings of > 200 Hz were observed near the injection site, which was also the sclerotic tissue. Their study characterizing ripples and fast ripples defined *ripples* as oscillations occurring at 100–200 Hz and lasting 50–150 ms, while *fast ripples* were the 200–500 Hz oscillations lasting 10–100 ms (Bragin et al., 1999). Although sometimes frequency bands of pathological oscillations may overlap with physiological oscillations (Ibarz et al., 2010; Pail et al., 2020), one study suggests that the peak amplitudes of pathological oscillations are highly variable compared to the more consistent physiological recordings (Ewell et al., 2019). Apart from features of the HFOs, the locations in which they occur are also of importance. For instance, according to Engel et al. (2009), oscillations occurring at 250–600 Hz in the hippocampus would be considered pathological, while in the neocortex, they may be facilitating physiological processes. Additionally, pathologic oscillations seem to occur regardless of the brain state, while physiological HFOs are linked closely with specific tasks (Ewell et al., 2019). Buzsáki (2015) theorized that the threshold of conversion from an HFO to a pathological HFO is minimal, therefore in highly excitable circuits such as the hippocampus, a perturbation of normal HFO is likely to lead to seizure disorders. The appearance of these HFOs during the latent and, more frequently during chronicity implies that a progressive change in the network generates this activity (**Figure 1**; Assenza et al., 2020).

In a Ca^{2+} imaging study, Lillis et al. (2015) found an increase in local hippocampal synchronization stemming from the recruitment of more cells from the early stages following induction of epilepsy. In the chronic phase, there are more HFOs than in the healthy or the early seizure stages, and more than in the acutely epileptic brain, suggesting a progressive series of changes such as network reorganization throughout TLE development that could lead to long-term pathophysiology (Lévesque et al., 2018). Another finding following seizure induction was that the earlier the HFOs were exhibited during latency, the shorter the latency (Jiruska et al., 2017). This relationship could be one of the explanations for why some latencies are shorter than others. It also leads us to the natural assumption that perhaps the latent period represents the rewiring of the brain and that there is a threshold for these aberrant activities, which, when met, begins the chronic stage of TLE. When the latent period transitions into the chronic phase, there is also a change in the site of HFO generation, from the hippocampus to the entorhinal cortex (Jiruska et al., 2017), and an increased duration of the HFOs near the beginning of SRS (Lévesque et al., 2018). The dynamics and presentation of HFOs, once understood, can be used to detect TLE stages and serve as a warning before the looming first SRS.

Song and colleagues observed stronger temporal lobe coherence during resting states in people with chronic epilepsy versus healthy controls (Song et al., 2013). The theta, gamma, and beta power are heightened during the ictal part of the seizure, while delta power is high in the interictal stages (Sharma et al., 2018). A study in the early 90 s showed a correlation between theta oscillations and the attenuation of seizures. Stimulating the medial septum at 4–8 Hz after a pentylenetetrazole-induced seizure stopped the ongoing seizures within seconds, while the lesioning of the medial septum removed the theta waves and heightened susceptibility to and frequency of seizures (Miller et al., 1994), further emphasizing the theta-SWR dichotomy even in pathology. Recent evidence supports

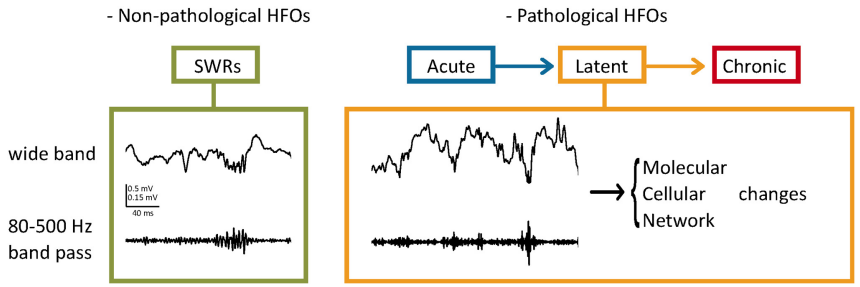

FIGURE 1 | Pathological HFOs and their possible role during the latent phase of TLE. **(Left)** SWRs as an example of non-pathological HFOs. In the hippocampus, HFOs (80–200 Hz) called ripples are associated with high amplitude activities (Sharp Wave Ripples, SWRs) and contribute to neuronal plasticity and memory consolidation. **(Right)** Pathological HFOs during the latent phase of TLE. Higher frequencies of oscillations (200–500 Hz) are observed between the acute and chronic stages without behavioral expression of seizures. Neuronal activities leading to the pathological HFOs are suggested to result in long-term molecular and cellular changes. Circuit rewiring caused by these changes might make the more brain areas prone to SRSs, leading to further progression of TLE.

this claim through experiments using continuous deep brain stimulation on the medial septum in animal models of TLE. The results were significant reductions in seizure severity, the incidence of generalized seizures and SE, and the total number of generalized seizures. The 5 Hz stimulation yielded the most significant effects on all measurements (Wang et al., 2021). A slice preparation experiment showed that directly stimulating the GABA-ergic neurons in the medial septum (MS) achieves the same effect (Hristova et al., 2021). The results coincide with the already established role of the MS that is the generation and input of theta oscillations to the hippocampus (Buzsáki, 2002; Watson et al., 2019).

High-frequency oscillations may also be a crucial seizure-prediction tool that shows the locations of seizure generation and the time window to the subsequent seizure, and possibly, they could define the stage of the epileptogenesis (Ibarz et al., 2010). In a human study using intracranial EEG and HFO detection systems, machine learning algorithms could reliably recognize patterns of brain activity that preceded the seizures up to 30 min and discern them from non-seizure-related activity (Scott et al., 2021). Due to higher HFO instances in the ipsilateral hippocampus rather than the contralateral side can be used as a biomarker for the seizure focus (Řehulka et al., 2019) path. Non-invasive tools have already been developed for better detection with minimal discomfort for people with TLE (Cai et al., 2021). As such, not only can HFOs be used to predict the first spontaneous seizure (after latency), but they could also be used to predict the ongoing seizures throughout chronicity and their site of generation (**Table 1** summarizes the important studies which observed pathological HFOs either in the human and rodents). Therefore, we can appreciate the potential utilization of HFOs in the clinical setting for people with either acute and chronic epilepsy.

CELLULAR UNDERPINNINGS OF HIGH-FREQUENCY OSCILLATIONS

The cellular mechanisms underlying the generation of pathological HFOs are still unclear, and more work is needed to understand them. There are, however, some theories that have been suggested to understand how HFOs arise. For example, some research states that the generation of pathological HFOs during seizures is due to the synchronous firing of pyramidal cells and the relative reduction of activity from the interneurons (Pail et al., 2020).

Jiruska et al. (2017) also posit that the pHFOs represent this fast (order of milliseconds) synchronous firing within aberrantly connected principal cell population (Zijlmans et al., 2012) which is different from normal ripples whose origin is believed to be the activity of interneurons and the summation of their IPSPs in an area (Engel et al., 2009; Pail et al., 2020). Physiological HFOs are said to emanate from the activity of cells in the pyramidal layer of the CA1 and interneurons such as the basket cells, especially PV^+ cells responding to the bursting of CA3 neurons with a surge of IPSPs (Chrobak and Buzsáki, 1996; Bragin et al., 1999). During an SWR, a physiological oscillation, Ramadan et al. (2009) suggest that the activity of both excitatory and inhibitory neurons in the CA3 is at its peak, but that the firing rate of pyramidal neurons is higher than that of interneurons, causing the synchronous depolarization of cells of the CA1 downstream. From a study utilizing computer simulations, Ibarz and colleagues suggested that both in-phase firing and out-of-phase firing of principal cells in the hippocampus could lead to fast ripples observed in the epileptic brain. Additionally, the degree of synchrony in cellular discharge was found to be much more pronounced in the dentate gyrus than in other parts of the hippocampus, emphasizing that the elicitation of pathologic HFOs is complex and may look different on the single-cell level compared to the population behavior (Ibarz et al., 2010). The pathologic HFOs may also arise due to increased overall excitability caused by interneuron cell death following repeated seizures (Walker, 2015). The demographics of the remaining neurons may impact the molecular characteristics of the region, too, that is, causing a differential release of neurotransmitters or expression of receptors leading to an imbalance in neurotransmission (Menendez de la Prida et al., 2015). Another factor for elicitation of HFOs could be the breaking of the dentate gate. The dentate gate theory states that due to the nature of the granule cells and the local inhibitory

TABLE 1 | Studies evaluating pathological HFOs (pHFOs) in the epileptogenic regions.

Study	Subjects	Recording location	Detection parameters	Findings/Conclusion
Bragin et al., 1999	Rats (KA), Humans	Hippocampus (CA1, DG), Entorhinal cortex	Depth electrodes, microelectrodes	Fast ripples (250–500 Hz) were only found in the hippocampus of KA-treated rats and epileptic humans; fast ripples are defined as pathologic.
Staba et al., 2002	Humans	Hippocampus, Entorhinal cortex	Depth electrodes	More HFOs were detected in the hippocampal sites ipsilateral to onset location compared to contralateral sites.
Worrell et al., 2004	Humans	Temporal, frontal lobe	Video-EEG during sleep and wakefulness	pHFOs found in seizure onset zones and could predict onset within a specific timeframe in neocortical epilepsy.
Burnos et al., 2014	Humans	Various: Amygdala; Entorhinal cortex; Frontal anterior; Frontal lobe; Frontal posterior; Hippocampus; Mesial temporal lobe; Perirhinal cortex; Temporal basal anterior; Temporal basal posterior; Temporal depth frontal; Temporal depth lateral	iEEG	Location of pHFOs overlapped with the location of onset.
Řehulka et al., 2019	Humans	Hippocampus, amygdala	Depth electrodes	Ripples were more prominent in epileptic rather than non-epileptic brains. Higher frequencies were observed near sclerotic tissue.
Scott et al., 2021	Humans	Temporal, frontal lobe	iEEG	Pre-ictal and inter-ictal HFOs can in some cases be differentiated, and changes in the frequency of the HFOs can be used as predictors of seizures.
Jiruska et al., 2010	Rats (low-calcium ACSF perfusion of slices)	Hippocampus (CA1)	Glass pipettes, extracellular field potentials	HFOs build up before the seizure onset.
Ibarz et al., 2010	Rats (KA), Computer simulations	Hippocampus (DG, CA1, CA3), computational models	Silicon probes, computational models	Populations spikes and emergent spikes cause fast ripples, region-specific differences in synchronicity during HFOs.
Salami et al., 2014	Rats (Pilocarpine)	Hippocampus (CA1), Entorhinal cortex	Depth electrodes	pHFO dynamics and distribution changes during latency and chronic stage, inter-ictal spikes change before and after the first spontaneous seizure.
Jones et al., 2015	Mice (KA)	Hippocampus (CA1, DG)	Glass pipettes and silicon probes	pHFOs begin in the early latent period in CA1, and the majority are observed in DG. Peak amplitudes increase with epileptogenesis.
Ewell et al., 2019	Rats (KA)	Hippocampus (CA1)	LFP and single-unit recordings with tetrodes	pHFOs found only in epileptic brains independent of brain state and are associated with inter-ictal spikes.

circuitry, the dentate gyrus essentially acts as a gate that keeps the probability of seizures low. However, in epilepsy, there seems to be a malfunction in the regulation of this gate, and therefore the granule cells may become overexcitable (Krook-Magnuson et al., 2015). This makes sense when we consider some literature that has found that pathological HFOs are never observed in the dentate gyrus of healthy brains but are a hallmark of those that develop epilepsy (Engel et al., 2009). Importantly, these HFOs are observed in the seizure-generating areas ipsilateral to the site of drug injection and the site of tissue sclerosis within the hippocampus (Krook-Magnuson et al., 2015).

Hippocampal sclerosis may be one of the causes of local network reorganization (Walker, 2015) during the latent period. Since there is substantial neural damage induced from the hypertoxicity during the seizure development, the affected tissues endure atrophy and gliosis (Curia et al., 2008; Walker, 2015) throughout latency (Kim and Cho, 2018). A second cause may be the presence of HFOs within the latent period, which intensifies as the chronic stage nears. HFOs have been shown to facilitate synaptic changes in healthy neurons; however, if the HFOs occur more frequently and in different regions (Lévesque et al., 2018) than in healthy brains, this could lead to abnormal synaptic rewiring within the latent period (Janz et al., 2017) which may result in the increased propensity toward seizures. Thus, the relationship between HFOs and the extent of sclerosis in TLE may be another chicken and egg problem.

FUTURE DIRECTIONS

Growing evidence suggests that pathological HFOs within the latent period are associated with network rewiring, leading to changes in their expression as epileptogenesis continues. If this is the case, could stopping network rewiring also stop the HFOs? Could stopping the HFOs prevent the TLE development? In 2013, Krook-Magnuson and colleagues developed a method that could detect a seizure onset and optogenetically silence the activity of the hippocampal pyramidal cells in chronic

mice. This intervention resulted in a significant reduction in the seizure duration (Krook-Magnuson et al., 2013). One can imagine adapting this approach to detect the HFOs preceding the actual seizure, eliciting inhibition on the seizure focus, effectively preventing the seizure from happening at all.

Since closed-loop devices like the one described above may be invasive, though, inhibition through drugs could offer a less invasive solution (Smith et al., 2016; Vlasov et al., 2018). More specifically, since HFOs typically arise from around the seizure focus, we could investigate the applications of a DREADD mediated inhibition of the cells in the identified area following early detection of HFOs to prevent a seizure.

Löscher et al. (2015) states that many preventative interventions in the form of antiepileptic drugs (AEDs) have not been successful in attenuating chronic seizures. These results could be due to the wrong line of treatment for the type of epilepsy or the non-ideal timing of the therapy. An alternative approach to circumvent that would be to design an experiment for transiently reducing overall neural activity after a seizure rather than targeting a specific circuit to stop the overall network rewiring and aberrant synaptic plasticity changes. Some animals in the wild can achieve this brain state through the process of hibernation, in which neural activity reduces upon temperature reduction (Walker et al., 1977). This long-lasting hypothermic and hypometabolic state was artificially induced in non-hibernating animals using a DREADD mediated activation of hypothalamic Q-neurons (Takahashi et al., 2020). During this Q-neuron-induced hypothermia and hypometabolism (QIH), neural activity was substantially reduced in the whole brain without any observed tissue damage following hibernation. This tool would be a fascinating approach to help us gain insights into mechanisms of latent period, plasticity changes, and their role in TLE development. More research is needed to delineate the stages of TLE so that we may be better able to evaluate and perhaps halt the progression of TLE from the perspective of pathological oscillations.

AUTHOR CONTRIBUTIONS

Both authors listed have made a substantial, direct, and intellectual contribution to the work, and approved it for publication.

ACKNOWLEDGMENTS

TM acknowledges support from OIST graduate school. KT acknowledges support from MEXT Grant-in-Aid for Scientific Research (21H02585) and OIST.

REFERENCES

Andersen, P. (2007). *The Hippocampus Book*. New York: Oxford University Press.

Assenza, G., Lanzone, J., Insola, A., Amatori, G., Ricci, L., Tombini, M., et al. (2020). Thalamo-cortical network dysfunction in temporal lobe epilepsy. *Clin. Neurophysiol.* 131, 548–554. doi: 10.1016/j.clinph.2019.10.017

Başar, E., and Güntekin, B. (2008). A review of brain oscillations in cognitive disorders and the role of neurotransmitters. *Brain Res.* 1235, 172–193. doi: 10.1016/j.brainres.2008.06.103

Belchior, H., Lopes-Dos-Santos, V., Tort, A. B., and Ribeiro, S. (2014). Increase in hippocampal theta oscillations during spatial decision making. *Hippocampus* 24, 693–702. doi: 10.1002/hipo.22260

Bone, B., Fogarasi, A., Schulz, R., Gyimesi, C., Kalmar, Z., Kovacs, N., et al. (2012). Secondarily generalized seizures in temporal lobe epilepsy. *Epilepsia* 53, 817–824. doi: 10.1111/j.1528-1167.2012.03435.x

Bragin, A., Engel, J. Jr., Wilson, C. L., Fried, I., and Mathern, G. W. (1999). Hippocampal and entorhinal cortex high-frequency oscillations (100-500 Hz) in human epileptic brain and in kainic acid-treated rats with chronic seizures. *Epilepsia* 40, 127–137. doi: 10.1111/j.1528-1157.1999.tb02065.x

Burnos, S., Hilfiker, P., Sürücü, O., Scholkmann, F., Krayenbühl, N., Grunwald, T., et al. (2014). Human Intracranial High Frequency Oscillations (HFOs) detected by automatic time-frequency analysis. *PLoS One* 9:e94381. doi: 10.1371/journal.pone.0094381

Buzsáki, G. (2002). Theta Oscillations in the Hippocampus. *Neuron* 33, 325–340. doi: 10.1016/s0896-6273(02)00586-x

Buzsáki, G. (2015). Hippocampal sharp wave−ripple: a cognitive biomarker for episodic memory and planning. *Hippocampus* 25, 1073–188. doi: 10.1002/hipo.22488

Buzsáki, G., and Schomburg, E. W. (2015). What does gamma coherence tell us about interregional neural communication? *Nat. Neurosci.* 18, 484–489. doi: 10.1038/nn.3952

Buzsáki, G., and Wang, X. (2012). Mechanisms of gamma oscillations. *Ann. Rev. Neurosci.* 35, 203–225. doi: 10.1146/annurev-neuro-062111-150444

Cai, Z., Sohrabpour, A., Jiang, H., Ye, S., Joseph, B., Brinkmann, B. H., et al. (2021). Noninvasive high-frequency oscillations riding spikes delineates epileptogenic sources. *Proc. Natl. Acad. Sci. U. S. A.* 118:e2011130118. doi: 10.1073/pnas.2011130118

Cho, K., Lybrand, Z. R., Ito, N., Brulet, R., Tafacory, F., Zhang, L., et al. (2015). Aberrant hippocampal neurogenesis contributes to epilepsy and associated cognitive decline. *Nat. Commun.* 6:6606. doi: 10.1038/ncomms7606

Chrobak, J. J., and Buzsáki, G. (1996). High-frequency oscillations in the output networks of the hippocampal–entorhinal axis of the freely behaving rat. *J. Neurosci.* 16, 3056–3066. doi: 10.1523/jneurosci.16-09-03056.1996

Curia, G., Longo, D., Biagini, G., Jones, R. S., and Avoli, M. (2008). The pilocarpine model of temporal lobe epilepsy. *J. Neurosci. Methods* 172, 143–157. doi: 10.1016/j.jneumeth.2008.04.019

Curia, G., Lucchi, C., Vinet, J., Gualtieri, F., Marinelli, C., Torsello, A., et al. (2014). Pathophysiogenesis of mesial temporal lobe epilepsy: is prevention of damage antiepileptogenic? *Curr. Med. Chem.* 21, 663–688. doi: 10.2174/09298673206613111915220

Engel, J. Jr. (2014). Approaches to refractory epilepsy. *Ann. Indian Acad. Neurol.* 17, S12–7. doi: 10.4103/0972-2327.128644

Engel, J. Jr., Bragin, A., Staba, R., and Mody, I. (2009). High-frequency oscillations: what is normal and what is not? *Epilepsia* 50, 598–604. doi: 10.1111/j.1528-1167.2008.01917.x

Ewell, L. A., Fischer, K. B., Leibold, C., Leutgeb, S., and Leutgeb, J. K. (2019). The impact of pathological high-frequency oscillations on hippocampal network activity in rats with chronic epilepsy. *ELife* 8:e42148. doi: 10.7554/elife.42148

Gowers, W. R. (1901). *Epilepsy and Other Chronic Convulsive Diseases: Their Causes, Symptoms and Treatment*. Philadelphia: P. Blakistons Son & Co.

Hamilton, H. K., Roach, B. J., Cavus, I., Teyler, T. J., Clapp, W. C., Ford, J. M., et al. (2020). Impaired potentiation of theta oscillations during a visual cortical plasticity paradigm in individuals with schizophrenia. *Front. Psychiatry* 11:590567. doi: 10.3389/fpsyt.2020.590567

Henderson, K. W., Gupta, J., Tagliatela, S., Litvina, E., Zheng, X., Zandt, M. A., et al. (2014). Long-term seizure suppression and optogenetic analyses of synaptic connectivity in epileptic mice with hippocampal grafts of GABAergic interneurons. *J. Neurosci.* 34, 13492–13504. doi: 10.1523/jneurosci.0005-14.2014

Herweg, N. A., Solomon, E. A., and Kahana, M. J. (2020). Theta oscillations in human memory. *Trends Cogn. Sci.* 24, 208–227. doi: 10.1016/j.tics.2019.12.006

Hristova, K., Martinez-Gonzalez, C., Watson, T. C., Codadu, N. K., Hashemi, K., Kind, P. C., et al. (2021). Medial septal GABAergic neurons reduce seizure duration upon optogenetic closed-loop stimulation. *Brain* 144, 1576–1589. doi: 10.1093/brain/awab042

Ibarz, J. M., Foffani, G., Cid, E., Inostroza, M., and Menendez de la Prida, L. (2010). Emergent dynamics of fast ripples in the epileptic hippocampus. *J. Neurosci.* 30, 16249–16261. doi: 10.1523/jneurosci.3357-10.2010

Jadhav, S. P., Kemere, C., German, P. W., and Frank, L. M. (2012). Awake hippocampal sharp-wave ripples support spatial memory. *Science* 336, 1454–1458. doi: 10.1126/science.1217230

Janz, P., Savanthrapadian, S., Häussler, U., Kilias, A., Nestel, S., Kretz, O., et al. (2017). Synaptic remodeling of entorhinal input contributes to an aberrant hippocampal network in temporal lobe epilepsy. *Cereb. Cortex* 27, 2348–2364. doi: 10.1093/cercor/bhw093

Jiruska, P., Alvarado-Rojas, C., Schevon, C. A., Staba, R., Stacey, W., Wendling, F., et al. (2017). Update on the mechanisms and roles of high-frequency oscillations in seizures and epileptic disorders. *Epilepsia* 58, 1330–1339. doi: 10.1111/epi.13830

Jiruska, P., Csicsvari, J., Powell, A. D., Fox, J. E., Chang, W. C., Vreugdenhil, M., et al. (2010). High-frequency network activity, global increase in neuronal activity, and synchrony expansion precede epileptic seizures *in vitro*. *J. Neurosci.* 30, 5690–5701. doi: 10.1523/jneurosci.0535-10.2010

Jones, R. T., Barth, A. M., Ormiston, L. D., and Mody, I. (2015). Evolution of temporal and spectral dynamics of pathologic high-frequency oscillations (pHFOs) during epileptogenesis. *Epilepsia* 56, 1879–1889. doi: 10.1111/epi.13218

Kandratavicius, L., Balista, P., Lopes-Aguiar, C., Ruggiero, R., Umeoka, E., Garcia-Cairasco, N., et al. (2014). Animal models of epilepsy: use and limitations. *Neuropsychiatric Dis. Treat.* 10, 1693–1705. doi: 10.2147/ndt.s50371

Kiernan, J. A. (2012). Anatomy of the Temporal Lobe. *Epilepsy Res. Treat.* 2012, 1–12. doi: 10.1155/2012/176157

Kim, J., and Cho, K. (2018). The pilocarpine model of temporal lobe epilepsy and EEG monitoring using radiotelemetry system in mice. *J. Vis. Exp.* 132:56831. doi: 10.3791/56831

Krook-Magnuson, E., Armstrong, C., Bui, A., Lew, S., Oijala, M., and Soltesz, I. (2015). *In vivo* evaluation of the dentate gate theory in epilepsy. *J. Physiol.* 593, 2379–2388. doi: 10.1113/jp270056

Krook-Magnuson, E., Armstrong, C., Oijala, M., and Soltez, I. (2013). On-demand optogenetic control of spontaneous seizures in temporal lobe epilepsy. *Nat. Commun.* 4:1376. doi: 10.1038/ncomms2376

Kucewicz, M. T., Cimbalnik, J., Matsumoto, J. Y., Brinkmann, B. H., Bower, M. R., Vasoli, V., et al. (2014). High frequency oscillations are associated with cognitive processing in human recognition memory. *Brain* 137, 2231–2244. doi: 10.1093/brain/awu149

Lee, A. K., and Wilson, M. A. (2002). Memory of sequential experience in the hippocampus during slow wave sleep. *Neuron* 36, 1183–1194. doi: 10.1016/s0896-6273(02)01096-6

Lee, H., Jung, S., Lee, P., and Jeong, Y. (2017). Altered intrinsic functional connectivity in the latent period of epileptogenesis in a temporal lobe epilepsy model. *Exp. Neurol.* 296, 89–98. doi: 10.1016/j.expneurol.2017.07.007

Lévesque, M., and Avoli, M. (2013). The kainic acid model of temporal lobe epilepsy. *Neurosci. Biobehav. Rev.* 37, 2887–2899. doi: 10.1016/j.neubiorev.2013.10.011

Lévesque, M., Shiri, Z., Chen, L., and Avoli, M. (2018). High-frequency oscillations and mesial temporal lobe epilepsy. *Neurosci. Lett.* 667, 66–74. doi: 10.1016/j.neulet.2017.01.047

Lillis, K. P., Wang, Z., Mail, M., Zhao, G. Q., Berdichevsky, Y., Bacskai, B., et al. (2015). Evolution of network synchronization during early epileptogenesis parallels synaptic circuit alterations. *J. Neurosci.* 35, 9920–9934. doi: 10.1523/jneurosci.4007-14.2015

Löscher, W., Hirsch, L. J., and Schmidt, D. (2015). The enigma of the latent period in the development of symptomatic acquired epilepsy — Traditional view versus new concepts. *Epilepsy Behav.* 52, 78–92. doi: 10.1016/j.yebeh.2015.08.037

Louie, K., and Wilson, M. A. (2001). Temporally structured replay of awake hippocampal ensemble activity during rapid eye movement sleep. *Neuron* 29, 145–156. doi: 10.1016/s0896-6273(01)00186-6

Maguire, J. (2016). Epileptogenesis: more than just the latent period. *Epilepsy Curr.* 16, 31–33. doi: 10.5698/1535-7597-16.1.31

Menendez de la Prida, L., and Huberfeld, G. (2019). Inhibition and oscillations in the human brain tissue *in vitro*. *Neurobiol. Dis.* 125, 198–210. doi: 10.1016/j.nbd.2019.02.006

Menendez de la Prida, L., Staba, R. J., and Dian, J. A. (2015). Conundrums of high-frequency oscillations (80–800 Hz) in the epileptic brain. *J. Clin. Neurophysiol.* 32, 207–219. doi: 10.1097/wnp.0000000000000150

Miller, J. W., Turner, G. M., and Gray, B. C. (1994). Anticonvulsant effects of the experimental induction of hippocampal theta activity. *Epilepsy Res.* 18, 195–204. doi: 10.1016/0920-1211(94)90040-x

Oliva, A., Fernández-Ruiz, A., Oliveira, E. F., and Buzsáki, G. (2018). Origin of gamma frequency power during hippocampal sharp-wave ripples. *Cell Rep.* 25, 1693–1700.e4. doi: 10.1016/j.celrep.2018.10.066

Pail, M., Cimbálník, J., Roman, R., Daniel, P., Shaw, D. J., Chrastina, J., et al. (2020). High frequency oscillations in epileptic and non-epileptic human hippocampus during a cognitive task. *Sci. Rep.* 10:18147. doi: 10.1038/s41598-020-74306-3

Panayiotopoulos, C. P. (2005). *The Epilepsies: Seizures, Syndromes and Management: Based on the ILAE Classifications and Practice Parameter Guidelines*. Chipping Norton: Bladon Medical Pub.

Paschen, E., Elgueta, C., Heining, K., Vieira, D. M., Kleis, P., Orcinha, C., et al. (2020). Hippocampal low-frequency stimulation prevents seizure generation in a mouse model of mesial temporal lobe epilepsy. *Elife* 9:e54518. doi: 10.7554/elife.54518

Paz, R., Bauer, E. P., and Pare, D. (2008). Theta synchronizes the activity of medial prefrontal neurons during learning. *Learn. Memory* 15, 524–531. doi: 10.1101/lm.932408

Ramadan, W., Eschenko, O., and Sara, S. J. (2009). Hippocampal sharp wave/ripples during sleep for consolidation of associative memory. *PLoS One* 4:e6697. doi: 10.1371/journal.pone.0006697

Rattka, M., Brandt, C., Bankstahl, M., Bröer, S., and Löscher, W. (2011). Enhanced susceptibility to the GABA antagonist pentylenetetrazole during the latent period following a pilocarpine-induced status epilepticus in rats. *Neuropharmacology* 60, 505–512. doi: 10.1016/j.neuropharm.2010.11.005

Řehulka, P., Cimbálník, J., Pail, M., Chrastina, J., Hermanová, M., and Brázdil, M. (2019). Hippocampal high frequency oscillations in unilateral and bilateral mesial temporal lobe epilepsy. *Clin. Neurophysiol.* 130, 1151–1159. doi: 10.1016/j.clinph.2019.03.026

Ren, E., and Curia, G. (2021). Synaptic reshaping and neuronal outcomes in the temporal lobe epilepsy. *Int. J. Mol. Sci.* 22:3860. doi: 10.3390/ijms22083860

Salami, P., Lévesque, M., Benini, R., Behr, C., Gotman, J., and Avoli, M. (2014). Dynamics of interictal spikes and high-frequency oscillations during epileptogenesis in temporal lobe epilepsy. *Neurobiol. Dis.* 67, 97–106. doi: 10.1016/j.nbd.2014.03.012

Scott, J. M., Gliske, S. V., Kuhlmann, L., and Stacey, W. C. (2021). Viability of preictal high-frequency oscillation rates as a biomarker for seizure prediction. *Front. Hum. Neurosci.* 14:612899. doi: 10.3389/fnhum.2020.612899

Seidenbecher, T., Laxmi, T. R., Stork, O., and Pape, H. (2003). Amygdalar and hippocampal theta rhythm synchronization during fear memory retrieval. *Science* 301, 846–850. doi: 10.1126/science.1085818

Sharma, S., Puttachary, S., Thippeswamy, A., Kanthasamy, A. G., and Thippeswamy, T. (2018). Status Epilepticus: behavioral and electroencephalography seizure correlates in kainate experimental models. *Front. Neurol.* 9. doi: 10.3389/fneur.2018.00007

Shibley, H., and Smith, B. N. (2002). Pilocarpine-induced status epilepticus results in mossy fiber sprouting and spontaneous seizures in C57BL/6 and CD-1 mice. *Epilepsy Res.* 49, 109–120. doi: 10.1016/s0920-1211(02)00012-8

Sinel'Nikova, V. V., Shubina, L. V., Gol'Tyaev, M. V., Loseva, E. V., and Kichigina, V. F. (2013). Detection of c-Fos expression in the brains of animals with a pilocarpine model of temporal lobe epilepsy. *Neurosci. Behav. Physiol.* 43, 1084–1091. doi: 10.1007/s11055-013-9853-6

Skaggs, W. E., and McNaughton, B. L. (1996). Replay of neuronal firing sequences in rat hippocampus during sleep following spatial experience. *Science* 271, 1870–1873. doi: 10.1126/science.271.5257.1870

Smith, K. S., Bucci, D. J., Luikart, B. W., and Mahler, S. V. (2016). DREADDS: use and application in behavioral neuroscience. *Behav. Neurosci.* 130, 137–155. doi: 10.1037/bne0000135

Song, J., Tucker, D. M., Gilbert, T., Hou, J., Mattson, C., Luu, P., et al. (2013). Methods for examining electrophysiological coherence in epileptic networks. *Front. Neurol.* 4:55. doi: 10.3389/fneur.2013.00055

Staba, R. J., Wilson, C. L., Bragin, A., Fried, I., and Engel, J. Jr. (2002). Quantitative analysis of high-frequency oscillations (80–500 hz) recorded in human epileptic hippocampus and entorhinal cortex. *J. Neurophysiol.* 88, 1743–1752. doi: 10.1152/jn.2002.88.4.1743

Sullivan, D., Csicsvari, J., Mizuseki, K., Montgomery, S., Diba, K., and Buzsáki, G. (2011). Relationships between hippocampal sharp waves, ripples, and fast gamma oscillation: influence of dentate and entorhinal cortical activity. *J. Neurosci.* 31, 8605–8616. doi: 10.1523/jneurosci.0294-11.2011

Takahashi, T. M., Sunagawa, G. A., Soya, S., Abe, M., Sakurai, K., Ishikawa, K., et al. (2020). A discrete neuronal circuit induces a hibernation-like state in rodents. *Nature* 583, 109–114. doi: 10.1038/s41586-020-2163-6

Tsanov, M., and Manahan-Vaughan, D. (2009). Long-term plasticity is proportional to theta-activity. *PLoS One* 4:e5850. doi: 10.1371/journal.pone.0005850

Vlasov, K., Dort, C. J., and Solt, K. (2018). Optogenetics and Chemogenetics. *Methods Enzymol.* 603, 181–196. doi: 10.1016/bs.mie.2018.01.022

Walker, J. M., Glotzbach, S. F., Berger, R. J., and Heller, H. C. (1977). Sleep and hibernation in ground squirrels (Citellus spp): electrophysiological observations. *Am. J. Physiol. Regul. Integr. Comp. Physiol.* 233, R213–R221. doi: 10.1152/ajpregu.1977.233.5.r213

Walker, M. (2015). Hippocampal sclerosis: causes and prevention. *Semin. Neurol.* 35, 193–200. doi: 10.1055/s-0035-1552618

Wang, Y., Shen, Y., Cai, X., Yu, J., Chen, C., Tan, B., et al. (2021). Deep brain stimulation in the medial septum attenuates temporal lobe epilepsy via entrainment of hippocampal theta rhythm. *CNS Neurosci. Ther.* 27, 577–586. doi: 10.1111/cns.13617

Watson, T. C., Obiang, P., Torres-Herraez, A., Watilliaux, A., Coulon, P., Rochefort, C., et al. (2019). Anatomical and physiological foundations of cerebello-hippocampal interaction. *Elife* 8:e41896. doi: 10.7554/elife.41896

Wilson, M. A., and McNaughton, B. L. (1994). Reactivation of hippocampal ensemble memories during sleep. *Science* 265, 676–679. doi: 10.1126/science.8036517

Worrell, G. A., Parish, L., Cranstoun, S. D., Jonas, R., Baltuch, G., and Litt, B. (2004). High-frequency oscillations and seizure generation in neocortical epilepsy. *Brain* 127, 1496–1506. doi: 10.1093/brain/awh149

Zhang, X., Zhong, W., Brankačk, J., Weyer, S. W., Müller, U. C., and Tort, A. B. (2016). Impaired theta-gamma coupling in APP-deficient mice. *Sci. Rep.* 6:21948. doi: 10.1038/srep21948

Zhou, Y., Qiu, L., Wang, H., and Chen, X. (2020). Induction of activity synchronization among primed hippocampal neurons out of random dynamics is key for trace memory formation and retrieval. *FASEB J.* 34, 3658–3676. doi: 10.1096/fj.201902274r

Zijlmans, M., Jiruska, P., Zelmann, R., Leijten, F. S., Jefferys, J. G., and Gotman, J. (2012). High-frequency oscillations as a new biomarker in epilepsy. *Ann. Neurol.* 71, 169–178. doi: 10.1002/ana.22548

Conflict of Interest: The authors declare that the research was conducted in the absence of any commercial or financial relationships that could be construed as a potential conflict of interest.

Publisher's Note: All claims expressed in this article are solely those of the authors and do not necessarily represent those of their affiliated organizations, or those of the publisher, the editors and the reviewers. Any product that may be evaluated in this article, or claim that may be made by its manufacturer, is not guaranteed or endorsed by the publisher.

frontiers in Behavioral Neuroscience

ORIGINAL RESEARCH
published: 24 December 2021
doi: 10.3389/fnbeh.2021.774999

Non-thermal Electroporation Ablation of Epileptogenic Zones Stops Seizures in Mice While Providing Reduced Vascular Damage and Accelerated Tissue Recovery

*Emma Acerbo[1†], Sawssan Safieddine[1†], Pascal Weber[1], Boris Botzanowski[1], Florian Missey[1], Marcel Carrère[1], Robert E. Gross[2], Fabrice Bartolomei[1], Romain Carron[1,3], Viktor Jirsa[1], Ivo Vanzetta[4], Agnès Trébuchon[1] and Adam Williamson[1,5]**

[1] Institut de Neurosciences des Systèmes, UMR 1106, Aix-Marseille Université, Marseille, France, [2] Department of Neurosurgery, Emory University School of Medicine, Atlanta, GA, United States, [3] Department of Functional and Stereotactic Neurosurgery, Timone University Hospital, Aix-Marseille Université, Marseille, France, [4] Institut de Neurosciences de la Timone, CNRS, Aix-Marseille Université, Marseille, France, [5] Center for Bioelectronic Medicine, Department of Medicine, Solna, Karolinska Institutet, Stockholm, Sweden

OPEN ACCESS

Edited by:
Yuichi Takeuchi,
Hokkaido University, Japan

Reviewed by:
Tomoyuki Miyazaki,
Yokohama City University, Japan
Kiyoshi Egawa,
Hokkaido University, Japan

***Correspondence:**
Adam Williamson
adam.williamson@univ-amu.fr;
adam.williamson@ki.se

[†] These authors have contributed equally to this work

Specialty section:
This article was submitted to Pathological Conditions, a section of the journal Frontiers in Behavioral Neuroscience

Received: 13 September 2021
Accepted: 08 November 2021
Published: 24 December 2021

Citation:
Acerbo E, Safieddine S, Weber P, Botzanowski B, Missey F, Carrère M, Gross RE, Bartolomei F, Carron R, Jirsa V, Vanzetta I, Trébuchon A and Williamson A (2021) Non-thermal Electroporation Ablation of Epileptogenic Zones Stops Seizures in Mice While Providing Reduced Vascular Damage and Accelerated Tissue Recovery. Front. Behav. Neurosci. 15:774999. doi: 10.3389/fnbeh.2021.774999

In epilepsy, the most frequent surgical procedure is the resection of brain tissue in the temporal lobe, with seizure-free outcomes in approximately two-thirds of cases. However, consequences of surgery can vary strongly depending on the brain region targeted for removal, as surgical morbidity and collateral damage can lead to significant complications, particularly when bleeding and swelling are located near delicate functional cortical regions. Although focal thermal ablations are well-explored in epilepsy as a minimally invasive approach, hemorrhage and edema can be a consequence as the blood-brain barrier is still disrupted. Non-thermal irreversible electroporation (NTIRE), common in many other medical tissue ablations outside the brain, is a relatively unexplored method for the ablation of neural tissue, and has never been reported as a means for ablation of brain tissue in the context of epilepsy. Here, we present a detailed visualization of non-thermal ablation of neural tissue in mice and report that NTIRE successfully ablates epileptic foci in mice, resulting in seizure-freedom, while causing significantly less hemorrhage and edema compared to conventional thermal ablation. The NTIRE approach to ablation preserves the blood-brain barrier while pathological circuits in the same region are destroyed. Additionally, we see the reinnervation of fibers into ablated brain regions from neighboring areas as early as day 3 after ablation. Our evidence demonstrates that NTIRE could be utilized as a precise tool for the ablation of surgically challenging epileptogenic zones in patients where the risk of complications and hemorrhage is high, allowing not only reduced tissue damage but potentially accelerated recovery as vessels and extracellular matrix remain intact at the point of ablation.

Keywords: resective surgery, ablation, two photon, epilepsy, electroporation

INTRODUCTION

The primary method of treatment for patients suffering from drug-resistant focal-onset epilepsy is resective surgery (Wiebe et al., 2001). In the most common type of drug-resistant epilepsy, mesial temporal lobe epilepsy (MTLE), while associated with high-rates of seizure freedom surgical resection can often impact neurocognitive function. For drug-resistant MTLE, focal thermal ablation is a less-invasive method being explored for surgical treatment to achieve high-degrees of seizure freedom while maintaining memory and other cognitive functions associated with the basal and lateral temporal areas (Bezchlibnyk et al., 2018; Gross et al., 2018). Although, radio-frequency (RF) ablation and laser interstitial thermal therapy (LITT, aka laser ablation) are the methods with the most attention, achieving reasonable seizure-free rates with less negative impact on neurocognitive function, (Gross et al., 2015) there remain technical questions about these two methods of thermal ablation, primarily thermal injury to surrounding tissues, edema due to hemorrhage (Howenstein and Sato, 2010) and poor directionality.

Here we investigate irreversible electroporation, a common method of focal ablation outside of the brain, but which may be feasible to use in brain tissue to avoid the primary concerns of focal RF and laser ablation in epilepsy. Indeed, in spite of the numerous focal ablations performed using irreversible electroporation in tumor removal, (Davalos et al., 2005; Golberg and Yarmush, 2013) it has not yet been adopted in the ablation of neural tissue clinically. The NTIRE mechanism itself is well-understood. Electroporation induces the formation of pores in the cell membrane due to the application of an electric field with a relatively high field intensity (typically in the kV/cm range), however, with a very short pulse duration (in the μs range) to avoid thermal heating (Kinosita and Tsong, 1977). Classically, electroporation was a technique used to insert plasmids into mammalian cells (Chu et al., 1987). Here, we visualize and investigate the possibility of using non-thermal irreversible electroporation (NTIRE) in the somatosensory cortex, posterior parietal cortex, and hippocampus of mice. For this purpose, we induce pores in the target neurons to be ablated, allowing the influx and efflux of ions and molecules, irreversibly disturbing the intra- and extracellular concentration gradients. The target neurons are not able to recover from these abrupt, non-thermally induced physiological changes, and subsequently die (Joshi and Schoenbach, 2002). There are many studies showing the negative impact of elevated temperatures on tissue, creating necrosis and tissue damage past a certain threshold (Moritz, 1947; Yarmolenko et al., 2011). Here, in applying multiple temporally short pulses of electric fields, it's possible to create irreversible electroporation without heat-related damage (Joshi and Schoenbach, 2002).

We found that neural cells can be ablated in specific regions while the blood-brain barrier remains intact in the same region. Vasoconstriction and leaking from the blood-brain barrier during and after the NTIRE event is investigated as a function of vessel size, with larger vessels essentially temporarily contracting after the electroporation without any significant degree of leakage and small vessels temporarily contracting with only a mild degree of leakage. However, both vessel groups remain intact, while target neurons around the vessels are destroyed. Additionally, re-innervation of fibers into ablated regions and activation of dendritic cells indicates a possible acceleration of recovery in the ablated brain region compared to a thermal ablation where coagulated tissue renders a brain region permanently dead.

MATERIALS AND METHODS

Surgeries and Electrodes Placement

All surgical procedures were approved by the National Animal Studies Committee of France (authorization no. APAFIS20359-2019041816357133v5). We used 27 OF1 (Charles Rivers, Les Oncins, France) adult mice 8–10 weeks old, 30–40 g in weight. We used also 6 mice with Thy1-cyan fluorescent protein (CFP)-23, LysM-green fluorescent protein (GFP), CD11c-yellow fluorescent protein (YFP). Mice were deeply anesthetized with ketamine–xylazine (120 mg/kg, 12 mg/kg, respectively) in saline with (IP) intra-peritoneal injection and supplemented when need it (60 mg/kg, 6 mg/kg). Ocry-gel (Laboratoire TVM, Lempdes, France) was applied to maintain eye moisture and surgical anesthesia was verified by a lack of toe pinch reflex. The hair around the surgical site was shaved, and the skin was cleaned with iodine solution (Vétoquinol). The skin of the skull was incised, and the fascia was gently removed using a scalpel.

For the placement electrode on the cortex, a U-shaped clip were placed on the skull of the left side and glued with primer dental cement (GACD, France) followed by blockout resin photopolymerized by an optic UV lamp (GACD, France). This clip served to fix mice during surgery procedure and image acquisition under the microscope, to a holder. A craniotomy was carried out on the right hemisphere of the head using a high-speed drill with a carbide bur (size = round 1/4; World Precision Instruments, Hitchin, England). The brain was kept free of debris by repeated rinsing with phosphate buffered saline (PBS) during implant and surgery.

Two 50 μm platinum-iridium microelectrodes (Phymep) were placed on the dura matter of the brain and fixed on the skull by primer dental cement followed by the photopolymerized block resin. Prior to the surgery, a glass window of 5 mm diameter and 0.17 mm thickness (Thermo Fisher Scientific, France) was cleaned and dried. Once the electrodes were positioned, the glass window was placed over the skull and electrodes. Gentle pressure was applied to maintain the glass in place while dental cement was applied to the edges of the glass and the surrounding bone and muscle. Finally, an additional layer of dental cement was applied over the primer to reinforce the structure.

For the deep brain ablation, groups of OF1 underwent a surgical procedure as described above. However, instead of placing **two** wires on the cortex, an implantable electrode was placed into the brain in order to reach the hippocampus. For that, a craniotomy was performed by drilling a hole for the electrode (PT electrode twisted 5 mm, Bilaney Consultant**s**, Germany) (Coordinates: ML: −2.04, AP: +2.07, DV: 1.29 determined by the Paxinos atlas) and another one for the reference in the cerebellum. At the end, electrodes were cemented with Dentalon (PHYMEP, France).

Non-thermal Irreversible Electroporation and Thermal Irreversible Electroporation Lesion

The electroporator device (Electro cell B10-CNRS) is connected through the two wires placed on the brain of the mice. The delivered voltage values depend on the space between the two wires, but it was always equal to 1,750 V/cm. The width of the pulse for both the positive and negative phase was 50 μs the frequency was 10 Hz with 10 repetitions. All TIRE and NTIRE stimulations were performed with the electroporator device as it is possible to configure parameters of stimulation (**Supplementary Figure 1**).

Microscopic Imaging

For the microscopy, animals were injected with 50 μl of Dextran, Rhodamine B, 10,000 MW, Neutral (Thermo Fisher Scientific) (3 mg/ml) in saline was injected in the ophthalmic venous sinus using the retro-orbital method. During imaging, the animals were freely breathing, and the microscope chamber was heated to ∼32°C. We used a tunable femtosecond pulsed laser (Mai-Tai, Spectra Physics, Évry, France) coupled to a Zeiss two-photon microscope (LSM 780) equipped with a Plan-Apochromat 20× water immersion objective lens (NA = 1.0) and five non-descanned detectors (NDD). For each image stack laser, intensity and sometimes the gain, were adjusted according to imaging depth in order to maximize image intensity while minimizing saturation throughout the image stack. We always imaged the region between the two wires using the following strategy. The window was epi-illuminated with LED lights on the side of the objective. To determine the vasoconstriction percentage, blood vessels where divided into two groups: large blood vessel ≥20 μm and small blood vessel <20 μm. Images were analyzed using the ZEN 2.6 software, the diameter of blood vessels before and after stimulation was taken, and the percentage of vasoconstriction was calculated.

Kindling Protocol

For depth NTIRE and TIRE ablation of epileptic foci, mice with implantable hippocampal -CA3- electrode (Twisted Pair, Plastic One®), after 2 days post-surgery, were connected to a data acquisition system (Intan Technologies, United States) in order to record and stimulate. After finding the after discharge (AD) threshold for each mouse (the minimum current applied to evoke a seizure) the following parameters were applied: 50 Hz, 500 μ s pulse width, train of 500 stimulation pulses, with current set at the AD threshold (see **Supplementary Figure 2** for more details). This stimulation was repeated 10 times every 10 min (Lothman et al., 1985; Musto et al., 2009). After that, NTIRE or TIRE ablation was performed with the electroporator device (under anesthesia) and epilep**ti**form events were recorded within the following 12 h.

Analysis Spikes Rate

To detect specific events as spikes, we performed a semi-automatic detection on the signal. The detection part was processed by using Delphos software, a detector of spikes and oscillations used mainly in clinical research (Roehri et al., 2018). Before to analyzed the signal, it has been downsample to 3,750 Hz and filtered in between 20 and 40 Hz. All the spikes detection were reviewed by a single person (EA) via AnyWave software, a visualization software for electrophysiological data (Colombet et al., 2015). To asses the number of epileptic spikes, each mice underwent a 1 h recording before NTIRE treatment and 1 h after the treatment (for non-treatment group, delay in between the two recording session was the same as NTIRE group). Epileptic spikes were detected and an average of the spikes/min was calculated.

Finite Element Method

Finite Element Method calculations were performed with the COMSOL Multiphysics 5.5 software. The physic used was "Electrical Current." A custom mouse brain mesh model was designed on Blender software and then imported in COMSOL Multiphysics 5.5. The distance and the voltage applied between the electrodes were taken in account to recreate as closely as possible the experimental conditions of the Cortical NTIRE ablation, 245 V between $\simeq$ 1.4 mm. All plots were made and exported with the built-in tool of COMSOL Multiphysics 5.5 (**Supplementary Figure 3**).

Histology

Conventional histology was performed on twelve section. Four days after the stimulation mice were perfused with saline followed by 4% paraformaldehyde, then brain was carefully removed from the skull and transferred to 4% PFA for post fixation. After 1 day of post-fixation, brain was washed three times in 0.12 PB and then immersed in 20% sucrose in 0.12 PB for 24 h. The day after brain was frozen, with the ventral surface placed on a metal plate, cooled by a surrounding bath of dry ice. Brains were stored at −80°C until cut. The brain tissue was sectioned into coronal section of 30 μm in thickness on Leica CM3500 cryostat (Leica Microsystems Inc., Bannockburn, IL, United States).

For cell counting: all tissue sections lying between the two electrodes were collected. Brain sections to be stained with Nissl Eosin were directly mounted on the microscopic glasses (Polysine™ Microscope Adhesion Slides – Thermo Fisher Scientific) and left for 24 h in the oven.

Then, sections were placed in alcohol 95% two times for 10 min, followed by 5 min in chloroform. Then, they were hydrated by alcohol 95, 80, and 75% for 2 min each. Next, sections were soaked 10 times slowly in distilled water before staining them in the heated (60°C) Nissl's solution for 1 min. A second wash with water is done for 1 min before immersion of the sections in acetic formalin solution for 6 min. Washing with water for 1 min is done before passing to the dehydration step in alcohol 80, 90, 95, 100, and 100% for 2 min each. Nissl's sections were used for assessing the cell death.

Statistics

Date were analyzed using R software. Vasoconstriction, cell loss and spike rate data were separated into groups regarding the ablation protocol (NTIRE, TIRE, and no treatment). After a common normality verification using Shapiro test, groups

were compared with *T*-test or Wilcoxon-test depending on the presence or absence of a normal distribution, respectively.

Figures 2, **3**: 9 NTIRE mice were analyzed to assess the percentage of vasoconstriction on NTIRE mice. To determine the vasoconstriction percentage broadly, blood vessels where divided into two groups: large blood vessels ≥20 μm and small blood vessels <20 μ m.

Figure 4: 4 OF1 mice were sacrificed, and histological analysis of cell loss was performed for cortex cell-density data, with contralateral cortex used as the control for cell density.

Figure 5: 12 OF1 mice were kindled as described above and six received NTIRE ablations, the six other were not treated to show that there is no decrease of spikes during time. After a common normality verification using Shapiro test, Wilcoxon test were performed.

RESULTS

Experimental Set Up

The experimental setup is introduced in **Figures 1A,B**, where microelectrodes are mounted on the somatosensory or posterior parietal cortex of mice. When the NTIRE event is visualized in real-time using a 2-photon fluorescence microscope, a brief contraction of vessels can be seen but they remain intact. However, neurons in the region of the NTIRE are destroyed, as depicted in **Figure 1C**. A thermal ablation, or thermal irreversible electroporation (TIRE) also uses a high electric field, but typically the pulse width is larger creating a thermal event and subsequent coagulation necrosis of tissue – vessels, neurons, and all tissues in the ablated region are destroyed. Then we wanted to compare if the tissue damage in the epileptic hippocampus after NTIRE ablations is reduced compared to epileptic mice receiving a thermal ablation of the same region. To better understand this, the parameters of non-thermal ablations are discussed in detail in **Figure 2** and **Supplementary Figure 1**.

Non-thermal Irreversible Electroporation Induces Vessels Contraction Without Ablation

The primary parameters of interest in a thermal versus non-thermal ablation are power and electric field. The electric field must be sufficiently high to cause the irreversible poration of cell membranes. An ablation is performed with identical electric field values, high enough to cause irreversible poration, here 1,750 V/cm (**Supplementary Figure 1**). However, in NTIRE ablation, the associated power is only 200 mW, creating a non-thermal event. As can be seen in the image, the cortex immediately after the NTIRE event is visibly unchanged. For TIRE, the associated power is 11 W, creating a very thermal event. As can be seen in the image, the cortex immediately after the TIRE event shows a increase in bleeding. Because of absence of bleeding in the NTIRE process, mice can be monitored for longer periods of time without significant reduction in imaging quality of the two photon visualization. Consequently, mice were monitored up to 37 days after NTIRE ablation, with no visual destruction of vessels seen for the duration of the monitoring (**Figure 2B**). As seen in **Figure 2C**, blood plasma flow slows, with red blood cells seen individually in the vessels (panel, t = 1 min 45 s) as the speed of blood plasma flow has decreased. Flow recovers for vessels of all sizes after several minutes, however, (right panel) the difference between large and small vessels is simply the percentage of contraction – with no discernable long-term effects. Indeed, it was the short-term effects on vessels which were quite interesting immediately after NTIRE, namely the leakage and the percentage of contraction. Then, the contraction and leakage as been analyzed as a function of diameter. In **Figure 2D**, a section of cortex can be seen with vessels down to a depth of approximately 400 μm. Vessels of numerous sizes can be seen before and after, without any damage to the vessels. Vessel diameters due to the NTIRE have completely recovered. On the panel E, data showing typical contractions in a section of tissue is grouped into large vessels (greater than 20 μm diameter) and small vessels (less than 20 μm diameter). The percentage of vasocontraction is more dramatic for smaller vessels than larger vessels (*t_test:* p-value = 0.02622). Interestingly, this corresponds well to leakage, which is measured as a change in fluorescence measured 10 μm outside of vessels. So, three example vessels are shown, with 60, 44, and 10 μm diameters. The change in fluorescence outside of all vessels of 60 μm in diameter or greater is negligible, which is an important result as damage and leaking to such large vessels would create a significant hemorrhage. The change in fluorescence outside of vessels of large-medium vessels 30–40 μm in diameter (40 μm in the example) is small and relatively fast (**Figure 2F**). The interesting measurements are from vessels less than 20 μm, (10 μm diameter in the example) where fluorescence increases substantially. Although the vessels are not destroyed, leakage will likely allow a small amount of blood into the surrounding tissue. The result is that leakage from a vessel due to NTIRE seems to scale with the percentage of vasoconstriction of a given vessel, with an increased percentage in vasoconstriction from smaller vessels correlating with increased leakage. However, independent of size, vessels remain intact over time with contraction and leakage limited to the initial time immediately after NTIRE. In contrast, the consequences for neurons due to NTIRE is not temporary, as seen in **Figures 3A,B** and **Supplementary Figure 4**.

Non-thermal Irreversible Electroporation Can Ablate Neurons

As depicted in **Figure 3**, ablation of neurons scales very closely with the electric field. In **Figure 3A** a section of cortex directly between the two micro electrodes can be seen. **Figure 3B** shows a loss of neurons can be seen in the region above 400 μm which, as shown in **Figure 3C**, correspond to a field strength of ∼800 V/cm; this correlates well with the threshold for irreversible electroporation. The electric field below the depth of 400 μm is not zero, but not high enough to create the irreversible poration and ablation. Although the region of cortex is ablated, meaning the neurons have been destroyed, clearly no evidence of coagulation or thermal events can be seen in any of the tissue slices. Around 70% of the neurons in the neocortex are eliminated

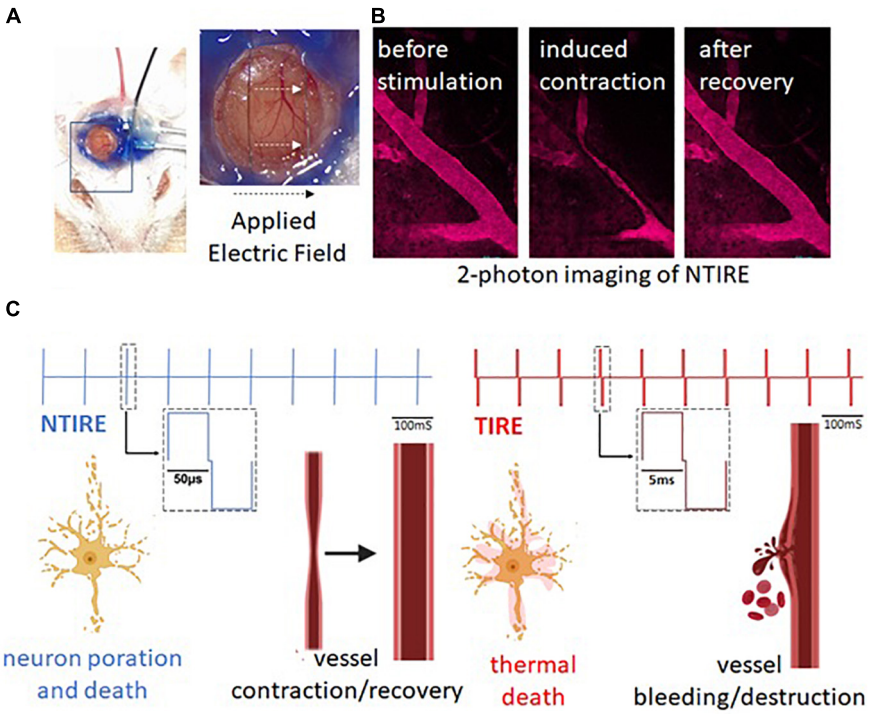

FIGURE 1 | Visualizing vessel contraction and the concept of NTIRE to ablate epileptic foci. **(A)** Mice are implanted with microelectrodes and cranial windows. In the simplest configuration, the electric field for NTIRE or TIRE is applied between the two microelectrodes under the cranial window (white arrows). **(B)** 2-photon fluorescence imaging is used to visualize the contraction or destruction of blood vessels due to the applied electric field. **(C)** The primary difference between NTIRE (non-thermal) and TIRE (thermal) ablation process is the duty cycle of the stimulation. NTIRE uses very short pulses per period at high-voltage which ablate neurons non-thermally via electroporation while vessels remain in place. TIRE uses longer pulses per period which coagulate tissue, ablating neurons thermally and causing destruction of vessels and bleeding (detailed discussion of NTIRE and thermal versus non-thermal ablation parameters in **Supplementary Figure 1**).

in the first 200 μm with a decrease in the number of ablated cell with depth (**Supplementary Figure 4**).

Unlike the thermal ablation which destroys vessels and neurons immediately and leaves the brain with a coagulated region, NTIRE does not show a complete cell loss right after the stimulation (corresponding well with histology). However, already at 7 min, a cell and dendrite loss already started (**Figure 4A**). The panel B, shows a section of cortex highlighting an individual pair of neurons in the field between the two microelectrodes. Before (top left panel) and several minutes after (middle panel) the NTIRE event is performed, the neurons are clearly visible. Indeed, neurons can often be visible for more than 24 h after NTIRE. The peak clearance of neurons is at approximately day 3; any neurons visible at or after day 3 will not be removed. Interestingly, as seen in the **Figure 4B** (right panel) for the same section of cortex, although the neurons have died and been cleared away, enervation of fibers from a region below the ablated cortex can be seen. This is a very interesting result, as this is not the case in a thermally coagulated section of neural tissue, where there is induction of axonal sprouting and synchronous activity (Carmichael and Chesselet, 2002). This could indicate an accelerated time-line for recovery, compared to the case of a thermal ablation, avoiding also the possible generation of epilepsy following cortical injury (Prince et al., 2009). Day 3, and also day 4, corresponds to a definite and visible increase in dendritic cells, specifically around the vessels in a region which has experienced the NTIRE event (**Supplementary Figure 5**). Day 7 seems to be the peak of dendritic cell concentration. In general, however, due to the lack of a thermal coagulated necrosis of tissue, it seems that the immune response and recovery is much similar to a mild stroke, with recovery on a much faster time-scale compared to thermal ablation. This is likely related to the fact that vasculature and extracellular matrix is completely in place, and there is no sign of tissue scarring.

Non-thermal Irreversible Electroporation Can Suppress Epileptiform Activities (Interictal Spikes)

Figure 5 shows the results of the NTIRE ablation applied to epileptic foci in the mouse hippocampus. As seen in **Figure 5A**, a two-electrode implant is placed at the border of CA3 in the mouse hippocampus. Animals had previously been rendered epileptic with a standard kindling protocol at this location (detail in the Supplementary Material). Animals under continuous video and electrophysiological supervision displayed behavioral epileptic state and pathological electrophysiological activity. As shown in **Figure 5B**, all the animals were kindled and were having burst of interictal spikes. For the ones

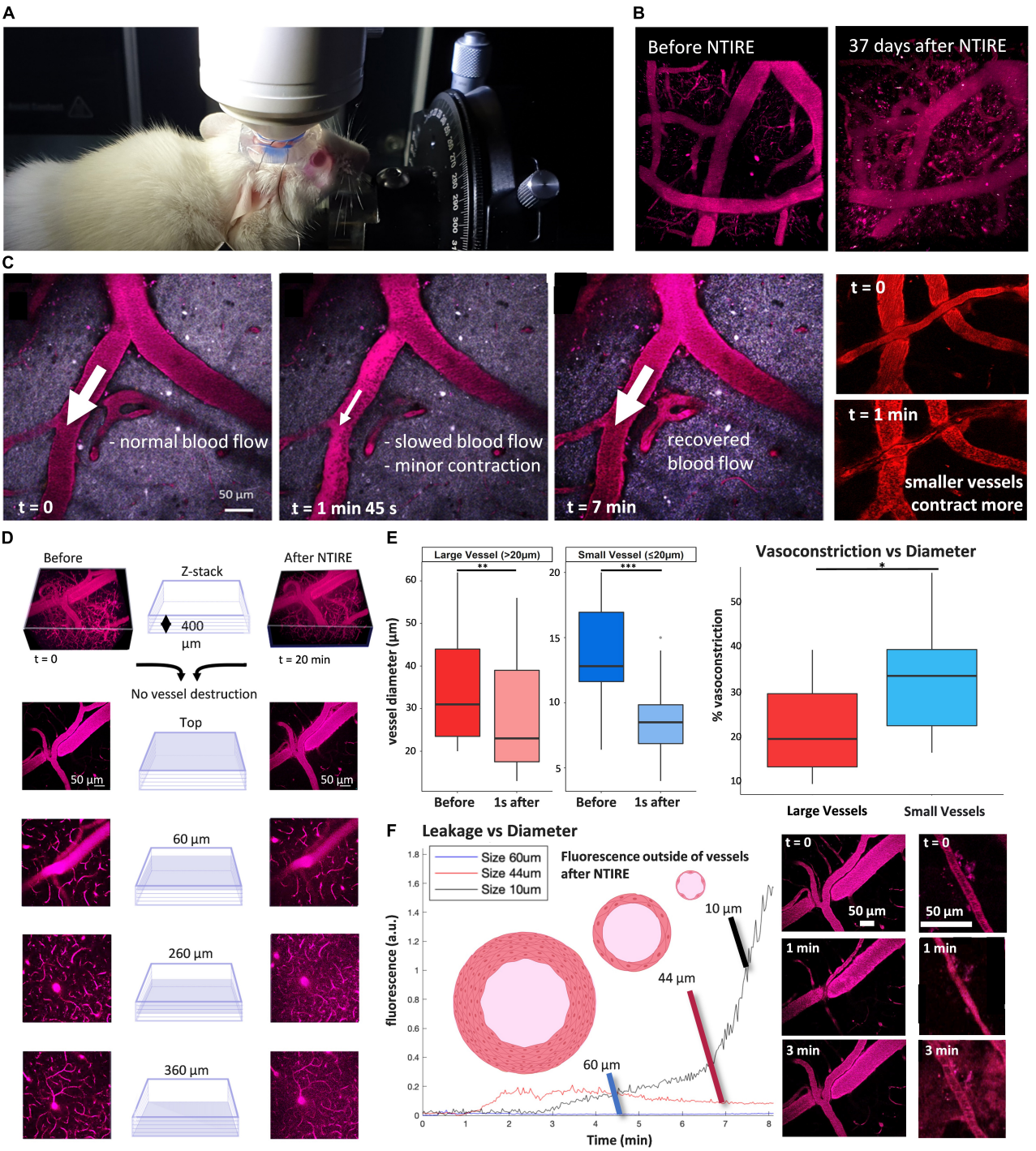

FIGURE 2 | Principal of NTIRE: Contraction, Recovery, and Leakage. **(A,B)** Mice and blood vessel integrity were monitored for a maximum of 37 days after the NTIRE process, with no discernable loss of vessels in the time window. **(C)** Blood flow (represented by the white arrows) is normal, then slowed in the minutes after the NTIRE event, and recovers for all vessels by 7 min. **(D)** 400 µm × 400 µm block of cortex taken between the two microelectrodes (schematically seen in **Figure 1**). Imaging immediately before and 7 min after NTIRE (1,750 V/cm, 10 Hz) reveals no obvious destruction of vessels, independent of vessel size. **(E) Contraction:** The average contraction of vessels due to NTIRE is measured, for vessels above vs. bellow 20 µm diameter, before and 1 s after NTIRE [Large vessels: *p* value (Shapiro test) >0.05, *p*-value (paired *t*-test) = 0.0003741. Small vessels: *p*-value (Shapiro test) <0.05, *p*-value (paired Wilcoxon test) = 0.001953]. Recovery takes approximately 1 min. The percentage of vasoconstriction for smaller vessels (diameter less than 20 µm) approaches 50% [*p* value (Shapiro test) >0.05, *p*-value (paired *t*-test) = 0.02622]. **(F) Leakage:** Leakage from vessels is estimated by considering the increase in fluorescence at a distance of 10 µm from an individual vessel. In the example here, the leakage from smaller vessels (diameter less than 20 µm – seen in the example panels, bottom right) continues for many minutes and is greater than from larger vessels, where the largest vessels (+60 µm) simply show no leak.

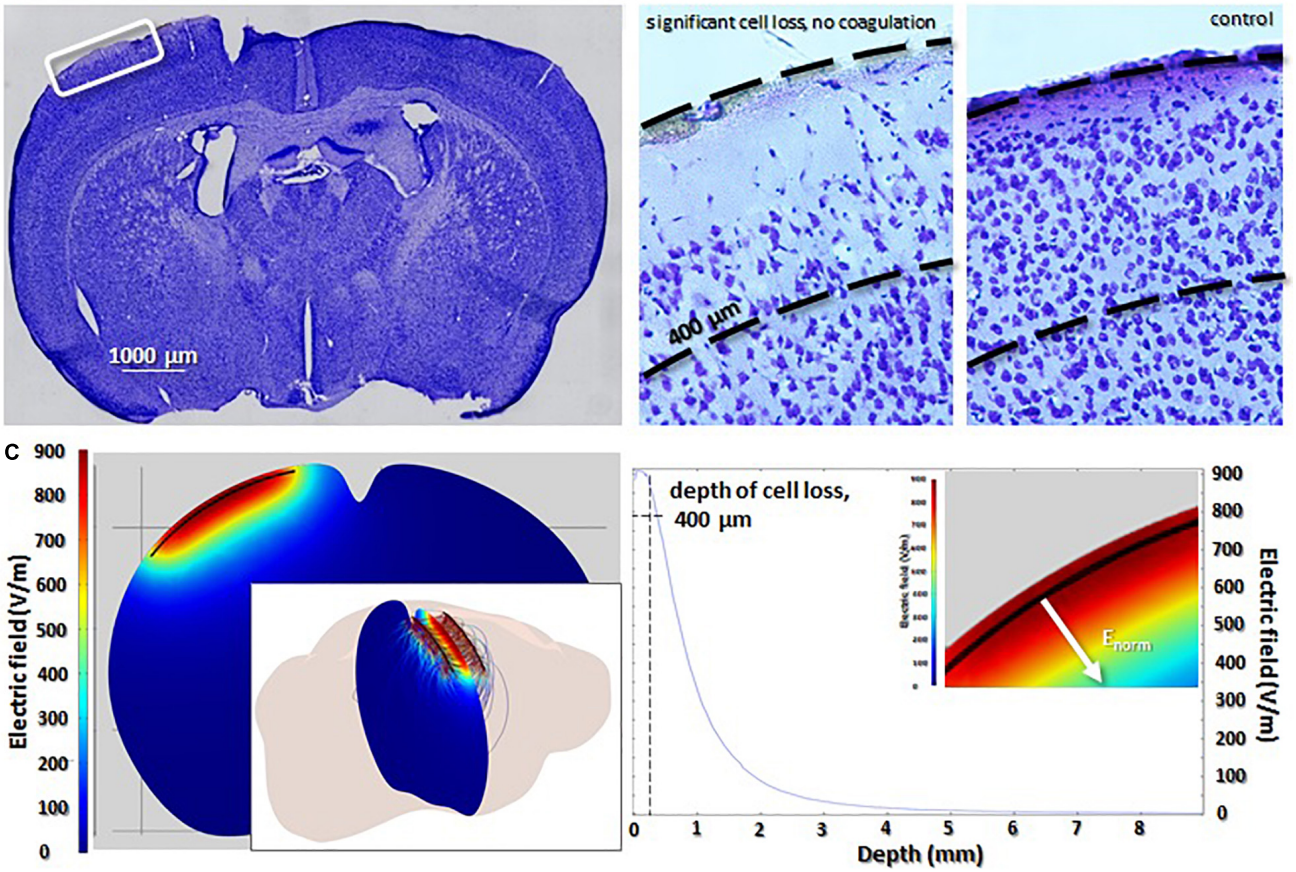

FIGURE 3 | Ablation of neurons using NTIRE. **(A)** Coronal section highlighting the location of microelectrodes on the cortex. **(B)** A magnified view of the highlighted region in **(A)**. Significant cell loss is seen down to a depth of approximately 400 µm. Control sections (left panel) highlight the density of cells without the NTIRE ablation. **(C)** Finite-element method simulations representing the penetration of the electric field into the tissue during one pulse of the NTIRE ablation (detailed discussion of NTIRE pulses in **Supplementary Figure 1**). The depth of the electric field perpendicular to the microelectrodes. Clearly, the depth of cell loss at approximately 400 µm corresponds to an electric field of 800 V/cm. Values of electric field below this number seem to not cause NTIRE ablation. In the inset, absorption of the electric field is shown in the cortex.

treated with an NTIRE ablation no longer displayed behavioral seizures and no longer showed pathological electrophysiological activity (representative of behavioral epileptic state available in **Supplementary Material**). The ablation rendering the animal seizure-free is important, but the lack of coagulated tissue in the NTIRE ablation has perhaps additional and positive consequences regarding recovery after ablation. In order to demonstrate this impact on hippocampal oscillation, a ratio of the detected interictal spikes (spikes detection after treatment/spikes detection before treatment) as been performed. The No treatment group has a ratio ∼1 meaning that there is no decrease of the number of spikes detection with time. But NTIRE ablation induced a significative reduction of the interictal spiking (p value = 0.02597) is a technique of ablation that can also be performed at depth like in an epileptic focus located in the hippocampus, similar cell death is seen with a corresponding reduced tissue damage and lack of thermal coagulation (**Supplementary Figure 1C**).

DISCUSSION

Non-thermal irreversible electroporation is a well-established method for the ablation of many types of tissue and tumors (Garcia et al., 2010, 2011, p. 2; Ellis et al., 2011; Hjouj et al., 2012). The phenomenon of irreversible electroporation occurs when an applied electric field in the targeted tissue region is above a critical value, typically taken between 1,500 V/cm and 2,500 V/cm (Yarmolenko et al., 2011; Savic et al., 2016). Usually, the electric field needed to achieve irreversible electroporation is associated with significant tissue heating and thermal damage. However, Davalos et al. (2005) showed that irreversible electroporation can be generated without thermal damage by applying certain pulse parameters, and that NTIRE can be used to destroy considerable volumes of tissue *in vivo* without heating (Rodriguez et al., 2015). Indeed, researchers have shown the use of NTIRE in small and large animal models in the prostate, (Hjouj et al., 2012) liver (Garcia et al., 2011) and on implanted mouse

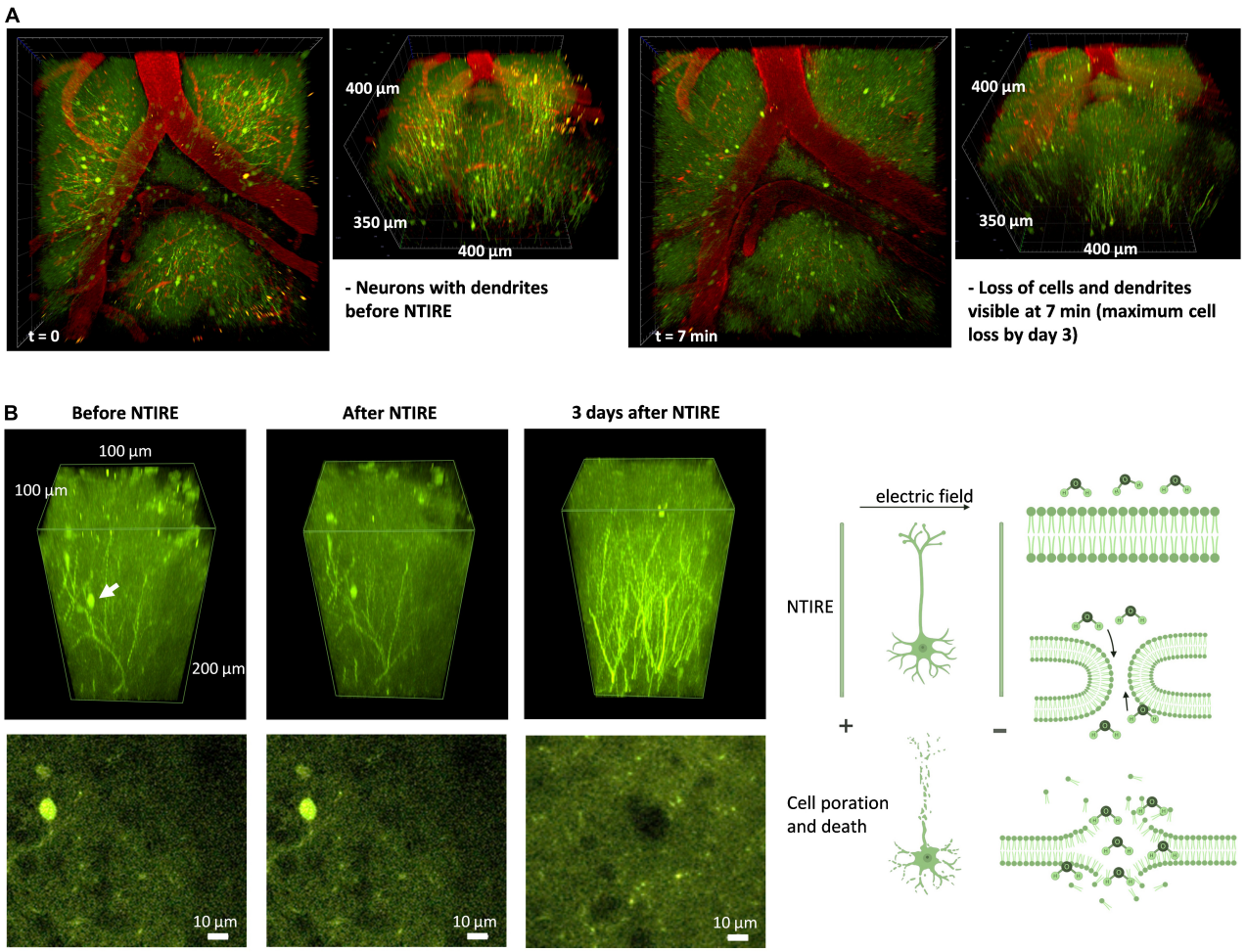

FIGURE 4 | Principal of NTIRE: Ablation timeline for individual neurons and new projections. **(A)** Initial cell death and destruction of dendrites is seen in the initial minutes. Unlike the thermal ablation which destroys vessels and neurons immediately and leaves the brain with a coagulated region, NTIRE does not show complete cell loss until day 3 (corresponding well with histology) and shows numerous signs of allowing the ablated brain region to recovery from the ablation to some degree. **(B)** We follow the time course of an example neuron (white arrow) in a section of cortex which has been ablated with NTIRE using the microelectrodes (top panels) and a slice at the depth of the neuron (bottom panels). The neuron before and 10 min after NTIRE shows no specific change, although the irreversible electroporation event has taken place, and the neuron is on a trajectory toward cell death. Interesting the majority of neurons will be cleared away by day 3, corresponding well with histology (**Supplementary Figure 4**). Arrival of immune cells, Dendritic Cells seen here, at days 3 and 4, in particular seemingly concentrating themselves outside of vessels. By day 7 the peak concentration of Dendritic Cells is reached. Before and immediately after NTIRE, no change is seen (**Supplementary Figure 5**).

sarcomas (Ellis et al., 2011). Studies outside the CNS have shown that NTIRE preserves the extracellular matrix and major blood vessels. In NTIRE studies outside the CNS, ablation is fast to apply and fast to resolve, permitting early repopulation of the ablated zone with healthy cells (Joshi and Schoenbach, 2002; Hjouj et al., 2012).

This work here describes the first time an NTIRE procedure has been coupled to live two-photon imaging in a mouse model, to follow its effects as they evolve. Focal lesions were created in the right somatosensory and parietal cortex of the mouse, and subsequently in the hippocampus to destroy seizure foci. Our results have shown that very short pulses durations per period, and correspondingly low RMS-voltages and low powers, cause only vasoconstriction of the vessels while destroying neurons. This finding indicates that NTIRE could be used safely in the brain to ablate pathophysiological structures while blood vasculature is maintained, in significant contrast to thermal ablation methods (Rossmeisl et al., 2013). We did not observe large-scale edema and swelling following the NTIRE ablations, in contrast to findings following thermal ablation with TIRE. The method may present a distinct new tool in epilepsy as a new option to treat seizure foci, rather than complete resective surgery or present thermal ablation techniques such as radiofrequency or LITT.

Our NTIRE ablations produce a sharply delineated volume of ablated tissue making it, as we have shown, suitable for treatment of epileptic foci in deep structures. The negligible heat generation during the ablation leaves extracellular matrix and major blood vessels undamaged. As described in this paper, we have shown several advantages over thermal ablation techniques related to

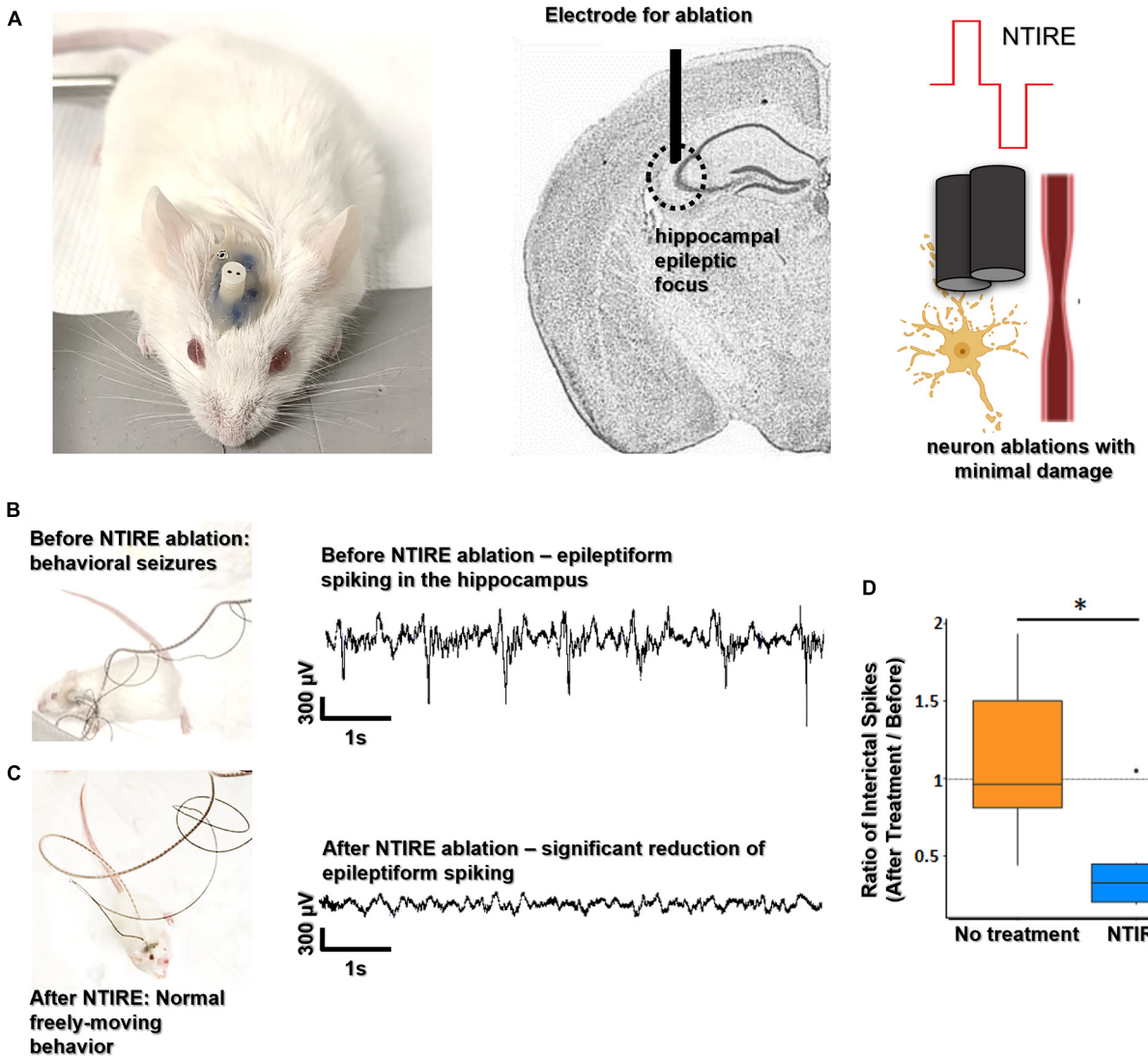

FIGURE 5 | NTIRE ablation of hippocampal seizure foci. **(A)** A hippocampal seizure focus created via a standard kindling protocol (details in the section "Materials and Methods") and an electrode is placed at the boarder of CA3. A two-electrode implant (100 μm electrode diameter, 50 μm spacing) used for the kindling protocol is then used for the treatment. **(B,C)** Video monitoring (representative of behavioral epileptic state available in **Supplementary Material**) and electrophysiological recordings in the hippocampus of animals prior to ablation show behavioral epileptic state and pathological epileptiform activity. Video monitoring and electrophysiological recordings in animals after ablation show no evidence of behavioral seizures and electrophysiological activity has a significant decrease in interictal epileptiform activity. **(D)** Evaluation of electrophysiological effects due to the NTIRE ablation (n = 12). The ratio (after treatment on before NTIRE) of epileptiform spikes during is dramatically reduced for the NTIRE mice (orange, n = 6) compared to the no treatment group (purple, n = 6), and no further behavioral seizures were observed. Wilcoxon test as been performed (*p-value = 0.02597).

bleeding and vasculature, but a second and very interesting finding is that, since NTIRE ablates tissue non-thermally rather than causing cell death through coagulative necrosis (as in thermal methods such as RF and laser ablation), it may accelerate the tissue recovery and regeneration process. The possibility of tissue to regenerate within the ablated epileptic foci, in part certainly due to the undamaged vasculature and lack of scarring, must be studied in detail in longer term experiments. However, our preliminary results show the recruitment of immune system cells, much more like brain recovery from mild stroke rather than a full thermal coagulative necrosis.

CONCLUSION

The results of our experiments indicate that the advantages of NTIRE over thermal ablation technologies in the brain are significant. The improved safety profile of the NTIRE method in epilepsy should accelerate clinical exploration and translation. Indeed, our preliminary results are the first step toward using NTIRE as a focal ablation treatment clinically in epilepsy. Our results are perfectly in line with the results of previous studies that have shown that NTIRE, in tissue outside the brain, has many beneficial properties compared to thermal ablations,

including better regeneration of tissue in the ablated zone and correspondingly improved avoidance of scar formation (Davalos et al., 2005). Currently, NTIRE is used in patients with tumors in organs such as the kidney, pancreas, lungs, and prostate (Rodriguez et al., 2015; Savic et al., 2016). An additional benefit, which might be ideal for epilepsy, is that the method allows work in tissue regions and organs with high densities of blood vessels, such as the insula of the brain, due to the insignificant impact on vascularization (Maor et al., 2007). Compared to thermocoagulation, the method completely avoids emboli and thrombosis after treatment (Davalos and Rubinsky, 2008). Even in cases of extremely high exposure to NTIRE, specific cases where clinicians want to electroporate tumor cells to allow the injection of chemotherapies, the BBB remains disrupted for 3 days post treatment and is reversed by 8 days (Hjouj et al., 2012). We hope that the results presented here stimulate further research into the NTIRE method as a significant alternative to thermal processes in the focal ablation process currently used to treat numerous epilepsies.

DATA AVAILABILITY STATEMENT

The raw data supporting the conclusions of this article will be made available by the authors, without undue reservation.

ETHICS STATEMENT

The animal study was reviewed and approved by the National Animal Studies Committee of France (authorization no. APAFIS20359-2019041816357133v5).

AUTHOR CONTRIBUTIONS

AW conceived the project and wrote the manuscript with input from the other authors, including MC, IV, RG, RC, VJ, AT, and FB. EA, SS, and PW performed the experiments. BB performed finite-element simulations. EA and FM analyzed the neural data. All authors contributed to the article and approved the submitted version.

FUNDING

This research was supported by funds from the European Research Council (ERC) under the European Union's Horizon 2020 research and innovation programme (grant agreement Nos. 716867 and 963976). This research was also supported by the French government program managed by the French National Research Agency (ANR) (grant No. BLAT80C/U208/AN19HRJNMF). AW and SS acknowledge funding from the Excellence Initiative of Aix-Marseille University A*MIDEX, a French "Investissements d'Avenir" program.

ACKNOWLEDGMENTS

AW thank Franck Debarbieux for his help regarding the access to his animal facility.

SUPPLEMENTARY MATERIAL

The Supplementary Material for this article can be found online at: https://www.frontiersin.org/articles/10.3389/fnbeh.2021.774999/full#supplementary-material

REFERENCES

Bezchlibnyk, Y. B., Willie, J. T., and Gross, R. E. (2018). A neurosurgeon's view: laser interstitial thermal therapy of mesial temporal lobe structures. *Epilepsy Res.* 142, 135–139. doi: 10.1016/j.eplepsyres.2017.10.015

Carmichael, S. T., and Chesselet, M.-F. (2002). Synchronous neuronal activity is a signal for axonal sprouting after cortical lesions in the adult. *J. Neurosci.* 22, 6062–6070. doi: 10.1523/JNEUROSCI.22-14-06062.2002

Chu, G., Hayakawa, H., and Berg, P. (1987). Electroporation for the efficient transfection of mammalian cells with DNA. *Nucleic Acids Res.* 15, 1311–1326. doi: 10.1093/nar/15.3.1311

Colombet, B., Woodman, M., Badier, J. M., and Bénar, C. G. (2015). AnyWave: a cross-platform and modular software for visualizing and processing electrophysiological signals. *J. Neurosci. Methods* 242, 118–126. doi: 10.1016/j.jneumeth.2015.01.017

Davalos, R. V., Mir, L. M., and Rubinsky, B. (2005). Tissue ablation with irreversible electroporation. *Ann. Biomed. Eng.* 33, 223–231. doi: 10.1007/s10439-005-8981-8

Davalos, R. V., and Rubinsky, B. (2008). Temperature considerations during irreversible electroporation. *Int. J. Heat Mass Transfer* 51, 5617–5622. doi: 10.1016/j.ijheatmasstransfer.2008.04.046

Ellis, T. L., Garcia, P. A., Rossmeisl, J. H., Henao-Guerrero, N., Robertson, J., and Davalos, R. V. (2011). Nonthermal irreversible electroporation for intracranial surgical applications. *J. Neurosurg.* 114, 681–688. doi: 10.3171/2010.5.JNS091448

Garcia, P. A., Pancotto, T., Rossmeisl, J. H., Henao-Guerrero, N., Gustafson, N. R., Daniel, G. B., et al. (2011). Non-thermal irreversible electroporation (N-TIRE) and adjuvant fractionated radiotherapeutic multimodal therapy for intracranial malignant glioma in a canine patient. *Technol. Cancer Res. Treat.* 10, 73–83. doi: 10.7785/tcrt.2012.500181

Garcia, P. A., Rossmeisl, J. H., Neal, R. E., Ellis, T. L., Olson, J. D., Henao-Guerrero, N., et al. (2010). Intracranial Nonthermal irreversible electroporation: *in vivo* analysis. *J. Membr. Biol.* 236, 127–136. doi: 10.1007/s00232-010-9284-z

Golberg, A., and Yarmush, M. L. (2013). Nonthermal irreversible electroporation: fundamentals, applications, and challenges. *IEEE Trans. Biomed. Eng.* 60, 707–714. doi: 10.1109/TBME.2013.2238672

Gross, R. E., Mahmoudi, B., and Riley, J. P. (2015). Less is more: novel less-invasive surgical techniques for mesial temporal lobe epilepsy that minimize cognitive impairment. *Curr. Opin. Neurol.* 28, 182–191. doi: 10.1097/WCO.0000000000000176

Gross, R. E., Stern, M. A., Willie, J. T., Fasano, R. E., Saindane, A. M., Soares, B. P., et al. (2018). Stereotactic laser amygdalohippocampotomy for mesial temporal lobe epilepsy. *Ann. Neurol.* 83, 575–587. doi: 10.1002/ana.25180

Hjouj, M., Last, D., Guez, D., Daniels, D., Sharabi, S., Lavee, J., et al. (2012). MRI study on reversible and irreversible electroporation induced blood brain barrier disruption. *PLoS One* 7:e42817. doi: 10.1371/journal.pone.0042817

Howenstein, M. J., and Sato, K. T. (2010). Complications of radiofrequency ablation of hepatic, pulmonary, and renal neoplasms. *Semin. Intervent. Radiol.* 27, 285–295. doi: 10.1055/s-0030-1261787

Joshi, R. P., and Schoenbach, K. H. (2002). Mechanism for membrane electroporation irreversibility under high-intensity, ultrashort electrical pulse

conditions. *Phys. Rev. E Stat. Nonlin. Soft Matter Phys.* 66:052901. doi: 10.1103/PhysRevE.66.052901

Kinosita, K., and Tsong, T. Y. (1977). Voltage-induced pore formation and hemolysis of human erythrocytes. *Biochim. Biophys. Acta* 471, 227–242. doi: 10.1016/0005-2736(77)90252-8

Lothman, E. W., Hatlelid, J. M., Zorumski, C. F., Conry, J. A., Moon, P. F., and Perlin, J. B. (1985). Kindling with rapidly recurring hippocampal seizures. *Brain Res.* 360, 83–91. doi: 10.1016/0006-8993(85)91223-5

Maor, E., Ivorra, A., Leor, J., and Rubinsky, B. (2007). The effect of irreversible electroporation on blood vessels. *Technol. Cancer Res. Treat.* 6, 307–312. doi: 10.1177/153303460700600407

Moritz, A. R. (1947). Studies of thermal injury: III. The pathology and pathogenesis of cutaneous burns. An experimental study. *Am. J. Pathol.* 23, 915–941.

Musto, A. E., Samii, M. S., and Hayes, J. F. (2009). Different phases of afterdischarge during rapid kindling procedure in mice. *Epilepsy Res.* 85, 199–205. doi: 10.1016/j.eplepsyres.2009.02.020

Prince, D. A., Parada, I., Scalise, K., Graber, K., Jin, X., and Shen, F. (2009). Epilepsy following cortical injury: cellular and molecular mechanisms as targets for potential prophylaxis. *Epilepsia* 50, 30–40. doi: 10.1111/j.1528-1167.2008.02008.x

Rodriguez, A., Tatter, S., and Debinski, W. (2015). Neurosurgical techniques for disruption of the blood–brain barrier for Glioblastoma treatment. *Pharmaceutics* 7, 175–187. doi: 10.3390/pharmaceutics7030175

Roehri, N., Pizzo, F., Lagarde, S., Lambert, I., Nica, A., McGonigal, A., et al. (2018). High-frequency oscillations are not better biomarkers of epileptogenic tissues than spikes. *Ann. Neurol.* 83, 84–97. doi: 10.1002/ana.25124

Rossmeisl, J. H., Garcia, P. A., Roberston, J. L., Ellis, T. L., and Davalos, R. V. (2013). Pathology of non-thermal irreversible electroporation (N-TIRE)-induced ablation of the canine brain. *J. Vet. Sci.* 14:433. doi: 10.4142/jvs.2013.14.4.433

Savic, L., Chapiro, J., Hamm, B., Gebauer, B., and Collettini, F. (2016). Irreversible electroporation in interventional oncology: where we stand and where we go. *Rofo* 188, 735–745. doi: 10.1055/s-0042-104203

Wiebe, S., Blume, W. T., Girvin, J. P., Eliasziw, M., and Effectiveness and Efficiency of Surgery for Temporal Lobe Epilepsy Study Group (2001). A randomized, controlled trial of surgery for temporal-lobe epilepsy. *N. Engl. J. Med.* 345, 311–318. doi: 10.1056/NEJM200108023450501

Yarmolenko, P. S., Moon, E. J., Landon, C., Manzoor, A., Hochman, D. W., Viglianti, B. L., et al. (2011). Thresholds for thermal damage to normal tissues: an update. *Int. J. Hyperthermia* 27, 320–343. doi: 10.3109/02656736.2010.534527

Conflict of Interest: The authors declare that the research was conducted in the absence of any commercial or financial relationships that could be construed as a potential conflict of interest.

Publisher's Note: All claims expressed in this article are solely those of the authors and do not necessarily represent those of their affiliated organizations, or those of the publisher, the editors and the reviewers. Any product that may be evaluated in this article, or claim that may be made by its manufacturer, is not guaranteed or endorsed by the publisher.

frontiers in Behavioral Neuroscience

ORIGINAL RESEARCH
published: 28 January 2022
doi: 10.3389/fnbeh.2021.799271

Sleep-Wake Rhythm and Oscillatory Pattern Analysis in a Multiple Hit Schizophrenia Rat Model (Wisket)

Leatitia Gabriella Adlan[1†], Mátyás Csordás-Nagy[2†], Balázs Bodosi[1], György Kalmár[2], László G. Nyúl[3], Attila Nagy[1], Gabriella Kekesi[1], Alexandra Büki[1] and Gyongyi Horvath[1]*

[1] Department of Physiology, Albert Szent-Györgyi Medical School, University of Szeged, Szeged, Hungary, [2] Department of Technical Informatics, Faculty of Science and Informatics, Institute of Informatics, University of Szeged, Szeged, Hungary, [3] Department of Image Processing and Computer Graphics, Faculty of Science and Informatics, Institute of Informatics, University of Szeged, Szeged, Hungary

Electroencephalography studies in schizophrenia reported impairments in circadian rhythm and oscillatory activity, which may reflect the deficits in cognitive and sensory processing. The current study evaluated the circadian rhythm and the state-dependent oscillatory pattern in control Wistar and a multiple hit schizophrenia rat model (Wisket) using custom-made software for identification of the artifacts and the classification of sleep-wake stages and the active and quiet awake substages. The Wisket animals have a clear light-dark cycle similar to controls, and their sleep-wake rhythm showed only a tendency to spend more time in non-rapid eye movement (NREM) and less in rapid eye movement (REM) stages. In spite of the weak diurnal variation in oscillation in both groups, the Wisket rats had higher power in the low-frequency delta, alpha, and beta bands and lower power in the high-frequency theta and gamma bands in most stages. Furthermore, the significant differences between the two groups were pronounced in the active waking substage. These data suggest that the special changes in the oscillatory pattern of this schizophrenia rat model may have a significant role in the impaired cognitive functions observed in previous studies.

Keywords: oscillatory activity, EEG, schizophrenia, circadian rhythm, multiple hit model

OPEN ACCESS

Edited by:
Jun Nagai,
RIKEN Center for Brain Science (CBS), Japan

Reviewed by:
Kenichiro Nagahama,
Johns Hopkins Medicine, United States
Jasna Saponjic,
University of Belgrade, Serbia

***Correspondence:**
Gyongyi Horvath
horvath.gyongyi@med.u-szeged.hu

[†] These authors have contributed equally to this work and share first authorship

Specialty section:
This article was submitted to Pathological Conditions, a section of the journal Frontiers in Behavioral Neuroscience

Received: *21 October 2021*
Accepted: *30 December 2021*
Published: *28 January 2022*

Citation:
Adlan LG, Csordás-Nagy M, Bodosi B, Kalmár G, Nyúl LG, Nagy A, Kekesi G, Büki A and Horvath G (2022) Sleep-Wake Rhythm and Oscillatory Pattern Analysis in a Multiple Hit Schizophrenia Rat Model (Wisket). Front. Behav. Neurosci. 15:799271. doi: 10.3389/fnbeh.2021.799271

INTRODUCTION

Schizophrenia is a chronic and multidimensional neuropsychiatric disorder with devastating consequences for patient outcomes. Although not included in its diagnostic criteria, sleep disturbances are consistently reported in patients, including disrupted circadian rhythms of activity, sleep-wake, and oscillatory patterns obtained by electroencephalography (EEG) (Felder et al., 1994; Sponheim et al., 1994, 2003; Omori et al., 1995; Wirz-Justice et al., 2001; Symond et al., 2005; Rockstroh et al., 2007; Bob et al., 2008; Boutros et al., 2008; Afonso et al., 2011; Pritchett et al., 2012; Başar, 2013; Lakatos et al., 2013; Uhlhaas and Singer, 2013; Featherstone et al., 2015; Tam et al., 2015; Manoach et al., 2016; Newson and Thiagarajan, 2019). All these abnormalities may be implicated in impaired sleep-dependent memory consolidation and may represent an endophenotype for schizophrenia that contributes to abnormal cognitive and sensory performances (Manoach et al., 2016). Unfortunately, the results are very controversial and they may depend on the subtypes or phases of this disease or type of drug treatment. Furthermore, the EEG abnormalities are neither consistent nor unique in schizophrenia as most of these signs are also reported in other

mental disorders such as major depression and autism spectrum disorder (Cohrs, 2008; O'Reilly et al., 2017).

Rodent models are essential for understanding brain function in health and disease. Several animal models of schizophrenia have abnormalities in their circadian rhythm and oscillatory pattern, but most of these results obtained in mutant mice with modification of only one gene transcription, e.g., disrupted-in-schizophrenia 1 (DISC1) gene, metabotropic glutamate 5 receptors (mGLUR5), voltage gated L-type calcium channels, serine racemase enzyme (responsible for N-methyl-D-aspartate (NMDA) receptor function), GluA1 subunit of α-amino-3-hydroxy-5-methyl-4-izoxazolepropionic acid (AMPA) receptors, or stable tubule only polypeptide (STOP) (Ahnaou et al., 2015b; Kumar et al., 2015; Profitt et al., 2016; Ang et al., 2018; Aguilar et al., 2020). Only few studies investigated single hit rat models (Ahnaou et al., 2007; Phillips et al., 2012a; Valdés-Cruz et al., 2012). Most of these animal models possess few disturbances in their sleep-wake rhythm and/or oscillatory pattern, with some contradictions between the studies.

Since the etiology of schizophrenia involves the interaction among genetic, developmental, and environmental factors, multiple hit translational models might provide animals with a high level of constructive and face validities with a wider range of schizophrenia-related signs. Therefore, a triple hit rat model, named Wisket, was developed in our laboratory by combining developmental (postweaning social isolation for 4 weeks), pharmacological (NMDA receptor antagonist, ketamine, and treatment intraperitoneally: 30 mg/kg, 4 ml/kg body weight, daily, 5 times/week, 15 injections in total), and genetic (selective breeding based on behavioral phenotype for more than 30 generations) manipulations, as described previously (**Supplementary Figure 1**; Horvath et al., 2017, 2021a). Animals with decreased pain sensitivity, impaired sensory gating, and cognitive functions were selected for breeding. A wide range of disturbances was observed in Wisket animals, including impaired pain sensitivity, sensory gating, cognition and alterations in opioid, cannabinoid, oxytocin, and dopamine receptors' (D_2R and D_1R) signaling and/or expression (Petrovszki et al., 2013; Szûcs et al., 2016b,a, 2020; Horvath et al., 2017, 2021b; Banki et al., 2020). Furthermore, the Wisket model rats exhibited altered daily rhythm in the gross motor activity and body temperature investigated by telemetry, and changes in oscillatory patterns and evoked potentials detected in a short-term EEG paradigm (Horvath et al., 2015, 2016). To characterize further the possible disturbances in these animals, the aim of this study was to determine their sleep-wake rhythm and oscillatory pattern with the application of EEG in freely moving conditions.

Traditionally, the classification of the wake-sleep stages in the EEG records is performed by trained human experts *via* visual inspection of the EEG features, which is a laborious task prone to interindividual variability and it also requires considerable time and specialized knowledge about sleep in rodents. Considerable progress in computational technologies has made possible an improvement in automated sleep scoring algorithms (Miladinović et al., 2019; Yamabe et al., 2019). Therefore, the aim of this study was to characterize the sleep/wake states architecture and sleep/wake-related oscillations in the Wisket rat model of schizophrenia by more accurate software.

MATERIALS AND METHODS

Animals

Male, adult Wistar (control) and Wisket rats (4–6 months old) were involved in the study. All experiments were carried out with the approval of the Hungarian Ethical Committee for Animal Research (registration number: XIV/1248/2018) and in accordance with the guidelines set by the Government of Hungary and EU Directive 2010/63EU for animal experiments. The animals were kept with a 12 h light/dark cycle under conditions of controlled temperature (23 ± 1°C) and humidity (55 ± 10%).

Surgical Procedure

The whole setup of the surgery was similar as described previously (Bodosi et al., 2000, 2004; Horvath et al., 2016). Briefly, the rats were anesthetized with a mixture of ketamine hydrochloride (Calypsol, Gedeon Richter Plc., Budapest, Hungary; 72 mg/kg) and xylazine (CP-Xylazin, Produlab Pharma B.V. Raamsdonksveer, Netherlands, 8 mg/kg) administered intraperitoneally, and transferred into a stereotaxic frame. For EEG recording, each animal was implanted with stainless steel screws over the parietal cortex (from bregma: −2.3 and 2.4 mm right to the midline), occipital cortex (ground electrode: −6.1 and 2.4 mm right to the midline), and the cerebellum (reference: −10.5 and 0.5 mm right to the midline). A thermistor was placed over the left parietal cortex to record brain cortical temperature (Tc). Finally, the electrodes were connected with enamel-coated copper wires to a miniature connector, which was fixed to the skull with dental cement.

Experimental Paradigm

After the surgery, the rats were housed individually in custom-made clear plexiglass cages (25 cm × 28 cm × 50 cm), to avoid the removal of the implanted devices by their cage mate. The rats were in visual, auditory, and olfactory contact with other rats to minimalize the effect of isolation rearing (Hurst et al., 1999). They were allowed to recover for 1 week with access to water and food *ad libitum*. The room was sound attenuated. During this period, the rats were connected to the recording tether and habituated to the experimental conditions. After the recovery period, EEG was recorded for 23 h (1 h was devoted to taking care of the animals). However, due to technical reasons (the animals frequently disrupted the recording cable close to the light phase), 21 h-long EEG recordings were analyzed, including the total length of the light phase (12 h), and 9 h of the dark phase.

Two series of experiments were performed. In the first (matched) series, four rats (representing both control and Wisket animals; n = 8/group) were recorded simultaneously in each recording session. Furthermore, to determine whether the changes obtained between the two groups in the first series can be reproduced independently of the environmental circumstances, the second series of experiments was performed with a different

group of animals, where the animals were unmatched (5 controls and 6 Wiskets, investigated on different days).

Data Recording, Correction, and Classification

Cables from the electrodes were connected to a miniature microcontroller-based transmitter unit powered by a rechargeable Li-ion battery and tied to the cables. The housing of the cables was attached to a plastic bearing above the cage providing free rotation. Signals were amplified (2000×) and filtered (0.5−48 Hz), and were digitized by an inbuilt analog-to-digital converter at a sampling rate of 128 Hz. The resolution was 12 bits. The motor activity of the rats was detected by a 3 − axis accelerometer (type: LIS3LV02DQ; range: 0 − 6 G) within the unit, as described earlier (Bodosi et al., 2000, 2004). For scoring, the signals were transmitted at 2.4 GHz to a receiver unit attached to the PC over a USB connection. These units, including all PC and microcontroller programs, were developed and produced by one of the authors (BB). Data were analyzed in an 8-s epoch offline.

The EEG recordings contained artifacts, caused by short contact losses of the electrodes due to animal movements. During these periods, the EEG signal clipped and these sections' spectra would mislead the spectrum-analysis approach presented in the article. To correct these sections, the EEG signals were preprocessed. First, the clipping signal parts were detected, and then they were analyzed and substituted. The replacement signal had the same length as the faulty section and was generated as a well-formed (colored) white Gaussian noise, which noise's spectrum was formed to match the spectrum of the EEG signal surrounding the faulty section. Thus, the replacement does not affect the aggregated spectrum-based features extracted at the later stages of the analysis. The preprocessing method corrected 2% of the EEG dataset.

The next task was to classify the EEG signal into three wake-sleep stages: awake, non-rapid eye movement (NREM), and rapid eye movement (REM) stages. To achieve this automated classification, a machine-learning model was trained to predict the class label for 8 s-long EEG signal segments. To train such a model, we had access to a dataset containing 36 manually classified recorded days and approximately 10, 000 hand-labeled segments for each day. Our approach was to extract handcrafted features from the segments and use only these to predict a label. The generated features are the following: mean amplitude and SD values for the different frequency bands, the SD of the motion data, and a Petrosian Fractal Dimension value (Petrosian, 1995) of the EEG data. Then, the states of vigilance were determined over 8 s epochs as NREM sleep (high-amplitude slow waves, low level of body movements); REM sleep (highly regular theta activity in the EEG, low level of body movements with occasional twitches); and wakefulness (less regular theta activity, frequent body movements). Established in earlier studies, the awake stage was subdivided into two substages: active and quiet/inactive awake (Vyazovskiy and Tobler, 2005; Mofleh and Kocsis, 2021). The basis of the subdivision was the motor activity: longer than 1 s movement duration during the 8 s period referred to active substage. Based on these indicators, we trained a random forest classifier (Breiman, 2001), which achieved 92.8% accuracy measured with 10-fold cross-validation. This automated classifier method was used to predict labels for the EEG data served as the basis of the analysis results presented later in this article.

After the categorization of the states of vigilance, power spectra were computed by Fast Fourier Transform (FFT) for each stage and substages under a condition of 0.125°Hz resolution with a Hanning window. Total absolute power was calculated as the sum of squares of all frequency values contained in a given band. Relative band powers were expressed as power ratios of each frequency band to the total (z-score) in each 8 s bin. The resulting power spectra were divided and analyzed in different frequency ranges: delta (0.5−4 Hz), theta (4−8 Hz), alpha (8 − 12 Hz), beta (12 − 30 Hz), and low gamma (30–48 Hz) bands.

Data and Statistical Analyses

The parameters were quantified and analyzed as means of values per hour for the 21 h (daily) and separately for the light and dark phases (diurnal). The mean duration per hour and the number and duration of episodes in different stages were determined. Regarding the detailed analysis of the oscillatory pattern, our preliminary data analysis revealed a separate or even opposite tendency in relative powers in narrow frequency ranges. Therefore, based on earlier results, we performed the statistical analysis for all of the data within a frequency band (delta, theta, alpha, beta, and gamma) to reveal fine-grained alterations between the two groups (Saravanapandian et al., 2020).

Data are expressed as means ± SEM. The parameters were compared with repeated and/or factorial ANOVA. When the global test was significant, the Fisher least significant difference (LSD) *post-hoc* test was used for the evaluation of the effects of various parameters. Statistical analysis was performed with STATISTICA 13.5.0.17 (TIBCO Software Inc., United States). Differences were considered significant for $p < 0.05$.

RESULTS

Sleep-Wake Rhythm

Factorial ANOVA of the time spent in the different stages (awake, NREM, and REM) during the whole investigated period showed significant effects of the stage [$F_{(2,42)} = 282.62$; $p < 0.001$; **Table 1**]. Thus, both groups of animals spent a significantly shorter time in the REM stage compared to awake or NREM stages. The separate analysis of the active and quiet substages revealed significant effects of substage [$F_{(1,28)} = 29.82$; $p < 0.001$], thus, both groups of animals spent less time in quiet awake than in active awake substage (**Table 1**). Regarding the light:dark (diurnal) rhythm (phases), the ANOVA showed significant effects of the stage [$F_{(2,42)} = 268.94$; $p < 0.001$) and phase and stage interaction [$F_{(2,42)} = 81.49$; $p < 0.001$), thus, the animals in both groups spent more time in awake and less in NREM and REM stages of sleep during the dark phase compared to the light condition without significant differences between the two groups (**Table 1**). Furthermore, the separate analysis of the diurnal rhythm of the active and quiet substages revealed significant effects of substage [$F_{(1,28)} = 29.92$; $p < 0.001$], phase

TABLE 1 | The mean per hour° ± °SEM duration of different stages and substages, the number and length of episodes in control and Wisket animals for the whole period and by light and dark phases.

STAGES/substages	Group	Duration (min)		No. of episodes		Length of episodes (s)		Total power	
AWAKE	Control	26.5 ± 0.89		25.9 ± 1.54		89.7 ± 11.17		0.021 ± 0.0017	
	Wisket	25.4 ± 1.01		23.9 ± 1.35		107.7 ± 22.72		0.025 ± 0.0019	
Active	Control	17.8 ± 1.76						0.022 ± 0.0018	
	Wisket	17.3 ± 1.96						0.025 ± 0.0020	
Quiet	Control	8.7 ± 1.46						0.019 ± 0.0017	
	Wisket	8.1 ± 1.47						0.023 ± 0.0017	
NREM	Control	26.4 ± 1.46		25.5 ± 1.65		64.0 ± 5.46		0.041 ± 0.0020	
	Wisket	28.2 ± 0.73		23.3 ± 1.42		73.9 ± 3.58		0.044 ± 0.0043	
REM	Control	**7.2 ± 0.94**		20.2 ± 3.77		21.8 ± 1.49		0.021 ± 0.0018	
	Wisket	**6.4 ± 0.46**		17.2 ± 1.86		22.5 ± 2.57		0.026 ± 0.0024	
		Light	***Dark***	***Light***	***Dark***	***Light***	***Dark***	***Light***	***Dark***
AWAKE	Control	20.2 ± 0.94	*34.8 ± 2.04*	27.5 ± 1.56	***23.7 ± 1.90***	60.5 ± 14.02	128.7 ± 16.08	0.021 ± 0.0017	0.021 ± 0.0017
	Wisket	17.1 ± 1.90	*36.6 ± 2.57*	25.6 ± 1.43	***21.5 ± 1.57***	49.2 ± 10.00	185.7 ± 22.85	0.024 ± 0.0021	0.025 ± 0.0018
Active	Control	12.9 ± 1.58	*24.3 ± 2.61*					0.022 ± 0.0019	0.021 ± 0.0017
	Wisket	11.1 ± 1.54	*25.6 ± 3.11*					0.025 ± 0.0022	0.026 ± 0.0019
Quiet	Control	7.3 ± 1.08	*10.5 ± 2.12*					0.019 ± 0.0014	0.019 ± 0.0015
	Wisket	5.9 ± 1.00	*11.0 ± 3.10*					0.023 ± 0.0017	0.023 ± 0.0018
NREM	Control	31.1 ± 1.20	*20.1 ± 2.09*	28.4 ± 2.09	*21.7 ± 1.38*	69.4 ± 5.31	56.7 ± 6.05	0.040 ± 0.0021	0.042 ± 0.0022
	Wisket	34.4 ± 1.29	*19.9 ± 1.94*	26.2 ± 1.17	*19.5 ± 1.92*	81.7 ± 4.85	63.4 ± 4.34	0.044 ± 0.0044	0.046 ± 0.0043
REM	Control	8.7 ± 1.29	*5.1 ± 0.75*	22.7 ± 4.41	*16.8 ± 3.05*	24.6 ± 2.12	**18.1 ± 1.74**	0.021 ± 0.0020	0.021 ± 0.0017
	Wisket	8.5 ± 0.76	*3.5 ± 0.72*	21.0 ± 2.02	*12.0 ± 2.06*	26.2 ± 3.56	**16.9 ± 1.51**	0.027 ± 0.0025	0.025 ± 0.0022

Bolded data mean significant differences compared to NREM and awake stages. Data in italic letters show significant differences compared to the light phase. The underlined data show significant differences compared to active substages.

$[F_{(1,28)} = 48.87; p < 0.001]$, and substage and phase interaction $[F_{(1,28)} = 13.05; p < 0.005]$, thus both groups of animals spent a long time in both types of awake substages during the dark than in the light phase (**Table 1**).

The number and the length of episodes did not differ significantly between the two groups analyzed for the whole investigated period (**Table 1**). Regarding the diurnal rhythm in the number of episodes in awake, NREM, and REM stages, the ANOVA showed significant effects of the stage $[F_{(2,42)} = 5.81; p < 0.01]$ and phase $[F_{(1,42)} = 91.71; p < 0.001]$, thus, both groups of animals had fewer number in bouts of all stages during the dark phase, with a moderate tendency of decreased numbers in Wisket animals (**Table 1**). The analysis of the mean length of the episodes also showed significant effects of the stage $[F_{(2,42)} = 24.75; p < 0.001]$, phase $[F_{(1,42)} = 7.18; p < 0.05]$, and the stage and phase interaction $[F_{(2,42)} = 15.01; p < 0.001]$, thus, both groups of animals had shorter REM sleep episodes compared to awake and NREM stages, and longer awake bouts during the dark phase (**Table 1**).

Regarding the unmatched groups, the Wisket animals, similarly to the matched series, did not show significant changes in these parameters compared to the control ones (data are not shown).

Oscillatory Pattern

The oscillatory pattern of the EEG was analyzed next. Since no diurnal changes were obtained in the oscillations, power spectra were analyzed for the whole session independently of stages, and then for the three sleep-wake stages (REM, NREM, and awake) and the active and quiet awake substages, separately. To demonstrate the fine-grained distribution of the relative power, the ANOVA analysis was performed for all the data obtained within the different frequency bands (delta, theta, alpha, beta, and gamma).

Regarding the analysis of total absolute power, only a tendency of enhanced power was obtained in the Wisket animals by stages, substages, and the light-dark phases (**Table 1**).

Regarding the entire relative power irrespective of the stages in the delta band ($0.5 - 4$ Hz), factorial ANOVA showed significant effects of frequency $[F_{(28,406)} = 157.82; p < 0.001]$ and group and frequency interaction $[F_{(28,406)} = 1.52; p < 0.05]$. The *post hoc* analyses revealed that the Wisket animals had significantly higher total relative power compared to control ones in the interval of $1.38 - 1.75$ Hz (**Figure 1A**).

The analysis of the delta power by stages revealed significant effects of frequency $[F_{(28,1218)} = 337.79; p < 0.001]$, stage $[F_{(2,1218)} = 1638.03; p < 0.001]$, group and frequency interaction $[F_{(28,4065)} = 2.41; p < 0.001]$, group and stage interaction $[F_{(2,1218)} = 25.60; p < 0.001]$, frequency and stage interaction $[F_{(56,1218)} = 46.25; p < 0.001]$, and group, frequency, and stage interaction $[F_{(56,1218)} = 1.48; p < 0.05]$. The *post hoc* analysis disclosed that the delta power was the lowest during the REM stage in both groups, with significantly lower in its middle range ($1.88 - 2.5$ Hz) in the model rats compared to control animals. Furthermore, the pattern of the delta spectrum differed between the two groups in the NREM stage, i.e., the Wisket animals had

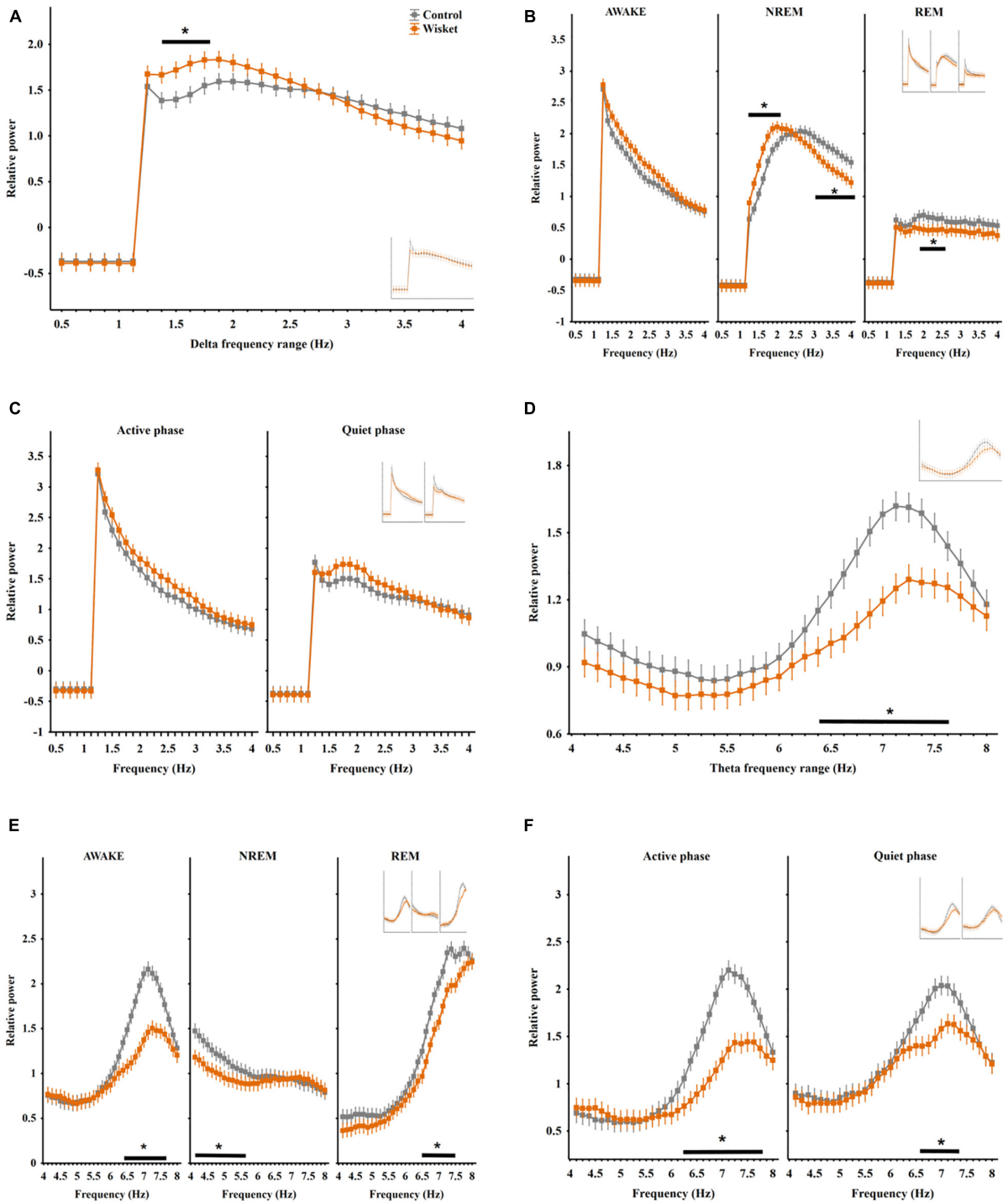

FIGURE 1 | Relative EEG power differences between the two groups at the delta and theta frequency bands. **(A)** Total relative delta power (0.5–4 Hz). **(B)** Delta power in different stages. **(C)** Delta power in active and quiet awake substages. **(D)** Total relative theta power (4–8 Hz). **(E)** Theta power in different stages. **(F)** Theta power in active and quiet awake substages. Curves inserted in reduced size show the results obtained from unmatched control and Wisket animals. The symbol * shows QQsignificant ($p° < °0.05$) differences between the two groups.

higher power at the lower frequency range (1.25 − 2 Hz), while they had significantly lower power at the higher frequency range (3 − 4 Hz) compared to control rats (**Figure 1B**).

The separate analysis of the delta band by substages revealed significant effects of group [$F_{(1,812)} = 16.75$; $p < 0.001$], frequency [$F_{(28,812)} = 195.11$; $p < 0.001$], substage

[$F_{(1,812)}$ = 40.67; p < 0.001)], and frequency and substage interaction [$F_{(28,812)}$ = 13.11; p < 0.001]. Thus, the Wisket animals had a trend for higher delta power in both awake substages (**Figure 1C**).

Regarding the total relative power irrespective of the stages in the theta band (4 − 8°Hz), factorial ANOVA showed significant effects of group [$F_{(1,448)}$ = 10.58; p < 0.001] and frequency [$F_{(31,448)}$ = 25.05; p < 0.001]. The *post hoc* analysis showed that the Wisket animals had significantly lower power compared to control ones at the higher frequency theta band (6.38 − 7.62 Hz interval; **Figure 1D**).

The analysis of the theta power by stages revealed significant effects of group [$F_{(1,1344)}$ = 206.48; p < 0.001], frequency [$F_{(31,1344)}$ = 113.34; p < 0.001], stage [$F_{(2,1344)}$ = 51.38; p < 0.001], group and frequency interaction [$F_{(31,1344)}$ = 2.64; p < 0.001], group and stage interaction [$F_{(2,1344)}$ = 10.92; p < 0.001], frequency and stage interaction [$F_{(62,1344)}$ = 55.54; p < 0.001] and group, frequency, and stage interaction [$F_{(62,1344)}$ = 1.48; p < 0.001]. Thus, the pattern of the theta spectrum differed between the stages with the lowest rise of the curve during NREM (**Figure 1E**). Furthermore, during NREM sleep the theta power at the lower frequency band (4.12 − 5.62 Hz) was significantly lower, while during awake and REM stages the higher frequency bands (6.38 − 7.62 Hz and 6.5 − 7.5 Hz, respectively) were lower in the Wisket animals compared to controls.

The separate analysis of the theta band by substages revealed significant effects of group [$F_{(1,896)}$ = 123.00; p < 0.001], frequency [$F_{(31,896)}$ = 63.92; p < 0.001], substage [$F_{(1,896)}$ = 120.98; p < 0.001], group and frequency interaction [$F_{(31,896)}$ = 5.71; p < 0.001], group and substage interaction [$F_{(1,896)}$ = 9.44; p < 0.005] and frequency and substage interaction [$F_{(31,896)}$ = 3.64; p < 0.001]. Thus, the Wisket animals in both active and quiet substages had significantly lower total power (6.25 − 7.75 and 6.62 − 7.38 Hz, respectively, **Figure 1F**).

Regarding the total relative power in the alpha band (8 − 12 Hz), factorial ANOVA showed significant effects of group [$F_{(1,448)}$ = 52.00; p < 0.001] and frequency [$F_{(31,448)}$ = 170.77; p < 0.001]. The Wisket animals had significantly higher relative power compared to control ones at the lower range of alpha band (8.5 − 9.38 Hz interval; **Figure 2A**).

The analysis of the alpha power by stages revealed significant effects of group [$F_{(1,1344)}$ = 167.26; p < 0.001], frequency [$F_{(31,1344)}$ = 354.09; p < 0.001], stage [$F_{(2,1344)}$ = 980.07; p < 0.001], group and frequency interaction [$F_{(31,1344)}$ = 3.94; p < 0.001], group and stage interaction [$F_{(2,1344)}$ = 81.04; p < 0.001], frequency and stage interaction [$F_{(62,1344)}$ = 48.09; p < 0.001] and group, frequency, and stage interaction [$F_{(62,1344)}$ = 1.63; p < 0.005]. The pattern of the alpha spectrum differed between the stages with the lowest rise of the curve during NREM, and the Wisket animals had higher relative alpha power in awake and REM stages in the lower frequency bands (8.38 − 9.75 Hz and 8.25 − 10 Hz, respectively) compared to control rats (**Figure 2B**).

The separate analysis of the alpha band by substages disclosed significant effects of group [$F_{(1,896)}$ = 126.58;

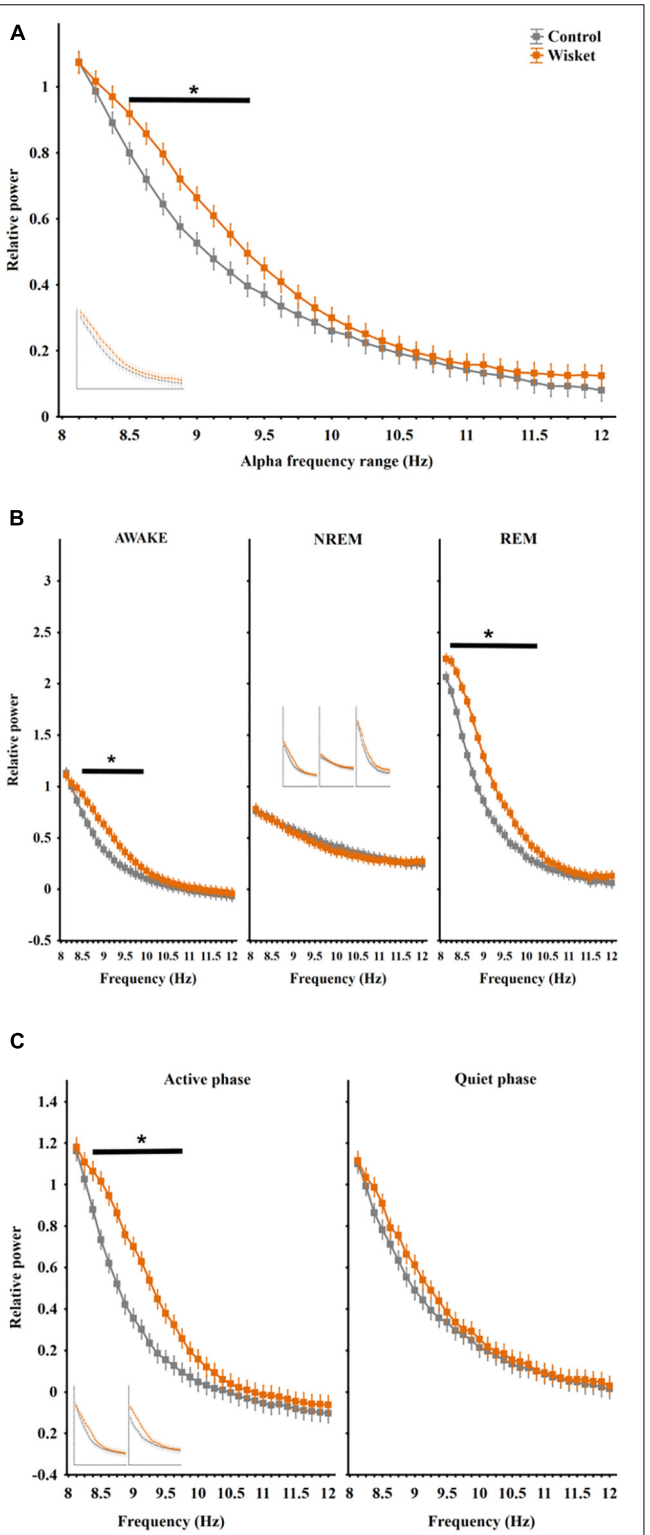

FIGURE 2 | Relative EEG power differences between the two groups at the alpha frequency band. **(A)** Total relative alpha power (8–12 Hz). **(B)** Alpha power in different stages panel. **(C)** Alpha power in active and quiet awake substages. Curves inserted in reduced size show the results obtained from unmatched control and Wisket animals. The symbol * shows significant (p° < °0.05) differences between the two groups.

$p < 0.001$], frequency [$F_{(31,896)} = 230.56$; $p < 0.001$), substage [$F_{(1,896)} = 92.76$; $p < 0.001$], group and frequency interaction [$F_{(31,896)} = 2.90$; $p < 0.001$], group and substage interaction [$F_{(1,896)} = 30.94$; $p < 0.001$], and frequency and substage interaction [$F_{(31,896)} = 2.02$; $p < 0.001$]. The *post hoc* comparison revealed that the Wisket animals had significantly higher relative power at the lower frequency alpha band (8.38 − 9.75 Hz) compared to controls during the active awake substage (**Figure 2C**).

Regarding the relative power during the whole investigated period in the beta band (12–30 Hz), factorial ANOVA showed significant effects of group [$F_{(1,2016)} = 344.18$; $p < 0.001$], frequency [$F_{(143,2016)} = 235.91$; $p < 0.001$], and group and frequency interaction [$F_{(143,2016)} = 4.18$; $p < 0.001$]. Thus, the Wisket animals had significantly higher total relative power compared to control ones at the lower frequency beta band (12.12 − 18.38 Hz interval; **Figure 3A**).

The analysis of the beta power by stages showed significant effects of group [$F_{(1,6048)} = 625.89$; $p < 0.001$], frequency [$F_{(143,6048)} = 390.36$; $p < 0.001$], stage [$F_{(2,6048)} = 1415.83$; $p < 0.001$), group and frequency interaction [$F_{(143,6048)} = 4.24$; $p < 0.001$], group and stage interaction [$F_{(2,6048)} = 35.80$; $p < 0.001$], and frequency and stage interaction [$F_{(286,6048)} = 44.05$; $p < 0.001$]. The pattern of the beta spectrum differed between the stages with the highest steepness of the curve during NREM, and the Wisket animals had higher relative power in all stages at the lower beta frequency band (awake: 12.12 − 19.38 Hz, NREM: 12.88 − 17.5 Hz, REM: 12.12 − 15.75 Hz; **Figure 3B**).

The separate analysis of the beta band by substages revealed significant effects of group [$F_{(1,4032)} = 541.50$; $p < 0.001$], frequency [$F_{(143,4032)} = 312.70$; $p < 0.001$], substage [$F_{(1,4032)} = 649.00$; $p < 0.001$], group and frequency interaction [$F_{(143,4032)} = 5.00$; $p < 0.001$], and frequency and substage interaction [$F_{(143,4032)} = 20.90$; $p < 0.001$]. Thus, the Wisket animals had significantly higher relative power at the lower frequency beta band compared to controls primarily during the active awake substage (active: 12.12 − 19.38 Hz, quiet: 12.38 − 12.5 Hz; **Figure 3C**).

As regards the relative power during the whole period in the gamma band (30 − 48 Hz), factorial ANOVA showed significant effects of group [$F_{(1,2002)} = 588.00$; $p < 0.001$) and frequency [$F_{(142,2002)} = 20.00$; $p < 0.001$). The *post hoc* analysis disclosed that the Wisket animals had significantly lower whole relative power compared to control ones at the higher gamma frequency band (39 − 48 Hz interval; **Figure 3D**).

The analysis of the gamma power by stages revealed significant effects of group [$F_{(1,6006)} = 332.00$; $p < 0.001$], frequency [$F_{(142,6006)} = 39.00$; $p < 0.001$], stage [$F_{(2,6006)} = 9538.00$; $p < 0.001$], and frequency and stage interaction [$F_{(284,6006)} = 7.00$; $p < 0.001$]. The *post hoc* analysis showed that the pattern of the gamma spectrum differed between the stages with the lowest steepness of curve values during NREM, and the Wisket animals had lower relative gamma power, primarily during the awake stage at the higher frequency range (44.25 − 48 Hz; **Figure 3E**).

The separate analysis of the gamma band by substages revealed significant effects of group [$F_{(1,4004)} = 478.00$; $p < 0.001$], frequency [$F_{(142,4004)} = 17.00$; $p < 0.001$], substage [$F_{(1,4004)} = 8230.00$; $p < 0.001$], group and substage interaction [$F_{(1,4004)} = 54.00$; $p < 0.001$], and frequency and substage interaction [$F_{(142,4004)} = 3.00$; $p < 0.001$]. Thus, the Wisket animals had significantly lower relative power at the higher frequency gamma band compared to controls, primarily during the active awake substage (active: 42.62 − 48 Hz, quiet: 46.16 − 48 Hz; **Figure 3F**).

Regarding the data of unmatched series, the curves were inserted into the figures in reduced size (**Figures 1–3**). Most of the observed changes in the matched Wisket animals could also be obtained in the unmatched animals.

DISCUSSION

The main objective of the present study was to assess changes in sleep architecture and oscillatory pattern of a multiple hit schizophrenia rat model. The Wisket animals have a clear light-dark cycle similar to controls, and their wake-sleep rhythm showed only a tendency to alterations. However, important signs of abnormalities in their oscillatory pattern were obtained by applying a fine-grain analysis within different frequency bands. In spite of the lack of the diurnal variation in the oscillation in both groups, the Wisket rats showed higher relative power in the low-frequency delta, alpha, and beta bands and lower relative power in the high-frequency theta and gamma bands in most stages and substages. The same pattern of differences could be observed between the unmatched groups even with the low number of animals, suggesting that these alterations are stabile with high reproducibility. Furthermore, the automated categorization of the stages and substages had a high level of correlation with the manual classification.

The automated sleep stage discrimination was carried out using software developed in-house, to assign each epoch to one of the three stages. While visual EEG classification is still considered the gold standard for sleep scoring, the considerable progress in computational technologies has made possible the improvement of automated sleep scoring algorithms (Miladinović et al., 2019; Yamabe et al., 2019). Conventional methods for identifying and removing EEG artifacts are subjective and time consuming, that are commonly dealt with based on qualitative and subjective criteria. The artifacts can be repaired or rejected (Jas et al., 2017). While the method of excluding artifacts from the analysis is very often employed, it leads to the loss of several data. Therefore, we presented an automated algorithm for unified reception and repairing these artifacts in EEG signals. The algorithm allowed us to automate the preprocessing of EEG data. The automated nature of this method minimized the burden of human inspection, supporting scalability and reliability data analysis.

It is very important for an automatic classification to achieve the accuracy level required for practical research usage. Generally, the inter-rater agreement rate of the manual sleep stage scoring results in rodents is reported to be approximately 95%. While we found 92.8% agreement between the manual and automated classification, we assume that this level should also provide

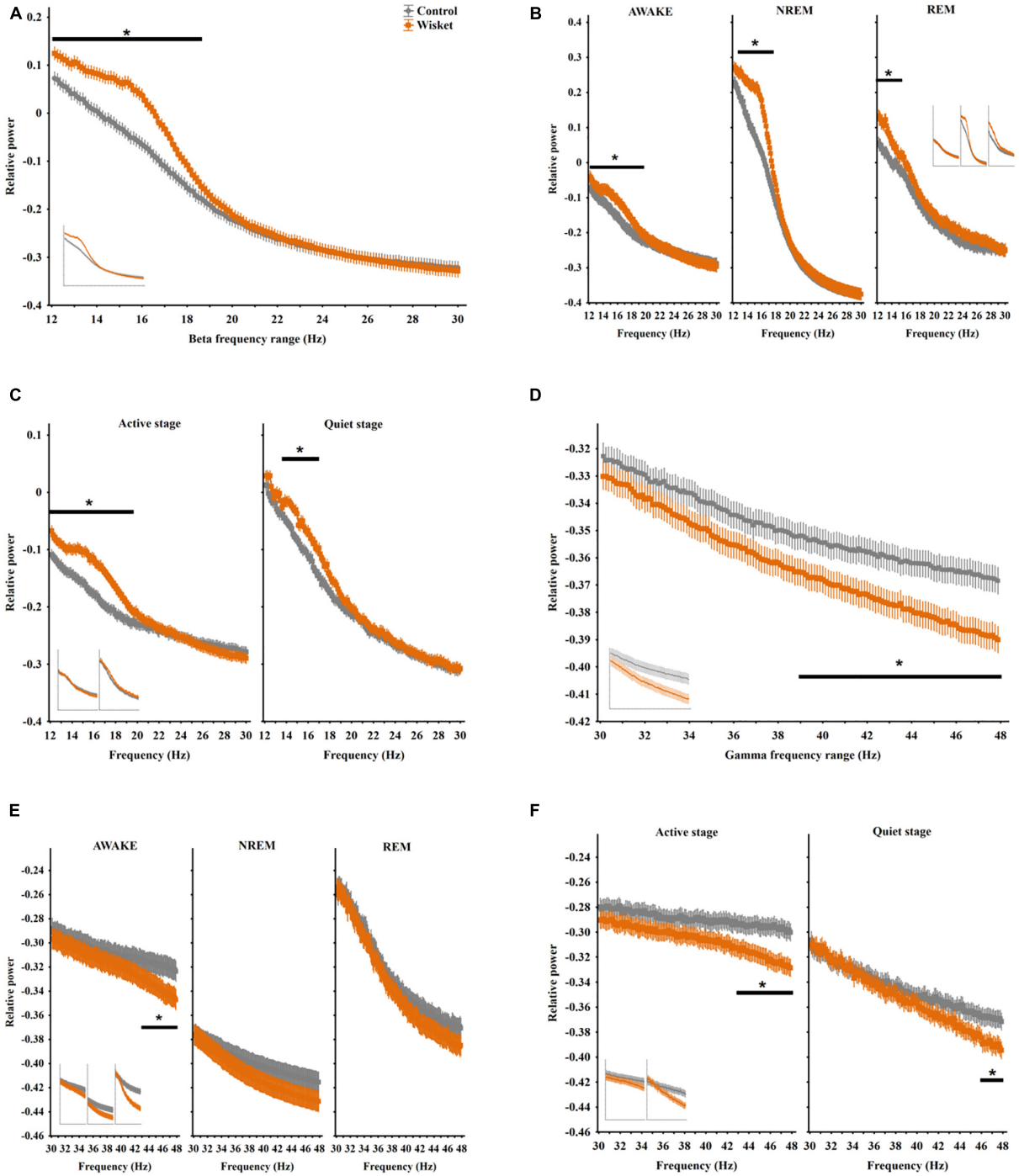

FIGURE 3 | Relative EEG power differences between the two groups at the beta and gamma frequency bands. **(A)** Total relative beta power (12–30 Hz). **(B)** Beta power in different stages. **(C)** Beta power in active and quiet awake substages. **(D)** Total relative gamma power (30–48 Hz). **(E)** Gamma power in different stages. **(F)** Gamma power in active and quiet awake substages. Curves inserted in reduced size show the results obtained from unmatched control and Wisket animals. The symbol * shows significant ($p° < °0.05$) differences between the two groups.

reliable data. This was supported by the very similar data obtained with different groups of animals.

Normal wake-sleep rhythm is an important physiological process underlying the maintenance of physical, mental, and emotional health. Sleep disorder is one of the most common signs in patients with schizophrenia, that correlates with cognitive and affective abnormalities (Cohrs, 2008; Poulin et al., 2010; Pritchett et al., 2012; Winsky-Sommerer et al., 2019).

Most of the studies suggest reduced sleep duration and enhanced sleep fragmentation; however, sleep-onset insomnia can counterintuitively increase total sleeping time in some patients compared to healthy controls (Poulin et al., 2010). Although direct comparison of clinical and preclinical data is difficult, especially because rats, unlike humans, are polycyclic sleepers, the Wisket animals had almost normal diurnal variation in their sleep-wake pattern. This is in agreement with some previous reports obtained in different schizophrenia models, including DISC1 gene mutant mice and rats with prenatal intervention or neonatal hippocampal lesion (Ahnaou et al., 2007; Phillips et al., 2012b; Valdés-Cruz et al., 2012; Profitt et al., 2016; Dittrich et al., 2017). The Wisket rats spent a slightly reduced time awake during the light phase accompanied by a moderately prolonged period in NREM sleep. Furthermore, a tendency of decreased REM sleep duration was detected compared to the control group. This phenomenon was accompanied by a mild decrease in the number of episodes in all stages. Apparently, these results seem to be in contrast with some human data or results obtained in animal models of schizophrenia (Phillips et al., 2012a; Pritchett et al., 2012; Profitt et al., 2016; Winsky-Sommerer et al., 2019). However, the decreased incidence of REM sleep episodes accompanied by enhanced NREM duration was also detected in mGLUR5 mutant mice (Ahnaou et al., 2015b; Ang et al., 2018). These signs may be derived from a chronic imbalance between the ascending and descending systems, of which activities are known to trigger or to dampen the occurrence of NREM and REM sleep states, respectively (Brown et al., 2012). Therefore, less sequential transitions in the NREM-REM sleep cycle might correlate with impaired cognition processes obtained in Wisket animals (Kekesi et al., 2015; Horvath et al., 2017). The unchanged fragmentation of the episodes seems to be in contrast with the earlier results obtained with telemetry, where decreased motor activity with the fragmented pattern was observed in the Wisket animals (Horvath et al., 2015). However, telemetry is only suited to monitor gross motor activity, it cannot differentiate between the activity stages, and it cannot detect fine movements (Horvath et al., 2015). Furthermore, the micro-arousals (shorter than 8 s long fragments of the awake stage) that were not involved in the EEG analysis might have modified the results (Kang et al., 2015).

In summary, the wake-sleep phenotype of Wisket rats may mimic only a slight abnormality observed in a small subset of patients with schizophrenia but does not reflect disease-related sleep abnormalities overall (Kaskie et al., 2017). However, all these changes might have a significant influence on the oscillatory pattern in different frequency bands. Neuronal oscillations represent a fundamental mechanism enabling coordinated activity during normal brain functioning and are, therefore, an instrumental research target for neuronal and neuropsychiatric disorders. The oscillatory pattern may depend on the strength and kinetics of inhibitory and excitatory synaptic interactions and data suggest that ineffective inhibitory control of sensory processing is characteristic in schizophrenia (Gyorgy and Andreas, 2004; Orekhova et al., 2008; Uhlhaas and Singer, 2013). Altered oscillatory activity in the different EEG frequency bands has been reported in patients, which may contribute to their abnormal sensory and cognitive performance (Felder et al., 1994; Sponheim et al., 1994, 2003; Omori et al., 1995; Symond et al., 2005; Rockstroh et al., 2007; Bob et al., 2008; Boutros et al., 2008; Lakatos et al., 2013; Uhlhaas and Singer, 2013; Csukly et al., 2016). Unfortunately, the results are controversial and they may depend on the subtypes or phases of this disease (Adler et al., 1982; Braff and Geyer, 1990; Sponheim et al., 2003; Başar, 2013; Uhlhaas and Singer, 2013). In agreement with earlier studies, the oscillatory pattern did not show differences between the dark and light phases neither in the control nor in the Wisket groups (Ahnaou et al., 2015a; Profitt et al., 2016; Aguilar et al., 2020). However, several differences in EEG power spectra across the three different stages were detected between the two groups but at different frequency ranges. Oscillations in different frequency bands may have different underlying mechanisms, which subserve different functions. Thus, the differences in cortical oscillations might suggest very complex disturbances in the Wisket animals.

Regarding the delta wave, it is originated from the reticular nucleus of the thalamus, where GABAergic neurons are tonically activated *via* NMDA receptors, thereby regulating the activity of thalamic relay neurons projecting to the prefrontal cortex (Lisman, 2012). Thus, the interplay among spontaneous synaptic inputs, intrinsic neural properties, and coupled thalamocortical network oscillations generates EEG power in this frequency range (Crunelli and Hughes, 2010). It is mainly associated with brain quiescence and the closing of thalamic gates for external input, but such activity has also been related to unexpectedly high levels of spontaneous neuronal activity, which may serve important cognitive processes such as memory consolidation (Steriade, 2006). This frequency band during the NREM stage plays important role in the recovery function of sleep and the beneficial cognitive effects of sleep (Borbély, 2001; Borbély et al., 2016).

Augmented low-frequency oscillations were observed in unmedicated, first-episode, and chronic patients with schizophrenia (Sponheim et al., 1994; Knott et al., 2001; Rockstroh et al., 2007; Boutros et al., 2008; Newson and Thiagarajan, 2019). Other data suggest that delta band power increased in patient with negative symptoms, while it decreased in patients with positive symptom domains (Begic et al., 2000). It was suggested that the abnormal slow wave activity is a manifestation of disrupted formation of neural circuits, facilitating histological anomalies, like gray matter loss.

In our experiments, only a tendency of enhancement in the delta band power was found during the awake stage (at both the active and quiet substages) compared to the controls. However, the Wisket animals showed significantly enhanced delta activity in its lower frequency range during the NREM phase, while it decreased in the higher frequency range of the delta band during the NREM and REM stages. The higher power in the lower frequency delta band might suggest enhanced requirements of sleep (Borbély, 2001). The reduced delta power during NREM sleep at the higher frequency range could arise from cortical dysfunction, altered thalamocortical input, or both, while the enhancement in the slow oscillations at the higher delta band was thought to indicate less exchange of excitation (Rockstroh et al., 2007). Regarding the earlier preclinical studies, a tendency

of enhancement in delta power in both wakefulness and NREM sleep was found 2 months after neonatal hippocampal lesion (Ahnaou et al., 2007). STOP mutant mice also showed an increase in relative power in the delta band (0.5–4 Hz) during NREM (Profitt et al., 2016). In agreement with our data, AMPA receptor mutant mice had higher power in a lower frequency range (0.75–1.5 Hz), while mGLUR5 receptor mutant mice had lower delta power at a higher frequency range during NREM compared to control animals (Ahnaou et al., 2015b; Ang et al., 2018).

The cortico-hippocampal circuits are key generators of theta rhythm, which has an important role in cognition and memory formation (Buzsáki, 2002; Gyorgy and Andreas, 2004; Buzsáki and Moser, 2013). Theta oscillations dominate during motor activity or when the rats remain motionless but alert (Buzsáki, 2002). REM sleep in rodents is characterized by a prominent theta rhythm in EEG recording (as was observed in both groups of rats), reflecting hippocampal activity (Boyce et al., 2016). Its generation depends on GABA neurons in the medial septum projecting to the hippocampus, thus, the silencing of these neurons during REM sleep led to decreased theta power and impairments in memory consolidation.

Inconsistent changes in theta band power were observed in patients with schizophrenia (Winterer and Weinberger, 2004; Javitt et al., 2008; Lakatos et al., 2013; Grove et al., 2021) depending on the dominant symptom domain, i.e., in patients with positive symptoms, there was no change, while in case of negative signs, it increased (Gerez and Tello, 1995; Begic et al., 2000; Winterer and Weinberger, 2004; Javitt et al., 2008; Lakatos et al., 2013; Grove et al., 2021).

In Wisket rats, the significantly lower relative power of the higher frequency band was observed during the awake (both the active and quiet substages) and REM stages. In contrast, they had significantly lower power at the lower frequency range of theta band during NREM. Optogenetic inhibition of REM theta power impairs sleep-dependent memory consolidation in mice (Boyce et al., 2016). Therefore, our observation of decreased theta power in REM might explain the memory impairment in Wisket rats reported earlier (Kekesi et al., 2015; Horvath et al., 2017). Regarding the schizophrenia models, the results are controversial. Enhancement of power in theta bands was observed in both wakefulness and NREM sleep in neonatal hippocampal lesioned rats (Ahnaou et al., 2007). In contrast, but agreement with our data, STOP or AMPA receptor mutant mice had lower relative power in the theta band (Profitt et al., 2016; Ang et al., 2018), suggesting reduced arousal level during the active stage (Leemburg et al., 2010).

The oscillation in the alpha band is related primarily to the thalamus, thus, the alterations in this frequency band may suggest dysfunction of the inhibitory input of thalamic neurons (Markand, 1990; Begic et al., 2000). There are limited and inconsistent data regarding the role and significance of alpha oscillations in schizophrenia. Either higher alpha power associated with negative symptoms or reduced alpha band activity in patients with both negative or positive signs of schizophrenia were reported (Gerez and Tello, 1995; Begic et al., 2000; Boutros et al., 2008; Featherstone et al., 2015; Newson and Thiagarajan, 2019).

While Wisket animals showed significantly enhanced relative power at the lower frequency alpha band during awake (primarily in active substage) and REM stages, it might be related to the negative symptoms. In agreement with our results, hippocampal lesion increased the alpha power during the awake stage (Ahnaou et al., 2007), but AMPA receptor or STOP mutant schizophrenia model mice demonstrated decreases in the alpha power during the REM phase (Profitt et al., 2016; Ang et al., 2018).

Beta oscillations are believed to be generated broadly across multiple neocortical structures and are involved in adaptation to repetitive sensory stimuli, attention, affective processing, alertness, and synchronization of large ensembles of neurons (Uhlhaas and Singer, 2013; Featherstone et al., 2015). Both decreased and increased beta oscillatory activities were detected in patients with schizophrenia (Javitt et al., 2008; Uhlhaas and Singer, 2013; Csukly et al., 2016). The enhancement in the beta band might be due to global cortical hyperexcitability or attention disturbances observed in these patients (Begic et al., 2000; Newson and Thiagarajan, 2019).

Our data clearly showed that Wisket animals had significantly enhanced beta power at the lower frequency range in all stages compared to control animals, but this difference was most prominent during active awake substage. These alterations might play role in the impaired cognitive behavior of Wisket model rats observed earlier (Horvath et al., 2019; Saravanapandian et al., 2020). Preclinical data are also inconsistent in the beta wave changes. STOP and AMPA receptor and voltage-gated calcium channel mutant mice had lower beta power during NREM and/or REM stages, the AMPA receptor mutant animals had higher beta power during awake, while the calcium channel mutant mice had lower power in this stage (Kumar et al., 2015; Profitt et al., 2016; Ang et al., 2018). In contrast, the hippocampal lesion did not cause changes in this frequency band (Ahnaou et al., 2007).

Gamma oscillations have received great interest because of their role in sensory and cognitive functions such as selective attention, short- and long-term memory, and multisensory integration (Traub et al., 1999; Gyorgy and Andreas, 2004; Uhlhaas and Singer, 2013; Featherstone et al., 2015; Tatard-Leitman et al., 2015). The primary generators of gamma oscillations are in the cortex, where subsets of GABAergic interneurons modulate the glutamatergic pyramidal cell activity, while the pyramidal neurons appear to control the strength, duration, and long-range synchronization of the GABAergic interneurons. Abnormal gamma oscillations have been associated with positive, negative, and cognitive symptoms of schizophrenia (Lee et al., 2001; Uhlhaas and Singer, 2013; Featherstone et al., 2015). Many studies observed reduced oscillatory activity that may reflect the deficits in cognitive and sensory processing related to negative symptoms in schizophrenia (Kwon et al., 1999; Symond et al., 2005; Hong et al., 2010; Koychev et al., 2012; Uhlhaas and Singer, 2013). However, contrasting findings of increased gamma activities in schizophrenia also exist, and it is reportedly relevant to positive symptoms (Gerez and Tello, 1995; Norra et al., 2004; Javitt et al., 2008; Başar, 2013; Lakatos et al., 2013; Baradits et al., 2019).

Our results showed that Wisket animals had a significant decrease in the relative power of the higher band of gamma

wave (between 39 and 48 Hz) compared to the controls, which was dominant during the awake stage (primarily in the active substage). It is well-known that gamma band oscillations are associated with multiple cognitive functions, and gamma activity increases during alert or attentive wakefulness, especially above 40 Hz (Maloney et al., 1997; Uhlhaas and Singer, 2013). Therefore, this phenomenon in Wisket rats may indicate a lower level of arousal or alertness during wakefulness, but could also be related to the impaired cognitive functions obtained earlier in the Wisket animals (Franken et al., 1994; Horvath et al., 2019). Earlier preclinical data are controverting in this respect. In agreement with our data, the animals after chronic NMDA antagonists treatment or with voltage-gated calcium channel mutation also displayed no change or reduction in gamma power (Kittelberger et al., 2012; Featherstone et al., 2014; Kumar et al., 2015; Sullivan et al., 2015), but elevated gamma activity was recorded during sleep in mGluR5 mutant mice (Aguilar et al., 2020).

LIMITATIONS

There are several limitations in our recording system: the maximum recording duration and the limited number of channels, and a lack of deep hippocampal electrodes. Furthermore, as we used a tethered option rather than wireless recording, the rats were singly housed in cages, to provide appropriate circumstances for fully recovering after the surgery and prevent the destruction of the EEG devices and cables. It is well known that long-term single housing (more than 1 week), especially in young animals, affects several biological parameters (Weiss et al., 2004; Makinodan et al., 2012; Yamamuro et al., 2018). However, in this study, the social isolation was performed during adulthood for only 1 week, and the animals were kept in visual, auditory, and olfactory contact with other rats during the whole experimental period to minimalize the effect of isolation rearing (Hurst et al., 1999). It should also be mentioned that we used a limited gamma frequency range in our analysis; therefore, it could not be excluded from further impairments in the higher frequency band in Wisket animals. A further limitation is the lower sampling rate of the EEG recordings (128 Hz), which would have limited the fine analyses of the oscillatory pattern in the higher gamma frequency band.

CONCLUSION

Our data first characterized the sleep-wake rhythm and oscillatory pattern of a multiple hit rat model of schizophrenia. The results indicate that the Wisket rats have only a tendency to alterations in their sleep-wake pattern with normal circadian rhythm. On the other hand, the investigation of the oscillatory patterns in different frequency bands revealed complex alterations in all stages and substages of the sleep-wake rhythm.

Wakefulness and sleep are promoted by the ascending arousal and descending inhibitory pathways, respectively, operating with several neurotransmitters, including dopamine, glutamate, and GABA systems (Saper et al., 2005). The Wisket rats have impairment in several receptor systems (Szûcs et al., 2016a, 2020; Büki et al., 2019; Banki et al., 2020; Horvath et al., 2021b), which might be involved in both the development of schizophrenia-like behavioral signs and the connected particular brain oscillation (Svensson et al., 1987; Hajos et al., 2008; Kittelberger et al., 2012).

A better understanding of the characteristics of sleep disturbance and oscillatory activity in this schizophrenia model may help to address fundamental relationships among the behavioral, neurochemical, and electrophysiological parameters, as well as to develop novel drug targets and therapies to treat this disorder.

DATA AVAILABILITY STATEMENT

The raw data supporting the conclusions of this article will be made available by the authors, without undue reservation.

ETHICS STATEMENT

The animal study was reviewed and approved by Hungarian Ethical Committee for Animal Research.

AUTHOR CONTRIBUTIONS

LA contributed to data collection, interpretation of the results, and manual classification. MC-N developed data classification software and tested by comparison with manual classification. BB did animal surgery, conducted the experiments, and developed the data recording system. GyK developed data classification software and contributed to statistical analysis. LN supervised software development and performed proofreading. AN supervised the experiments and manual classification of data and performed proofreading. GaK contributed to the interpretation of the results and performed proofreading. AB contributed to statistical analysis. GH conceived of the presented idea, planned the experiments, performed statistical analysis, and wrote the first draft of the manuscript.

FUNDING

This study was supported by a grant from SZTE ÁOK-KKA Grant No. 2019/270-62-2.

SUPPLEMENTARY MATERIAL

The Supplementary Material for this article can be found online at: https://www.frontiersin.org/articles/10.3389/fnbeh.2021.799271/full#supplementary-material

Supplementary Figure 1 | Interventions in the Wisket animals to develop the triple-hit schizophrenia model. TF, tail-flick test to determine pain sensitivity; PPI, prepulse inhibition test to measure sensory gating; Ambitus, a reward-based cognitive test to determine motor activity and learning capability.

REFERENCES

Adler, L. E., Pachtman, E., Franks, R. D., Pecevich, M., Waldo, M. C., and Freedman, R. (1982). Neurophysiological evidence for a defect in neuronal mechanisms involved in sensory gating in schizophrenia. *Biol. Psychiatry* 17, 639–654.

Afonso, P., Brissos, S., Figueira, M. L., and Paiva, T. (2011). Schizophrenia patients with predominantly positive symptoms have more disturbed sleep-wake cycles measured by actigraphy. *Psychiatry Res.* 189, 62–66. doi: 10.1016/j.psychres.2010.12.031

Aguilar, D. D., Strecker, R. E., Basheer, R., and McNally, J. M. (2020). Alterations in sleep, sleep spindle, and EEG power in mGluR5 knockout mice. *J. Neurophysiol.* 123, 22–33. doi: 10.1152/jn.00532.2019

Ahnaou, A., Raeymaekers, L., Steckler, T., and Drinkenbrug, W. H. I. M. (2015b). Relevance of the metabotropic glutamate receptor (mGluR5) in the regulation of NREM-REM sleep cycle and homeostasis: evidence from mGluR5 (-/-) mice. *Behav. Brain Res.* 282, 218–226. doi: 10.1016/j.bbr.2015.01.009

Ahnaou, A., Langlois, X., Steckler, T., Bartolome-Nebreda, J. M., and Drinkenburg, W. H. I. M. (2015a). Negative versus positive allosteric modulation of metabotropic glutamate receptors (mGluR5): indices for potential pro-cognitive drug properties based on EEG network oscillations and sleep-wake organization in rats. *Psychopharmacology* 232, 1107–1122. doi: 10.1007/s00213-014-3746-4

Ahnaou, A., Nayak, S., Heylen, A., Ashton, D., and Drinkenburg, W. H. I. M. (2007). Sleep and EEG profile in neonatal hippocampal lesion model of schizophrenia. *Physiol. Behav.* 92, 461–467. doi: 10.1016/j.physbeh.2007.04.020

Ang, G., McKillop, L. E., Purple, R., Blanco-Duque, C., Peirson, S. N., Foster, R. G., et al. (2018). Absent sleep EEG spindle activity in GluA1 (Gria1) knockout mice: relevance to neuropsychiatric disorders. *Transl. Psychiatry* 8:154. doi: 10.1038/s41398-018-0199-2

Banki, L., Büki, A., Horvath, G., Kekesi, G., Kis, G., Somogyvári, F., et al. (2020). Distinct changes in chronic pain sensitivity and oxytocin receptor expression in a new rat model (Wisket) of schizophrenia. *Neurosci. Lett.* 714:134561. doi: 10.1016/j.neulet.2019.134561

Baradits, M., Kakuszi, B., Bálint, S., Fullajtár, M., Mód, L., Bitter, I., et al. (2019). Alterations in resting-state gamma activity in patients with schizophrenia: a high-density EEG study. *Eur. Arch. Psychiatry Clin. Neurosci.* 269, 429–437. doi: 10.1007/s00406-018-0889-z

Başar, E. (2013). Brain oscillations in neuropsychiatric disease. *Dialogues Clin. Neurosci.* 15, 291–300. doi: 10.31887/dcns.2013.15.3/ebasar

Begic, D., Hotujac, L., and Jokic-Begic, N. (2000). Quantitative EEG in "positive" and "negative" schizophrenia. *Acta Psychiatr. Scand.* 101, 307–311.

Bob, P., Palus, M., Susta, M., and Glaslova, K. (2008). EEG phase synchronization in patients with paranoid schizophrenia. *Neurosci. Lett.* 447, 73–77. doi: 10.1016/j.neulet.2008.09.055

Bodosi, B., Gardi, J., Hajdu, I., Szentirmai, E., Obal, F., and Krueger, J. M. (2004). Rhythms of ghrelin, leptin, and sleep in rats: effects of the normal diurnal cycle, restricted feeding, and sleep deprivation. *Am. J. Physiol. Regul. Integr. Comp. Physiol.* 287, R1071–R1079. doi: 10.1152/ajpregu.00294.2004

Bodosi, B., Obál, F., Gardi, J., Komlódi, J., Fang, J., and Krueger, J. M. (2000). An ether stressor increases REM sleep in rats: possible role of prolactin. *Am. J. Physiol. Regul. Integr. Comp. Physiol.* 279, R1590–R1598. doi: 10.1152/ajpregu.2000.279.5.r1590

Borbély, A. A. (2001). From slow waves to sleep homeostasis: new perspectives. *Arch. Ital. Biol.* 139, 53–61. doi: 10.4449/aib.v139i1.204

Borbély, A. A., Daan, S., Wirz-Justice, A., and Deboer, T. (2016). The two-process model of sleep regulation: a reappraisal. *J. Sleep Res.* 25, 131–143. doi: 10.1111/jsr.12371

Boutros, N. N., Arfken, C., Galderisi, S., Warrick, J., Pratt, G., and Iacono, W. (2008). The status of spectral EEG abnormality as a diagnostic test for schizophrenia. *Schizophr. Res.* 99, 225–237. doi: 10.1016/j.schres.2007.11.020

Boyce, R., Glasgow, S. D., Williams, S., and Adamantidis, A. (2016). Sleep research: causal evidence for the role of REM sleep theta rhythm in contextual memory consolidation. *Science* 352, 812–816. doi: 10.1126/science.aad5252

Braff, D. L., and Geyer, M. A. (1990). Sensorimotor gating and schizophrenia: human and animal model studies. *Arch. Gen. Psychiatry* 47, 181–188.

Breiman, L. (2001). Random forests. *Mach. Learn.* 45, 5–32. doi: 10.1023/A:1010933404324

Brown, R. E., Basheer, R., McKenna, J. T., Strecker, R. E., and McCarley, R. W. (2012). Control of sleep and wakefulness. *Physiol. Rev.* 92, 1087–1187. doi: 10.1152/physrev.00032.2011

Büki, A., Horvath, G., Benedek, G., Ducza, E., and Kekesi, G. (2019). Impaired GAD1 expression in schizophrenia-related WISKET rat model with sex-dependent aggressive behavior and motivational deficit. *Genes Brain Behav.* 18:e12507. doi: 10.1111/gbb.12507

Buzsáki, G. (2002). Theta oscillations in the hippocampus. *Neuron* 33, 325–340. doi: 10.1016/S0896-6273(02)00586-X

Buzsáki, G., and Moser, E. I. (2013). Memory, navigation and theta rhythm in the hippocampal-entorhinal system. *Nat. Neurosci.* 16, 130–138. doi: 10.1038/nn.3304

Cohrs, S. (2008). Sleep disturbances in patients with schizophrenia: impact and effect of antipsychotics. *CNS Drugs* 22, 939–962. doi: 10.2165/00023210-200822110-00004

Crunelli, V., and Hughes, S. W. (2010). The slow (1 Hz) rhythm of non-REM sleep: a dialogue between three cardinal oscillators. *Nat. Neurosci.* 13, 9–17. doi: 10.1038/nn.2445

Csukly, G., Farkas, K., Marosi, C., and Szabó, Á (2016). Deficits in low beta desynchronization reflect impaired emotional processing in schizophrenia. *Schizophr. Res.* 171, 207–214. doi: 10.1016/j.schres.2016.01.031

Dittrich, L., Petese, A., and Jackson, W. S. (2017). The natural Disc1-deletion present in several inbred mouse strains does not affect sleep. *Sci. Rep.* 7:5665. doi: 10.1038/s41598-017-06015-3

Featherstone, R. E., McMullen, M. F., Ward, K. R., Bang, J., Xiao, J., and Siegel, S. J. (2015). EEG biomarkers of target engagement, therapeutic effect, and disease process. *Ann. N. Y. Acad. Sci.* 1344, 12–26.

Featherstone, R. E., Nagy, L. R., Hahn, C. G., and Siegel, S. J. (2014). Juvenile exposure to ketamine causes delayed emergence of EEG abnormalities during adulthood in mice. *Drug Alcohol Depend.* 134, 123–127. doi: 10.1016/j.drugalcdep.2013.09.017

Felder, C. C., Singer-Lahat, D., and Mathes, C. (1994). Voltage-independent calcium channels. Regulation by receptors and intracellular calcium stores. *Biochem. Pharmacol.* 48, 1997–2004. doi: 10.1016/0006-2952(94)90498-7

Franken, P., Dijk, D. J., Tobler, I., and Borbély, A. A. (1994). High-frequency components of the rat electrocorticogram are modulated by the vigilance states. *Neurosci. Lett.* 167, 89–92. doi: 10.1016/0304-3940(94)91034-0

Gerez, M., and Tello, A. (1995). Selected quantitative EEG (QEEG) and event-related potential (ERP) variables as discriminators for positive and negative schizophrenia. *Biol. Psychiatry* 38, 34–49. doi: 10.1016/0006-3223(94)00205-H

Grove, T. B., Lasagna, C. A., Martínez-Cancino, R., Pamidighantam, P., Deldin, P. J., and Tso, I. F. (2021). Neural Oscillatory Abnormalities During Gaze Processing in Schizophrenia: evidence of Reduced Theta Phase Consistency and Inter-areal Theta-Gamma Coupling. *Biol. Psychiatry Cogn. Neurosci. Neuroimaging* 6, 370–379. doi: 10.1016/j.bpsc.2020.08.013

Gyorgy, B., and Andreas, D. (2004). Neuronal Oscillations in Cortical Networks. *Science* 304, 1926–1929.

Hajos, M., Hoffmann, W. E., and Kocsis, B. (2008). Activation of cannabinoid-1 receptors disrupts sensory gating and neuronal oscillation: relevance to schizophrenia. *Biol. Psychiatry* 63, 1075–1083.

Hong, L. E., Summerfelt, A., Buchanan, R. W., O'Donnell, P., Thaker, G. K., Weiler, M. A., et al. (2010). Gamma and delta neural oscillations and association with clinical symptoms under subanesthetic ketamine. *Neuropsychopharmacology* 35, 632–640. doi: 10.1038/npp.2009.168

Horvath, G., Adam, G., Tuboly, G., Kekesi, G., Büki, A., Ducza, E., et al. (2021a). Caffeine - treat or trigger? Disparate behavioral and long-term dopaminergic changes in control and schizophrenia-like Wisket rats. *Physiol. Behav.* 236:113410. doi: 10.1016/J.PHYSBEH.2021.113410

Horvath, G., Kis, G., Kekesi, G., Büki, A., Adlan, L. G., Szûcs, E., et al. (2021b). Interaction of clozapine with metformin in a schizophrenia rat model. *Sci. Rep.* 11:16862. doi: 10.1038/s41598-021-96478-2

Horvath, G., Kekesi, G., Petrovszki, Z., and Benedek, G. (2015). Abnormal motor activity and thermoregulation in a schizophrenia rat model for translational science. *PLoS One* 10:e0143751. doi: 10.1371/journal.pone.0143751

Horvath, G., Liszli, P., Kekesi, G., Büki, A., and Benedek, G. (2017). Characterization of exploratory activity and learning ability of healthy and "schizophrenia-like" rats in a square corridor system (AMBITUS). *Physiol. Behav.* 169, 155–164. doi: 10.1016/j.physbeh.2016.11.039

Horvath, G., Liszli, P., Kekesi, G., Büki, A., and Benedek, G. (2019). Cognitive training improves the disturbed behavioral architecture of schizophrenia-like rats, "Wisket". *Physiol. Behav.* 201, 70–82. doi: 10.1016/j.physbeh.2018.12.011

Horvath, G., Petrovszki, Z., Kekesi, G., Tuboly, G., Bodosi, B., Horvath, J., et al. (2016). Electrophysiological alterations in a complex rat model of schizophrenia. *Behav. Brain Res.* 307, 65–72. doi: 10.1016/j.bbr.2016.03.051

Hurst, J. L., Barnard, C. J., Tolladay, U., Nevision, C. M., and West, C. D. (1999). Housing and welfare in laboratory rats: effects of cage stocking density and behavioural predictors of welfare. *Anim. Behav.* 58, 563–586. doi: 10.1006/ANBE.1999.1165

Jas, M., Engemann, D. A., Bekhti, Y., Raimondo, F., and Gramfort, A. (2017). Autoreject: automated artifact rejection for MEG and EEG data. *Neuroimage* 159, 417–429. doi: 10.1016/j.neuroimage.2017.06.030

Javitt, D. C., Spencer, K. M., Thaker, G. K., Winterer, G., and Hajos, M. (2008). Neurophysiological biomarkers for drug development in schizophrenia. *Nat. Rev. Drug Discov.* 7, 68–83. doi: 10.1038/nrd2463

Kang, D., Ding, M., Topchiy, I., Shifflett, L., and Kocsis, B. (2015). Theta-rhythmic drive between medial septum and hippocampus in slow-wave sleep and microarousal: a Granger causality analysis. *J. Neurophysiol.* 114, 2797–2803. doi: 10.1152/jn.00542.2015

Kaskie, R. E., Graziano, B., and Ferrarelli, F. (2017). Schizophrenia and sleep disorders: links, risks, and management challenges. *Nat. Sci. Sleep* 9, 227–239. doi: 10.2147/NSS.S121076

Kekesi, G., Petrovszki, Z., Benedek, G., and Horvath, G. (2015). Sex-specific alterations in behavioral and cognitive functions in a "three hit" animal model of schizophrenia. *Behav. Brain Res.* 284, 85–93. doi: 10.1016/j.bbr.2015.02.015

Kittelberger, K., Hur, E. E., Sazegar, S., Keshavan, V., and Kocsis, B. (2012). Comparison of the effects of acute and chronic administration of ketamine on hippocampal oscillations: relevance for the NMDA receptor hypofunction model of schizophrenia. *Brain Struct. Funct.* 217, 395–409. doi: 10.1007/s00429-011-0351-8

Knott, V., Labelle, A., Jones, B., and Mahoney, C. (2001). Quantitative EEG in schizophrenia and in response to acute and chronic clozapine treatment. *Schizophr. Res.* 50, 41–53.

Koychev, I., El-Deredy, W., Mukherjee, T., Haenschel, C., and Deakin, J. F. W. (2012). Core dysfunction in schizophrenia: electrophysiology trait biomarkers. *Acta Psychiatr. Scand.* 126, 59–71. doi: 10.1111/j.1600-0447.2012.01849.x

Kumar, D., Dedic, N., Flachskamm, C., Voulé, S., Deussing, J. M., and Kimura, M. (2015). Cacna1c (Cav1.2) modulates electroencephalographic rhythm and rapid eye movement sleep recovery. *Sleep* 38, 1371D–1380D. doi: 10.5665/sleep.4972

Kwon, J. S., O'Donnell, B. F., Wallenstein, G. V., Greene, R. W., Hirayasu, Y., Nestor, P. G., et al. (1999). Gamma frequency-range abnormalities to auditory stimulation in schizophrenia. *Arch. Gen. Psychiatry* 56, 1001–1005. doi: 10.1001/archpsyc.56.11.1001

Lakatos, P., Schroeder, C. E., Leitman, D. I., and Javitt, D. C. (2013). Predictive suppression of cortical excitability and its deficit in schizophrenia. *J. Neurosci.* 33, 11692–11702. doi: 10.1523/JNEUROSCI.0010-13.2013

Lee, K. H., Williams, L. M., Haig, A., Goldberg, E., and Gordon, E. (2001). An integration of 40 Hz Gamma and phasic arousal: novelty and routinization processing in schizophrenia. *Clin. Neurophysiol.* 112, 1499–1507. doi: 10.1016/S1388-2457(01)00584-3

Leemburg, S., Vyazovskiy, V. V., Olcese, U., Bassetti, C. L., Tononi, G., and Cirelli, C. (2010). Sleep homeostasis in the rat is preserved during chronic sleep restriction. *Proc. Natl. Acad. Sci. U. S. A.* 107, 15939–15944. doi: 10.1073/pnas.1002570107

Lisman, J. (2012). Excitation, inhibition, local oscillations, or large-scale loops: what causes the symptoms of schizophrenia?. *Curr. Opin. Neurobiol.* 22, 537–544. doi: 10.1016/j.conb.2011.10.018

Makinodan, M., Rosen, K. M., Ito, S., and Corfas, G. (2012). A critical period for social experience-dependent oligodendrocyte maturation and myelination. *Science* 337, 1357–1360. doi: 10.1126/SCIENCE.1220845

Maloney, K. J., Cape, E. G., Gotman, J., and Jones, B. E. (1997). High-frequency gamma electroencephalogram activity in association with sleep-wake states and spontaneous behaviors in the rat. *Neuroscience* 76, 541–555. doi: 10.1016/S0306-4522(96)00298-9

Manoach, D. S., Pan, J. Q., Purcell, S. M., and Stickgold, R. (2016). Reduced Sleep Spindles in Schizophrenia: a Treatable Endophenotype That Links Risk Genes to Impaired Cognition?. *Biol. Psychiatry* 80, 599–608. doi: 10.1016/j.biopsych.2015.10.003

Markand, O. M. (1990). Alpha rhythms. *J. Clin. Neurophysiol.* 7, 163–189.

Miladinović, D., Muheim, C., Bauer, S., Spinnler, A., Noain, D., Bandarabadi, M., et al. (2019). SPINDLE: end-to-end learning from EEG/EMG to extrapolate animal sleep scoring across experimental settings, labs and species. *PLoS Comput. Biol.* 15:e1006968. doi: 10.1371/journal.pcbi.1006968

Mofleh, R., and Kocsis, B. (2021). Delta-range coupling between prefrontal cortex and hippocampus supported by respiratory rhythmic input from the olfactory bulb in freely behaving rats. *Sci. Rep.* 11:8100. doi: 10.1038/s41598-021-87562-8

Newson, J. J., and Thiagarajan, T. C. (2019). EEG Frequency Bands in Psychiatric Disorders: a Review of Resting State Studies. *Front. Hum. Neurosci.* 12:521. doi: 10.3389/fnhum.2018.00521

Norra, C., Waberski, T. D., Kawohl, W., Kunert, H. J., Hock, D., Gobbelé, R., et al. (2004). High-Frequency somatosensory thalamocortical oscillations and psychopathology in schizophrenia. *Neuropsychobiology* 49, 71–80. doi: 10.1159/000076413

Omori, M., Koshino, Y., Murata, T., Murata, I., Nishio, M., and Sakamoto, K. (1995). Quantitative EEG in never-treated schizophrenic patients. *Biol. Psychiatry* 38, 305–309.

O'Reilly, C., Lewis, J. D., and Elsabbagh, M. (2017). Is functional brain connectivity atypical in autism? A systematic review of EEG and MEG studies. *PLoS One* 12:e0175870. doi: 10.1371/journal.pone.0175870

Orekhova, E. V., Stroganova, T. A., Prokofyev, A. O., Nygren, G., Gillberg, C., and Elam, M. (2008). Sensory gating in young children with autism: relation to age, IQ, and EEG gamma oscillations. *Neurosci. Lett.* 434, 218–223. doi: 10.1016/j.neulet.2008.01.066

Petrosian, A. (1995). "Kolmogorov complexity of finite sequences and recognition of different preictal EEG patterns," in *Proceedings of the IEEE Symposium on Computer-Based Medical Systems*, (Lubbock: IEEE), 212–217. doi: 10.1109/cbms.1995.465426

Petrovszki, Z., Adam, G., Tuboly, G., Kekesi, G., Benedek, G., Keri, S., et al. (2013). Characterization of gene-environment interactions by behavioral profiling of selectively bred rats: the effect of NMDA receptor inhibition and social isolation. *Behav. Brain Res.* 240, 134–145. doi: 10.1016/j.bbr.2012.11.022

Phillips, K. G., Bartsch, U., McCarthy, A. P., Edgar, D. M., Tricklebank, M. D., Wafford, K. A., et al. (2012a). Decoupling of Sleep-Dependent Cortical and Hippocampal Interactions in a Neurodevelopmental Model of Schizophrenia. *Neuron* 76, 526–533. doi: 10.1016/j.neuron.2012.09.016

Phillips, K. G., Cotel, M. C., McCarthy, A. P., Edgar, D. M., Tricklebank, M., O'Neill, M. J., et al. (2012b). Differential effects of NMDA antagonists on high frequency and gamma EEG oscillations in a neurodevelopmental model of schizophrenia. *Neuropharmacology* 62, 1359–1370. doi: 10.1016/j.neuropharm.2011.04.006

Poulin, J., Chouinard, S., Pampoulova, T., Lecomte, Y., Stip, E., and Godbout, R. (2010). Sleep habits in middle-aged, non-hospitalized men and women with schizophrenia: a comparison with healthy controls. *Psychiatry Res.* 179, 274–278. doi: 10.1016/j.psychres.2009.08.009

Pritchett, D., Wulff, K., Oliver, P. L., Bannerman, D. M., Davies, K. E., Harrison, P. J., et al. (2012). Evaluating the links between schizophrenia and sleep and circadian rhythm disruption. *J. Neural Transm.* 119, 1061–1075. doi: 10.1007/s00702-012-0817-8

Profitt, M. F., Deurveilher, S., Robertson, G. S., Rusak, B., and Semba, K. (2016). Disruptions of sleep/wake patterns in the Stable Tubule Only Polypeptide (STOP) null mouse model of schizophrenia. *Schizophr. Bull.* 42, 1207–1215. doi: 10.1093/schbul/sbw017

Rockstroh, B. S., Wienbruch, C., Ray, W. J., and Elbert, T. (2007). Abnormal oscillatory brain dynamics in schizophrenia: a sign of deviant communication in neural network?. *BMC Psychiatry* 7:44. doi: 10.1186/1471-244X-7-44

Saper, C. B., Scammell, T. E., and Lu, J. (2005). Hypothalamic regulation of sleep and circadian rhythms. *Nature* 437, 1257–1263. doi: 10.1038/nature04284

Saravanapandian, V., Frohlich, J., Hipp, J. F., Hyde, C., Scheffler, A. W., Golshani, P., et al. (2020). Properties of beta oscillations in Dup15q syndrome. *J. Neurodev. Disord.* 12:22. doi: 10.1186/s11689-020-09326-1

Sponheim, S. R., Clementz, B. A., Iacono, W. G., and Beiser, M. (1994). Resting EEG in first-episode and chronic schizophrenia. *Psychophysiology* 31, 37–43. doi: 10.1111/j.1469-8986.1994.tb01023.x

Sponheim, S. R., Iacono, W. G., Thuras, P. D., Nugent, S. M., and Beiser, M. (2003). Sensitivity and specificity of select biological indices in characterizing psychotic patients and their relatives. *Schizophr. Res.* 63, 27–38. doi: 10.1016/S0920-9964(02)00385-7

Steriade, M. (2006). Grouping of brain rhythms in corticothalamic systems. *Neuroscience* 137, 1087–1106. doi: 10.1016/j.neuroscience.2005.10.029

Sullivan, E. M., Timi, P., Hong, L. E., and O'Donnell, P. (2015). Reverse translation of clinical electrophysiological biomarkers in behaving rodents under acute and chronic NMDA receptor antagonism. *Neuropsychopharmacology* 40, 719–727. doi: 10.1038/npp.2014.228

Svensson, K., Alföldi, P., Hajós, M., Rubicsek, G., Johansson, A. M., Carlsson, A., et al. (1987). Dopamine autoreceptor antagonists: effects on sleep-wake activity in the rat. *Pharmacol. Biochem. Behav.* 26, 123–129. doi: 10.1016/0091-3057(87)90544-2

Symond, M. B., Harris, A. W. F., Gordon, E., and Williams, L. M. (2005). "Gamma synchrony" in first-episode schizophrenia: a disorder of temporal connectivity?. *Am. J. Psychiatry* 162, 459–465. doi: 10.1176/appi.ajp.162.3.459

Szûcs, E., Dvorácskó, S., Tömböly, C., Büki, A., Kékesi, G., Horváth, G., et al. (2016b). Decreased CB receptor binding and cannabinoid signaling in three brain regions of a rat model of schizophrenia. *Neurosci. Lett.* 633, 87–93. doi: 10.1016/j.neulet.2016.09.020

Szûcs, E., Büki, A., Kékesi, G., Horváth, G., and Benyhe, S. (2016a). Mu-Opioid (MOP) receptor mediated G-protein signaling is impaired in specific brain regions in a rat model of schizophrenia. *Neurosci. Lett.* 619, 29–33. doi: 10.1016/j.neulet.2016.02.060

Szûcs, E., Ducza, E., Büki, A., Kekesi, G., Benyhe, S., and Horvath, G. (2020). Characterization of dopamine D2 receptor binding, expression and signaling in different brain regions of control and schizophrenia-model Wisket rats. *Brain Res.* 1748:147074. doi: 10.1016/j.brainres.2020.147074

Tam, S. K. E., Pritchett, D., Brown, L. A., Foster, R. G., Bannerman, D. M., and Peirson, S. N. (2015). Sleep and circadian rhythm disruption and recognition memory in schizophrenia. *Methods Enzymol.* 552, 325–349. doi: 10.1016/bs.mie.2014.10.008

Tatard-Leitman, V. M., Jutzeler, C. R., Suh, J., Saunders, J. A., Billingslea, E. N., Morita, S., et al. (2015). Pyramidal cell selective ablation of N-methyl-D-aspartate receptor 1 causes increase in cellular and network excitability. *Biol. Psychiatry* 77, 556–568. doi: 10.1016/j.biopsych.2014.06.026

Traub, R. D., Whittington, M. A., Buhl, E. H., Jefferys, J. G. R., and Faulkner, H. J. (1999). On the mechanism of the $\gamma \rightarrow \beta$ frequency shift in neuronal oscillations induced in rat hippocampal slices by tetanic stimulation. *J. Neurosci.* 19, 1088–1105. doi: 10.1523/jneurosci.19-03-01088.1999

Uhlhaas, P. J., and Singer, W. (2013). High-frequency oscillations and the neurobiology of schizophrenia. *Dialogues Clin. Neurosci.* 15, 301–313. doi: 10.31887/dcns.2013.15.3/puhlhaas

Valdés-Cruz, A., Negrete-Díaz, J. V., Magdaleno-Madrigal, V. M., Martínez-Vargas, D., Fernández-Mas, R., Almazán-Alvarado, S., et al. (2012). Electroencephalographic activity in neonatal ventral hippocampus lesion in adult rats. *Synapse* 66, 738–746. doi: 10.1002/syn.21563

Vyazovskiy, V. V., and Tobler, I. (2005). Theta activity in the waking EEG is a marker of sleep propensity in the rat. *Brain Res.* 1050, 64–71. doi: 10.1016/j.brainres.2005.05.022

Weiss, I. C., Pryce, C. R., Jongen-Rêlo, A. L., Nanz-Bahr, N. I., and Feldon, J. (2004). Effect of social isolation on stress-related behavioural and neuroendocrine state in the rat. *Behav. Brain Res.* 152, 279–295. doi: 10.1016/J.BBR.2003.10.015

Winsky-Sommerer, R., de Oliveira, P., Loomis, S., Wafford, K., Dijk, D. J., and Gilmour, G. (2019). Disturbances of sleep quality, timing and structure and their relationship with other neuropsychiatric symptoms in Alzheimer's disease and schizophrenia: insights from studies in patient populations and animal models. *Neurosci. Biobehav. Rev.* 97, 112–137. doi: 10.1016/j.neubiorev.2018.09.027

Winterer, G., and Weinberger, D. R. (2004). Genes, dopamine and cortical signal-to-noise ratio in schizophrenia. *Trends Neurosci.* 27, 683–690. doi: 10.1016/j.tins.2004.08.002

Wirz-Justice, A., Haug, H. J., and Cajochen, C. (2001). Disturbed circadian rest-activity cycles in schizophrenia patients: an effect of drugs?. *Schizophr. Bull.* 27, 497–502. doi: 10.1093/oxfordjournals.schbul.a006890

Yamabe, M., Horie, K., Shiokawa, H., Funato, H., Yanagisawa, M., and Kitagawa, H. (2019). MC-SleepNet: large-scale sleep stage scoring in mice by deep neural networks. *Sci. Rep.* 9:15793. doi: 10.1038/s41598-019-51269-8

Yamamuro, K., Yoshino, H., Ogawa, Y., Makinodan, M., Toritsuka, M., Yamashita, M., et al. (2018). Social Isolation During the Critical Period Reduces Synaptic and Intrinsic Excitability of a Subtype of Pyramidal Cell in Mouse Prefrontal Cortex. *Cereb. Cortex* 28, 998–1010. doi: 10.1093/CERCOR/BHX010

Conflict of Interest: The authors declare that the research was conducted in the absence of any commercial or financial relationships that could be construed as a potential conflict of interest.

Publisher's Note: All claims expressed in this article are solely those of the authors and do not necessarily represent those of their affiliated organizations, or those of the publisher, the editors and the reviewers. Any product that may be evaluated in this article, or claim that may be made by its manufacturer, is not guaranteed or endorsed by the publisher.

frontiers in Behavioral Neuroscience

CASE REPORT
published: 16 February 2022
doi: 10.3389/fnbeh.2022.798375

Case Report: Event-Related Desynchronization Observed During Volitional Swallow by Electroencephalography Recordings in ALS Patients With Dysphagia

Akari Ogawa[1,2], *Satoko Koganemaru*[2,3]*, *Toshimitsu Takahashi*[3], *Yuu Takemura*[4], *Hiroshi Irisawa*[4], *Masao Matsuhashi*[5], *Tatsuya Mima*[6], *Takashi Mizushima*[4] and *Kenji Kansaku*[3]

[1] Cognitive Motor Neuroscience, Human Health Sciences, Graduate School of Medicine, Kyoto University, Kyoto, Japan, [2] Department of Regenerative Systems Neuroscience, Human Brain Research Center, Graduate School of Medicine, Kyoto University, Kyoto, Japan, [3] Department of Physiology, Dokkyo Medical University, Shimotsuga-gun, Tochigi, Japan, [4] Department of Rehabilitation Medicine, Dokkyo Medical University, Shimotsuga-gun, Tochigi, Japan, [5] Department of Epilepsy, Movement Disorders and Physiology, Graduate School of Medicine, Kyoto University, Kyoto, Japan, [6] The Graduate School of Core Ethics and Frontier Sciences, Ritsumeikan University, Kyoto, Japan

OPEN ACCESS

Edited by:
Ryo Momosaki,
Mie University, Japan

Reviewed by:
David M. Niddam,
Brain Research Center, National Yang-Ming University, Taiwan
Maria Sheila Guimarães Rocha,
Hospital Santa Marcelina, Brazil
Hiroaki Hashimoto,
Osaka University, Japan

***Correspondence:**
Satoko Koganemaru
kogane@kuhp.kyoto-u.ac.jp

Specialty section:
This article was submitted to Pathological Conditions, a section of the journal Frontiers in Behavioral Neuroscience

Received: 20 October 2021
Accepted: 24 January 2022
Published: 16 February 2022

Citation:
Ogawa A, Koganemaru S, Takahashi T, Takemura Y, Irisawa H, Matsuhashi M, Mima T, Mizushima T and Kansaku K (2022) Case Report: Event-Related Desynchronization Observed During Volitional Swallow by Electroencephalography Recordings in ALS Patients With Dysphagia. Front. Behav. Neurosci. 16:798375. doi: 10.3389/fnbeh.2022.798375

Dysphagia is a severe disability affecting daily life in patients with amyotrophic lateral sclerosis (ALS). It is caused by degeneration of both the bulbar motor neurons and cortical motoneurons projecting to the oropharyngeal areas. A previous report showed decreased event-related desynchronization (ERD) in the medial sensorimotor areas in ALS dysphagic patients. In the process of degeneration, brain reorganization may also be induced in other areas than the sensorimotor cortices. Furthermore, ALS patients with dysphagia often show a longer duration of swallowing. However, there have been no reports on brain activity in other cortical areas and the time course of brain activity during prolonged swallowing in these patients. In this case report, we investigated the distribution and the time course of ERD and corticomuscular coherence (CMC) in the beta (15–25 Hz) frequency band during volitional swallow using electroencephalography (EEG) in two patients with ALS. Case 1 (a 71-year-old man) was diagnosed 2 years before the evaluation. His first symptom was muscle weakness in the right hand; 5 months later, dysphagia developed and exacerbated. Since his dietary intake decreased, he was given an implantable venous access port. Case 2 (a 64-year-old woman) was diagnosed 1 year before the evaluation. Her first symptom was open-nasal voice and dysarthria; 3 months later, dysphagia developed and exacerbated. She was given a percutaneous endoscopic gastrostomy. EEG recordings were performed during volitional swallowing, and the ERD was calculated. The average swallow durations were 7.6 ± 3.0 s in Case 1 and 8.3 ± 2.9 s in Case 2. The significant ERD was localized in the prefrontal and premotor areas and lasted from a few seconds after the initiation of swallowing to the end in Case 1. The ERD was localized in the lateral sensorimotor areas only at the initiation of swallowing in Case 2. CMC was not observed in either case. These results suggest that compensatory processes for cortical motor

outputs might depend on individual patients and that a new therapeutic approach using ERD should be developed according to the individuality of ALS patients with dysphagia.

Keywords: event-related desynchronization, amyotrophic lateral sclerosis, dysphagia, electroencephalography, cerebral cortex

INTRODUCTION

Amyotrophic lateral sclerosis (ALS) is a degenerative disorder affecting the upper and lower motor neurons (Brooks, 1996). Dysphagia is a disability caused by oropharyngeal muscle weakness during disease progression; most ALS patients encounter this problem, which severely affects their activities of daily living (ADL) and quality of life (QOL). In general, damage to the upper and lower motoneurons results in dynamic cortical reorganization in multiple regions (Elbert and Rockstroh, 2004; Jurkiewicz et al., 2007; Fortanier et al., 2019). However, there have been few studies on cortical reorganization during swallowing in ALS patients with dysphagia (Li et al., 2009a; Teismann et al., 2011).

In previous studies using PET and functional MRI (fMRI), cortical activation was widely observed in the primary motor (M1), somatosensory, supplementary, and pre-motor cortices during volitional swallowing in healthy subjects (Ertekin and Aydogdu, 2003; Michou and Hamdy, 2009). ALS patients with dysphagia showed less cortical activity in the bilateral sensorimotor areas during volitional self-paced swallowing, compared with healthy subjects in a previous magnetoencephalography (MEG) study using event-related desynchronization (ERD) (Teismann et al., 2011). ERD is a decrease in power spectral density in the alpha (10–12 Hz) and beta frequency bands (15–25 Hz) observed during voluntary movements and is thought to reflect motor-related cortical activity (Pfurtscheller and Lopes Da Silva, 1999; Li et al., 2018; Chen et al., 2020; Spadone et al., 2020; Xie et al., 2021). The ERDs within the beta frequency band (13–30 Hz) in bilateral sensorimotor areas were less prominent in patients with ALS, and the lower the ERD, the more severe the dysphagia they had (Teismann et al., 2011), suggesting that the reduced ERD reflected the disturbed function of the degenerated cortico-motoneurons. Although the previous report showed lower activities in the sensorimotor areas (Teismann et al., 2011), there have been no report of the whole brain areas during swallow. In general, corticomotoneuronal lesions reorganize the wide-spread brain areas probably for compensation of the motor function (Ward et al., 2004; Ward, 2005). Therefore, other brain areas than sensorimotor areas would be recruited during swallowing in patients with dysphagia. In addition, swallow durations are often prolonged due to disturbances in the oral and pharyngeal phases in ALS patients (Ertekin et al., 2000; Teismann et al., 2011; Jani and Gore, 2016). However, there have been no reports about the time course of ERDs during prolonged swallowing in patients with ALS.

Recently, we have succeeded in recording ERDs within beta frequency band during swallowing in healthy subjects using electroencephalography (EEG), which is a convenient method for evaluating cortical activity in clinical practice (Koganemaru et al., 2021). Therefore, we investigated the time course of the ERD within beta band frequency in the whole brain areas in the prolonged swallow duration in two ALS patients using EEG.

Corticomuscular coherence (CMC) has also been reported in EEG studies using motor tasks of the upper and lower limbs (Mima and Hallett, 1999a). CMC is supposed to indicate corticomotoneuronal activation (Mima and Hallett, 1999a). Since predominant CMC was observed in the bilateral sensorimotor, premotor, and inferior prefrontal areas during volitional swallowing in healthy volunteers in our preliminary EEG study (Koganemaru et al., 2021), we also investigated CMC during swallowing in ALS patients.

We hypothesized that the ERD during the swallow could be found in other cortical areas than the medial sensorimotor areas, it would be changed within a prolonged swallow period and CMC would be reduced due to cortico-bulbar degeneration in the dysphagic ALS patients. There has been no previous report showing ERD in the multiple cortical areas, the time course of ERD and the CMC in ALS patients. Therefore, we investigated them in the two ALS patients.

CASE DESCRIPTION

Cases

Case 1 was a 71-year-old right-handed man. He became aware of muscle weakness in his right hand at the age of 69 years. He was diagnosed with ALS at the age of 70 years. At the age of 71 years, dietary intake decreased due to exacerbation of dysphagia (**Table 1**, in detail). He was admitted to the hospital for the construction of an implantable venous access port for nutrition intake. He could take water without thickening, jelly, and enzyme-degraded food by adjusting it to a mouthful volume. The % vital capacity (%VC) was maintained (%VC, 84.8%) and the forced expiratory volume was decreased (FEV1.0%, 52.2%). The patient's ADL score was independent. In the video-fluorography (VF) evaluation, pharyngeal phase difficulty was found.

Case 2 was a 64-year-old right-handed woman. She developed an open-nasal voice and dysarthria and was diagnosed with ALS at the age of 63 years (**Table 1**, in detail). The patient was admitted to the hospital to construct percutaneous endoscopic gastrostomy (PEG) due to exacerbated dysphagia. On admission, she showed tongue atrophy, limited elevation, and inversion of the tongue. She could consume pasted food due to impaired mastication and dysphagia. The oral phase was more disturbed by the weak movements of the mandible and tongue in the VF. The %VC decreased (73.9%) and the FEV1.0% was maintained (88.0%). The patient's ADL score was independent.

TABLE 1 | Clinical findings of Case 1 and Case 2.

Years	Clinical findings
Case 1	
0 (Onset)	Aware of right-hand weakness
0.4	Developed open-nasal voice and hoarseness
1.1	Showed swallow difficulty
	• Diagnosed with ALS according to the following findings: • Upper motor neuron deficits: • Exaggerated jaw jerk and abnormal sucking reflex • Exaggerated deep tendon reflexes of right biceps and triceps brachii muscles and left patella • Lower motor neuron deficits: • Fasciculation of tongue, bilateral forearm and lower leg muscles • Weakness of bilateral deltoid, right biceps and triceps brachii, right finger flexor and extensor, bilateral iliopsoas, hamstrings and quadriceps muscles • Atrophy of tongue, vocal cord, bilateral thenar and right first dorsal interossei muscles • Hoarseness due to vocal cord atrophy and swallowing difficulty • Needle EMG findings: fibrillation, positive sharp wave, fasciculation, large or polyphasic motor unit potentials and reduced recruitments in the right trapezius, biceps brachii, extensor digitorum, erector spinae (the level of Th10) and tibialis anterior muscles • No sensory disturbances nor ataxia • Normal laboratory data (blood and cerebrospinal fluid test), brain and spinal MR images without explainable findings for the symptoms
	Edaravone administered
1.6	Admitted to the hospital to construct totally implantable central venous access port ALSFRS-R 36 MWST: 3a, RSST: 1 Evaluated EEG
Case 2	
0 (Onset)	Developed open-nasal voice and dysarthria
0.5	• Diagnosed with ALS according to the following findings: • Upper motor neuron deficits: • Exaggerated deep tendon reflexes of bilateral biceps brachii muscles and patellae • Lower motor neuron deficits: • Fasciculation of tongue and inferior eyelids • Weakness of neck flexor, bilateral deltoid, biceps and triceps brachii, and extensor digitorum muscles • Atrophy of tongue • Facial nerve palsy • Needle EMG findings: fibrillation, positive sharp wave, fasciculation, and reduced interference and recruitments in the right trapezius, biceps brachii, extensor digitorum, erector spinae (the level of Th10) and tibialis anterior muscles • Dysarthria • No sensory disturbances nor ataxia • Normal laboratory data (blood test and cerebrospinal fluid test), normal brain and spinal MR images
	Edaravone administered (60 mg/day for 14 days)
1	Starting to use the bilevel positive airway pressure
1.5	• Admitted to constructed PEG • Evaluated EEG • ALSFRS-R 37 • MWST: 4, RSST: 2

ALSFRS-R, ALS functional rating scale-revised (Cedarbaum et al., 1999); MWST, modified water swallowing test; RSST, repetitive saliva swallowing test.

EEG and EMG Recordings

The patients were comfortably seated in an armchair during recording. The EEG signals were recorded using 32 electrodes. EEG electrodes were eego^{TM} sports active electrodes (ANT Neuro, Netherlands) and attached inside the EEG cap according to the 10–20 international electrode system. The EEG signals were amplified using an eego^{TM} sports amplifier. A CPz electrode was selected as the reference electrode. The impedance of all the electrodes was $<$15 kΩ. Data were recorded and saved at a sampling rate of 1 kHz. We concurrently recorded surface EMG using two pairs of bipolar silver electrodes attached to bilateral submental group muscles and the left orbicularis oris muscle according to previous studies (Okitsu et al., 1998; Nederkoorn et al., 1999; Ding et al., 2002; Vaiman, 2007). The electrodes were connected to a bipolar eego^{TM} sports amplifier (ANT Neuro, Netherlands). Swallowing movements were recorded with a triple-axis accelerometer placed on the anterior part of the participant's neck, similar to previous studies (Suntrup et al., 2014, 2015; Jestrovic et al., 2018; Suntrup-Krueger et al., 2018). Head movements during volitional swallowing were monitored using two cameras. An experimenter injected 2 mL of water into the oral cavity via a flexible tube with 3.3-mm diameter connected to the syringe before each swallow during the experiment. The patients were asked to perform volitional swallowing without moving their heads at their own pace with a waiting time of $>$3 s after the water infusion according to the previous report (Koganemaru et al., 2021). The tip of the tube was placed on the right of the mouth between the buccal part of the teeth and cheek, and fixed on the skin with tape, similar to the previous MEG studies (Suntrup et al., 2014, 2015; Suntrup-Krueger et al., 2018). They repeated the volitional swallow for 1 h to evaluate 100–150 times of voluntary swallow with 15–20 s of inter-intervals.

Data Analysis

Pre-processing

We removed artifacts of the blink, electrooculographic activities, and muscle activities related with swallow movements from the EEG signals using independent component analysis (ICA) (Hyvärinen and Oja, 2000) using the EEGLAB MATLAB toolbox (Math Works Inc., USA) (Delorme and Makeig, 2004). We segmented EEG signals based on the onset and offset of each swallow, as determined by rectified EMG signals from submental group muscles according to previous MEG studies (Teismann et al., 2011; Suntrup et al., 2014, 2015; Suntrup-Krueger et al., 2018). The beginning of the main muscle activation (M1) was defined as the time point at which the amplitude of the rectified EMG signal continuously increased by more than 100% (**Figure 1**). Moreover, the onset of the first visible EMG activity of the swallowing movement (M0) was manually set to determine the total swallow duration (from M0 to M2). The end of the swallow specific muscle activity (M2) was defined as the time point when the amplitude of the rectified EMG signal continuously decreased by more than 50%, as in previous studies (Suntrup et al., 2014, 2015; Suntrup-Krueger et al., 2018). To analyze the event-related EEG signals, the onset of swallowing (E1) was defined as (M1–0.4 s) and the offset of the swallowing

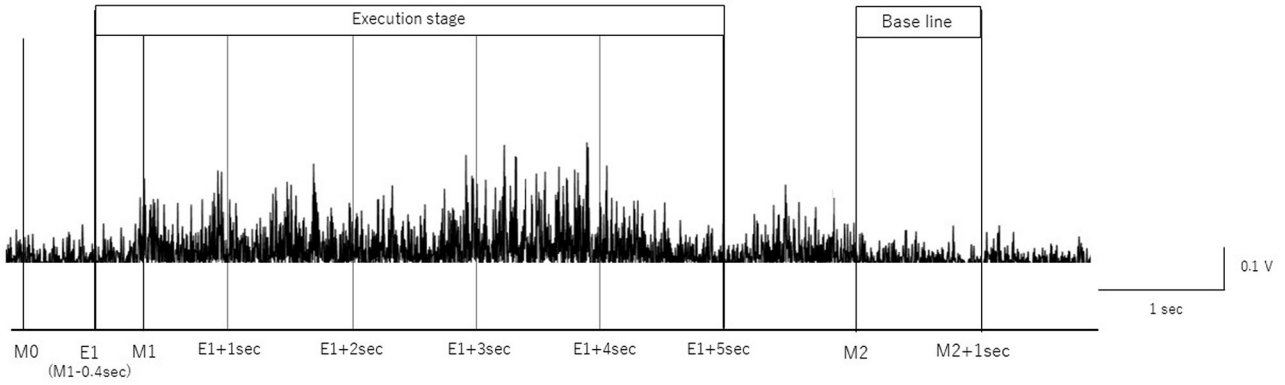

FIGURE 1 | Definition of onset and offset of swallow. The onset and offset of volitional swallowing are defined according to swallow-related submental group muscle activities form Case 1. M0 is the E1 is the time to initiate swallowing, M1 is the time to start the main muscle activation, and M2 is the time to return to baseline. The surface EMG of the submental group muscle trace during a single swallow is shown.

as M2, according to previous studies (Dziewas et al., 2009; Teismann et al., 2011; Suntrup et al., 2015). The time intervals are defined as follows:

(1) Execution stage: −0.4 to 4.6 s divided by 1 s duration in reference to M1 (from E1 to E1+ 5 s)

(2) Resting-stage: 0–1 s in reference to M2.

EEG Analysis

Event-Related Desynchronization

We calculated the power spectral density of the segmented EEG denoised by ICA using fast Fourier transform (FFT). We applied the FFT to 1,000 ms segments spanning the activation stage (from E1 to E1 + 5 s, divided into 1,000 ms intervals). The baseline for ERD analysis was 1,000 ms segments spanning the resting stage (from M2 s to M2 + 1.0 s). The upper and lower limits of the FFT were 500 and 1 Hz, respectively. The evaluated frequency ranged from 15 to 25 Hz. The ERD was calculated by taking the logarithm of the averaged power spectrum and subtracting that in the baseline from that in the activation stage. We obtained the average ERD of all channels in each patient in the beta (15–25 Hz) frequency. The 95% confidence limit for the EEG power was calculated for the number of trials (n) in each patient using the following equation (Halliday et al., 1995).

$$\textbf{Confidence limit } (95\%) = \pm (0.851) * (n)^{-1/2}$$

Corticomusclar Coherence

By using FFT, we computed the cross- and auto-spectra in the frequency domain of the EEG signals and rectified EMG signals from submental group muscles in the activation phase. The FFT was applied to 1,000 ms segments spanning from E1 to E1 + 5 s in the same way as with the calculation of ERD. The coherence is defined as cross-spectra normalized by auto-spectra, and it expressed by the following equation, in which $f_{xx}(j), f_{yy}(j)$, and $|f_{xy}(j)|$ denote auto-spectra and cross-spectra at frequency j (Mima and Hallett, 1999a).

$$|R_{xy}(j)|^2 = \frac{|f_{xy}(j)|^2}{f_{xx}(j) f_{yy}(j)}$$

The 95% confidence limit was calculated for the number of trials (n) in each patient using the following equation (Mima and Hallett, 1999a).

$$\textbf{Confidence limit } (95\%) = 1 - (0.05)^{1/(n-1)}$$

ASSESSMENT

The number of volitional swallows in each patient was 120 times in Case 1 and 89 times in Case 2 during EEG recording. The averages of each swallow duration were 7.6 ± 3.0 s in Case 1 and 8.3 ± 2.9 s in Case 2. We visually inspected head movements monitored by cameras and found no head movements during swallowing in either case. During the recordings including the volitional swallow task, no adverse events occurred. During the volitional swallowing task, no aspiration occurred and the patients did not execute the double or more swallowing and did not swallow the saliva. We removed ∼5% of the trials with <5 s of swallow duration so that we could investigate brain activity during prolonged swallow movements. **Figures 2**, **3** show the EMG of submental group muscles and the topographic mapping of the averaged ERD or event-related synchronization (ERS) every 1 s. The 95% confidence limit for the ERD were ± 0.0777 in Case 1 and ± 0.0918 in Case 2. Thus, the ERD smaller than this limit is judged to be non-zero. In Case 1, no significant ERD was found in any channels until 3 s after the onset of the swallowing. After then, significant ERD was found in the bilateral prefrontal areas (corresponding to the Fp1, Fpz, and Fp2) and the right premotor area (corresponding to the F4 channel) 3–4 s after and in those areas (corresponding to the Fp1, Fp2, and F4 channels) 4–5 s after the onset of the swallow. In Case 2, significant ERD

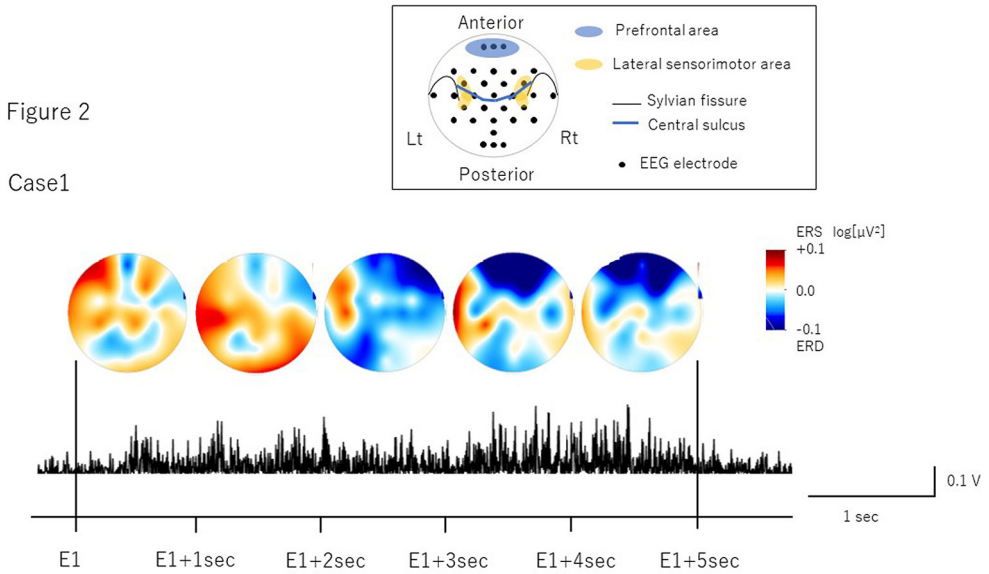

FIGURE 2 | The topographic mapping of the averaged ERD/ERS and the EMG of submental group muscles in Case 1. The topographic mapping display of the swallow-related ERD or ERS every 1 s and the EMG of submental group muscles during a single swallow in Case 1 are shown. ERD/S are color-coded on the topomap display. ERD is prominent in the bilateral prefrontal areas from 3 s after the onset of swallowing to the end of swallowing.

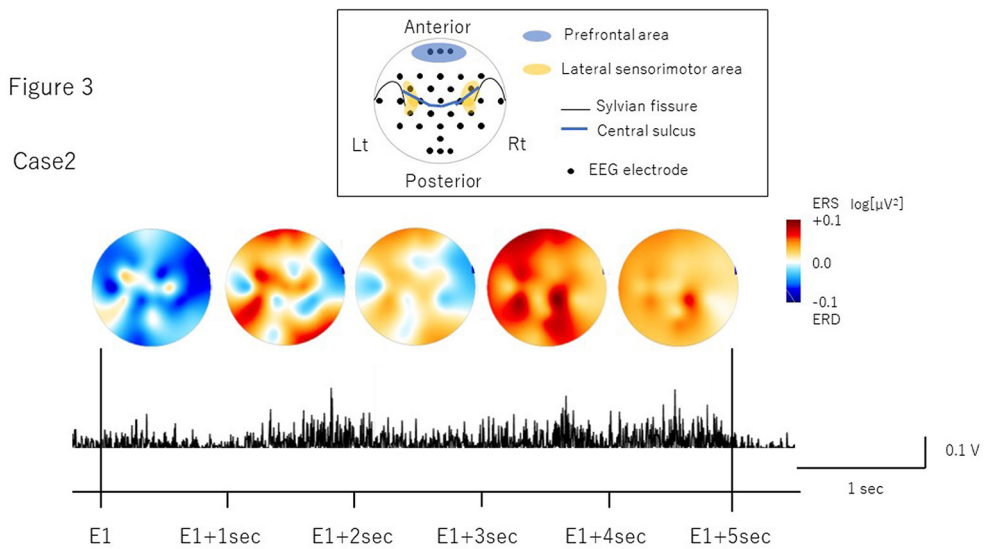

FIGURE 3 | The topographic mapping of the averaged ERD/ERS and the EMG of submental group muscles in Case 2. The topographic mapping display of the swallow-related ERD or ERS every 1 s and the EMG of submental group muscles during a single swallow in Case 2 are shown. ERD/S are color-coded on the topomap display. ERD is prominent in the right lateral sensorimotor areas at the beginning of swallowing.

was found in the right lateral sensorimotor area (corresponding to the CP6 and FC6), and the right premotor area (corresponding to the F4 channel) and the bilateral temporal areas (T7 and T8 channels) at the beginning of the swallow but was absent from 1 to 5 sec after the onset of swallowing. The 95% confidence limit for the CMC were 0.0249 in Case 1 and 0.0335 in Case 2. Thus, the CMC larger than this limit is judged to be non-zero. However, as CMC was lower than the limit in each channel in both cases, significant CMC was not found during volitional swallowing.

DISCUSSION

We found the significant ERD in other cortical areas than medial sensorimotor cortices, the individual timing of ERD emergence and no significant CMC during the volitional swallow in two ALS patients with dysphagia showing a prolonged swallow duration.

In Case 1, we found ERD in the prefrontal areas around the time when the EMG activity reached the peak, which mostly corresponded to the pharyngeal phase (Nederkoorn

et al., 1999; Vaiman, 2007). The prefrontal cortex is related to higher motor function, such as inhibition of reaction, control of voluntary movements, and cognitive functions such as attention and working memory (Faw, 2003). In previous studies, ERDs were observed in the dorsolateral prefrontal cortex during self-paced movements, reflecting cognitive processes supporting movement tasks such as motor memory, estimation of time interval for motor preparation, and attention (Rektor et al., 2006; Sochurková et al., 2006). Therefore, the ERD in the prefrontal areas in Case 1 suggests that swallowing was forced with cognitive efforts to compensate for reduced motor outputs due to the possible degeneration of the cortico-bulbar tracts and the lower cranial motor neurons. In Case 2, we found the ERD in the right lateral sensorimotor areas most likely corresponding to the tongue representation. This suggests that activation may be related to weakened tongue movements during the oral phase. In a previous EEG study, ERD was induced in the lateral sensorimotor areas when the tongue was thrusting (Sakihara and Inagaki, 2015). Activation has also been reported in more medial sensorimotor areas during volitional swallowing in healthy volunteers (Hamdy et al., 1996; Dziewas et al., 2009). ERD in the more lateral areas during volitional swallow in Case 2 suggests that activation in the tongue-related areas may reflect an increase in motor outputs to the weakened tongue muscles to transfer into the pharynx as well as compensation for reduced activity of the M1 pharyngeal areas located more medially. Furthermore, significant ERD were found in the bilateral temporal areas in Case 2. Previous reports showed the temporal lesion produced dysphagia and the brain activity was increased in the dysphagic patients (Hamdy et al., 1998; Li et al., 2009b). The detailed mechanism of temporal activities has not been clarified. However, it may be related to the compensation for the swallowing dysfunction.

Although there was almost no difference of the ALS severity according to the scores of ALSFRS-R between Case 1 and 2, Case 1 showed hoarseness due to incomplete vocal closure caused by vocal atrophy. It suggests that Case 1 required more efforts to compensate the incomplete closure of the vocal cord and to prevent aspiration during the swallowing than Case 2, who showed no dysfunction of vocal cord.

As for laterality, the previous MEG study found significant ERD lateralization to the left hemisphere in healthy subjects and to the right hemisphere in ALS patients with both moderate and severe dysphagia (Teismann et al., 2011). In this case report, the both cases showed the lateralization to the right hemisphere as well as the previous report.

Previous MEG studies analyzed ERD just for one second during swallowing (Teismann et al., 2011). However, patients with dysphagia often show a duration of more than several seconds during swallowing. The timing of the ERD appearance differed between Cases 1 and 2. It might be related to the more severely affected period, for example, the period before or after the EMG peak. Further investigation is necessary in more patients with ALS. The current EEG method to evaluate ERD during the swallow may be used in the assessment of effortfulness of the swallow and in determining the therapeutic target phase in swallow rehabilitation. Our finding may extend the knowledge about the mechanism and alteration of cortical involvement in the swallow in dysphagic ALS.

Recently, ERD has been used to restore motor function in the BMI techniques in patients with neurological diseases (Ramos-Murguialday et al., 2013; Ono et al., 2014). In this case report, we clarified the difference of time-course of ERD emergence in the individual ALS patients. If ERD during the swallow can be used in the swallow rehabilitation, the target timing of the ERD needs to be considered. Our findings would be useful in new swallow rehabilitation using ERD. Furthermore, a simpler method using EEG with a fewer electrodes and online analysis of ERD would be necessary for clinical application in future.

We did not find a significant CMC in either case. CMC can measure the cortical control of peripheral motor neurons (Mima and Hallett, 1999a,b). A previous study reported that CMC in ALS patients was significantly diminished relative to healthy subjects during a light hand grip (Proudfoot et al., 2018). The CMC was not significant during volitional swallowing in this study, probably due to cortico-bulbar dysfunction in ALS.

In this study, we characterized the time course and the distribution of ERD during prolonged volitional swallowing in two ALS patients with dysphagia. Although they showed severe dysphagia, which caused difficulties in oral intake, the time course and distribution were different. This suggests that different processes occur for degeneration and compensation in patients with dysphagic ALS. Further studies are necessary in a larger number of patients with ALS.

PATIENT PERSPECTIVE

Case 1 stated that he hoped his result would be helpful for understanding of the impairments of brain activation related to dysphagia in ALS. Case 2 stated that she hoped she could contribute to developing a new therapy to improve dysphagia in ALS by participating in the EEG evaluation.

DATA AVAILABILITY STATEMENT

The raw data supporting the conclusions of this article will be made available by the authors, without undue reservation.

ETHICS STATEMENT

The studies involving human participants were reviewed and approved by the Committee of Medical Ethics of Dokkyo Medical University. The patients/participants provided their written informed consent to participate in this study.

AUTHOR CONTRIBUTIONS

SK designed the study and collected and interpreted the data. AO contributed to data analysis and wrote the initial draft of the manuscript. TT, YT, HI, MM, TMim, TMiz, and KK have contributed to data collection and interpretation and critically

reviewed the manuscript. All authors approved the final version of the manuscript.

FUNDING

This work was supported by a Grant-in-Aid for Exploratory Research (20K21770), Grants-in-Aid for Scientific Research (B) (21H03308) (SK), Grants-in-Aid for Scientific Research (A) (19H01091) (TMim), Grants-in-Aid for Scientific Research (A) (19H01126), and (B) (19H03939) (KK) from the Japan Society for the Promotion of Science.

ACKNOWLEDGMENTS

The authors would like to thank A. Sugawara and M. Hayakawa for their technical assistance with the experiments.

SUPPLEMENTARY MATERIAL

The Supplementary Material for this article can be found online at: https://www.frontiersin.org/articles/10.3389/fnbeh.2022.798375/full#supplementary-material

REFERENCES

Brooks, B. R. (1996). Clinical epidemiology of amyotrophic lateral sclerosis. *Neurol. Clin.* 14, 399–420. doi: 10.1016/S0733-8619(05)70264-4

Cedarbaum, J. M., Stambler, N., Malta, E., Fuller, C., Hilt, D., Thurmond, B., et al. (1999). The ALSFRS-R: a revised ALS functional rating scale that incorporates assessments of respiratory function. BDNF ALS study group (phase III). *J. Neurol. Sci.* 169, 13–21. doi: 10.1016/S0022-510X(99)00210-5

Chen, S., Li, Y., Shu, X., Wang, C., Wang, H., Ding, L., et al. (2020). Electroencephalography Mu rhythm changes and decreased spasticity after repetitive peripheral magnetic stimulation in patients following stroke. *Front. Neurol.* 11, 546599. doi: 10.3389/fneur.2020.546599

Delorme, A., and Makeig, S. (2004). EEGLAB: an open source toolbox for analysis of single-trial EEG dynamics including independent component analysis. *J. Neurosci. Methods* 134, 9–21. doi: 10.1016/j.jneumeth.2003.10.009

Ding, R., Larson, C. R., Logemann, J. A., and Rademaker, A. W. (2002). Surface electromyographic and electroglottographic studies in normal subjects under two swallow conditions: normal and during the Mendelsohn manuever. *Dysphagia* 17, 1–12. doi: 10.1007/s00455-001-0095-3

Dziewas, R., Teismann, I. K., Suntrup, S., Schiffbauer, H., Steinstraeter, O., Warnecke, T., et al. (2009). Cortical compensation associated with dysphagia caused by selective degeneration of bulbar motor neurons. *Hum. Brain Mapp.* 30, 1352–1360. doi: 10.1002/hbm.20603

Elbert, T., and Rockstroh, B. (2004). Reorganization of human cerebral cortex: the range of changes following use and injury. *Neuroscientist* 10, 129–141. doi: 10.1177/1073858403262111

Ertekin, C., and Aydogdu, I. (2003). Neurophysiology of swallowing. *Clin. Neurophysiol.* 114, 2226–2244. doi: 10.1016/S1388-2457(03)00237-2

Ertekin, C., Aydogdu, I., Yüceyar, N., Kiylioglu, N., Tarlaci, S., and Uludag, B. (2000). Pathophysiological mechanisms of oropharyngeal dysphagia in amyotrophic lateral sclerosis. *Brain* 123 (Pt. 1), 125–140. doi: 10.1093/brain/123.1.125

Faw, B. (2003). Pre-frontal executive committee for perception, working memory, attention, long-term memory, motor control, and thinking: a tutorial review. *Conscious. Cogn.* 12, 83–139. doi: 10.1016/S1053-8100(02)00030-2

Fortanier, E., Grapperon, A. M., Le Troter, A., Verschueren, A., Ridley, B., Guye, M., et al. (2019). Structural connectivity alterations in amyotrophic lateral sclerosis: a graph theory based imaging study. *Front. Neurosci.* 13, 1044. doi: 10.3389/fnins.2019.01044

Halliday, D. M., Rosenberg, J. R., Amjad, A. M., Breeze, P., Conway, B. A., and Farmer, S. F. (1995). A framework for the analysis of mixed time series/point process data–theory and application to the study of physiological tremor, single motor unit discharges and electromyograms. *Prog. Biophys. Mol. Biol.* 64, 237–278. doi: 10.1016/S0079-6107(96)00009-0

Hamdy, S., Aziz, Q., Rothwell, J. C., Power, M., Singh, K. D., Nicholson, D. A., et al. (1998). Recovery of swallowing after dysphagic stroke relates to functional reorganization in the intact motor cortex. *Gastroenterology* 115, 1104–1112. doi: 10.1016/S0016-5085(98)70081-2

Hamdy, S., Aziz, Q., Rothwell, J. C., Singh, K. D., Barlow, J., Hughes, D. G., et al. (1996). The cortical topography of human swallowing musculature in health and disease. *Nat. Med.* 2, 1217–1224. doi: 10.1038/nm1196-1217

Hyvärinen, A., and Oja, E. (2000). Independent component analysis: algorithms and applications. *Neural Netw.* 13, 411–430. doi: 10.1016/S0893-6080(00)00026-5

Jani, M. P., and Gore, G. B. (2016). Swallowing characteristics in amyotrophic lateral sclerosis. *NeuroRehabilitation* 39, 273–276. doi: 10.3233/NRE-161357

Jestrovic, I., Coyle, J. L., Perera, S., and Sejdic, E. (2018). Influence of attention and bolus volume on brain organization during swallowing. *Brain Struct. Funct.* 223, 955–964. doi: 10.1007/s00429-017-1535-7

Jurkiewicz, M. T., Mikulis, D. J., Mcilroy, W. E., Fehlings, M. G., and Verrier, M. C. (2007). Sensorimotor cortical plasticity during recovery following spinal cord injury: a longitudinal fMRI study. *Neurorehabil. Neural Repair* 21, 527–538. doi: 10.1177/1545968307301872

Koganemaru, S., Mizuno, F., Takahashi, T., Takemura, Y., Irisawa, H., Matsuhashi, M., et al. (2021). Event-related desynchronization and corticomuscular coherence observed during volitional swallow by electroencephalography recordings in humans. *Front. Hum. Neurosci.* 15, 643454. doi: 10.3389/fnhum.2021.643454

Li, H., Huang, G., Lin, Q., Zhao, J.-L., Lo, W.-L. A., Mao, Y.-R., et al. (2018). Combining movement-related cortical potentials and event-related desynchronization to study movement preparation and execution. *Front. Neurol.* 9, 822. doi: 10.3389/fneur.2018.00822

Li, S., Chen, Q., Yu, B., Xue, K., Luo, C., Xu, Y., et al. (2009a). Structural and functional changes mapped in the brains of amyotrophic lateral sclerosis patients with/without dysphagia: a pilot study. *Amyotroph. Lateral Scler.* 10, 280–287. doi: 10.3109/17482960902893342

Li, S., Luo, C., Yu, B., Yan, B., Gong, Q., He, C., et al. (2009b). Functional magnetic resonance imaging study on dysphagia after unilateral hemispheric stroke: a preliminary study. *J. Neurol. Neurosurg. Psychiatry* 80, 1320–1329. doi: 10.1136/jnnp.2009.176214

Michou, E., and Hamdy, S. (2009). Cortical input in control of swallowing. *Curr. Opin. Otolaryngol. Head Neck Surg.* 17, 166–171. doi: 10.1097/MOO.0b013e32832b255e

Mima, T., and Hallett, M. (1999a). Corticomuscular coherence: a review. *J. Clin. Neurophysiol.* 16, 501–511. doi: 10.1097/00004691-199911000-00002

Mima, T., and Hallett, M. (1999b). Electroencephalographic analysis of cortico-muscular coherence: reference effect, volume conduction and generator mechanism. *Clin. Neurophysiol.* 110, 1892–1899. doi: 10.1016/S1388-2457(99)00238-2

Nederkoorn, C., Smulders, F. T., and Jansen, A. (1999). Recording of swallowing events using electromyography as a non-invasive measurement of salivation. *Appetite* 33, 361–369. doi: 10.1006/appe.1999.0268

Okitsu, T., Arita, M., Sonoda, S., Ota, T., Hotta, F., Honda, T., et al. (1998). The surface electromyography on suprahyoid muscles during swallowing. *Jpn. J. Rehabil. Med.* 35, 241–244. doi: 10.2490/jjrm1963.35.241

Ono, T., Shindo, K., Kawashima, K., Ota, N., Ito, M., Ota, T., et al. (2014). Brain-computer interface with somatosensory feedback improves functional recovery from severe hemiplegia due to chronic stroke. *Front. Neuroeng.* 7, 19. doi: 10.3389/fneng.2014.00019

Pfurtscheller, G., and Lopes Da Silva, F. H. (1999). Event-related EEG/MEG synchronization and desynchronization: basic principles. *Clin. Neurophysiol.* 110, 1842–1857. doi: 10.1016/S1388-2457(99)00141-8

Proudfoot, M., Van Ede, F., Quinn, A., Colclough, G. L., Wuu, J., Talbot, K., et al. (2018). Impaired corticomuscular and interhemispheric cortical beta oscillation coupling in amyotrophic lateral sclerosis. *Clin. Neurophysiol.* 129, 1479–1489. doi: 10.1016/j.clinph.2018.03.019

Ramos-Murguialday, A., Broetz, D., Rea, M., Läer, L., Yilmaz, O., Brasil, F. L., et al. (2013). Brain-machine interface in chronic stroke rehabilitation: a controlled study. *Ann. Neurol.* 74, 100–108. doi: 10.1002/ana.23879

Rektor, I., Sochurková, D., and Bocková, M. (2006). Intracerebral ERD/ERS in voluntary movement and in cognitive visuomotor task. *Prog. Brain Res.* 159, 311–330. doi: 10.1016/S0079-6123(06)59021-1

Sakihara, K., and Inagaki, M. (2015). Mu rhythm desynchronization by tongue thrust observation. *Front. Hum. Neurosci.* 9, 501. doi: 10.3389/fnhum.2015.00501

Sochurková, D., Rektor, I., Jurák, P., and Stancák, A. (2006). Intracerebral recording of cortical activity related to self-paced voluntary movements: a bereitschaftspotential and event-related desynchronization/synchronization. SEEG study. *Exp. Brain Res.* 173, 637–649. doi: 10.1007/s00221-006-0407-9

Spadone, S., Croce, P., Zappasodi, F., and Capotosto, P. (2020). Pre-stimulus EEG microstates correlate with anticipatory alpha desynchronization. *Front. Hum. Neurosci.* 14, 182. doi: 10.3389/fnhum.2020.00182

Suntrup, S., Teismann, I., Wollbrink, A., Warnecke, T., Winkels, M., Pantev, C., et al. (2014). Altered cortical swallowing processing in patients with functional dysphagia: a preliminary study. *PLoS ONE* 9:e89665. doi: 10.1371/journal.pone.0089665

Suntrup, S., Teismann, I., Wollbrink, A., Winkels, M., Warnecke, T., Pantev, C., et al. (2015). Pharyngeal electrical stimulation can modulate swallowing in cortical processing and behavior - magnetoencephalographic evidence. *Neuroimage* 104, 117–124. doi: 10.1016/j.neuroimage.2014.10.016

Suntrup-Krueger, S., Ringmaier, C., Muhle, P., Wollbrink, A., Kemmling, A., Hanning, U., et al. (2018). Randomized trial of transcranial direct current stimulation for poststroke dysphagia. *Ann. Neurol.* 83, 328–340. doi: 10.1002/ana.25151

Teismann, I. K., Warnecke, T., Suntrup, S., Steinsträter, O., Kronenberg, L., Ringelstein, E. B., et al. (2011). Cortical processing of swallowing in ALS patients with progressive dysphagia–a magnetoencephalographic study. *PLoS ONE* 6, e19987. doi: 10.1371/journal.pone.0019987

Vaiman, M. (2007). Standardization of surface electromyography utilized to evaluate patients with dysphagia. *Head Face Med.* 3, 26. doi: 10.1186/1746-160X-3-26

Ward, N. S. (2005). Mechanisms underlying recovery of motor function after stroke. *Postgrad. Med. J.* 81, 510–514. doi: 10.1136/pgmj.2004.030809

Ward, N. S., Brown, M. M., Thompson, A. J., and Frackowiak, R. S. (2004). The influence of time after stroke on brain activations during a motor task. *Ann. Neurol.* 55, 829–834. doi: 10.1002/ana.20099

Xie, J., Peng, M., Lu, J., Xiao, C., Zong, X., Wang, M., et al. (2021). Enhancement of event-related desynchronization in motor imagery based on transcranial electrical stimulation. *Front. Hum. Neurosci.* 15, 635351. doi: 10.3389/fnhum.2021.635351

Conflict of Interest: The authors declare that the research was conducted in the absence of any commercial or financial relationships that could be construed as a potential conflict of interest.

Publisher's Note: All claims expressed in this article are solely those of the authors and do not necessarily represent those of their affiliated organizations, or those of the publisher, the editors and the reviewers. Any product that may be evaluated in this article, or claim that may be made by its manufacturer, is not guaranteed or endorsed by the publisher.

Advantages of publishing in Frontiers

OPEN ACCESS
Articles are free to read for greatest visibility and readership

FAST PUBLICATION
Around 90 days from submission to decision

HIGH QUALITY PEER-REVIEW
Rigorous, collaborative, and constructive peer-review

TRANSPARENT PEER-REVIEW
Editors and reviewers acknowledged by name on published articles

Frontiers
Avenue du Tribunal-Fédéral 34
1005 Lausanne | Switzerland

Visit us: www.frontiersin.org
Contact us: frontiersin.org/about/contact

REPRODUCIBILITY OF RESEARCH
Support open data and methods to enhance research reproducibility

DIGITAL PUBLISHING
Articles designed for optimal readership across devices

FOLLOW US
@frontiersin

IMPACT METRICS
Advanced article metrics track visibility across digital media

EXTENSIVE PROMOTION
Marketing and promotion of impactful research

LOOP RESEARCH NETWORK
Our network increases your article's readership